

Department Biologie II
Anthropologie und Humangenetik
Ludwig-Maximilians-Universität München

Cloning in Cattle: Nuclear architecture and epigenetic status of chromatin during reprogramming of donor cell nuclei



Daniela Köhler

Dissertation an der Fakultät für Biologie
der Ludwig-Maximilians-Universität München
Eingereicht am 23.10.2008

Cloning in cattle: Nuclear architecture and epigenetic status of chromatin during reprogramming of donor cell nuclei

Dissertation an der Fakultät für Biologie, Department II
der Ludwig-Maximilians-Universität München (LMU)

Vorgelegt von
Dipl.Biol. Daniela Köhler

Gutachter:
Erstgutachter: Prof. Dr. Thomas Cremer
Zweitgutachter: Prof. Dr. Manfred Schliwa

Tag der mündlichen Prüfung: 19.März 2009

Einmal kündigte der Physiker Leo Szilard seinem Freund Hans Bethe an, er wolle eventuell ein Tagebuch führen: “ Ich habe nicht vor etwas zu veröffentlichen. Ich möchte die Tatsachen nur festhalten, damit Gott Bescheid weiß.” Daraufhin fragte Bethe: “Glauben sie nicht, dass Gott die Tatsachen schon kennt?” – “Ja”, erwiderte Szilard, “die Tatsachen kennt er. Aber diese Version der Tatsachen kennt er noch nicht.”

Hans Christian von Baeyer, Das Atom der Falle

Contents:

1. Summary	1
1.1. Abstract	1
1.2. Zusammenfassung	3
2. Introduction: Positions of chromosome territories (CTs) and sub-domains in the cell nucleus	5
2.1. Goals of the study	5
2.2. Organization in a cell nucleus	7
2.2.1. Discovery of CTs	7
2.2.2. The Chromosome-Territory-Interchromatin-Compartment (CT-IC) model	9
2.2.2.1. Intermingling and loops	11
2.2.2.2. Computer-based models	12
2.2.3. Different compartments within a nucleus	12
2.2.3.1. Chromatin structure	13
2.2.3.2. Euchromatin and Heterochromatin	13
2.2.3.3. Nuclear lamina	15
2.2.3.4. Nucleolus, Speckles and other nuclear bodies	16
2.2.4. Distribution pattern of CTs: radial distribution and neighborhoods	16
2.2.4.1. Prometaphase rosettes	17
2.2.4.2. Interphase nuclei	17
2.2.4.3. Sperm heads	18
2.2.4.4. Tissues and cancer	18
2.2.4.5. Gene-rich and gene-poor chromosomes	19
2.2.4.6. Differentiation and development	20
2.2.4.7. Chromatin mobility & gene expression	21
2.2.5. Evolutionary conserved pattern	23
2.2.6. Influence of nuclear shape on CT distribution	24
2.2.7. Preimplantation embryos as a model system	25
2.2.7.1. Diagnostics in preimplantation embryos	25
3. Material & Methods:	27
3.1. Cell and embryo material	27
3.1.1. Human Diploid Fibroblasts (HDF)	27
3.1.2. Lymphocytes (human/bovine)	27
3.1.3. Bovine Fetal Fibroblasts (BFF)	28
3.1.4. Bovine embryos	28
3.1.5. Mouse embryos	28
3.2. Cell culture	29
3.2.1. Media	29

3.2.2. Unfreezing, culture and freezing down	29
3.2.3. Growing cells on glass coverslips	29
3.3. Generation of embryonic specimen	30
3.3.1. Extraction of oocytes	30
3.3.2. <i>In-vitro</i> fertilization (IVF)	31
3.3.3. Nuclear Transfer (NT)	32
3.4. Metaphase preparation	33
3.4.1. Treatment of cells	33
3.4.2. Drop cells	34
3.4.3. Post-treatment for conservation	34
3.4.4. Pepsin-treatment of slides	35
3.5. Fixation of cells for 3D fluorescence in situ hybridization (FISH)	35
3.6. Fixation of embryos	36
3.7. Probe amplification and labeling	39
3.7.1. Origin of bovine probes	39
3.7.2. Nucleotide labeling	39
3.7.3. Secondary DOP-PCR	41
3.7.4. Whole Genome Amplification (WGA) by Multiple Displacement Amplification (MDA)	42
3.7.5. Label DOP-PCR	43
3.7.6. Nick translation (NT)	44
3.7.7. Preparation of C ₀ t-1 DNA	45
3.8. Probe precipitation	47
3.9. 2D FISH	47
3.9.1. 2D FISH set up	47
3.9.2. 2D FISH detection	48
3.10. 3D FISH	49
3.10.1. 3D FISH on cells	49
3.10.1.1. 3D FISH set up on cells	49
3.10.1.2. Detection of 3D FISH on cells	50
3.10.2. 3D FISH on embryos	50
3.10.2.1. 3D FISH set up on embryos	50
3.10.2.2. Detection of FISH signals on embryos	51
3.11. Microscopy	53
3.11.1. Stereomicroscope	53
3.11.2. Light microscope	53
3.11.3. Fluorescent microscope	53
3.11.4. Confocal laser scanning microscope (CLSM)	54

3.12. Data evaluation	55
3.12.1. Shift correction	55
3.12.2. Deconvolution	55
3.12.3. Image J	56
3.12.4. Quantitative data evaluation	57
3.12.4.1. Three dimensional – Relative Radial Distribution (3D-RRD)	58
3.12.4.2. Absolute Distance to Surface (ADS) or Enhanced Absolute Distance to Surface (eADS)	58
3.12.5. Photoshop (CS2, Adobe systems, Inc., S. Jose)	59
3.12.6. Amira	59
3.12.7. Statistics	59
4. Results:	60
4.1. Similarity of chromosome arrangement is lost after two cell cycles in HeLa and normal diploid cells	60
4.2. Distribution of gene-rich and gene-poor CTs in dependency on nuclear shape and cell cycle	61
4.2.1. Human fibroblasts data with flat shaped nuclei	61
4.2.1.1. Cell cycle dependent distribution of big vs. small chromosomes (HSA 1 vs. HSA 20)	61
4.2.1.2. Cell cycle dependent distribution of gene-rich vs. gene-poor chromosomes (HSA 17 vs. HSA Y)	63
4.2.1.3. Cell cycle dependent distribution of gene-poor vs. gene-rich chromosomes (HSA 18 vs. HSA 19)	64
4.2.2. Inducing a change of nuclear shape by growing fibroblasts on micropattern	67
4.2.2.1. Morphology and shape of nuclei from fibroblasts grown on micropattern	68
4.2.2.2. Distribution of human chromosomes 18 and 19 in human fibroblast cells	70
4.2.2.2.1. Cigar shaped cells	70
4.2.2.2.2. Round shaped cells	72
4.2.2.3. Distribution of human orthologous chromosomes 18 and 19 in fibroblasts of Wolf's guenon	73
4.2.2.3.1. Cigar shaped cells	74
4.2.2.3.2. Round shaped cells	75
4.2.2.4. Distribution of bovine chromosomes 19 and 20 in fibroblast nuclei of Cattle	76
4.2.2.4.1. Bovine fetal fibroblasts (BFF451-1): “normal” flat shape	77
4.2.2.4.2. Cigar shaped bovine fetal fibroblasts (BFF451-1)	77
4.2.2.4.3. Round shaped bovine fetal fibroblasts (BFF 451-1)	78
4.3. FISH on 3D preserved bovine preimplantation embryos	80
4.3.1. Establishment of a FISH protocol on 3D preserved embryos	80
4.3.2. Embryo attachment	80
4.3.3. Choosing the best wells to securely handle embryos	80
4.3.4. Modifications of the fixation protocol	81

4.3.5. Set up FISH: denaturation and hybridization _____	81
4.3.6. Modifications and improvements for probe detection in embryos _____	82
4.3.7. Recording embryos at the confocal laser scanning microscope (CLSM) _____	83
4.4. Gene-rich and gene-poor chromosomes in bovine species _____	84
4.4.1. Bovine karyotype _____	84
4.4.2. Probe optimization _____	85
4.4.3. 3D distribution of CTs 19 and 20 in diploid bovine fibroblast nuclei _____	87
4.4.4. 3D distribution of CTs 19 and 20 in diploid bovine lymphocyte nuclei _____	87
4.4.5. 3D radial distribution of CTs 19 and 20 in IVF embryos _____	88
4.4.5.1. Zygotes – early, mid and late _____	90
4.4.5.2. Day 2 embryos: 4-8 cells per embryo _____	91
4.4.5.3. Day 3 embryos: 10-16 cells per embryo _____	92
4.4.5.4. Blastocysts: ICM vs TE _____	93
4.4.6. Global DNA distribution _____	94
4.4.7. Test of FISH on embryos of another species: the mouse model _____	96
4.4.7.1. Modifications of the FISH protocol for mouse preimplantation embryos _____	96
4.4.7.2. Gene rich and gene poor chromosomes in mouse _____	97
4.5. Localization of an Oct4-GFP transgene in NT embryos _____	97
4.5.1. The reporter gene construct GOF18- Δ PE-EGFP _____	98
4.5.2. Oct4-GFP (GOF) – the transgene and its localization _____	99
4.5.3. GOF distribution in BFF451-1 nuclei _____	100
4.5.4. Distribution of GOF in NT embryos of different developmental stages _____	101
4.5.4.1. Distribution in day 2 embryos _____	102
4.5.4.2. Distribution in day 4 embryos _____	102
4.5.4.3. Distribution in day 7 embryos _____	103
4.5.4.4. Comparing the GOF distribution in different developmental stages _____	106
4.5.4.4.1. GOF in relation to CT 13 _____	106
4.5.4.4.2. GOF in relation to the nucleus _____	107
4.5.4.4.3. CT 13 in relation to the nucleus _____	107
5. Discussion: Establishment of CT pattern during early preimplantation development and potential influences related to nuclei shape and cell cycle stage _____	109
5.1. Symmetry of sister cells _____	109
5.2. Radial CT distribution in somatic cells _____	110
5.2.1. Influence of the cell cycle _____	110
5.2.2. Implications of evaluation methods _____	112
5.2.3. Positions in xy- and z-dimension _____	114
5.2.4. Changes in shape: “blown up” fibroblasts _____	115
5.2.5. Invaginations of the nuclear lamina _____	116

5.2.6.	Comparison between different species _____	117
5.3.	Early bovine embryos _____	118
5.3.1.	Gene-density correlated distribution pattern of CTs in adult bovine cells _____	118
5.3.2.	FISH on 3D preserved early bovine embryos _____	119
5.3.3.	Distribution of gene-rich and gene-poor CTs in nuclei of early bovine embryos _____	120
5.3.4.	Localization of a developmentally regulated Oct4-GFP transgene _____	124
5.3.5.	Remodeling of the Oct4-GFP transgene during nuclear transfer _____	126
5.3.6.	Remodeling during early differentiation events _____	130
5.3.7.	Future perspectives/outlook _____	131
6.	<i>References:</i> _____	133
7.	<i>Appendix</i> _____	143
7.1.	Tables of results and statistics _____	143
7.1.1.	Distribution of CTs 18 & 19 in human fibroblasts during cell cycle _____	143
7.1.2.	Distribution of gene poor and gene rich chromosomes in artificially shaped fibroblasts from different species _____	147
7.1.3.	Distribution of gene rich and gene poor chromosomes in bovine preimplantation embryos _____	150
7.1.4.	Distribution of the transgene GOF and its harboring CT during nuclear transfer and early development _____	154
7.2.	Material and technical equipment _____	158
7.2.1.	Chemicals, enzymes and reagents _____	158
7.2.2.	Media, buffers and solutions _____	161
7.2.3.	Equipment and instrumentation _____	162
7.3.	Manuscript: Similarity of chromosome arrangement is lost after two cell cycles in HeLa and normal diploid cells _____	166
8.	<i>Abbreviations</i> _____	191
9.	<i>Table of figures</i> _____	192
10.	<i>Publications</i> _____	193
10.1.	Publications: _____	193
10.2.	Posters/Oral Presentations: _____	194
11.	<i>Curriculum Vitae</i> _____	196
12.	<i>Acknowledgement</i> _____	197

1. Summary

1.1. Abstract

In mammalian cell nuclei chromosome territories (CTs) occupy positions correlating with their gene-density and chromosome size. While this global radial order has been well documented, the question of whether a global neighborhood order is also maintained has remained a controversial matter. To answer this question I grew clones (of HeLa, HMEC and human diploid fibroblast cells) for up to 5 divisions (32 cells) and performed 3D FISH experiments to visualize the nuclear positions of 3 different CT pairs. Using different landmark-based registration approaches I assessed the similarity of CT arrangements in daughter cells and cousins. As expected from a symmetrical chromatid movement during mitotic anaphase and telophase, I was able to confirm previous findings of a pronounced similarity of CT arrangements between daughter cells. However, already after two cell cycles the neighborhood order in cousins was nearly completely lost. This loss indicates that a global neighborhood order is not maintained.

Further, I could show in the present thesis that a gene density correlated distribution of CTs, which has already been shown in different cell types of various species appears to be independent of the cell cycle. Moreover I could provide evidence that the nuclear shape plays a major role in defining the extent of this gene-density correlated distribution, as nuclei of human, old world monkey and bovine fibroblasts showed an increased difference in the radial distribution of gene poor/dense CTs when their nuclei were artificially reshaped from a flat ellipsoid to a nearly spherical nucleus.

The observation that a gene-density correlated distribution of CTs has been found in nuclei from birds to humans argues for a significant, yet undiscovered functional impact. So far CTs have been investigated mainly in cultured cells and to some extent in tissues, yet little is known about the origin and fate of CTs during early development. To gain insights into the very early organization of CTs in preimplantation embryos I have developed a fluorescence in situ hybridization (FISH) protocol, which enables the visualization of CTs in three dimensionally preserved embryos. Using this protocol I have investigated CTs of bovine chromosomes 19 and 20, representing the most gene-rich and gene-poor chromosomes, respectively. Equivalent to the distributions described in other species I could confirm a gene density related spatial CT arrangement in bovine fibroblasts and lymphocytes with CT 19 being localized more internally and CT 20

more peripherally. Importantly, I did not find a gene density related distribution of CTs 19 and 20 in early embryos up to the 8-cell stage. Only in embryos with more than 8 cells a significant difference in the distribution of both chromosomes became apparent that increased upon progression to the blastocyst stage. Since major genome activation in bovine embryos occurs during the 8- to 16-cell stage, my findings suggest an interrelation between higher order chromatin arrangements and transcriptional activation of the embryonic genome.

Using another experimental set up I analyzed the topology of a developmentally regulated transgene utilizing bovine nuclear transfer (NT) embryos derived from fetal fibroblasts, which harbored a mouse Oct4/GFP reporter construct integrated at a single insertion site on bovine chromosome 13. I analyzed the intranuclear distribution of the transgene as well as its position in relation to its harboring chromosome in donor cell nuclei and day 2 NT embryos, where the transgene is still inactive as well as in day 4 NT embryos, where transgene expression starts, and day 7 NT embryos, where expression is highly increased. Compared to donor cell nuclei I found a more peripheral location of both BTA 13 CTs and the Oct4/GFP transgene in day 2, day 4 and day 7 NT embryos, although there was a trend of the transgene and both BTA 13 CTs to re-localize towards the nuclear interior from d2 to d7 embryos. Moreover, I found the transgene located at the surface of its harboring CT 13 in donor fibroblasts, whereas during preimplantation development of NT embryos it became increasingly internalized into the chromosome 13 territory, reaching a maximum in d7 NT embryos, i.e. at the developmental stage when its transcription levels are highest. These latter experiments show that the transfer of a somatic nucleus into a chromosome depleted oocyte triggers a large scale positional change of CTs 13 and of an Oct4/GFP transgene and indicate a redistribution of this developmentally regulated Oct4/GFP transgene during activation and upregulation in developing NT embryos.

1.2. Zusammenfassung

In den Zellkernen aller bisher untersuchten Säugetiere findet man die Anordnung der Chromosomenterritorien (CTs) korreliert mit der Gendichte und Größe der einzelnen Chromosomen. Nachbarschaftsanordnungen der einzelnen CTs jedoch werden sehr kontrovers diskutiert. Um diesbezüglich neue Erkenntnisse zu gewinnen habe ich verschiedene humane Zelllinien als Klone einzelner Zellen bis hin zum 32-Zellstadium (5 Teilungen) wachsen lassen und auf diesen FISH Experimente mit Sonden für 3 verschiedenen CTs durchgeführt. Mittels Auswertungen, die auf einer Landmark-basierten Registrierung einzelner CTs beruht, wurde die Ähnlichkeit der CT Anordnungen in den verschiedenen Kernen von Töchtern und Kusinen gemessen. Da sich, wie angenommen, die Chromatiden in der Anaphase symmetrisch auseinander bewegen, findet sich in den Tochterkernen nach der Mitose eine sehr symmetrische Anordnung der CTs, die aber bereits in den Kusinen ersten Grades verschwunden ist, was gegen eine generelle Vererbung der Nachbarschaftsanordnungen spricht.

Darüberhinaus konnte ich in der vorliegenden Arbeit zeigen, dass die von der Gendichte abhängige Verteilung der CTs in verschiedenen Spezies jeweils Zellzyklus unabhängig ist. Des Weiteren konnte ich zeigen, dass die Form der Kerne eine entscheidende Rolle spielt für die jeweilige Ausprägung der CT Verteilungen. In Fibroblasten Zellkernen verschiedener Spezies (Mensch, Meerkatze/Primat, Rind), die artifiziell von ihrer ursprünglich flachen in eine eher kugelige Form gebracht wurden zeigte sich bei zunehmender Kugelform ein größerer Unterschied zwischen den Verteilungen von genreichen und genarmen CTs.

Eine gendichte abhängige Verteilung von CTs wurde in Zellkernen verschiedenster Spezies gefunden, von Vögeln bis hin zum Menschen, was für ihre Bedeutung spricht, wenngleich der funktionelle Zusammenhang bisher nicht aufgedeckt werden konnte. Bisher lag der Fokus der Untersuchungen vor allem auf Kernen die aus Zellkulturen oder von Gewebeschnitten stammten. Weitaus weniger ist bekannt über die Entstehung von CTs während der frühen Entwicklung. Mich interessierte die Fragestellung der CT Etablierung während der frühen Embryonalentwicklung. Dafür habe ich zunächst das für Zellen gut etablierte Protokoll für „Fluoreszenz in situ Hybridisierung“ (FISH) so modifiziert, dass damit die Visualisierung von CTs in Embryonen möglich war, wobei zeitgleich deren 3D Morphologie erhalten blieb. Mit Hilfe dieses Protokolls habe ich die Rinderchromosomen (BTA, *Bos taurus*) 19 und 20, welche das genreichste bzw. genärmste Chromosom darstellen, in frühen in

in vitro fertilisierten (IVF) Embryonen untersucht. Zunächst konnte ich in Kernen von Fibroblasten und Lymphozyten von Rindern eine gendichte abhängige CT Verteilung bestätigen wie sie bereits für entsprechende Kerne anderer Spezies bekannt ist. Dabei ist das genreiche BTA 19 zur Kernmitte hin und das genarme BTA 20 zur Kernperipherie hin orientiert. Interessanterweise fand sich diese gendichte abhängige Verteilung nicht in den Kernen früher IVF Embryonen. Erst in Embryonen mit mehr als 8 Zellen wurde eine signifikante gendichte abhängige Verteilung sichtbar, die zum Blastozystenstadium hin noch deutlicher wurde. Da zwischen dem 8- und 16-Zellstadium die Hauptgenomaktivierung in Rinderembryonen stattfindet, lässt diese Beobachtung auf einen Zusammenhang zwischen CT Anordnung und Transkriptionsaktivierung schließen.

Mit Hilfe eines anderen Experimentansatzes habe ich die Anordnung eines entwicklungsgesteuerten Transgens in Rinderembryonen, die durch Kerntransfer gezeugt wurden, untersucht. Die dabei verwendeten Donorzellen enthielten ein murines Oct4-GFP Reporterkonstrukt das stabil an einem einzigen Locus auf Chromosom 13 integriert ist. In diesen Kernen habe ich die Anordnung des Transgens hinsichtlich der Lage im Kern und in Bezug auf seine Lage innerhalb des CTs analysiert. Zuerst in Donorzellen und Tag 2 Embryonen, in denen das Transgen inaktiv ist, dann in Tag 4 Embryos, in welchen das Transgen aktiviert wird und zuletzt in Tag 7 Embryos bei denen die Transkription des Transgens sehr hoch ist. Im Vergleich zu den Donorkernen war die Lokalisation von BTA 13 und Oct4-GFP in allen embryonalen Stadien deutlich peripherer, wenn gleich es einen Trend mit zunehmender embryonaler Entwicklung zur Re-lokalisierung von beiden zur Zellkern Mitte hin gibt. Darüber hinaus fand sich das Transgen in den Donorzellen an der Oberfläche des CTs, wohingegen es sich in den Embryonen mit zunehmender Entwicklung mehr und mehr innerhalb des CTs befand. Bemerkenswerterweise befand es sich in Tag 7 Embryos, in denen die Expression am höchsten ist, am weitesten innen. Diese Experimente zeigen deutlich, dass durch oder nach dem Transfer eines somatischen Zellkerns in eine Eizelle eine wesentliche Umpositionierung der untersuchten CTs und des Transgens stattfinden, welche vermutlich mit der Aktivierung von Entwicklungs- und anderen Genen, die für die frühe Embryonalentwicklung nötig sind, in Zusammenhang steht.

2. Introduction: Positions of chromosome territories (CTs) and sub-domains in the cell nucleus

2.1. Goals of the study

At present there are many publications about the preferred localization of CTs in a nucleus. Depending on the investigated species and cell types there is still an ongoing controversial discussion on how CTs are arranged in the nuclear space. Are CTs arranged in fixed neighborhood positions or is their spatial positioning random? Are there certain rules, like specific radial arrangements or relative positions to other compartments causing specific CT arrangements? How are these positions inherited? I used several approaches to address this topic.

In the first part I investigated whether CTs were inherited in fixed neighborhood patterns. Are CT arrangements in a mother nucleus similar to those in the daughter cells found after cell division? Therefore the clonal growth of different cell types was used for the analysis of a subset of chromosomes and their relative location towards each other over several cell cycles.

The detailed cell cycle dependent location of several chromosomes was investigated in the second part. All chosen chromosomes are representative for certain features such as chromosome size or gene density. These investigations should uncover controversial data published by several other groups concerning a different CT distribution during cell cycle stage.

Since the shape of nuclei seems to have a major influence on the general distribution of CTs, in the third part, the shape of nuclei was artificially altered to investigate the influence in one specific cell type.

In the fourth and last part we started to work, in collaboration with V. Zakhartchenko and E. Wolf from the Gencenter, Munich, on the 3D organization of CTs and chromosomal subdomains in bovine preimplantation embryos. To do that it was necessary to establish a FISH protocol on 3D preserved embryos. With this tool in our hands we started to investigate several questions concerning early embryo development. The radial distribution of gene-poor and gene-rich chromosomes was investigated previously in many different species and cell types. Using the bovine model we investigated if such a distribution pattern would be present from the very beginning of fertilization or if it was established later during development. This work was done utilizing in-vitro fertilized (IVF) embryos. Using in-vivo embryos would be

more precise because they would describe the ultimate native developmental stages but their generation is much more complex and complicate.

Another question was addressed using nuclear transfer (NT) embryos generated by using a transgenic fibroblast cell line. The transgene itself contains the sequence for an enhanced green fluorescent protein (EGFP), a promoter for the murine Oct4 and parts of the structural non-transcribed murine Oct4 gene. The transgene is expressed under control of the murine promoter which was shown to be active after the fourth cell cycle in embryos (Wuensch et al. 2007). The transgene and its harboring CT were identified with FISH technique in the donor cell line as well as in embryos of different developmental stages. Afterwards measurements concerning its location were performed. All measurements were done in relation to the nuclear border and respective to its harboring CT. Embryos were chosen from stages before and after major genome activation, representing the transgene in an active or inactive state.

In the following the main features of nuclear architecture are described. In Material & Methods (M&M) chapter all used techniques are described in detail, especially the protocol for FISH on embryos, which is described in the present work for the first time.

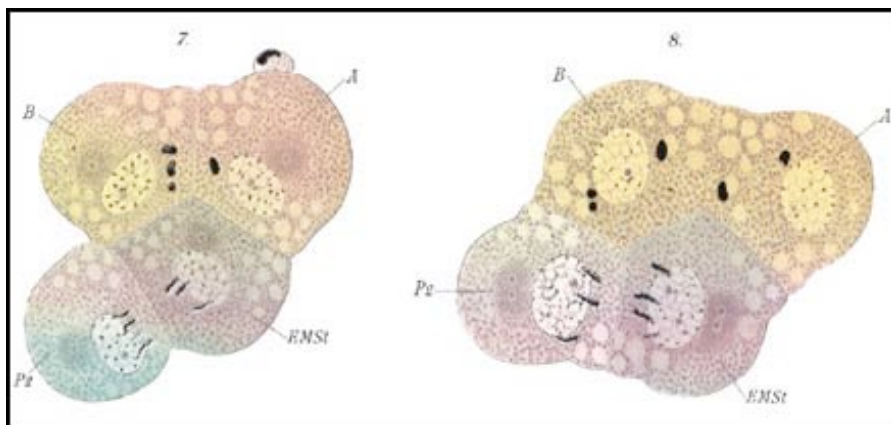


Fig. 1) Historical drawing by Theodor Boveri (1862-1915) depicting early development and chromosome diminution in *Ascaris megalocephala*, 1899; a four cell stage is shown with clearly discernible chromosomes; note that sister cells show a symmetrical order; for review see (Satzinger 2008);

2.2. Organization in a cell nucleus

All chromatin, the complex of DNA, histone and additionally associated non-histone proteins is highly organized in the cell nucleus a view that has emerged only the last decades (Cremer et al. 2006). While it is known since a long time that chromosomes exist in a well defined structure in mitosis and meiosis it was discovered only in the 80s of the 20th century that chromosomes remain in the interphase nucleus as chromosome territories (CTs) (reviewed by (Meaburn and Misteli 2007) and (Cremer and Cremer 2001)). Investigations trying to highlight any three dimensional order of CTs discovered several levels of topological organization varying in different types of cells and tissues (Cremer et al. 2006) (Lanctot et al. 2007).

2.2.1. Discovery of CTs

The human genome is organized in 23 chromosomes each in two homologues and each with different parental origin. The term “chromosome” refers to the Greek words “chroma” for color and “soma” for body – stainable bodies. Heinrich Wilhelm Waldeyer was first introducing the term “chromosome”. Chromatin was stained effectively with basophilic aniline dyes. One of the first publications describing “chromosomes” in plant mitotic events was by Wilhelm Hofmeister in 1848 already. During mitosis the chromosomes condense and are visible light microscopically as single X-shaped entities. During interphase the chromosomes are less densely packed but still occupy a distinct area in the nucleus. This was matter of debate for many years until the early 1980s, first of all because it was not clear if chromosomes possibly form de novo during mitosis and dissolve completely during interphase and secondly since it was not clear if interphase chromosomes would completely intermingle like “spaghetti in a bowl” (Cremer et al. 1993).

Carl Rabl was the first who supposed in 1885 the idea of a territorial organization of chromosomes existing throughout the whole cell cycle (Rabl 1885). Theodor Boveri, in 1909, formulated the hypothesis of chromosome individuality, where he postulated that each chromosome territory would occupy a certain part of the nucleus without losing its coherence and without mixing with the other territories (Boveri 1909; Cremer 1985). He also mentioned in his

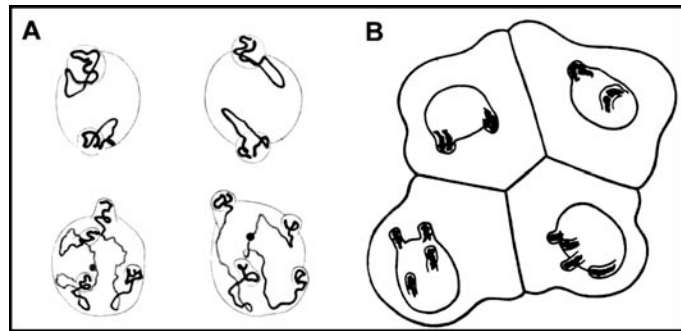


Fig. 2) Chromosome arrangements in blastomere nuclei of *P. equorum* ($2n = 2$) drawn by Theodor Boveri: (A) The two nuclei above and below each represent a pair of daughter nuclei from blastomeres studied at prophase of the two-cell stage. Chromosome ends are fixed within invaginations of the nuclear envelope. Note that chromosome arrangements and the positions of the invaginations are similar in each pair, whereas different pairs show striking differences. (B) Interphase blastomere cells from an embryo drawn at the four-cell stage. Chromosome arrangements within the nucleus are invisible, except for nuclear invaginations that indicate telomere positions. Each pair of daughter nuclei shows symmetrical positions of the invaginations, whereas a comparison of the two pairs reveals gross differences. Taken from (Walter et al. 2003);

theory that daughter cells are symmetrical in their CT arrangement (see Fig. 1 and 2) depending on the alignment of chromosomes during the metaphase plate (Boveri 1909).

However, these theories were neglected for a long time. The idea of a territorial organization of chromosomes during interphase was abolished due to the results of electron microscopical work in the 1960s and 1970s (Wischnitzer 1973). Instead it became popular to favor a “spaghetti”-like model, where chromosomes strongly decondense and intermingle in a cell nucleus.

Thomas Cremer et al., in the 1980s, showed by using a laser beam experiments that interphase chromosomes occupy discrete volumes in the nucleus (Cremer et al. 1980; Cremer et al. 1982; Cremer et al. 1982). With a microlaser beam local genome damage was induced within a small volume of the nucleus and metaphase spreads of those nuclei revealed that only a few chromosomes were concerned by this damage (Zorn et al. 1979). With the development of in-situ hybridization (ISH) and fluorescent in-situ hybridization (FISH) chromosomes were stainable as a whole and easily detectable at microscopes. These opportunities improved the possibilities for examination of chromosomal arrangements in cell nuclei (Manuelidis 1985; Schardin et al. 1985). The existence of CTs was proven rapidly for many cell types and also for tumor cells (Cremer et al. 1988; Lichter et al. 1988).

2.2.2. The **Chromosome-Territory-Interchromatin-Compartment (CT-IC)** model

The existence of a nuclear compartmentalization became clear during the late 1980s, when functional sub domains for associated e.g. with DNA replication, RNA processing, gene expression were described (Blobel 1985; Spector 1990; Haaf and Schmid 1991; Cremer et al. 1993). In 1993 the term interchromatin domain (ICD) was introduced (Zirbel et al. 1993). The ICD separates CTs and contains speckles and other nuclear bodies, like cajal or PML bodies (Spector 2001). This compartmentalization led to further models, like e.g. the chromosome-territory-interchromatin-compartment (CT-IC) model (Cremer et al. 1993; Cremer and Cremer 2001; Cremer et al. 2006). An overview of different models is given by T. Cremer (Cremer and Cremer 2001). A fundamental idea is that the network of the IC starts at the nuclear pore complexes (NPC), which are the gates for nuclear transport. In a recent study, using new high-resolution imaging techniques (three dimensional surface imaging microscopy, short 3D-SIM) developed by J.Sedat, it is shown that there are indeed chromatin free ICD channels emanating from the NPCs (Schermelleh et al. 2008). In the CT-IC model, the IC is described as the space between the CTs thereby expanding like a big network with lacunas throughout the nucleus. This interchromatin compartment provides space for non-chromatin domains, e.g. speckles, cajal-bodies and PML bodies (Cremer and Cremer 2001). Towards the interior branches of the IC expand between and into the CTs with bigger and smaller branches (Cremer and Cremer 2001). Transcription and splicing factors were found in the IC as well as other proteins like Rad51-foci (Cremer and Cremer 2001; Albiez et al. 2006). Our group recently confirmed the presence of a network-like IC by using hyperosmolar conditions which leads to a calcium dependent condensation of chromatin, and thus to an expanding of IC channels (Albiez et al. 2006). Lacunas became even more pronounced. This process was reversible and the channels kept their topography during multiple rounds of chromatin condensation/decondensation, arguing for a pre-existing network (Albiez et al. 2006).

Updated version of the CT-IC model (Albiez et al. 2006):

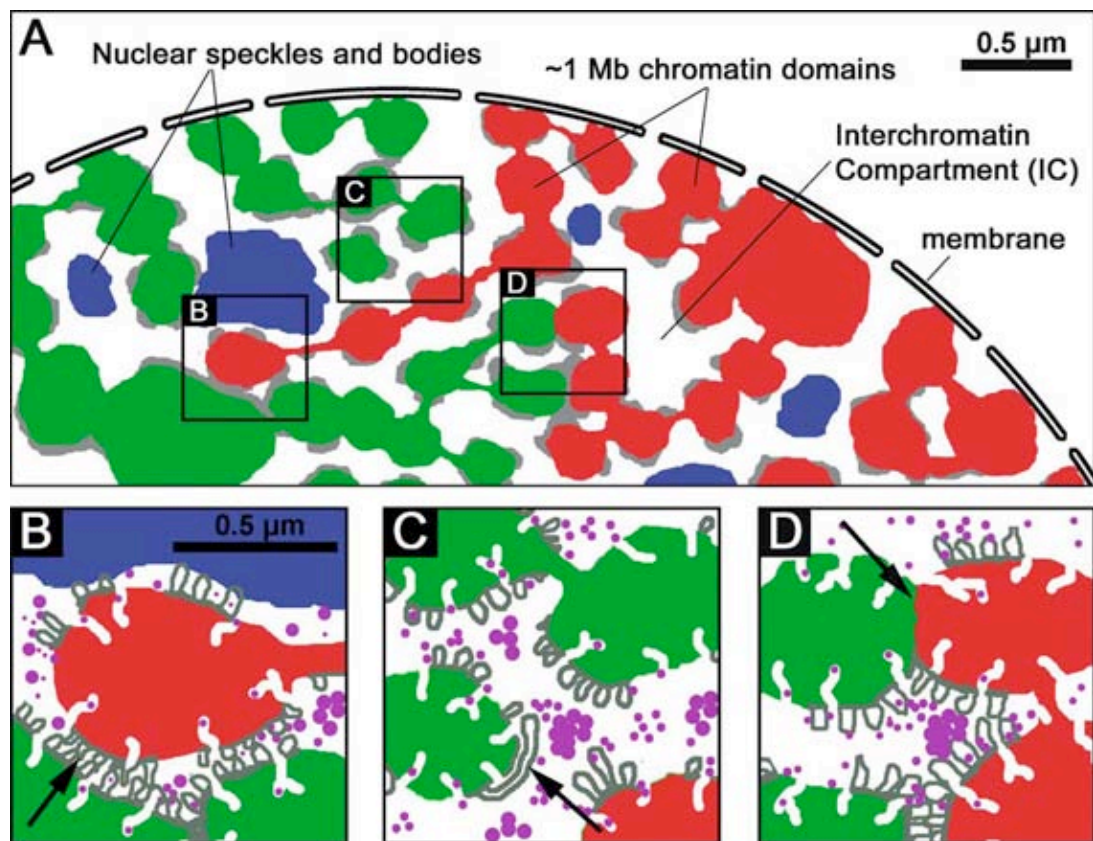


Fig. 3) Update of the chromosome territory-interchromatin compartment (CT-IC) model: A: Cartoon of a partial interphase nucleus with differentially colored higher-order chromatin domains (red and green) from neighboring CTs separated by the IC (white). This model postulates that the nucleus and each CT is built up from two structurally distinct compartments: a 3D network of chromatin domains with compaction levels much higher (10 times and more) than the compaction level of an extended 30 nm fiber (for details see text) and an integrated IC channel network with nuclear speckles and bodies (blue), which expands between these domains, independently of whether they belong to the same or different CTs. The width of the IC varies from the micrometer scale, e.g. IC lacunas containing large nuclear speckles, to nanometer scales (see B). Intrachromosomal, respectively interchromosomal, rearrangements can occur when double-strand breaks are induced in neighboring chromatin domains of the same respectively different CTs. Opportunities for rearrangements are increased, when constrained Brownian movements of neighboring chromatin domains result in a transient decrease of the width of small IC channels. The perichromatin region (gray) is located at the periphery of chromatin domains and forms a functionally important border zone (100-200 nm) with certain genes or segments thereof poised for, or in the process of, transcription. Although the CT-IC model postulates that permanently silenced genes are hidden in the interior of compact chromatin domains, the possibility that most or all genes are located at chromatin domain borders has not been excluded. BYD: Enlargements of nuclear sites indicated in A show ~1 Mb chromatin domains (red and green) and the interchromatin space (white) with nuclear speckles, bodies (blue), as well as preformed modules of the transcription and splicing machineries (pink). Diffusion of individual proteins into the interior of compact chromatin domains is likely not prevented. Several ~1 Mb chromatin domains may form still larger domains seen in EM images as chromatin clumps. The finest branches of the IC with a width ≈ 100 nm may penetrate into the interior of ~1 Mb chromatin domains and end between ~100 kb loop domains (not shown). B: The red ~1 Mb chromatin domain denotes the end of a higher-order chromatin protrusion, which expands from the respective red CT into the interior of the green CT (compare A). We assume that the expansion of these higher-order protrusions is guided by the IC. Locally decondensed chromatin loops contribute to the perichromatin region (gray). Note that the narrow IC channel allows for direct contact of loops from neighboring ~1 Mb chromatin domains (arrow). C: This enlargement shows somewhat wider IC channels compared to B. Note one larger decondensed loop (arrow) expanding along the perichromatin region. D: Direct contact between chromatin domains from neighboring CTs (arrow). The possible extent of intermingling of chromatin fibers at such connections is not known.

2.2.2.1. Intermingling and loops

In the CT-IC model chromatin is organized in ~1Mb domains (Note that the DNA content can range from a few hundred kb to several Mb (Jackson and Pombo 1998)) whereas the internal structure remains to be elucidated. The IC domain is believed to expand between and also partially into the interior of those ~1Mb domains. The perichromatin region is located at the periphery of chromatin domains and was described as the functional important zone of active transcription (see fig.3) (Albiez et al. 2006). Genes at the surface of ~1Mb domains are exposed towards the IC compartment. At these sites, interactions with nuclear bodies as well as with other components of the transcription and splicing machinery are possible (Albiez et al. 2006). Importantly no intermingling of CTs is described in this model in contrast to the suggestions of A. Pombo and their interchromosomal network (ICN) model (Branco and Pombo 2006). These authors suggest a border zone of neighboring CTs where chromatin would extensively intermingle (Foster and Bridger 2005; Branco and Pombo 2006). Chromatin loops in the CT-IC model are only possible in coordinated structures meaning the DNA structure of at least a 30nm fiber is kept and no decondensed DNA fibers occur. This prediction is not consistent with the results published by the group of W. Bickmore (Chubb and Bickmore 2003). They found loops expanding from the CTs positioning activated genes up to 1-2 μ m remote of their CT (Mahy et al. 2002). Cremer and co-workers however, found more condensed fingerlike protrusions from the CTs, which was shown by FISH experiments that stain the entire genomic region and not only a single gene somewhere on the loop (Albiez et al. 2006; Kupper et al. 2007). Even if it could not be excluded that small fractions of chromatin may exist in a 10 or 30nm fibers the majority of DNA, including loops, was compacted above the level of a 30nm fiber (Albiez et al. 2006). Investigations of a 2Mb gene-dense and highly active region on 11p15.5 showed a loop out from the CT (Kupper et al. 2007). FISH experiments with BAC probes of the major histocompatibility complex (MHC) locus on 6p21.3, which is one of the most gene-dense regions in the human genome showed looping out, if cells were induced with IFN- γ (Volpi et al. 2000). Chromatin became decondensed after IFN- γ treatment. This remodeling event is very fast (less than 10minutes) and was shown to precede expression, which started after several hours (Christova et al. 2007). The loops themselves were shown to form distinct structures, which were mediated by certain DNA anchoring sequences. These structures were believed to be crucial regulators for gene expression because they are responsible for the accessibility of DNA (Ottaviani et al. 2008).

2.2.2.2. Computer-based models

For the modelling of 3D organization of chromatin in the cell nucleus several computer-based models have been proposed, e.g. the spherical ~1Mb domain (SCD) model, which is a modified version of the multi-loop subcompartment (MLS) model (Cremer and Cremer 2001). The MLS model suggests that ~1Mb domains are built like rosettes with a series of ~100kb loops linked at a loop base spring (Munkel et al. 1999). The SCD model further made no assumption about the internal loop structure but this model supports the idea of the CT-IC model (Kreth et al. 2001). The 1Mb domains with a diameter of approximately 500nm are linked with each other, forming chains of chromatin and leaving free space in between (see fig.3).

The first quantitative model was presented by Sachs et al.: the random-walk/giant-loop (RW/GL) model (Sachs et al. 1995). Chromatin loops with a size of several Mb are backfolded to an underlying structure, but otherwise each giant loop is folded randomly. In a more recent work whole human lymphocyte cells were simulated. It was shown that using an initial probabilistic distribution fits best to experimental observations (Kreth et al. 2004). Again a spherical 1Mb chromatin domain model was used, combined with the latest data on chromosome length and density (Kreth et al. 2004). This model supports the concept of a probabilistic global gene positioning code depending on CT sequence length and gene density.

2.2.3. Different compartments within a nucleus

Every gene has its own promoter and enhancer/silencer regions. While promoter regions are mostly located closely to the coding region, enhancer/silencer regions can be located far away from the coding sequence. To explain the regulatory mechanism it was assumed that the promoter comes close to the coding region by folding back the chromatin fiber in an appropriate way thereby establishing functional expression site. The spatial positioning of genes within functional compartments was important for the expression and silencing of genes. There is increasing evidence that gene activation or silencing is often associated with a repositioning of the gene relative to nuclear compartments (Lanctot et al. 2007; Mateos-Langerak et al. 2007). In the following a brief overview of the state of the art is given concerning the interplay between nuclear architecture and the regulation of gene expression. First some basic knowledge about the chromatin structure and the general organization of chromatin in a cell nucleus is described, leading from a linear DNA sequence to a topological 3D model where a regulated transcription takes place.

2.2.3.1. Chromatin structure

The 2m length of diploid human DNA has to be arranged in a human cell nucleus with an average size of 10 to 20 μm . To understand how the genome is functionally organized one has to look first at the compaction of chromatin. For transcription a local accessibility of DNA for regulatory proteins is needed.

The first level of DNA packaging is the nucleosome. Each nucleosome consists of a histone octamer containing two proteins of each histone H2A, H2B, H3 and H4. The DNA double helix is wrapped around the nucleosomes by a length of 146bps. This structure of nucleosomes is widely known as the “beads on a string” confirmation (11nm in diameter) and was discovered by electron microscopy in 1974 (Olins and Olins 1974). The nucleosomes can be packed more densely by the so called linker histone protein H1. In that way the next level of compaction – the 30nm fiber – is reached. There are at least two models proposed for this fiber: a solenoid and a zigzag fiber (Tremethick 2007). In any case a compaction of 6-fold in comparison to the “beads on a string” confirmation is achieved. Everything between the 30nm fiber and the mitotic chromosome where the highest degree of compaction is reached (250-fold in comparison to interphase chromatin) remains still elusive. According to the two main models the 30nm fiber is organized in loops along the chromosome (Paulson and Laemmli 1977; Gasser and Laemmli 1986) or in a helical folding (Sedat and Manuelidis 1978).

2.2.3.2. Euchromatin and Heterochromatin

Histones have an influence on the chromatin package density and therefore on the accessibility of DNA for regulatory proteins which is important for the regulation of gene expression (Allis, Jenuwein, 2007). For a long time it was thought that transcription takes place on naked DNA and histones were generally suppressor proteins. However there was evidence that large regions of open DNA did not exist in eukaryotic cells (Clark and Felsenfeld 1971). Only with the discovery of nucleosomes as the fundamental chromatin subunit by Kornberg and Thomas in 1974 (Kornberg 1974), it became clear in subsequent experiments that histone tail modifications play an important role for the condensation state of chromatin and also for accessibility of DNA for regulatory proteins (Richmond et al. 1984; Luger et al. 1997). During the early 1980s it was shown in yeast that histone amino-terminal tails were essential for the up-regulation of genes as well as the establishment of silent chromatin domains (Wallis et al. 1980; Durrin et al. 1991). Acetyl was the first small chemical group which was shown to play a decisive role in gene regulation (Brownell et al. 1996). Other histone modifications like methylation and

phosphorylation were discovered soon and also the corresponding enzymes for these conversions were found. These findings played an important role in establishing the concept of epigenetics. The last decade brought a flood of publications dealing with the many faces of histone modifications and the role of eu- and heterochromatin in gene expression. For deeper insight comprehensive reviews (Jenuwein and Allis 2001; Bernstein and Allis 2005; Goldberg et al. 2007; Hake et al. 2007; Wang et al. 2007) and textbooks are available (Chromatin, Wolffe, 1997; Epigenetics, Allis, Jenuwein, 2007). 80 years ago, a classification into euchromatin and heterochromatin was formulated by Heitz (Heitz, 1928). Heterochromatin was the fraction of chromatin, which stays highly condensed as in mitosis throughout interphase while euchromatin gets decondensed. In the last decades a somewhat more detailed view emerged discriminating three main chromatin subtypes: euchromatin, facultative and constitutive heterochromatin. There were several typical properties of modified DNA and histones belonging to euchromatin or heterochromatin. The most important are listed in the following (Table 1):

	Euchromatin	Facultative Heterochromatin	Constitutive Heterochromatin
Character	dynamic	dynamic	stable
State	dispersed	condensed	highly condensed
Nucleosome array	irregular	regular	regular
Nuclease sensitive sites (HS)	+	-	-
Replication timing	early	mid	late
Banding pattern	R	G	C (subset of G)
Base content in humans ¹⁾	GC-rich	relatively AT-rich	mostly AT-rich
Genes	gene dense house keeping genes tissue specific genes	gene poor tissue specific genes inactive X chromosome	almost devoid of genes
Characteristic sequence	single copy short interspersed elements (SINES)	long interspersed elements (LINES)	repetitive sequences (satellite DNA) transposable elements
CpG islands	frequent	rare	absent
Excerpt of epigenetic marks ²⁾	H3/4 hyperacetylation H3K4me2/3 methylation H3K36 methylation R-methylation hypomethylated DNA	H3K27me3	H3/4 hypoacetylation H3K9me3 H4K20me3 methylated DNA RNAi

- 1) The base content is species specific, e.g. in cattle constitutive heterochromatin consists of GC-rich sequences;
- 2) All histone lysine methylations are named according to the Brno nomenclature (Turner 2005)

2.2.3.3. Nuclear lamina

The nuclear interior is separated from the cytoplasm by the nuclear envelope (NE). The NE consists of an inner nuclear membrane (INM), an outer nuclear membrane (ONM), the nuclear pore complexes (NPCs) and the lamina. The latter consists of a meshwork of proteins, mainly intermediate filaments (IF), like lamin A/C and lamin B, which are attached to the INM with lamin binding proteins, e.g. integrins. The lamina is an anchor site for chromatin thereby playing a major role in chromatin organization. But lamins do not only have structural function. They are important for several functions like DNA replication, transcription and DNA repair (reviewed in (Dechat et al. 2008)). There are different types of lamin, classified according to their sequence homologies, into A- and B-type lamins. In mammals there are two major A-type lamins – lamin A and C and two major B-type lamins – lamin B1 and B2. In germ cells additionally Lamin C2 is found (Furukawa et al. 1994). During differentiation different lamins are expressed. While B-type lamins are found in every cell type, lamin A/C is only found in correlation with differentiation, starting with the trophoblast formation, e.g. in mice lamin A/C is detectable on embryonic day 9 (Stewart and Burke 1987). Interestingly an influence on nuclei stability was reported: In undifferentiated human ES cells, where lamin A/C was missing, nuclei were highly deformable (Pajerowski et al. 2007).

The importance of lamins and their function is emphasized by the existence of several severe diseases, so called laminopathies that are caused by lamin mutations. Most of them are muscular dystrophies, like e.g. Emery-Dreifuss muscular dystrophy or progeroid syndromes, like e.g. Hutchinson-Gilford progeria syndrome (HGPS) or Werner's syndrome (WS). HGPS could be caused by at least 18 different LMNA mutations and causes a severe premature aging disease (reviewed in (Dechat et al. 2008)). The heterochromatic regions are enriched along the nuclear lamina and known to be involved in gene regulation (Lanctot et al. 2007). There exists a physical link between the heterochromatic protein HP1 β (which is an abundant component of heterochromatin) and the lamin B receptor (Ye and Worman 1996; Ye et al. 1997), which suggests a link between those two compartments.

Studies on the radial distribution of human CTs revealed a different localization of human chromosome 18, which is usually found at the nuclear border in wild type cells but which was localized in the nuclear interior in cells from laminopathy patients (Malhas et al. 2007; Meaburn et al. 2007). Histone marks, like H3K9me3, H3K27me3 or H4K20me3 were found to be different in patient fibroblast cells (Scaffidi and Misteli 2005; Shumaker et al. 2006). For example an increase in H4K20me3 might be related to telomere shortening observed in HGPS (Shumaker et al. 2006). Little is known yet about the detailed mechanisms of chromatin organization and lamins. But there is evidence that a close connection in organization and function is present (Shumaker et al. 2006). Lamins act as a dynamic molecular scaffold for chromatin and chromatin interacting or modifying proteins throughout the nucleus (Goldman et al. 2002; Gruenbaum et al. 2003). This scaffold may vary from cell type to cell type, dependent on the expression levels of the various lamin isoforms. In this way it may contribute to the determination of the specific functions of the respective cell (Dechat et al. 2008).

2.2.3.4. Nucleolus, Speckles and other nuclear bodies

Nucleoli, the places of rRNA synthesis, can vary in number and size between species and cell types. Despite the localization of acrocentric NOR-bearing chromosomes around the nucleolus, there was no fixed position of those CTs in relation to each other (Bolzer et al. 2005).

Speckles are believed to represent storage sites of splicing factors. They are located in the interchromatin domain and can possess a variable size and shape (Lamond and Spector 2003). Splicing factors can be recruited from the speckles to the transcription sites (Misteli et al. 1997).

There are several more nuclear bodies known, i.e. promyelotic leukaemia (PML) bodies or cajal bodies, all with distinct functions in transcription, replication or DNA repair (for detailed review (Spector 2001)).

2.2.4. Distribution pattern of CTs: radial distribution and neighborhoods

Since the discovery that chromosomes occupy distinct territories which persist throughout the interphase, it was questioned if those CTs are arranged in a fixed order in the nucleus. Are there fixed neighborhood patterns? How are homologues distributed in the nucleus? Do all nuclei show the same pattern? Is there a difference between various tissues? Several scenarios seemed to be possible and were subject of investigations. In the following chapters several studies addressing these questions are summarized.

2.2.4.1. Prometaphase rosettes

In the 1990s, there were several publications which argued in favor of a fixed neighborhood arrangement (Nagele et al. 1995; Nagele et al. 1998; Nagele et al. 1999; Nagele et al. 2001) and even a separation of the parental genomes in metaphase rosettes, the ring-like formation of chromosomes around the bundle of central microtubules of the mitotic spindle, was described (Nagele et al. 1995). In the work of Nagele et al. the angles between homologues were measured to get information about the spatial arrangement of CTs. In prometaphase rosettes all angles between 144° and 166° were found, which did not favor the idea of a random distribution where all angles should have been detected. All homologue chromosomes apparently had their homologues counterpart in an opposite position in the metaphase plate (Nagele et al. 1995). However, several other groups could not confirm these findings and supported a rather random arrangement in rosettes (Allison and Nestor 1999; Bolzer et al. 2005). A study from the Cremer group e.g. investigated prometaphase-rosettes with 24-color FISH experiments to visualize all human chromosomes simultaneously and revealed all possible angles between homologues, which argued against a parental separation as well as a fixed neighborhood pattern (Bolzer et al. 2005).

2.2.4.2. Interphase nuclei

In interphase nuclei several CTs were described to be in close proximity to each other, i.e. CT 8 and CT 11 (Nagele et al. 1999). Further more a correlation between the location during metaphase plate and the position in the interphase nuclei was found (Koss 1998; Nagele et al. 1999), which favored the idea of symmetrical daughter cells as a result of mitosis (Nagele et al. 1999). As an explanation, the association between CTs and a nuclear matrix was proposed (Nagele et al. 2001). Concerning the radial distribution, it was suggested that the less condensed homologue is located in the center of a nucleus while the condensed one is found at the periphery (Koss 1998).

However many observations argued against a fixed CT arrangement and neighborhood pattern (Lesko et al. 1995; Sun and Yokota 1999; Cremer et al. 2001; Cornforth et al. 2002; Parada et al. 2002; Bolzer et al. 2005). Studies in lymphocytes with centromere probes for CTs 7, 11 and 17 revealed a random distribution of these CTs (Lesko et al. 1995). With centromere probes for CTs 4, 6, 10 and 17 a random distribution was found in human fibroblast cells (Sun and Yokota 1999). Extensive studies in human amniotic fluid cells and fibroblasts with whole chromosome paint probes for CTs 1-5, 17-20 and the two sex chromosomes

revealed no specific side-by-side arrangements (Cremer et al. 2001). As already described for prometaphase stages a study from the Cremer group visualizing all individual chromosomes failed to detect a fixed neighborhood arrangements or CT pattern in human fibroblasts (Bolzer et al. 2005) or lymphocytes (Cornforth et al. 2002).

2.2.4.3. Sperm heads

In sperm head nuclei of several species, fixed CT arrangements were found, for example for the species *Planaria* (a fresh- and saltwater flatworm that belongs to the phylum of platyhelminthes) (Joffe et al. 1998), rat sperm (Meyer-Ficca et al. 1998) as well as in sperms of platypus (*Ornithorhynchus anatinus*, a semi-aquatic mammal, endemic in Australia and Tasmania, belonging to monotremes, the only mammal that lays eggs) (Watson et al. 1996). In several mammals the position of the X-chromosome seemed to be located always in the position where the sperm enters the oocyte (Luetjens et al. 1999; Greaves et al. 2001). This can cause, e.g. after intracytoplasmic sperm injection (ICSI) a prolonged condensation of the X chromosome (Luetjens et al. 1999). Many other species were described that showed a random CT distribution or at least no statistically detectable pattern, i.e. for grasshopper, salamander or chicken (Solovei et al. 1998; Luetjens et al. 1999; Greaves et al. 2001), concluding that a specific arrangement might only be present in individual species. Another study even argues that the position of CTs in human sperm would be important for its fertility and might therefore be used to estimate sperm quality (Finch et al. 2008).

2.2.4.4. Tissues and cancer

Cells of different tissues have different functions, which could be also reflected in chromosome positioning (Parada et al. 2004). Distinct translocation events are typical for certain tissues and very often involved in cancer (Mitelman 2000; Meaburn et al. 2007). These translocations required a spatial proximity of involved CTs (Bickmore and Teague 2002; Cornforth et al. 2002; Parada and Misteli 2002). In several publications such proximity patterns have been observed in cancer cells as well as in the corresponding healthy tissue cells (Kozubek et al. 1997; Lukasova et al. 1997; Parada et al. 2002; Roix et al. 2003; Kim et al. 2004). One example is the famous t9;22 translocation, which results in the fusion of the two genes BCR and ABL, thereby causing chronic myeloid leukemia. In proximity studies of those two loci in haematopoietic cells, it was found that they were more often juxtaposed than expected by chance (Kozubek et al. 1997; Lukasova et al. 1997).

2.2.4.5. Gene-rich and gene-poor chromosomes

Besides all controversy concerning the existence of CT neighborhood pattern, there seems to be a consensus of a well defined radial distribution pattern (Croft et al. 1999; Bridger et al. 2000; Boyle et al. 2001; Cremer and Cremer 2001; Bickmore and Teague 2002; Cremer et al. 2006; Lanctot et al. 2007; Misteli 2007). The typical location of gene-poor chromosomes is towards the nuclear periphery while gene-dense chromosomes are positioned towards the nuclear interior (Boyle et al. 2001). Best known examples are gene-poor CTs 18 and gene-rich CTs 19 in human cells, located at the nuclear border and center, respectively (Croft et al. 1999; Cremer et al. 2001). These localizations are established early in the cell cycle and maintained thereafter (Croft et al. 1999). Differences are also found concerning the volume occupied by chromosomes 18 and 19 which both have a similar size of 76Mb and 64Mb, respectively. CTs 19 are less condensed than CTs 18 (Croft et al. 1999).

Gene-density dependent pattern were also valid for subdomains, such as chromosome arms or chromosome bands (Sadoni et al. 1999; Gilbert et al. 2004; Kupper et al. 2007). Accordingly G-bands, which consist of gene poor chromatin, were located towards the periphery. In contrast, the gene rich R-bands were located more to the nuclear interior (Sadoni et al. 1999; Kupper et al. 2007). FISH experiments with chromosome arm specific probes for CT 18 revealed both arms localized to the periphery. P- and q- arm of CTs 19 were located near the nuclear core (Croft et al. 1999). Detailed studies of genes or BAC probes, assigned to a either gene-rich or gene-poor environment, were found orientated in the same way (Kupper et al. 2007). Gene expression, GC content and replication timing were surprisingly not found to be determining factors for radial positioning (Kupper et al. 2007).

This distributional motif fits to the concept of a compartmentalized nucleus, where chromatin at the periphery of nuclei is largely silenced and enriched in heterochromatin. An explanation for this organization might be the better accessibility of centered chromosomes for transcription factors (Parada et al. 2004; Cremer et al. 2006). Peripheral regions are occupied by highly condensed heterochromatin, engaged with heterochromatin proteins for stabilization (Cheutin et al. 2003). Decondensed chromatin, rather found in the center of a nucleus is found to correlate with gene-density (Gilbert et al. 2004). Access to decondensed chromatin regions is provided constantly (Dillon and Festenstein 2002). Functional properties concerning nuclear organization are still matter of debate (reviewed in (Cremer et al. 2006; Lanctot et al. 2007; Misteli 2007)).

Cells that have exit the cell cycle showed differences in their CT distributions (Bridger et al. 2000; Bolzer et al. 2005). In quiescent fibroblasts CTs 18 often moved to the interior and the differences to CTs 19 were less pronounced. After re-entry into the cell cycle CTs 18 moved back to the periphery after a short time, suggesting a direct link of positioning in cycling and quiescent cells. However, in senescent cells there was no difference between gene-rich and gene-poor CTs (Bridger et al. 2000). These results could be confirmed only in parts by our group. Using cells either in S-phase or G0 revealed a small difference in the distribution of CT 18 and CT 19, but without statistical significance (Bolzer et al. 2005).

In several tumor cell lines, gene-poor CTs 18 were again found at the nuclear periphery while gene-rich CTs 19 were found interior, even though some cell lines showed chromosomal imbalances, indicating that a gene-density distribution of chromosomes is a very common feature of nuclear architecture (Cremer et al. 2003).

In flat cells like human fibroblasts a gene-size dependent pattern is found, coexisting with the described gene-density dependent pattern, with big chromosomes located at the periphery of the nucleus, while small ones are found more internal (Bolzer et al. 2005). This is in accordance with results originally reported by Sun et al. (Sun et al. 2000).

2.2.4.6. Differentiation and development

The spatial organization of CTs can change during differentiation and development. In studies investigating mouse T-cell differentiation a global reorganization of centromeres, chromosomes and gene loci was found (Kim et al. 2004). During differentiation, centromeres were repositioned from a preferentially internal position in undifferentiated cells to a more peripheral position in differentiated mouse T-cells (Kim et al. 2004). In differentiated human and murine lymphocytes centromeres were found in clusters at the nuclear periphery (Weierich et al. 2003). In different mouse cell types it was shown that a radial distribution of CTs was not only shape dependent but also cell type specific (Mayer et al. 2005). Embryonic stem cells (ES) cells and differentiated cells, i.e. macrophages or myotubes, showed significant differences in the distribution of certain CTs (Mayer et al. 2005). The radial distribution was depending on gene-density and gene-size (Mayer et al. 2005). The spatial organization of CTs and proximity patterns was reported to be important for gene regulation during hematopoiesis (Kosak et al. 2007). Co-regulated genes are significantly colinear, forming gene clusters along chromosomes during murine

hematopoiesis with active genes centered in the middle of the nucleus (Kosak et al. 2007).

Pericentric heterochromatin was shown to aggregate during mouse myogenic differentiation and forming large chromocenters. This effect could be mimicked by an ectopic expression of MeCP2, which was found in increased levels in chromocenters (Brero et al. 2005). This reorganization of pericentric heterochromatin was found in correlation with certain epigenetic modifications, which recruit certain proteins, such as MeCP2. Through these mechanisms a stabilization of the transcriptional repression, mediated through binding of HP1, was suggested (Agarwal et al. 2007).

During early development a reorganization and reprogramming of chromatin was shown. There were several studies investigating pericentric chromatin (as it is a very prominent nuclear subcompartment) and epigenetic marks in this context in early mouse fertilization and development (Probst et al. 2007). Characteristic changes in the organization of pericentric heterochromatin were found at the transition from 1- to 2-cell stage. A difference between maternal and paternal pericentric regions was found, with the maternal one showing marks for H3K9me3, H4K20me3 and HP1 β while the paternal one showed only HP1 β marking (Probst et al. 2007). The typical somatic chromocenter formation is established with the burst of embryonic genome transcription and completed at blastocyst stage, which reflects the earliest state of differentiation (Martin et al. 2006). In a study in-vivo fertilized mice were compared to mice generated by nuclear transfer, revealing a rearrangement of chromocenters as it was typically found in 1-cell pronuclei in IVF embryos (Martin et al. 2006). Studies comparing the organization of kinetochores, pericentric heterochromatin and nucleoli in mouse embryos revealed that each stage of pre-implantation embryonic development is stage specific (Merico et al. 2007). The comparison between embryos obtained by IVF, parthenogenetic activation (P) and NT showed differences in the frequencies and time-course of nuclear architecture reprogramming events, but with the 8-cell stage the same distinct nuclear organization is achieved (Merico et al. 2007).

2.2.4.7. Chromatin mobility & gene expression

Deviating ideas exist concerning the topology of transcription (Lanctot et al. 2007; Misteli 2007; Trinkle-Mulcahy and Lamond 2008). On the one hand transcription sites were suggested to be randomly dispersed throughout the nucleus (Wansink et al. 1993). On the other hand models have been proposed that favor the existence of special transcription factories that are enriched in polymerases and contain many

genes at the same time (Cook 1999; Chakalova et al. 2005). The existence of preferred and clustered sites of transcription would implicate that activated genes move towards those sites.

Living cell experiments revealed that the movement of chromatin is limited to a radius of approximately 0.5 to 1 μ m during interphase (Abney et al. 1997; Edelmann et al. 2001; Walter et al. 2003; Gilbert et al. 2004). An exception was found during early G1 when chromatin moved even more than 2 μ m (Walter et al. 2003). FRAP experiments in HeLa cells where the chromatin was fluorescently labeled by stable expression of H2B fused to GFP showed a high stability of the bleached pattern from G1 to G2, indicating that chromatin is stable during that period (Walter et al. 2003). The same tendency of movement speed was observed for Cy3-scratch-labeled CTs, where also the inheritance of CTs through mitosis was observed. If a HeLa-H2B-GFP tagged cell was bleached except for a small segment at the border, a similar or scattered pattern was found in the next generation, indicating that changes can occur during mitosis. However the investigation of CT arrangements in daughter cells, revealed a striking similarity in the order of non-bleached patches, confirming the observations made by Boveri, who postulated already one decade ago that chromatin formation in daughter cells is highly symmetrical (see chapter 2.2.1.) (Boveri 1909; Walter et al. 2003). In contrast the studies with H2B-GFP and H2B-YFP tagged normal rat kidney cells performed by the Ellenberg group showed an overall inheritance of chromatin from one cell cycle to the next without global changes in the CT arrangement (Gerlich et al. 2003). Experimental set ups differed to some extent, while Gehrlich et al. bleached the halves of the nuclei Schermelleh et al. bleached nearly the whole nucleus except very small patches. The monitored areas differed in size and therefore occurring movements might be detectable to a different degree.

Several observations address the question of how far gene loci could move inside the nucleus (Vazquez et al. 2001; Chubb et al. 2002; Thomson et al. 2004; Chuang et al. 2006). A tendency of long-range movements was found to occur during G1 in interphase, which rather represents a short time window for large movements. After this a repositioning seemed only possible in small scales (Lanctot et al. 2007). Living cell data with the human cell line HT1080 confirmed the increased mobility of chromatin and individual loci during G1. This was arguing for a de novo establishment of chromatin positioning during that cell cycle stage (Thomson et al. 2004). An inheritance of CT arrangements from a mother cell to its descendants was not observed. Arrangements in daughter cell were found roughly symmetrical (Thomson et al. 2004). Many studies on chromatin mobility were done by the group

of A. Belmont using fluorescently labeled lac-operons, e.g. in *Drosophila melanogaster* spermheads (diameter of 10-17 μ m). Lac-operons provide an inducible system of genes that can be monitored through a fluorescent tag. Two types of movements were found in these experiments: rapid, local movements in the range of 0.3-0.7 μ m and slower movements in large-scale dimensions which were on average about 2.6 μ m (Vazquez et al. 2001).

Interactions of distinct gene loci with "silencing" compartments, like the nuclear periphery or nucleoli, could further lead to an immobilization of chromatin and a subsequent silencing of genes. Studies investigating different loci of the human genome revealed that loci around the nucleoli or at the periphery are significantly less mobile than more nucleoplasmic loci. Fluorescently labeled loci were monitored by tagging these loci to arrays of lacO, where GFP was fused to the Lac repressor (Chubb et al. 2002). Another study revealed that a transcriptionally inactive compartment like the nuclear periphery could not per se prevent transcription. Therefore a cumate inducible system was generated to attach active genes to the nuclear lamina. Observations revealed that first, repositioning to the lamina is only successful after a mitotic division of cells and secondly that the gene maintains its transcriptional competence shown by nascent transcripts found at the nuclear periphery (Kumaran and Spector 2008). A positioning of genes towards the nuclear periphery may allow both transcription or silencing and was postulated to modulate gene expression levels during differentiation and development (Trinkle-Mulcahy and Lamond 2008). Concerning differentiation and the localization of active genes close-by SC-35 domains a study by Moen et al. revealed that certain muscle genes co-localize with SC-35 domains in differentiated muscle cells but not in proliferative myoblasts or fibroblasts (Moen et al. 2004).

The question of how far chromatin sites can move during interphase and how gene expression is spatially organized is still discussed controversially. For further information the following reviews dealing with that topic are recommended (Fraser and Bickmore 2007; Lanctot et al. 2007; Misteli 2008; Trinkle-Mulcahy and Lamond 2008).

2.2.5. Evolutionary conserved pattern

Most studies on CT distribution have focused on human cells, but several other species, like mouse (Mayer et al. 2005), chicken (Habermann et al. 2001) or primate species (Muller and Wienberg 2001; Tanabe et al. 2002; Neusser et al. 2007) were also subjects of investigation, all revealing similar results concerning a gene-density depending radial distribution. Replication and transcription pattern were found that

resembled the ones found in mammalian cells, indicating a very high conservation of topological principles (Postberg et al. 2005).

Studies in primates revealed that certain motifs were evolutionary highly conserved (Tanabe et al. 2002). The gene-density dependent distribution of human CTs 18 and 19 or their orthologues were stained in cells of several great apes, namely chimpanzee, orangutan, gorilla or white-handed gibbon. The results were similar to those obtained in human cells (Tanabe et al. 2002).

In a recent study the distribution of CTs 18 and 19 orthologues in the old world monkey Wolf's guenon was examined. The karyotype of this species differs from the human one especially in chromosome size. While in humans the size of chromosomes varies from 50-250Mb, in Wolf's guenon all chromosomes are roughly of the same size (50-150Mb). Interestingly, the distribution of CTs 18 and 19 was gene-density related also in flat shaped fibroblasts (Neusser et al. 2007). This indicated that in principle a gene-density dependent distribution could be basically in all cells. In the case of human fibroblasts this pattern was somehow covered by the influence of gene size that might be a fact of fitting all chromosomes into those very flat cells.

2.2.6. Influence of nuclear shape on CT distribution

The shape of nuclei seems to have an influence on the positioning of CTs. In flat and ellipsoidal human fibroblasts the CT distribution differs from those in spherical cells like lymphocytes (Bolzer et al. 2005). The inner surface of nuclei might provide a different size for the attachment of CTs depending on the shape of the nucleus. The space that can be occupied by a CT might be restricted in flat cells. In the lab of D. Ingber investigations were performed, concerning the interactions of molecular components of the cell with the shape, stability and attachment to a given surface. They developed slides covered with different patterns of fibronectin, an extra-cellular matrix protein that is necessary for cell attachment. This forces cells to grow on this appropriately covered space, thereby inducing a specific shape of cells as well of nuclei (Chen et al. 1997; Maniotis et al. 1997; Ingber 2003; Arnold et al. 2004). Using this slides alterations in nuclei shape can be induced which allows a detailed investigation of possible changes in the field of nuclear architecture. I have used those slides to detect any influence of the nuclear shape on the distribution of CTs. The results of these experiments are described in this work (see chapter 4.2.2. and 5.2.4.).

2.2.7. Preimplantation embryos as a model system

Preimplantation embryos provide the possibility to study the earliest developmental processes. For development and differentiation reprogramming of parental DNA from the gametes is a major subject of investigation. Proper “programming” of chromatin including epigenetic marks are essential for successful development.

In sperm and egg nuclei chromatin is organized in a very unique way. Especially noticeable is the extreme condensation of DNA in sperm nuclei that needs to be reorganized and reconstructed after being injected into oocytes, starting with the replacement of protamines by histones (Morgan et al. 2005). Investigations concerning basic events are of great interest, like the structure and distribution of chromatin itself and other structural components of the nucleus during early development (Santos et al. 2005).

To get a comprehensive view of early developmental processes animal models of different species are of great importance. Several studies concerning technique improvement were done to reach a high rate of blastocyst- or -to-term development (Wolf et al. 1998; Zakhartchenko et al. 1999; Campbell et al. 2005; Aston et al. 2006). For example the success of different donor cells was tested, indicating that serum-starved cells in G0 gave better results in SCNT experiments in contrast to cycling ones (Zakhartchenko et al. 1999). To get insight in early reprogramming events nuclear architecture, chromatin and other cellular components as well as epigenetic marks are subject of investigation (Santos et al. 2003; Shi et al. 2003; Santos and Dean 2004). The potential of NT procedure to reprogram somatic donor cells to a totipotent stage is a promising tool for research and medicine (Wade and Kikyo 2002; Latham 2004). Using this technique it was possible to create patient specific embryonic stem cells (Paterson et al. 2003; Houdebine 2005; Kues et al. 2005). It became possible to produce cloned animals with novel genetic characteristic for gene-farming or xenotransplantations (Wolf et al. 1998). The effective production of bispecific antibodies in transgenic farm animals was reported (Grosse-Hovest et al. 2004). Animal models provide perfect experimental systems to study early development, reprogramming and differentiation processes. This hopefully gives insight to mechanisms in the evolution of certain human diseases and tools for adequate therapies as well.

2.2.7.1. Diagnostics in preimplantation embryos

Not allowed in Germany, there are many countries where the pre-implantation genetic screening (PGS) is a utilized tool in assisted reproductive technology (ART). Therefore blastomeres from a 6-8-cell stage can be taken for examination of

chromosome abnormalities (Munne et al. 1999; Munne et al. 2002). Human embryos, generated by IVF, can be subjected to PGS, and further used for detailed studies of CT arrangement in human embryos. Additionally comparisons to human tissue cells can be made.

Several studies concerning the spatial localization of CTs in human embryonic blastomeres were performed in such a way (McKenzie et al. 2004; Diblik et al. 2005; Diblik et al. 2007; Finch et al. 2008). The localization of several CTs (#13, 16, 18, 21, 22, X and Y) in aneuploid and euploid blastomeres from 6-8-cell stage embryos was compared. In chromosomally normal embryos a random distribution of all CTs was found. In aneuploid embryos the distribution was significantly different, but not in morphologically abnormal embryos (McKenzie et al. 2004). In another study the detailed positions of CTs 18 and X were studied in human blastomeres from day 3 and 4 embryos. For CT X no significant preferred localization was found but for CT 18 a preferred localization towards the periphery was observed. Significant difference was only found in aneuploid blastomeres (Diblik et al. 2005). In a further study the same authors investigated the localization of CT 18 and additionally the CTs #13, 16, 21, 22, X and Y, again in day 3 to day 4 blastomeres. The localization of CT 18 was only peripheral in aneuploid embryos. All other CTs investigated, including X, were distributed randomly (Diblik et al. 2007). The localization of the inactive X was described to be at the periphery (Dyer et al. 1989) but the onset of a shift to the periphery is not known (Diblik et al. 2007). In another study in the lab of D. Griffin, redundant human embryos from IVF procedures were grown until day 4 and further fixed for FISH (Finch et al. 2008). CTs # 13, 15, 16, 18, 21, 22, X and Y were analyzed in several different tissue cell types as well as morphologically and or genetically different groups of blastomeres. Comparisons between those groups revealed no differences between any of the investigated groups. To summarize their results the pattern for nearly all chromosomes in all non-embryonic cells (including amniotic fluid cells) were distributed significantly non-random. Sperm nuclei displayed a "chromocenter" pattern with all centromeres located in the interior. In all blastomeres no specific pattern was found at all. All chromosomes seemed to be randomly distributed. A few exceptions were only found in the group of aneuploid embryos. CTs 21 and 22 were centrally located, CT 18 more peripheral, like it was found in lymphocyte cells (Finch et al. 2008). Despite all the studies done so far, there are still many open questions about the order of CTs in early embryos going along with reprogramming and first differentiation steps.

3. Material & Methods:

The work consists of three parts for which the methodological spectrum did basically not differ.

3.1. Cell and embryo material

3.1.1. Human Diploid Fibroblasts (HDF)

Two different cell strains were used for the work - a male and a female one. For examinations of sister clone symmetry a female human primary diploid cell line, available in our lab, was used. For experiments concerning cell shape modifications and radial positions of chromosome territories during different cell cycle stages, a primary human diploid fibroblast culture from a skin biopsy of a 2-year old boy was used. Cells were kindly provided by the Department of medical genetics, LMU Munich. The karyotype was normal (46, XY) (Bolzer et al. 2005).

3.1.2. Lymphocytes (human/bovine)

Human lymphocytes were extracted freshly from blood of healthy persons in the group. Bovine lymphocytes were isolated using blood obtained from a local slaughterhouse. Quiescent peripheral lymphocytes were either mitogen-stimulated to obtain cycling cells or used unstimulated. Stimulation was applied by supplementing growth medium with Concanavalin A (5mg/ml), final concentration: 12.5µg/ml and Phythaemagglutinin (PHA-M; 5mg/ml), final concentration: 2.5µg/ml. Extraction of lymphocytes was performed the following way:

- 10ml of peripheral human blood was taken with a syringe from a healthy donor and filled into a 15ml falcon tube with 100µl Heparin. Bovine blood was filled at the slaughterhouse into 50ml falcon tubes with 200µl Heparin.
- Special 50ml Falcon tubes with Ficoll-disk (a filter disk placed in the Falcon to distinguish different blood phases) were prepared with 15ml of Ficoll and spin down shortly (30seconds) at 1000g that the liquid was beneath the disk.
- 10ml of blood were diluted with 10ml of PBS and filled gently into the prepared Ficoll tube.
- Spin down the blood-Ficoll-tube for 10min at 1000g.
- A cell culture flask (75cm²) was prepared with 20ml RPMI including following supplements: 50µl of Concanavalin A (stock conc.: 5mg/ml) and 10µl of PHA-M (stock conc.: 5mg/ml).

- The “buffy” coat was removed with a plastic pipette from the Ficoll tube. This is the layer of cells, which is above the disk and separates two clear liquid layers from each other. This layer contains the lymphocytes but no other blood cells like erythrocytes.
- The “buffy” coat was transferred into the prepared medium and incubated for 72h at 37°C and 5% CO₂.

3.1.3. Bovine Fetal Fibroblasts (BFF)

Bovine fibroblasts were kindly provided by V. Zakhartchenko (Institute of Molecular Animal Breeding and Biotechnology, Gene Center and Moorversuchsgut, LMU Munich). They are derived from blastocyst embryos generated by in vitro fertilization (IVF) or nuclear transfer (NT). Following BFF strain was used:

BFF451-1 are bovine female fetal fibroblasts from an embryo, generated by nuclear transfer with a stably transfected cell line. The transgene (see Fig. 33) contains a mouse Oct-3 promoter-driven sequence for enhanced fluorescent green protein (EGFP), which behaves similar to the endogenous Oct-3 (Yoshimizu et al. 1999). Oct-3 was shown to be crucial for early development in mice (Nichols et al. 1998) and the maintenance of pluripotency in embryonic stem cells (Niwa et al. 2000). The system is very useful as GFP expression can be used to distinguish between an on and an off state of the transgene (Wuensch et al. 2007). Topological aspects of the transgene were subject of the present study.

3.1.4. Bovine embryos

Bovine embryos were generated by V. Zakhartchenko and Co-workers. In the present study we used embryos generated by two different techniques (see chapter 3.3. for detailed description):

- *In-vitro* Fertilization (IVF)
- Nuclear Transfer (NT)

3.1.5. Mouse embryos

Mouse embryos were kindly provided by Dr. Renner-Müller (Gene center, LMU Munich). Embryos were generated in vivo by pairing super-ovulated female mice with male mice. The strain was FVB/N@Rj (Janvier, France). Zygotes were washed out and collected approximately 12 hours after fertilization. For transportation of zygotes HEPES buffered (M16) medium was used. Embryos were placed in a 4 well plate containing carbonate buffered (M11) medium for further growth in the incubator at 37°C and 5% CO₂ atmosphere. The blastocyst rate was about 70%.

3.2. Cell culture

3.2.1. Media

Before use, 1% Penicillin/Streptomycin and 10% fetal calf serum was added to all media. For selection of transgenic cell lines 2.5µg/ml gentamicin (G418, Gibco, Invitrogen, Karlsruhe; stock: 100mg/ml) was added.

- RPMI 1640 Medium was used for all tumor cell lines and lymphocytes.
- Dulbecco's MEM was used for fibroblast cells.
- HME cells were grown in a special and expensive HMEC media with supplements.
- M2 medium is a HEPES buffered medium that was used for embryo transport.
- M16 medium was used for cultivation of embryos.

3.2.2. Unfreezing, culture and freezing down

Aliquots of HeLa cells, that contain a quarter of the cells of a 75cm² culture flask with a 70% confluent culture were taken from liquid nitrogen storage, thawed quickly in a water bath at 37°C and transferred to 25cm² culture flask with 6ml pre-warmed medium. Medium was changed when cells were attached to culture flask bottom, approximately four to six hours later. In case of very sensitive cells, e.g. fibroblasts or HMEC, after thawing cells were transferred to 15ml Falcon tube and spun down for 10min at 192g. The supernatant containing DMSO enriched medium was removed and cells were re-suspended in fresh and pre-warmed medium before they were transferred to a culture flask. Cells were kept at 37°C and 5% CO₂. When reaching an almost confluent stage, cells were transferred to a 75cm² culture flask. Cells were split 1:4 (for fibroblast culture) or to 1:10 (for tumor cells) respectively if the culture was 70% confluent.

For further experiments aliquots of cells were frozen in liquid nitrogen. Therefore cells were treated with trypsin, removed to 15ml Falcon tubes and spun down for 10min with 192g. The cell pellet was resuspended in 10%DMSO/50%FCS/medium, 1.5ml aliquots of suspension were pipetted into 2ml cryo-tubes and frozen in an isopropanol box at -20°C for several hours to gently cool down the aliquots. Then the box was transferred to -80°C over night. The next day cells in were put into the liquid nitrogen tank for long time storage.

3.2.3. Growing cells on glass coverslips

For most experiments cells were grown on coverslips. Therefore coverslips were coated with Poly-L-Lysine to keep cells in good morphology. Poly-L-Lysine (working

conc. 1mg/ml) was incubated under sterile conditions for 45min. Then they were wiped shortly in H₂O bidest. and dried at RT. If not used immediately coverslips were irradiated with UV-light for 30min, stored in small petridishes, sealed with parafilm and kept at 4°C. Cells cultivated on Poly-L-Lysine turned out to be of advantage because cells attach and grow much better on this surface then on pure glass. Cells at a confluence of 70% are used for seeding onto coverslips. After trypsinization the cell suspension was poured at an adequate dilution onto pre-treated coverslips, medium was added and cells were grown in incubator at appropriate conditions (see above).

3.3. Generation of embryonic specimen

In the present study I have analyzed embryos that were generated either by *in-vitro* fertilization (IVF) or by nuclear transfer (NT). Generation of embryos was performed by V. Zakhartchenko, however methodological principles are briefly summarized in the following:

3.3.1. Extraction of oocytes

Both approaches have in common the collection and maturation of oocytes. Ovaries of freshly slaughtered cows were collected at the Munich slaughterhouse and transported in physiological saline at 25-30°C (see Fig. 4) to the Moorversuchsgut in Oberschleißheim (Zakhartchenko et al. 1997). Cumulus-oocyte complexes (COCs) were aspirated from the inner surface of the ovaries (Hiendleder et al. 2004). Oocytes were matured in TCM 199 media with stimulating supplements (10% estrous cow serum (ECS) containing 0.2 units/ml o-FSH) for 20-22 hours (Hiendleder et al. 2004). Matured oocytes were sorted by quality, which is based on great experience and skills of the people working there because few qualitative and quantitative evaluations were done on this subject. In this study only embryos of good quality were used. A hint for good quality is for example a homogenous and dark appearance of cytoplasm as well as a multilayered compact cumulus (Zakhartchenko et al. 1997). In general the quality control of oocytes and embryos is not very easy because stable parameters are missing for clear categorization.



Fig. 4) Bovine oocytes: collected from freshly slaughtered cattles, ready for transport.

3.3.2. *In-vitro* fertilization (IVF)

Details of the utilized in-vitro fertilization process is described by Hiendleder et al. (Hiendleder et al. 2004; Hiendleder et al. 2004; Hiendleder et al. 2004). Matured oocytes were washed in fertilization medium (Tyrode albumin lactate pyruvate) supplemented with sodium pyruvate (2.2mg/ml), heparin sodium salt (2 mg/ml), and BSA (6 mg/ml). For further use oocytes were transferred to drops of medium (400- μ l). Frozen spermatozoa were thawed and healthy ones start swimming upwards. The spermatozoas were subjected to that procedure for 90 min. Then the COCs and spermatozoa (2×10^6 cells/ml) were co-incubated for 18 h. To get zygotes free of cumulus complexes, they were vortexed, followed by several washings in synthetic oviductal fluid (SOF) culture medium enriched with 5% estrous cow serum (ECS), BME Vitamins100x (20 ml/ml;) and MEM. They were again transferred to 400- μ l droplets of medium covered with mineral oil for further development until they reach the desired stage. Incubation of embryos is at 39°C, 5% O₂, 5% CO₂ and 90% N₂ at maximum humidity. Time was measured from the time point when sperm was washed away until fixation. Additionally developmental stage was controlled by counting number of blastomeres as an indication for developmental stage (see Fig. 5 below). Some embryos do not develop in a “normal” way. They are slower than and were therefore not included in the analysis.

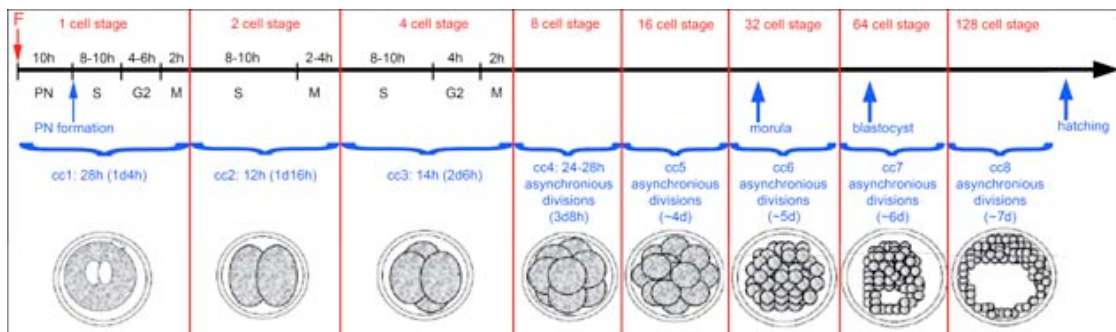


Fig. 5) Scheme of development of bovine IVF embryos: cell stage (red), cell cycle stage (black) and duration of cell stage (blue) is given in a schematic drawing. In the lower panel embryos at certain stages are depicted (taken from (Berg and Brehm 1989)).

3.3.3. Nuclear Transfer (NT)

The detailed procedure for nuclear transfer is described in Brüggerhoff et al. and Hiendleder et al. (Brüggerhoff et al. 2002; Hiendleder et al. 2003). For nuclear transfer the oocytes were enucleated with a micromanipulator (see Fig. 6a-c). During this process the zona pellucida is damaged. Single nuclei of a given cell culture were then positioned into the oocytes, by using the same hole in the zona pellucida as for the enucleating process (see Fig. 6d-f). After that the donor nucleus and the oocyte were affiliated by an electric pulse to induce fusion of both cells.

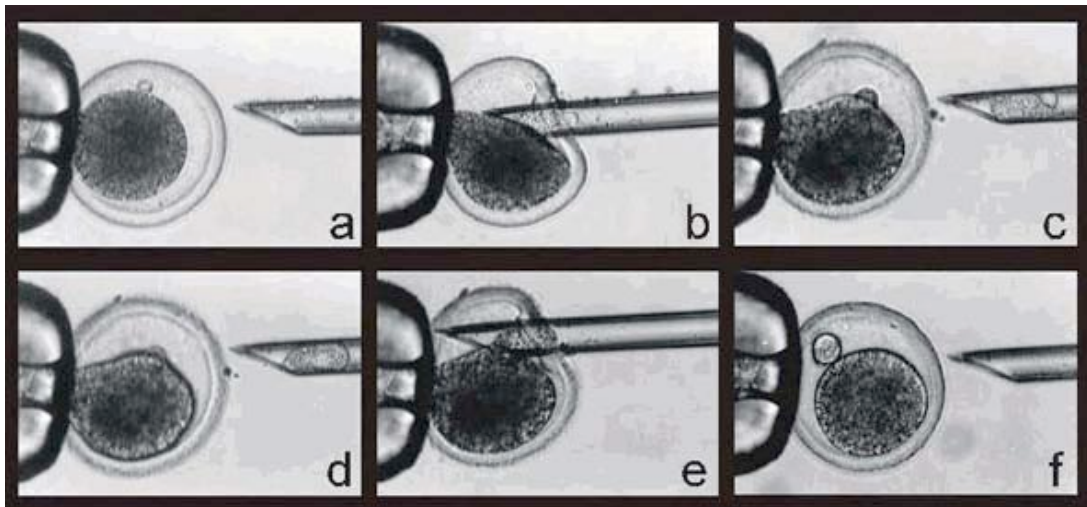


Fig 6) Nuclear transfer (NT): Images showing the process of NT, starting with the unfertilized oocyte (a), from which chromosomes are taken out (b, c) and donor nucleus is placed through the same hole in the zona pellucida next to the oocyte (d-e). Fusion of both cells (donor nucleus and oocyte) is induced by an electric pulse (not shown in the pictures; taken from <http://aet-d.de/de/klonen.htm>).

Embryos were then grown in medium at 39°C / 5% CO₂ until the appropriate developmental stage. In the present study utilized donor cells were always BFF451-1 cells, cultured for only a short period before frozen in small aliquots (1/40 of a 70% confluent T75 culture flask). Cells were thawed approximately one week before a nuclear transfer experiment. They were grown in a 24 well plate in DMEM, supplemented with 20% FCS. They were usually confluent the next day and kept in that stage until use. Most cells were in G0 due to contact inhibition. According to previous experiments of the Wolf group this cell stage has an advantage for nuclear transfer experiments, showing a higher blastocyst and to term development (Zakhartchenko et al. 1999).

3.4. Metaphase preparation

Metaphase spreads are used to test probes for their quality, hybridization efficiency (intensity and location). This includes also an improvement of detection schemes. Moreover the karyotype of cell lines can be checked for chromosome instabilities of the investigated chromosomes.

3.4.1. Treatment of cells

For the preparation of metaphase chromosomes cells were grown in twelve to 20ml appropriate medium in culture flasks (75cm²). For best results, when starting the treatment, the culture should contain many mitotic cells:

Add 10µg/ml colcemide (stock conc. 1mg/ml) and incubate 40min (bovine species) to 60min (all other species) at 37°C and 5% CO₂. Colcemide is a synthetical product similar to the natural agent colchicine, which is found in the autumn crocus (*colchicum autumnale*). It blocks microtubule assembly and therefore cells are arrested in mitosis (<http://www.biology-online.org/dictionary/Colchicine>, 03.12.2006). This increases the number of mitotic cells in culture. Since condensation of chromosomes continues, incubation time should not be too long since otherwise chromosomes are condensed too much and do not give proper results. (<http://www.mta-verband.at/zytogenetikforum/praxis/ernten.htm>, 03.12.2006)

After incubation, remove medium and keep it in a 50ml Falcon tube, because mitotic cells show poor adhesion.

- Wash cells briefly in 37°C pre-warmed 1xPBS.
- Add 2ml Trypsin/EDTA per flask and incubate for about 5min at 37°C to detach all cells from culture flask bottom.
- Use the former culture medium, to stop trypsinization. Transfer cell suspension completely to 50ml Falcon tube.
- Centrifuge cells down at 156g for 10min and remove supernatant.
- Resuspend cell pellet carefully. Then add slowly a 37°C pre-warmed hypotonic KCl-solution (0.6M = 0.56%) while shaking suspension smoothly all the time. Fill the tube up to 40ml.
- Incubate the suspension for 18 to 20min (depending on cell type and species) in hypotonic solution at 37°C. Afterwards add one drop of fixative solution (Methanol/Acetic acid; 3:1) and shake gently.
- Centrifuge for 10min at 156g and remove supernatant by using a water jet pump.
- Resuspend cells and add 5ml ice-cold fixative solution drop by drop. Fill up while mixing the suspension up to 10ml.

- Incubate the suspension for 25min at -20°C .
- Centrifuge cells at 263g for 10min and remove supernatant.
- Resuspend cells in little fixative solution and move suspension to a smaller 15ml Falcon tube. Fill up the tube with fixative to 10ml and incubate again at -20°C for 30min. (Cells can be stored in suspension at -20°C .)
- Repeat the washing step in fixative solution as many times as necessary to get clean metaphase spreads.

3.4.2. Drop cells

The cell suspension is dropped on glass slides (76x26mm). During this procedure cells are supposed to burst and condensed metaphase chromosomes are distributed on the glass surface. Cells are dropped the following way (Deng et al. 2003):

- A water bath with a defined size (31x30x16cm) and surface area (930cm²) is filled with water (11.16l) to a certain level (31x30x12cm) to optimize the most critical parameter which is humidity over the slide and get reproducible conditions. It is heated to 55°C .
- A metal box of selected size (16cmx10cm) is placed in there. Put one or two clean slides (without pre-cooling) in the metal box. Close the water bath so that the air is saturated with humidity.
- Resuspend cells on ice quickly, put one drop of suspension (use a plastic pipette) on each slide and close the water bath immediately.
- Let slides dry for about 3min and do not open the lid during that time.
- Metaphases need to be checked for their quality at the phase-contrast microscope. Slides are appropriately labeled including date and cell line. Store them until further use at RT.

3.4.3. Post-treatment for conservation

For better storage it is good to completely dehydrate metaphase preparation. This is achieved by the following treatments:

- Put all slides into coplin jars.
- Leave them in 70% Ethanol over night.
- Incubate them the next day for 5min in 100% Ethanol.
- Let them air dry.
- For artificial aging (increases the quality of metaphase spreads), incubate them for 1h at 60°C .

- Store them in appropriate boxes, including silica gel for protection against humidity, at -20°C .

3.4.4. Pepsin-treatment of slides

To increase probe accessibility metaphase spreads should be treated with pepsin to remove proteins and cytoplasm from the slides. This treatment is performed as follows:

- Prepare 0.01M HCl, 100ml per coplin jar. Warm up the solution at 37°C .
- Add pepsin (stock conc. 10%) to a final concentration of 0.002% to warm solution.
- Incubate slides in pepsin-HCl-solution for 5min to 10min, depending on cell type and quality of metaphase spreads, at 37°C .
- Remove slides and put them to 0.05M MgCl_2 -PBS solution to stop enzyme activity.
- Wash slides additionally two times in 1xPBS at RT.
- Dehydrate slides by an ethanol series, each for 3min: 70% \rightarrow 90% \rightarrow 100%.
- Air dry slides at RT.
- Check slides once more for successful treatment. Mark the slides as pepsin treated and store them at -20°C until further use.

3.5. Fixation of cells for 3D fluorescence in situ hybridization (FISH)

The fixation protocol for FISH is optimized to preserve the morphology of cells (Solovei et al. 2002). The individual steps can be summarized as follows:

- Cells were grown on coverslips at 37°C and 5% CO_2 atmosphere. When they reach the wanted density wash them briefly in 37°C pre-warmed 1xPBS.
- Incubate cells at RT in 4% freshly made paraformaldehyde (or in 3.7% formaldehyde) for 10min to fix cells by crosslinking DNA and proteins.
- Wash cells 3x4min in 1xPBS containing 0.05% Triton.
- Permeabilize cells for 20min in 0.5% Triton/1xPBS.
- Incubate cells for at least 1h or better O/N in 20% Glycerol/1xPBS.
- Put cells 4 times to liquid nitrogen until coverslip is completely frozen (you can hear a typical “crack” sound) and let them defreeze on a tissue at RT. Care should be taken that they do not dry out.
- Wash cells 3x4min in 0.05% Triton/1xPBS.
- Incubate cells in 0.1N HCl for 5 to 10min depending on cell type. Duration of HCl treatment is empirical. HeLa cells, as well as bovine cells are incubated for 10min, while human fibroblasts are only 5min incubated. Follow this process at the microscope to control HCl treatment.

- Wash cells 3x4min in 2xSSC.
- Incubate cells in 50% formamide in 2xSSC for at least O/N but better results were achieved by an incubation of 3 days at RT. If they are not immediately used store them at 4°C.

3.6. Fixation of embryos



Fig. 7) Embryo “work station”: the stereo-microscope Stemi 2000 from Zeiss company, Germany.

FISH, on three-dimensionally preserved embryos has not yet been applied in the group of T. Cremer and has to my knowledge not yet been published by anyone else. In literature protocols for stainings can be found, but nothing about a whole FISH procedure. I decided to start with a protocol similar to that for cells. A substantial difference with embryos is that one cannot handle them like cells because they do not easily attach to a surface. As a consequence all embryos need to be treated in solution manipulating them individually or at least in groups using micropipettes and a stereomicroscope to monitor individual steps (see Fig. 7).

An important aspect was that a freezing thawing step as used for cells was not applicable for embryos. For fixation, and detection as well, embryos were pipetted with a transferpettor or with a mouth pipette (see Fig. 8) using very thin glass pipettes, which are done by ourselves because handling is most sensitive then.

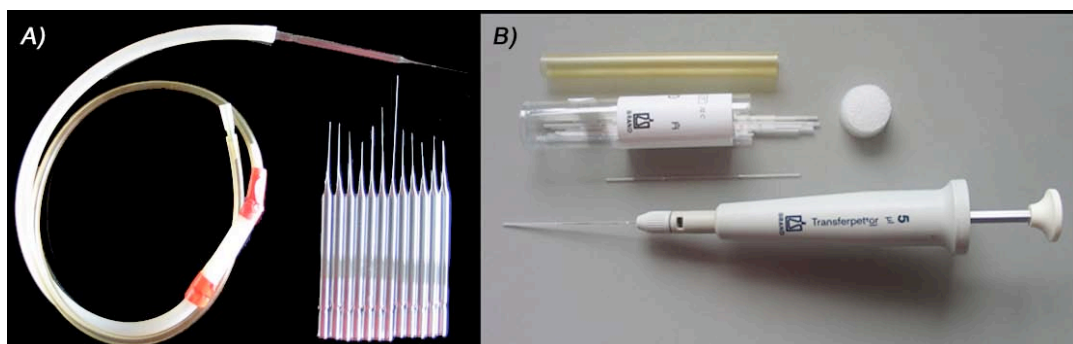


Fig. 8) Tools for pipetting embryos: A) a mouth pipette with individually glass-blown pipettes; B) a transferpettor with defined volume of 5µl and appropriate glass pipettes;

Embryos can be incubated in drops (when working with solutions, that do not contain Triton or any other strong

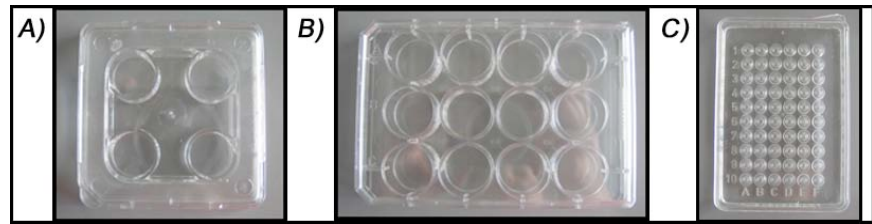


Fig. 9) Plastic stuff used for work with embryos: A) a 4-well-plate where embryos were grown; B) a 12-well-plate for fixation and detection and C) a 60-well-microtest plate, used for glycerol series.

detergent) on a Petri dish. Also 4-well or 12-well plates using 500 μ l or 1000 μ l of solution were used (see Fig. 9A, B). In drops embryos can be followed more easily and get not lost. In a bigger volume like 500 μ l or 1000 μ l embryos are sometimes hard to find and probably get lost. The advantage of those bigger volumes is that the dilution problem can be neglected. When using drops, sensitive steps require a stepwise equilibration of the new solution because there is always a dilution through the liquid from the Transferpettor. For some treatments the tracking of embryos is even difficult. Therefore all incubation steps in glycerol are done in microtest plates (Greiner Bio One, see Fig. 9C). However this procedure causes embryos to change their level of transparency / coloring (in the worst case, embryos can get nearly invisible or they start moving in all direction, rather than sinking). In the small wells of microtest plates embryos do not get lost because of the limited volume.

Another problem is the zona pellucida as it reduces the permeability of the embryo. It should therefore be removed completely so that embryonic cells are sensitive to permeabilization and finally probe penetration (see Fig. 10).

A disadvantage of removing it is that embryos are easily destabilized in their morphology and adhere much more easily to

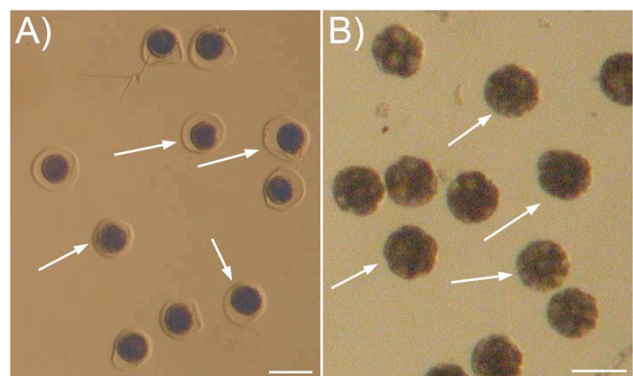


Fig. 10) Bovine embryos before fixation (A) with zona pellucida clearly visible around the embryo proper (white arrows) and after fixation (B) where zona pellucida is removed successfully (white arrows). Note that embryos on both pictures are not the same. In A) bovine IVF zygotes are shown while in B) bovine IVF embryos of day 4 are shown; Bars: 100 μ m.

any surface. To limit the latter problem BSA is added to nearly all solutions.

To establish a working protocol many variations were tested like e.g. removing the zona pellucida after fixation in 3.7% formaldehyde or different incubation length for the permeabilization (30-90min).

Finally the following protocol turned out to be most successful:

- Wash embryos briefly in 1xPBS at 37°C.
- Fix embryos for 10min in 3.7% formaldehyde/1xPBS at RT.
- Incubate embryos in 0.1N HCl until zona pellucida disappears. Time varies between 30sec and 2min. It is depending on the embryonic stage and on the method how embryos were generated. (NT embryos are in general more sensitive to HCl treatment than IVF embryos. Mouse 4 cell stages are incubated only in 0.01N HCl because of their bigger sensitivity.)
- Wash embryos two times each for 10min in 0.05% TritonX-100/1xPBS containing 0.1% BSA.
- Permeabilize embryos for 60min in 0.5% TritonX-100/1xPBS containing 0.1% BSA.
- Wash embryos another two times each for 10min in 0.05% TritonX-100 in 1xPBS + 0.1% BSA.
- Incubate embryos in 0.1N HCl for 2min.
- Wash embryos once in 1xPBS containing 0.05% TritonX-100 + 0.1% BSA for 10min.
- Wash embryos finally two times each for 10min in 2xSSC + 0.1% BSA + 0.01% TritonX-100.
- Leave embryos in 50% formamide/2xSSC containing 0.1% BSA (pH=7,0) for at least two days and nights.
- Repeat the following steps:
 - Wash embryos once for 10min in 2xSSC + 0.1% BSA + 0.01% TritonX-100.
 - Wash embryos two times each for 10min in 0.05% TritonX-100/1xPBS containing 0.1% BSA.
 - Permeabilize embryos for 60min in 0.5% TritonX-100/1xPBS containing 0.1% BSA and 0.02% RNase A.
 - Wash embryos another two times for 10min in 0.05% TritonX-100 in 1xPBS + 0.1% BSA.
 - Incubate embryos in 0.1N HCl for 2min.
 - Wash embryos once in 0.05% TritonX-100 in 1xPBS + 0.1% BSA for 10min.
 - Wash embryos finally two times for 10min in 2xSSC + 0.1% BSA + 0.01% TritonX-100.
- Leave embryos in 50% formamide/2xSSC containing 0.1% BSA (pH=7,0) for at least two days and nights.

3.7. Probe amplification and labeling

DNA is a double-stranded molecule that replicates in a semi-conservative way. Technology in our days makes it possible to copy nature by using its enzymes in a directed way. This results in a very efficient way to amplify desired DNA pieces. The development of the polymerase chain reaction (PCR) was an important methodological breakthrough for geneticists because of its nearly unlimited duplication possibilities of all kind of DNA probes. Additionally PCR (besides other technologies like e.g. nick translation) provides a way to mark the target DNA with special nucleotides to make them finally visible with certain techniques – an important tool for answering biological questions concerning DNA distribution in a cell nucleus.

3.7.1. Origin of bovine probes

Chromosome paint probes were kindly provided by Roscoe Stanyon. (Department of Animal Biology and Genetics, Laboratory of Anthropology, Florence). All chromosomes were originally obtained and separated by fluorescence activated chromosome sorting. This technique, shortly named “chromosome flow sorting” is separating chromosomes from a monodispersed suspension by their DNA content and their AT/GC ratio with the help of a flow cytometer (Gray et al. 1979). By DOP-PCR amplification chromosome paints can be made out of the sorted probes (Telenius et al. 1992). Since peaks were found very close together, i.e. different chromosomes showed very similar fluorescent properties, some “chromosome specific” probes were unfortunately highly cross-reacting with other chromosomes. However, probes for CTs 19 and 20 were only slightly cross-reacting with other chromosomes and this unspecific hybridization could be successfully suppressed by using a high concentration of repetitive C_0t -DNA.

3.7.2. Nucleotide labeling

For labeling any kind of DNA and RNA probes, fluorescence- or hapten-labeled nucleotides are necessary. There are many different labeling molecules commercially available. A cheaper possibility is to do them yourself. In the following there is a description how to make exemplarily Digoxigenin labeled dNTPs, which is published as well in CSH Protocols (Müller et al. 2007):

Dissolve 5mg of Digoxigenin (Dig) in **213µl DMSO → 40mM Dig.**

Mix:

- 10µl 20mM dUTP (Aminoallyl-dUTP)
- 15µl H₂O
- 10µl 0.2M bicarbonate buffer
- 10µl DMSO
- 10µl 40mM Digoxigenin

55 µl

Incubate solution for 3 – 4 hours at 30°C.

Add:

- 2µl 2M glycine (pH 8.0) to stop the reaction
- 4µl 1M Tris-HCl (pH 7.75) to stabilize the nucleotides
- 139 µl H₂O

200µl 2mM digoxigenin-dUTP

Make aliquots, e.g. 20µl 2mM Dig-dUTP per tube and store them at –20°C.

Accordingly one can label dUTPs with DNP (=Dinitrophenyl aminohexanoic acid; dissolve 25mg of DNP in **1.562ml DMSO → 40mM DNP**) and fluorescent labels like Texas Red (dissolve 5mg of Texas Red in **612µl DMSO → 10mM Texas Red**, use as well 10µl for mixture). For TAMRA there are different amounts (dissolve 10mg of TAMRA in **1560µl DMSO → 10mM TAMRA**, use 20µl of 10mM TAMRA-dUTP and only 10µl of H₂O – add in Step 4 only 134µl of H₂O). The protocol for Biotin is slightly different. There is no additional DMSO in the reaction mix:

Dissolve 100mg of Biotin (Bio) in **4.401ml DMSO → 40mM Bio.**

Mix:

- 10µl 20mM dUTP
- 15µl H₂O
- 10µl 0.2M bicarbonate buffer
- 5µl 40mM Biotin

40µl

It is most convenient to prepare a master mix of the PCR reagents, which contains all solutions except for DNA and Taq polymerase. It can be stored at -20°C.

Amplification set up (Table 3):

Number of cycles	Reaction	Temperature	Time
1	Initial denaturation	96 °C	3 min
35	Denaturation	94 °C	1 min
	Primer annealing	56 °C	1 min
	Extension	72 °C	2 min
1	Final extension	72 °C	5 min
	Time at all		3 hours

Check size of amplified probes on a 1% agarose-gel. Therefore mix 2µl of each probe with 3µl of loading buffer (6x). To estimate size and concentration of the PCR products a λ-Hind-DNA-Marker was used. With the described DOP-PCR one yield about 1.5 to 10µg of DNA, which corresponds to a concentration of 30 to 200ng/µl. The size of the DNA products should be between 200bp and 1.5kb. If the amount of the product is less one might repeat the DOP-PCR before using the probe.

3.7.4. Whole Genome Amplification (WGA) by Multiple Displacement Amplification (MDA)

We recently tested a new commercially available technique for amplifying whole genome DNA in a very efficient way. This is called GenomiPhi DNA Amplification Kit - from GE Healthcare, which consists of two buffers – a reaction and a sample buffer – plus an enzyme mix. The amplification is done continuously at a constant temperature and not in cycles with different temperature steps like in PCR. The utilized enzyme is Phi29 DNA polymerase. DNA sample is randomly fragmented and universal oligonucleotide primers and binding sites provide the amplification of the whole material. Denaturation is only necessary once at the beginning of the reaction. The big advantage of this reaction kit is that one can amplify DNA in the range of 5-10ng yielding up to 6-12µg of DNA with a length of 2-12kb. (http://www.sigmaaldrich.com/Area_of_Interest/Life_Science/Molecular_Biology/PCR/Product_Lines/Whole_Genome_Amplification.html, 04.12.2006; http://www.geneservice.co.uk/services/samples/WGA_service.jsp, 04.12.2006)

This technique is easy to perform and consists of only a few steps as detailed in the following:

- Pipette 9 μ l of sample buffer in a 0.6ml PCR tube.
- Add 1 μ l of template DNA and mix briefly.
- Denature for 3min at 95°C (use a thermocycler for accuracy).
- Prepare 9 μ l of reaction buffer in a second PCR tube.
- Add 1 μ l of enzyme to the reaction buffer and mix gently.
- Add reaction mix to sample mix, mix gently and incubate for 16 at 30°C in a thermocycler.
- Inactivate the reaction at 65°C for 10min.

All bovine probes (chromosome paints and the transgene GOF) were amplified with this GenomiPhi Amplification Kit. For bovine embryos it was necessary to get very high amounts of DNA probes for FISH experiments in order to obtain good hybridization signals.

3.7.5. Label DOP-PCR

Label DOP-PCR is one of several methods to generate labeled DNA probes, which compared to all other possibilities includes an amplification step. While amplifying a given template it includes a labeling of the DNA strands. The principle is equivalent to DOP-PCR as described above with the difference that a certain quantity of thymidine nucleotides is replaced by thymidine analogs, such as dUTP-Dig, dUTP-Bio (see also 3.7.2.). This way DNA probes are detectable by antibodies or if fluorescently tagged (dUTP-Tamra, dUTP-Cy3) directly visible after FISH experiments.

Label DOP-PCR (Table 4):

Reagents	Amount	Final concentration
GeneAmp PCR buffer (10x)	5 μ l	1 x
MgCl ₂ (25 mM)	4 μ l	2 mM
6-MW primer (100 μ M)	1 μ l	2 μ M
AGC mix (2 mM each)	2.5 μ l	100 μ M
dTTP (1 mM)	4 μ l	80 μ M
Labeled dUTP (2 mM)	2 μ l	40 μ M
H ₂ O	30 μ l	
DNA	1 μ l	30 - 200 ng
Taq polymerase (5 U/ μ l)	0.5 μ l	0.5 U/ μ l
Σ	50 μ l	

It is most convenient to prepare a master mix of the PCR reagents, which contains all solutions except for DNA, labeled nucleotides and Taq polymerase. It can be stored at -20°C.

Amplification set up for Label DOP-PCR (Table 5):

Number of cycles	Reaction	Temperature	Time
1	Initial denaturation	94 °C	3 min
20-25	Denaturation	94 °C	1 min
	Primer annealing	56 °C	1 min
	Extension	72 °C	30 sec
1	Final extension	72 °C	5 min
	Time at all		3 hours

Check size of labeled probes on a 1% agarose-gel. Therefore mix 2µl of each probe with 3µl of loading buffer (6x). For control of size and concentration add 5µl of appropriate marker, e.g. λ-Hind-Marker. The labeled chromosome probes should range between 200bp and 1.5kb.

3.7.6. Nick translation (NT)

Another way to label DNA is the application of nick translation. In this reaction labeled nucleotides are incorporated into template DNA but not amplified. That means that the amount of template DNA should be higher than in a comparable Label DOP-PCR. The advantage of nick translation is that the length of probes can be modified more accurate and the density of labeled nucleotides is higher.

In a nick translation the enzyme DNase is making nicks into the DNA templates and another enzyme, the DNA polymerase I is filling those gaps while including the labeled nucleotides into the DNA template. DNase (stock concentration: 2000 U/ml) is diluted in H₂O. Keep enzyme constantly on ice. The following reagents are pipetted into 1.5ml tubes (Table 6):

Reagents	Amount	Final concentration
DNA	2 µl	500 ng – 3 µg
NT buffer (10x)	5 µl	1x
β-Mercaptoethanol (100 mM)	5 µl	10 mM
dNTP mix (2.5 mM ACG, 0.5mM T)	5 µl	50 µM ACG; 1 µM T
Labeled dUTP (1 mM)	2.5 µl	50 µM
H ₂ O	28.5 µl	
DNase (1:200)	1 µl	0.16 U
DNA polymerase I (5 U/µl)	1 µl	0.1 U/µl
Σ	50 µl	

Incubate NT mixes for 90min at 15°C. To stop the reaction freeze tubes at -20°C to inactivate DNase. Check size of probes (use 2-5µl) on a 1% agarose gel. Use a Hind III marker for control of length. For bovine embryos it turned out that a size <500bp is optimal for hybridization. If the probes are still too long repeat DNase incubation at room temperature:

- Add 1µl of DNase (diluted 1:200 in H₂O) to the nicktranslation mix.
- Incubate for 10 to 30min at RT, depending on the length of probes.

- Stop the reaction by freezing tubes at -20°C to inactivate DNase.
- Test again on a 1% agarose gel.
- Once the correct size has been obtained the reaction is finally stopped by adding $1\mu\text{l}$ of 0.5M EDTA.

NT labeling was used for all bovine probes, according to the following NT set up (Table 7):

Number of bovine chromosome	DNA (~1 μg)	10x NT buffer	ME 0.1M	dNTP Mix	Labeled dUTP	H ₂ O	DNase 1:200	Pol I
BTA 18	2 μl	5 μl	5 μl	5 μl	2.5 μl DNP	29 μl	1 μl	1 μl
BTA 19	2 μl	5 μl	5 μl	5 μl	2.5 μl Dig	29 μl	1 μl	1 μl
BTA 20	2 μl	5 μl	5 μl	5 μl	2.5 μl Bio	29 μl	1 μl	1 μl
GOF	2 μl	5 μl	5 μl	5 μl	5 μl TAMRA	29 μl	1 μl	1 μl

Note that for probe labeling using fluorescently tagged dNTPs (e.g. Cy3-dUTP, FITC-dUTP, etc.), twice the amount of labeled nucleotides (5 μl instead of 2.5 μl , which corresponds to a final concentration of 100 μM) is helpful for proper results. The amount of added H₂O is reduced accordingly.

3.7.7. Preparation of C₀t-1 DNA

The genome of all species contains a high amount of repetitive DNA (about 25% of the genome consists of α -satellite sequences in eukaryotes (Campbell 1997)). Those repetitive sequences are found on all chromosomes, e.g. around the centromeres, which consists of α -satellite sequences or along the whole chromosomes where interspersed elements can be found (SINEs or LINEs). Since the probes used to highlight individual chromosomes contain such unspecific repetitive elements it was necessary to suppress them. For this purpose C₀t-1 DNA is added to the probe as competitor DNA. The value for C₀t-1 DNA reflects the time point when 50% of all DNA molecules are hybridized, while repetitive sequences hybridize first. This value is specific for each species and is determining the complexity of DNA.

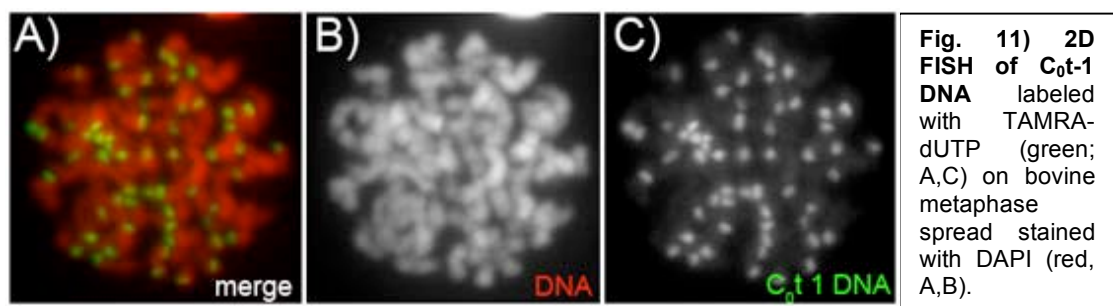
Since bovine Cot DNA is very expensive and the amount of used C₀t-1 DNA per experiment is very high we decided to generate bovine C₀t-1 DNA by ourselves, using bovine genomic DNA as a template. Genomic DNA is fragmented and denatured first. Then DNA is allowed to re-nature for a certain time where only the fraction of repetitive DNA can re-nature. The rest of the DNA in solution contains specific parts of the bovine genome and is degraded by a single strand specific DNase.

Fragmentation of DNA:

- Dilute 12 mg of bovine genomic DNA in 5ml TE, pH 8.0 → concentration of single stranded DNA at t=0: $c_0=2,4$ mg/ml;
- Fragmentation of DNA is accomplished in 50ml Falcon tubes on ice by sonication to get fragments of 300 to 600bp in length; (Our model W220F: use the adjustment between 6 and 7; be careful that the tip of the sonicator is exactly in the middle of the DNA solution to get regularly cut fragments;)
- Use the sonicator 7 times, each time for 2 min and make a 2 min break between so that the solution can cool down;
- To make sure that the fragments have the desired length, check on a 1% agarose gel;

Denaturation and DNA Degradation:

- Denature DNA at 96°C for 6 min
- Equilibrate at 65°C for 4 min
- Add 1205µl 5M NaCl → final conc.: 0.3M NaCl
- Reassociate DNA in 0.3M NaCl for 137sec at 65°C
- Stop the reassociation by adding 21.2ml ice-cold 2x nuclease –S1-buffer
- Add 12.5µl nuclease S1 (5000units)
- Incubate 30min at 37°C for the degradation of not reassociated single strand DNA
- Add 2x Vol of 100% Ethanol (in this case 84.845ml)
- Incubate over night at -20°C
- Centrifuge at 2300g for 30min
- Dry pellet for 5min in a speedvacuum (or for 30min at 60°C)
- Resuspend pellet in 5ml TE buffer
- Check size of the C_0t-1 DNA on a 1% agarose gel
- Measure DNA concentration in a photometer (should be around 1-5µg/µl)



The C_0t-1 DNA is finally tested for suppression quality in 2D experiments. Unspecific signals on other chromosomes should not be detected. Additionally C_0t-1 DNA itself was labeled by nick translation and used for DNA and RNA FISH experiments to visualize repetitive DNA (see Fig. 11) or global transcription of repetitive elements.

3.8. Probe precipitation

According to the experimental set up the designated probes (paint probes for whole chromosomes, centromere regions or the transgene GOF) are combined in a hybridization mixture. For 3D experiments the concentration is increased in comparison to 2D tests. The highest concentration is used in embryo FISH experiments because during set up the probe will be diluted.

In case of human probes the same amount of C₀t-1 DNA like probe amount is added. For bovine probes it turned out that a volume ratio of 4:1 C₀t-1 to probe yielded the best results.

3.9. 2D FISH

For testing the quality of probes the method of choice is 2D FISH on metaphase spreads. The morphology of cells is destroyed since a mixture of methanol and acetic acid is used as fixative. This leads to a dehydration of cells and a denaturation of proteins leading to a loss of the 3rd dimension, hence the name 2D FISH. The preparation of metaphase spreads is described in chapter 3.4. (metaphase preparation). Probes are prepared according to chapter 3.8. (probe precipitation).

3.9.1. 2D FISH set up

2D FISH was set up according to the following protocol:

- Denature metaphase slides for 2min (if slides are freshly dropped, then denature only 1min 30sec) in 70% Formamide/2xSSC (pH=7.4) at 74°C.
- Put slides directly to 70% ethanol, then in 90% ethanol and finally in 100% ethanol, each 3min.
- Air dry slides.
- Denature probes for 5min at 80°C.
- Cool down the probe in ice for 30sec and centrifuged for 30sec, to make sure that all liquid is at the bottom.
- Pre-anneal the probe at 37°C for 30min to allow repetitive sequences to hybridize with each other before putting them onto cells.
- Choose and mark (use a diamond pen) at the microscope an area with many and good metaphase spreads.
- Pipette 2-4µl of probe mixture to the designated area on the already denatured slide. (The amount of probe is depending on the size of coverslips, which equals the size of hybridized area. For a coverslip size of 12x12mm use 2µl of probe. If the size of the coverslip is 15x15mm or 20x20mm use 4 or 5µl of probe.)

- Cover the edges of glass with fixogum. Put the slides in a metal box in a water bath at 37°C. Let the probes hybridize at least overnight.

If you do not need a pre-annealing of probes, e.g. with centromeric regions, one can denature probes and metaphases in a single step:

- Put 2-4µl of probe to a chosen area on the slide.
- Cover the area with a coverslip of adequate size.
- Seal the coverslip with fixogum and let it dry at RT. (If you use directly labeled probes, avoid light exposure.)
- Denature slides at 75°C for 2min on a hotblock (a metal block that can be heated to the temperature exactly and where glass slides can be put on).
- Afterwards put the slides in a metal box in a water bath at 37°C and let probes hybridize at least overnight.

3.9.2. 2D FISH detection

All solutions have to be pre-warmed at the appropriate temperature. Metaphase slides can be washed in coplin jars. After incubation with fluorochromes conjugated antibodies try to minimize light exposure. Incubation steps are done in so called wet chambers - small black boxes filled with a few drops of water for keeping a humid atmosphere. Relevant washings and antibody-incubation steps are summarized in the following:

- Wash 3x5min at 37°C in 2xSSC.
- Wash 2x5min at 60°C in 0.1xSSC.
- Wash briefly in 4xSSCT at 37°C.
- Incubate slides 5min in blocking solution (4% BSA/4xSSCT) at 37°C.
- Incubate the first antibody (diluted in 2% BSA/4xSSCT) for 45min at 37°C.
- Wash 3x4min in 4xSSCT at 37°C.
- Incubate the secondary antibody (diluted in 2% BSA/4xSSCT) for 45min at 37°C.
- Wash 3x5min with 4xSSCT at 37°C.
- Counterstain nuclear DNA, using 4', 6-Diamidino-2-phenylindole (DAPI, final conc.=0.005µg/µl) for 5min at 37°C.
- Wash briefly in 4xSSCT.
- Add antifade (Vectashield) on hybridized area and put a coverslip on the according area, which is then sealed with transparent nailpolish.
- Check quality of FISH signals utilizing a fluorescence microscope.

The protocol is modified in following cases. For example if directly labeled probes are used, solutions are used at a maximum temperature of 40°C.

Detection schemes can be extended with as many layers as necessary for a successful detection. All layers are about 45min, washing steps in between are always 3x4min.

3.10. 3D FISH

3D FISH works in principle just as 2D FISH. The main difference is that the morphology of cells should be maintained and therefore it is absolutely necessary to avoid that cells dry out. However the treatment of cells for probe and antibody permeabilization and concurrently the preservation of morphology do need a compromise.

3.10.1. 3D FISH on cells

3.10.1.1. 3D FISH set up on cells

Cells and probes can either be denatured simultaneously or in separated steps. The easier way is to do it simultaneously, which is feasible if a very stringently controlled pre-annealing of the probe is not necessary. This is the case for all depleted human probes and repetitive sequences. If a simultaneous denaturation is possible the treatment is the following:

- Pipette 4µl of probe onto a slide.
- Place the coverslip with cells on it with cells facing the probe.
- Seal with fixogum and let it dry.
- Denature on a hotblock for 3min at 75°C.
- If cells and probe need to be denatured separately, the protocol is as follows:
- Denature coverslips for 2min in 70% Formamide/2xSSC (pH=7.4) at 74°C, shortly before use.
- Put slides directly to cold (-20°C) 70% Formamide/2xSSC (pH=7.4).
- Denature probes for 5min at 80°C.
- Cool down probes shortly on ice and centrifuged for 30sec, so that all liquid is at the bottom.
- In case of bovine paint probes pre-anneal at 37°C for 30min. (Time can vary and depends on species and quality and sort of probes.)
- Then pipette 2-8µl of probe mixture onto a fresh slide. The amount of probe depends on the size of cells-carrying coverslips. For example for a coverslip with

a size of 15x15mm use 4µl of probe, for a slide with a size of 20x20mm use 5µl of probe.

- Cover the edges of the coverslip with fixogum. Put the slides in a metal box at 37°C in a water bath. Let the probes hybridize for at least 2 nights.

3.10.1.2. Detection of 3D FISH on cells

Since cells are usually grown on 15x15mm (up to 20x20mm) coverslips all washing steps are done in 6well plates. Remove the coverslips from the slide and place them in 6well plates containing washing liquid:

- Wash 3x5min at 37°C in 2xSSC by shaking.
- Wash 2x5min at 60°C in 0.1xSSC by shaking.
- Wash shortly in 4xSSCT at 37°C.
- Incubate slides in blocking solution: 5min at 37°C in 4% BSA/4xSSCT.
- Incubate cells with first antibody for 45min at 37°C.
- Wash 3x4min with 4xSSCT at 37°C by shaking.
- Incubate with secondary antibody for 45min at 37°C.
- Wash 3x5min with 4xSSCT at 37°C by shaking.
- Counterstain DNA using Dapi (final conc.= 0.05µg/µl) for 5min at 37°C.
- Wash briefly in 4xSSCT.
- Put antifade to a proper coverslip and place hybridized area with cells facing down onto the antifade.
- Seal with nail polish.
- Results can be checked using an epifluorescence microscope.

3.10.2. 3D FISH on embryos

3.10.2.1. 3D FISH set up on embryos

Similar to 3D FISH on cells probes for 3D FISH on embryos were denatured simultaneously. However an equilibration time of embryos in the probe is necessary to ensure that the probe is penetrated into the

embryos before denaturation. As the handling of embryos is different from cells, proceed as described in the following:

- Prepare a proper slide with a metal ring on the surface (see Fig. 12): seal the outer rim of the metal ring with fixogum.
- Pipette 5µl of the probe exactly in the middle of the metal ring.



Fig. 12) Glass slide with metal ring (Brunel) placed on the top. Used for denaturation and hybridization of embryos in hybridization mixture.

- Pipette embryos into the probe.
- Cover the area of the metal ring carefully with mineral oil to avoid air-drying.
- Equilibrate embryos in the probe at 37°C for at least 2h in a humid environment.
- Denature embryos and probe afterwards on a hot block for 3min at 76°C.
- Hybridize embryos for at least 2 days at 37°C in humidified area.

3.10.2.2. Detection of FISH signals on embryos

Embryos cannot be attached easily and firmly to a surface. Consequently they have to be handled individually for each washing or incubation step. For detection 12well plates are used (see Fig. 13A). Each “well” is filled with about 1ml of solution to keep dilution factor as low as possible which is usually 1:100 considering that the transfer of 10 embryos adds 10 μ l of solution. Incubation of embryos in glycerol and all subsequent steps were performed in microtest plates (see Fig.13B) with about 4 μ l of liquid per well. When using microtest plates transfer the embryos always in two steps to a new solution to equilibrate them and minimize dilution effects. Monitor embryos during all steps with a stereomicroscope. Solutions if not stated otherwise contained 0.1% BSA and 0.1% TritonX-100 to prevent embryos from sticking to the pipette/plastic surfaces. They were all pre-warmed to 37°C but incubation itself is done at RT without shaking.

- Wash embryos 2x10min in 2xSSC.
- Wash embryos 10min in 50% formamide/2xSSC.
- Wash embryos 10min in 2xSSC.
- Wash embryos 10min in 0.1xSSC, pre-warmed at 60°C.
- Wash 10min with 4xSSCT.
- Incubate embryos in blocking solution: 10min at 37°C in 4% BSA/4xSSCT.
- Incubate embryos in the first antibody at 4°C overnight.
- Wash embryos 2x10min in 4xSSCT.
- Incubate embryos in the secondary antibody for 90min at 37°C in a humidified atmosphere.
- Wash embryos 2x10min in 4xSSCT.
- Counterstain nuclear DNA 20min in DAPI (final conc.= 0.05 μ g/ml).
- Place embryos in 2 steps in 20% Glycerol (microtest plate) and incubate them for 5min.
- Place embryos again in 2 steps in 40% Glycerol (microtest plate) and incubate for 5min.
- Place embryos in 2 steps in 60% Glycerol (microtest plate) and incubate for 5min.

- Finally incubate embryos in antifading medium Vectashield containing DAPI (final conc.= 0.5 μ g/ml (microtest plate).
- Place embryos on special μ -slides (Ibidi, Martinsried; see Fig. 13C), which are ideal for our purpose because visualization of embryos is possible directly through the bottom of the slides. Treat the slides before use with poly-lysine (final conc.=250 μ g/ml) to stick embryos to the surface. Suck off all liquid around the embryos. Embryos will keep their morphology as long as they are covered by a fine glycerol film, which will evaporate only very slowly, minimizing the risk that embryos might dry out. Embryos are left O/N at 4°C in order to attach to the surface. (Avoid light exposure!)
- Cover the embryos with antifading medium Vectashield containing DAPI (final conc.= 0.05 μ g/ml). Work very carefully so that embryos keep attached to the surface of the slide.

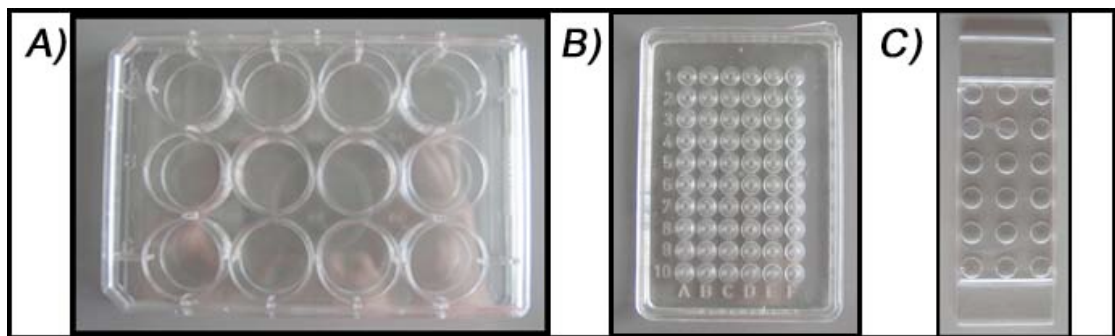


Fig. 13) Plastic stuff for detection of embryos: A) a 12-well-plate for solutions of detection; B) a microtest plate for glycerol series and C) a μ -slide (ibidi, Martinsried) for mounting embryos;

Check results of FISH on embryos at a confocal laser scanning microscope (CLSM).

If FISH was successful the relative positions of embryos in the respective well is recorded using a stereomicroscope, so that they can be easily found at the CLSM. A scheme of ibidi μ -slides is drawn and shown in Fig. 14.

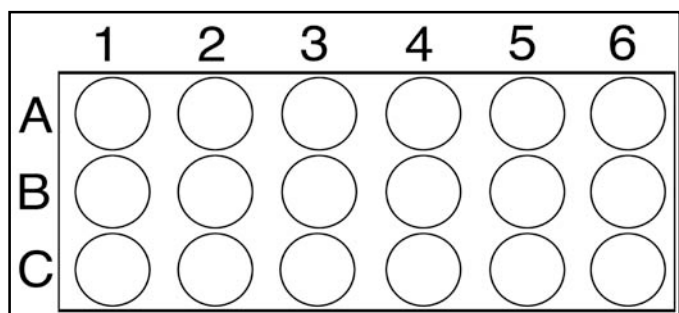


Fig. 14) Schematic drawing of a μ -slide (ibidi), used for mounting embryos. Location of embryos is plotted on the scheme to simplify a re-finding at CLSM.

3.11. Microscopy

3.11.1. Stereomicroscope

For the treatment of embryos it is necessary to work at a stereomicroscope (see Fig. 7) as embryos are handled individually and therefore are constantly monitored. We use a Stemi 2000 (Carl Zeiss, Jena) with a “N” stand including a transmitted light source that allows a maximum working space of ~20cm. The zoom is continuous up to 7.1x. As a light source a cooled halogen lamp was used which can illuminate the specimen from above or beneath, depending on the used fiber glass light guide.

3.11.2. Light microscope

This microscope “Axiovert 25C” is a phase contrast light microscope from the company Carl Zeiss, Jena. It is used mainly for cell culture as well as quality controls of fixed cells. The following objectives are available in our lab:

- CP Achromat 5x/0.12
- CP Achromat 10x/0.25 Ph1
- LD Achrostat 20x/0.3 Ph1
- Achrostat 40x/0.55 Ph2

Images can be taken with a Canon G5 digital camera (5 Megapixel resolution).

3.11.3. Fluorescent microscope

The epifluorescence microscope used was a Zeiss “Axiophot 2” equipped with the following objective lenses:

- Plan-Neofluar 16x/0.5
- Fluor 40x/1.3 Oil, Ph3
- Plan- Neofluar 40x/1.3 Oil
- Plan-Apochromat 63x/1.4 Oil
- Plan- Neofluar 100x/1.3 Oil

For the quality control of fluorochromes in the FISH experiments this microscope is used. A mercury lamp (100W) served as a light source for excitation of fluorochromes.

Images were taken with a Coolview CCD camera with a spectral response of 400-900nm and a CCD chip resolution of 753x576pixels. Cytovision software is from Applied Imaging Int, Newcastle.

Following filter sets were used for the visualization of the respective fluorochromes

(Table 8):

Fluorochromes	Excitation filter	Beam splitter	Emission filter
DAPI	BP 365	FT 395	LP 450-490
Alexa488/FITC	BP 450-490	FT 510	LP 515-565
CY3/TAMRA	BP 546	FT 580	LP 590
Alexa633/CY5/TOPRO3	BP 575-625	FT 645	BP 660-710
Triple filter	TBP 400/495/570	FT 410/505/585	TBP 460/530/610

3.11.4. Confocal laser scanning microscope (CLSM)

Confocal microscopy is used for all quantitative evaluations. The advantage of confocal microscopy is the better axial resolution. As a light source in this case lasers of definite wavelengths are used, to excite specifically individual fluorochromes. The scanning unit is responsible for the sequential excitation and is imaging a region of interest (ROI) voxel by voxel, lane by lane and from one plane to another. A pinhole, in front of the detector is eliminating light from other planes. Signals are detected by a photomultiplier. To collect high resolution images I used a HCX Plan-Apochromat 63x/1.40 oil objective lens. To localize embryos utilizing transmission light a Plan-Neofluar 10x/0.3 Ph1 objective lens was used.

Over time different CLSM types were used. Depending on the utilized CLSM the following set ups/parameters were used to visualize the according fluorochromes

(Table 9):

	Laser type, wavelength	Beamsplitter	Emission filter
Leica SP1			
Alexa488/FITC	Argon, 488nm		
CY3/TAMRA	Helium/Neon, 543nm		
Alexa633/CY5/ TOPRO3	Helium/Neon 633nm		
Zeiss LSM 410		FT 488/543	
Alexa488/FITC	Argon, 488nm, 15mW		BP 502-542
CY3/TAMRA	Helium/Neon, 543nm, 0.5mW		BP 575-640
Alexa633/CY5/ TOPRO3	Helium/Neon, 633nm, 5mW		LP 650

Leica TCS SP2			
DAPI	UV, 450nm, 50mW		AOTF*
Alexa488/FITC	Argon, 488nm, 20mW	TD 488/568/647	AOTF*
CY3/TAMRA	DPSS, 561nm, 10mW	RSP 525	*
TexasRed	Helium/Neon, 594nm, 2.5mW		AOTF*
Alexa633/CY5/ TOPRO3	Helium/Neon, 633nm, 10mW	RSP 650	AOTF*
Leica TCS SP5			
DAPI	Blue diode, 450nm, 50mW		AOTF*
Alexa488/FITC	Argon, 488nm, 20mW	TD 488/568/647	AOTF*
CY3/TAMRA	DPSS, 561nm, 10mW	RSP 525	AOTF*
TexasRed	Helium/Neon, 594nm, 2.5mW		AOTF*
Alexa633/CY5/ TOPRO3	Helium/Neon, 633nm, 10mW	RSP 650	AOTF*

*AOTF (**A**custo **O**ptical **T**unable **F**ilter): allows an interactive definition of the detected spectrum.

3.12. Data evaluation

3.12.1. Shift correction

For the correction of chromatic aberrations polychromatic beads (diameter = 500nm) are scanned with the same settings like for data collection. According to those image stacks chromatic shifts can be calculated and image stacks of collected data can be corrected appropriately. Those corrections are done using the software ImageJ 1.35k (<http://rsb.info.nih.gov/ij/>) and a plugin designed and implemented by B. Joffe from the Cremer group. Shift corrections in xy-dimension are usually so small that they can be neglected but in z-dimension shifts for the different channels need to be corrected.

3.12.2. Deconvolution

Fluorescent images, even taken at CLSM suffer from out-of-focus light, which decreases the image resolution. To get rid of this additional light, so called deconvolution programs are available. Deconvolution is a process of reversing the optical distortion that takes place in a microscope to create clearer images. Best images can be obtained by the assumption that a theoretical point source of light is in an optically perfect instrument, convolved with a **point spread function (PSF)**, that

is, a mathematical function that describes the distortion in terms of the pathways this point source takes through the instrument. Usually each point source contributes to a small area of fuzziness to the final image. Utilizing monochromatic beads (diameter = 175nm), which are imaged at the CLSM using similar settings as for data collection, the corresponding deconvolution corrections can be measured and implemented into the program set-up for deconvolution, in our case Huygens software. General parameters are necessary for proper results, such as numerical aperture of used objectives, lens medium refractive index and medium refractive index. They can be changed manually in the programs parameter file. This should ideally result in data stacks that are free from light of sections above and beneath the respective section (Albiez et al. in preparation). On the contrary there are several adjustable parameters for the set up that might be a source of error foremost applying thresholds, which is always based on subjectivity. Of course the obtained results should be discussed critically because this procedure is hardly depending on the chosen settings that if not chosen properly can lead to artificial images and therefore misinterpretations (Conchello and Lichtman 2005; Walter et al. 2006).

3.12.3. Image J

With this freely available Java based program (<http://rsb.info.nih.gov/ij/>) numerous image data processing can be performed. This includes chromatic shift correction, which is done utilizing a plugin. The single *.tif images recorded for one nucleus at the microscope are transformed to one single *.tif file (a so called image stack) containing all single images of an individual channel. RGB stacks (representing a multi-channel file containing three individual channels) and maximum intensity projections (reducing the stacks to one plane including the brightest voxel for a each xy-position from all the stack) can be created. For most of the data processing steps plugins are available. For the evaluation programs 3D-RRD and ADS (see below) thresholds have to be determined for each channel. This was accomplished with ImageJ as well. There is an option to fill holes in the DAPI structure, which is necessary if DAPI serves as a reference structure in the ADS program. For 3D-RRD and ADS programs the internal DAPI structure is not of interest, it is only used as a reference to determine the nuclear borders. Therefore it is convenient to reduce the image complexity of DAPI DNA counterstain and use a mask instead of the original data file, which will only consist of pixels with the maximum intensity (255) within the nucleus and of black pixels, e.g. with the intensity 0 outside of the nucleus. The calculation time of the programs are such, much shorter. In a second, also time reducing step, the size of the mask file could be reduced by multiplying it with a grid.

The result consists of an equivalent mask, which excludes 3 out of 4 pixels – a reduction of voxel density. This reduced stack is used for calculation of the counterstain curve.

Additionally, background signals can be cut out with the program by using functions like “clear” or “clear outside”. This is necessary if e.g. two nuclei are imaged simultaneously or if unspecific signals outside of the nucleus are present. In a certain evaluation of the NT embryo data set it was necessary to cut out the CTs harboring the GOF signal or not, respectively. Contrast enhancement should be avoided since evaluation programs are highly intensity dependent.

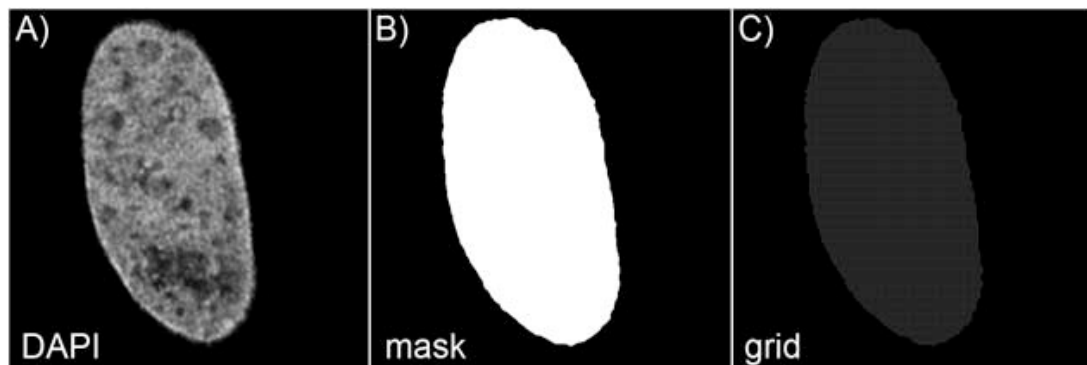


Fig. 15) Processing of DAPI channel: Original DAPI DNA counterstain (A); applied threshold (B) and reduced mask (C) of a reference channel; shown is a mid section of a BFF 451-1 nucleus.

3.12.4. Quantitative data evaluation

In the following a few remarks are made concerning the utilization of 2 different evaluation programs “relative radial distribution” (RRD) and “enhanced absolute distance to surface” (eADS):

Both programs are explained in chapter 3.12.4.1. and 3.12.4.2.. Note that the RRD program was only used for the evaluation of human fibroblast data concerning the distribution of chromosomes depending on the cell cycle stage. All other evaluations were performed with the eADS program and normalized afterwards to the smallest nuclear radius. For a comparison the same data set was exemplarily evaluated with both programs. The program RRD measures the distance of a given signal voxel to in relation to the center of the nucleus, while the ADS program is measuring the distance of a given signal voxel towards the nuclear border. Both programs normalize the results in relation to the nuclear diameter. In the RRD program 0% reflects the nuclear center, while 100% is depicting voxels at the nuclear periphery. On the contrary in the eADS program: 0% represents the nuclear border, while 100% is the nuclear center.

In the result part only the **normalized medians** are shown. Medians instead of means were preferred because the distribution of the curve itself can be neglected in this case. Normalization was done because all distances of all nuclei were comparable then. In the appendix a list of all detailed values can be found, including not only normalized data but also absolute values. It should be kept in mind that in the appendix absolute eADS values are given as negative numbers (in nm) for a location inside the reference structure, positive reflecting a position outside the reference structure. Normalized values are represented accordingly as a fraction, i.e. a value between 0 and 1 with negative or positive, depending whether the distance describes a position outside or inside the reference object. For simplicity the values are changed to commonly known percentage values between 0 and 100, with positive values depicting signals further inside the reference structure and negative once outside.

3.12.4.1. Three dimensional – **Relative Radial Distribution (3D-RRD)**

This program was developed by J. von Hase (Kirchhoff Institute for Physics (KIP), Heidelberg). It was mainly used for round and regularly shaped cells. It is described in (Cremer et al. 2001). Briefly it divides the nucleus into 25 concentric shells (3D) or rings (2D). All voxels of a given signal, defined by a determined threshold, which was individually done by hand, were assigned to a shell/ring. For all voxels of a certain signal the **average relative radius (ARR)** was calculated and normalized to the nuclear radius. 0% was representing a voxel at the nuclear center, 100% was a signal at the nuclear border. In this way a radial distribution is determined which can be used to calculate the preferential localization of this objects, e.g. the CTs.

3.12.4.2. **Absolute Distance to Surface (ADS) or Enhanced Absolute Distance to Surface (eADS)**

For the need of evaluating flat and irregular shaped cells a program called ADS was designed by J. von Hase (KIP, Heidelberg). A program that works analogously i.e. measures the distance of a signal to a given reference structure was developed by T. Thormeyer in the group of T. Cremer (Thormeyer 2005). Both programs follow the same principles of evaluation. For each voxel of a segmented fluorescent object, such as a CT, the shortest distance to the border of a segmented reference border such as the nucleus is determined. Segmentation of objects is accomplished by thresholding the respective images. Distances were assigned to equidistant shells. To compensate for different size and shape of the reference objects the distances can be normalized additionally with respect to their smallest radius. A median value

was calculated, which was representative for the curve. Be careful the percentage values were exactly the opposite with this program. 0% was reflecting a position at the nuclear periphery. 100% was depicting a signal at the nuclear center.

3.12.5. Photoshop (CS2, Adobe systems, Inc., S. Jose)

The program "Photoshop" is used for illustrating the results. RGB-pictures, including texts and other graphical objects, can be done very conveniently.

3.12.6. Amira

Former TGS Amira (Version 2.3), current Amira 4 is a 3D reconstruction program, now available from Mercury Computer Systems Inc. The striking feature of this program is that one can visualize objects in 3D and view them from all perspectives. Parts of such a 3D rendered object can be cut e.g. to visualize the inside of a nucleus. There are several possibilities of displaying images, e.g. *orthoslice* and *isosurface*. In the *orthoslice* mode the user can go stepwise through the stacks similar to ImageJ. The *isosurface* mode displays a 3D image after 3D rendering by using a certain threshold. The actual view of a specifically reconstructed 3D image data set can be stored as a "snapshot" image.

3.12.7. Statistics

All statistic evaluations were performed with the Systat program (San José, CA, USA; <http://www.systat.de/>). In general it was necessary to compare different distributions for their dissimilarity and especially the significance of the differences found. The program itself checks automatically for the curve distribution and gives further advises for sufficient significance tests. As far as a t-test is only applicable to normal distributed curves, a Mann-Whitney Rank Sum test, applicable to all curves, is performed.

4. Results:

All results concerning sister cell arrangements are described in the attached manuscript (see appendix 7.3.). Only a brief overview of those results is given in the following chapter. Thereafter results concerning cell cycle dependent CT distributions are described. In the following part all experiments concerning shape dependent CT patterns are shown and finally all results from experiments using bovine preimplantation embryos are described, starting with the results found for gene-rich and gene-poor CT arrangements, followed by the distributions of a Oct4-GFP transgene in an active and repressive state, respectively.

4.1. Similarity of chromosome arrangement is lost after two cell cycles in HeLa and normal diploid cells

Chromosomes occupy non-random tissue-specific positions in the interphase nucleus that correlate with the chromosome size and gene richness (Croft et al. 1999; Cremer et al. 2001; Bolzer et al. 2005); they can also have probabilistically preferred neighbors that might cause certain translocation frequencies (Parada et al. 2004; Meaburn and Misteli 2007). Earlier studies reached opposite conclusions about the degree of the transmission through mitosis of chromosome arrangement present in a given cell (Gerlich et al. 2003; Walter et al. 2003). The transmission was described as completely inherited by the Ellenberg group (Gerlich et al. 2003). In contrast findings in our group showed that only about one third of cells showed a transmission of CT pattern, whereas other cells can vary in their CT pattern (Walter et al. 2003). None of these studies, however, analyzed more than one cell cycle and used sufficiently rigorous measures for quantitatively assessing similarity of chromosome arrangement. Combining living cell studies and studies with fixed cells, also monitored during their growth, we studied the arrangement of 6-7 chromosomes in clones of up to 32 cells (5 divisions). Nuclear positions of chromosomes were visualized using FISH and the similarity in chromosome arrangements between cells of a clone was quantified using 3 different measures employing landmark based registration. Both, in HeLa and normal diploid cells, the similarity in chromosome arrangement was lost after only two cell cycles, implying a low level of transmission through mitosis. Despite the finding that in sister cells itself the similarity of CT arrangements can be very high also couples which differ in their CT arrangements were found. In a discussion of factors affecting the degree of the transmission we partially reconcile the contradicting results of earlier studies. For a detailed description and discussion see manuscript attached in the appendix (7.3.).

4.2. Distribution of gene-rich and gene-poor CTs in dependency on nuclear shape and cell cycle

4.2.1. Human fibroblasts data with flat shaped nuclei

By using 24-color-M-FISH, to distinguish all human chromosomes in a nucleus, the CT distribution in human fibroblasts was found to correlate with chromosome size (Bolzer et al. 2005). To test if this distribution was influenced by the cell cycle stage the following experiments were performed:

Human fibroblasts were grown on coverslips. The cell cycle stage of individual cells within a subconfluent culture was determined using the following parameter:

- BrdU was incorporated for 1h and detected afterwards by adequate antibodies.
- Ki-67, a cell-cycle specific nuclear protein was stained with according antibodies (Starborg et al. 1996; Bridger et al. 1998).

Cells in G0 neither revealed BrdU incorporation nor Ki-67 staining. Cells in S-phase showed both – BrdU and Ki-67 positive staining. According to the stage of S-phase, different pattern of BrdU incorporation could be distinguished (Solovei et al. 2006). Cells considered as different categories in the present study, clearly assigned to the S- or G0 stage were chosen for image acquisition and subsequent analysis. Evaluations were made in 2D and 3D, using the 2D-/3D-RRD program. As far as fibroblast cells are very flat the evaluation in 2D was done in comparison to detect any kind of differences in the evaluation methods. For CT 18 and CT 19 evaluations were additionally performed using the eADS program in order to compare both programs.

The cell cycle dependent radial distribution of three chromosome pairs were analyzed in each time 20 nuclei, whereas the pairs differed concerning their gene size and gene density:

4.2.1.1. Cell cycle dependent distribution of big vs. small chromosomes (HSA 1 vs. HSA 20)

Human chromosome 1 (247Mb; 10.9 genes/Mb) and human chromosome 20 (62Mb; 12.0 genes/Mb), both metacentric, without NOR regions (NOR bearing chromosomes are known to localize around the nucleoli), were chosen to represent the biggest and the smallest human chromosomes. Both chromosomes have a similar gene density (9 genes/Mb).

In 2D evaluations the results were more pronounced than in 3D: CTs 1 showed an ARR of 67% in S phase cells and at 71% in G0 cells. The small CTs 20 had an ARR of 55% in cycling cells and 47% in G0 cells.

Analysis of their 3D distribution showed that the big chromosomes 1 were located at the periphery in both investigated cell cycle stages. The ARR (=average relative radius) was 74% for G0 and 73% for cycling cells. In contrast, the small chromosomes 20 were located in the interior of the nucleus. The ARR in cycling cells revealed a value of 62% and 56% for G0 cells. A shift of CTs 20 towards the interior was observed in G0 cells.

The difference between the CTs 1 and 20 was significant in all investigated cases (3D and 2D G0, as well as 3D S-phase cells: $p < 0.001$ and 2D S-phase cells: $p = 0.006$). In comparison to the overall DNA distribution, significance tests revealed that chromosomes 1 were clearly shifted towards the nuclear border ($p < 0.001$), while chromosomes 20 were shifted significantly towards the interior ($p < 0.001$). Comparing the curves between G0 and S-phase revealed no significant differences for CT 1 (3D: $p = 0.957$; 2D: $p = 0.597$) and CT 20 (3D: $p = 0.086$; 2D: $p = 0.086$).

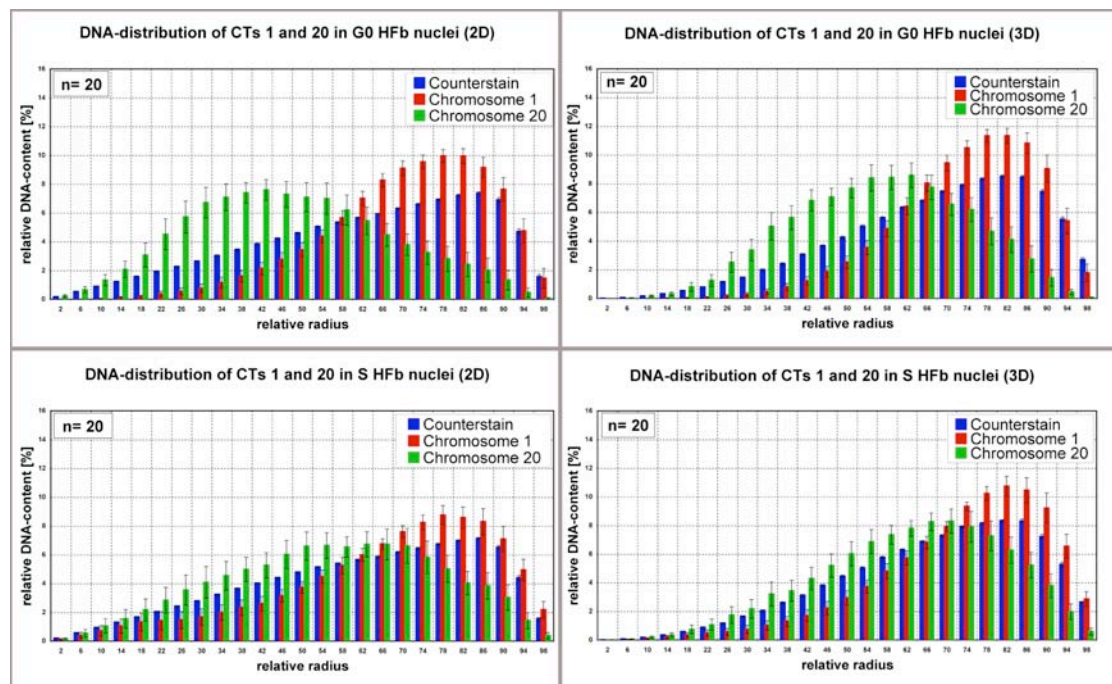


Fig. 16) 2D (left column) and 3D (right column) Relative Radial Distribution (RRD) of chromosomes 1 (red), 20 (green) and TOPRO DNA-counterstain (blue) in G0 (upper panel) and cycling (lower panel) human fibroblasts.

4.2.1.2. Cell cycle dependent distribution of gene-rich vs. gene-poor chromosomes (HSA 17 vs. HSA Y)

Human chromosomes 17 and Y were chosen because they are both small but different in their gene content. Differences in gene density dependent distributions are detectable with this pair of chromosomes. The small and gene-poor chromosomes Y (58Mb; 2.5 genes/Mb) were found shifted to the interior of the nucleus: in G0 cells the ARR was 43% for 2D and 59% for 3D evaluations, while the evaluation in cycling cells revealed an ARR of 34% in 2D and 51% in 3D. Comparing the curves of HSA Y from G0 and S-phase cells a significant difference was found for 3D evaluations ($p=0.016$) but not for 2D ($p=0.062$).

In comparison to CTs Y the small but gene-dense human chromosomes 17 (79Mb; 18.8 genes/Mb) were located more at the periphery. A significant difference between the distributions of both chromosomes (3D: $p=0.021$; 2D: $p=0.005$) was found for cycling cells but not for quiescent cells (3D: $p=0.860$; 2D: $p=0.108$). The ARR values for CTs 17 in G0 cells were 52% for 2D and 58% for 3D evaluations. In cycling cells the ARR was 50% in 2D and 58% in 3D. There is no significant difference found for HSA 17 between G0 and cycling cells (3D: $p=0.648$; 2D: $p=0.279$).

In comparison to the counterstain reference both chromosomes were located more internally with $p<0.001$ in all cell cycle stages.

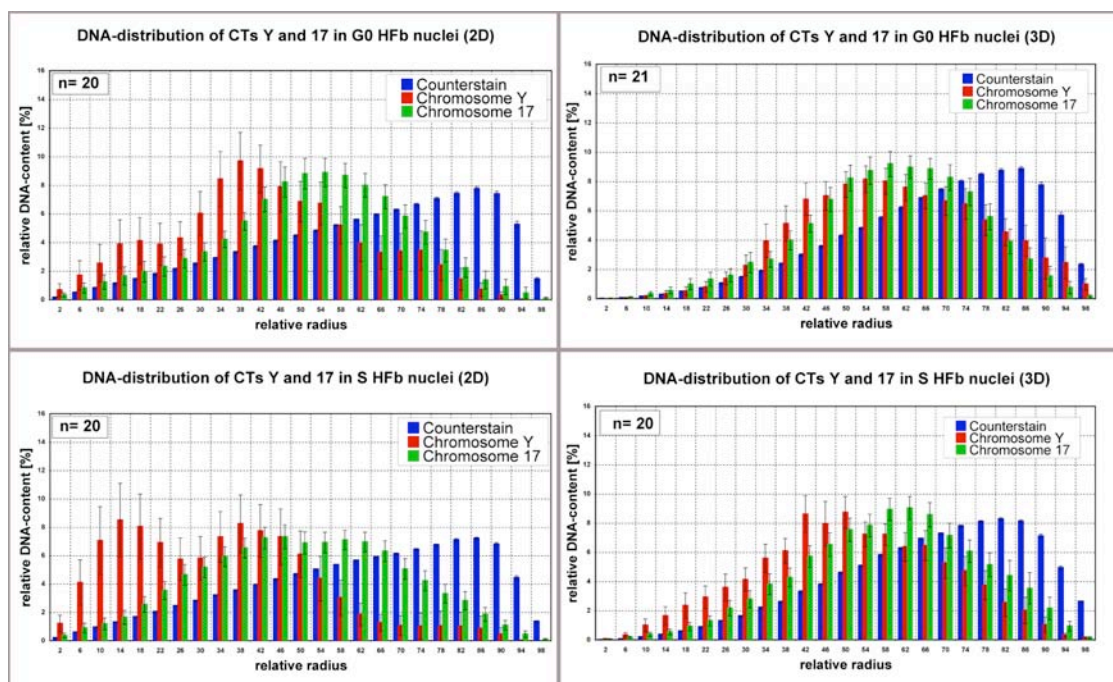


Fig. 17) 2D (left column) and 3D (right column) Relative Radial Distribution (RRD) of chromosomes Y (red), 17 (green) and TOPRO DNA-counterstain (blue) in G0 (upper panel) and cycling (lower panel) human fibroblasts.

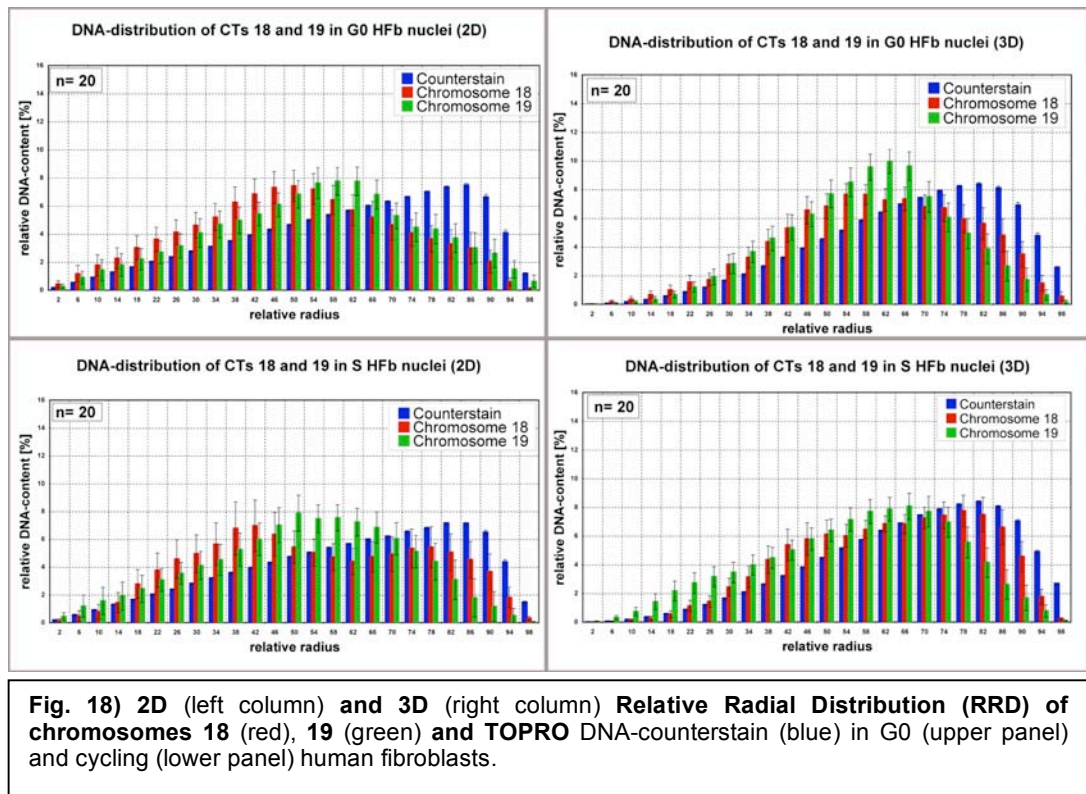
4.2.1.3. Cell cycle dependent distribution of gene-poor vs. gene-rich chromosomes (HSA 18 vs. HSA 19)

Additionally the very well investigated human chromosomes 18 and 19 were chosen for additionally cell cycle dependent experiments. Previous studies (see Introduction; 2.2.4.5.) showed contradictory results concerning their location. Human chromosomes 18 (76 Mb) and 19 (64 Mb) are both of comparable size but differ significantly in their gene-density. The gene content for CT 18 (5.2 genes/Mb) is very low in contrast to the most gene rich human chromosome 19 (25.5 genes/Mb) (http://www.ensembl.org/Homo_sapiens/index.html; ensembl release 49 – March 2008; 18.06.2008).

In both cell cycle stages, G0 and S-phase cells, CTs 19 were found more interior than CTs 18, showing a gene-density dependent distribution, however, differences were not significant if evaluation was done with the RRD program.

In 2D evaluations the ARR for CTs 18 was 50% in G0 and 54% in cycling cells, showing no significant difference ($p=0.448$). For CTs 19 the ARR in G0 was 54% and 51% in cycling cells, revealing again a similar result ($p=0.146$). The slight differences in the ARRs of CTs 18 compared to CTs 19 were statistically not significant ($p=0.457$ in G0 and $p=0.757$ in cycling cells).

The results using the 3D approach with the RRD software showed for CTs 18 an ARR of 60% and for CTs 19 an ARR of 58% in G0 cells. For cycling cells the ARR was 62% for CTs 18 and 56% for CTs 19. The statistic comparison between CTs 18 and 19 in G0 and S-phase cells revealed no significant difference in the distribution of both CTs ($p=0.675$ and $p=0.126$ respectively). The shifts of CTs 18 towards the periphery from G0 to S-phase (3D: $p=0.482$; 2D: $p=0.448$) and for CTs 19 (3D: $p=0.617$; 2D: 0.146) in the opposite direction were also not significant. CTs 18 and 19 in G0 and in cycling cells (in 2D and 3D) were shifted both towards the interior if compared to the overall chromatin distribution ($p<0.001$).



The results could be confirmed in parts using the eADS program. Similarly to the RRD program CTs 18 were generally located more at the periphery than CTs 19. However differences became significant using the eADS program. The normalized distributions of CTs 18 and 19 in G0 cells were significantly different ($p=0.039$). The median for CT 18 was 46% and for CT 19 58%. The difference between the nuclear localization of CTs 18 and 19 in S-phase cells was significantly different ($p=0.014$) for normalized values. For CT 18 the median was 46% and 51% for CT 19. The distributions of CTs 18 and CTs 19 compared between S and G0 cells revealed no significant differences ($p=0.465$ and $p=0.860$ respectively).

In an additional evaluation the distribution of all nuclei – mixing cells of S-phase and G0 - were evaluated together in eADS program, revealing again a significant difference between CTs 18 and CTs 19 with $p<0.001$. The median for CTs 18 was 46% and for CTs 19 56%. All curves for CTs 18 and 19 were significantly different ($p<0.001$) to the global DNA distribution as visualized by TOPRO staining.

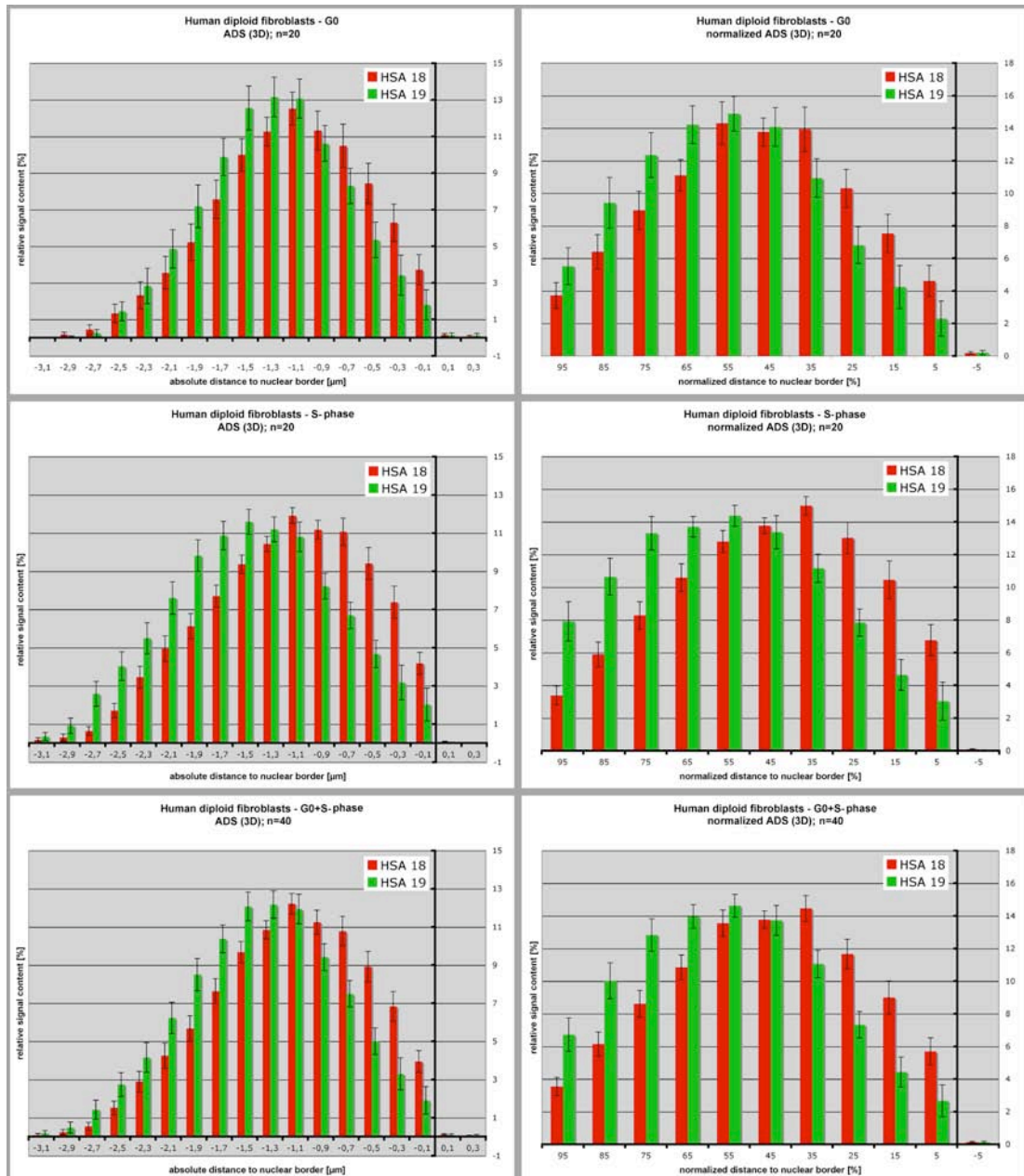


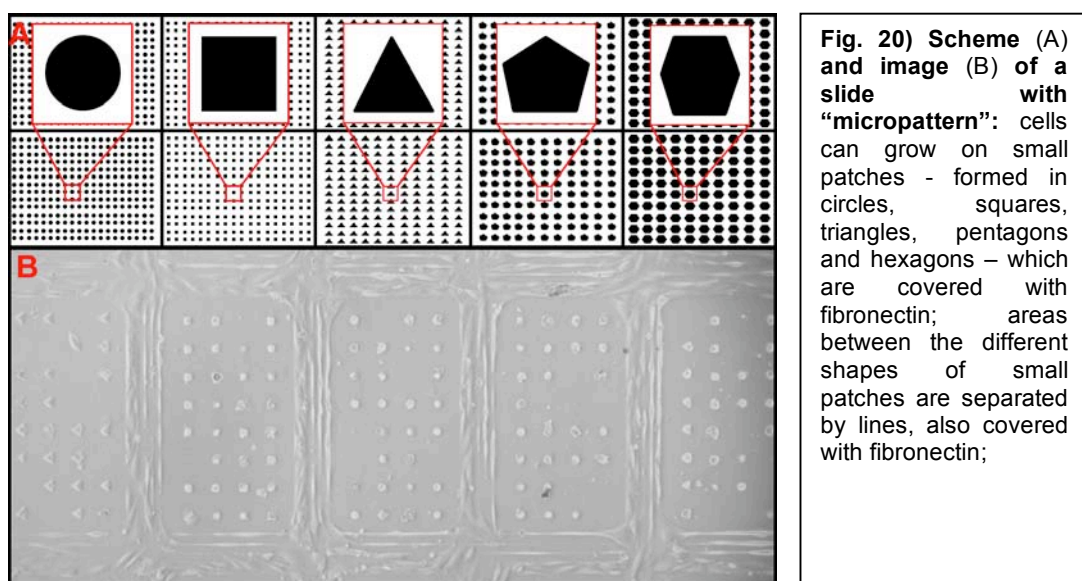
Fig. 19) Normalized (right column) and enhanced Absolute (left column) Distance to Surface (eADS) measurements of CTs 18 (red) and 19 (green) in G0 (upper panel), cycling (mid panel) and a mixed (lower panel) population of human fibroblast cells.

The results show the same tendencies in all evaluations despite the significances revealed some differences. Of course the reason for this might be attributed to the evaluation programs as well. A detailed comparison between both evaluation approaches – RRD and ADS – in one, two or three dimensions will be published in a manuscript together with J. von Hase (von Hase et al. submitted).

4.2.2. Inducing a change of nuclear shape by growing fibroblasts on micropattern

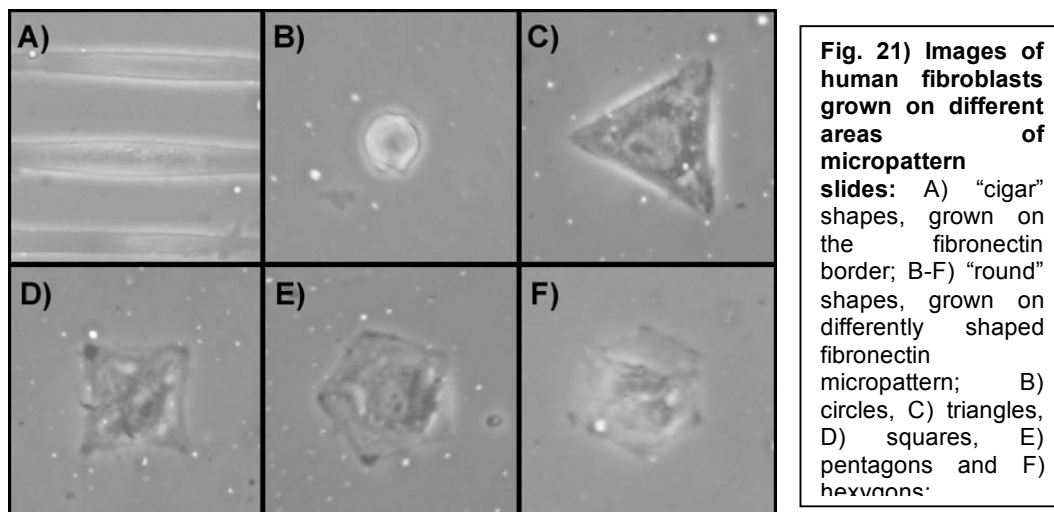
The result for the radial distribution of gene-rich and gene-poor chromosomes in human fibroblasts (Bolzer et al. 2005) differs from those in lymphocyte data (Croft et al. 1999; Cremer et al. 2001). In fibroblasts chromosomes were distributed predominantly according to their size, while in lymphocytes the gene density is the most influential parameter. A striking difference between those two cell types is the shape of their nuclei. To answer the questions whether the distribution of CTs is depending on the shape of nuclei the following experimental set up was used: The shape of nuclei in flat fibroblast nuclei was artificially altered by constricted growing conditions.

With special “micropatterned” slides, kindly provided by D. Ingber (Harvard Medical School, Boston, USA) cells were forced to attach on a very limited space, which resulted in differently shaped nuclei (see Fig. 20/21). Experiments were performed using fibroblasts of different species (Homo sapiens, Wolf’s guenon and Bos Taurus). The investigated chromosomes were the homologues of gene-poor and gene-rich chromosomes HSA 18 and 19, respectively and bovine gene-poor and gene-rich chromosomes BTA (*Bos Taurus*) 20 and 19. Lamin B was visualized as an additional outline for the nuclear borders and to detect invaginations of the nuclear lamina as it might act as an anchor for chromosomes. To compare the impact of different nuclear shapes on nuclear architecture spherical and cylindrical, “cigar” shaped nuclei were compared to the native flat ellipsoid nuclei.

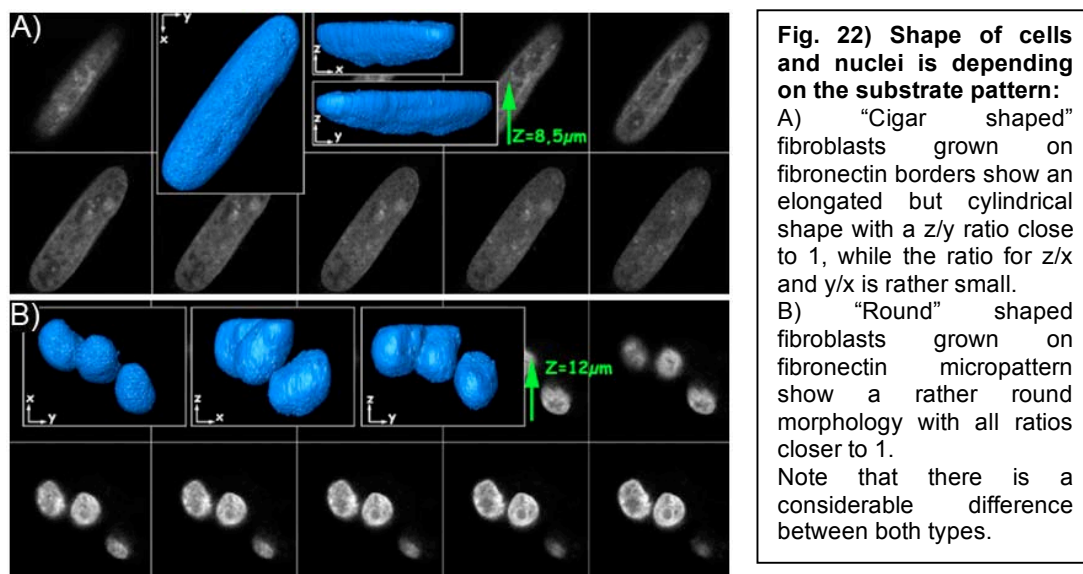


4.2.2.1. Morphology and shape of nuclei from fibroblasts grown on micropattern

The morphology of cells grown on micropattern slides is different to those grown on normal surfaces. Attachment of the cells was mediated by fibronectin, which was added to certain small areas on the slide. Cells could only grow on these areas and developed consequently a new morphology due the limited space (Ingber 2003). The slides were subdivided into different areas. Each area contained a different shape of micropattern – circles, triangles, squares, pentagons and hexagons (see Fig. 21 B-F) – whereas also the size of the various shapes varied. The areas including equally shaped micropattern were separated from each other by lines covered with fibronectin as well. Therefore one can find very elongated fibroblasts (so called “cigar”-shaped cells; see Fig. 21A) growing on those fibronectin borders and cells growing on the small and very defined micropattern, which adopted a spherical morphology (in the following called “round”-shaped cells).



Cigar-shaped cells were elongated but not as flat as normal fibroblasts. To characterize nuclei morphology the dimensions in x, y and z were measured. For consistence x is always the long diameter, y the short diameter and z the height of the nucleus. The relation between these values provides information about the roundness for each nucleus. The closer the value comes to 1 the rounder the shape is. For cigar-shaped cells grown on fibronectin borders their z/y diameter of the nucleus was nearly 1, which means that the smaller y-axis and height (z), were nearly the same. However there are elongated like usually grown fibroblasts (see Fig. 22A). In contrast the round-shaped fibroblasts micropattern were not perfectly spherical but the ratio of x- and y-axis in comparison to z-axis was remarkably increased, while x- and y-axis were nearly equal. This results in an overall round shape (see Fig. 22B).



The different medians of size and roundness-factors are graphically depicted in the diagrams shown in Fig. 23. One can clearly distinguish between so called round and cigar shaped cells, the latter one always show an elongated shape (note the big Y diameter). Note that the roundness-factors for all round cells come close to 1 in all cases, while for cigar shapes there is always a much smaller relation if Y is incorporated. For flat shaped fibroblasts (pink triangles in Fig. 23) the height would be on average $6\mu\text{m}$ (with a range from $5\mu\text{m}$ to $8\mu\text{m}$), in comparison all fibroblasts grown on micropattern had a height of $8\mu\text{m}$ (with a range from $5\mu\text{m}$ to $13\mu\text{m}$).

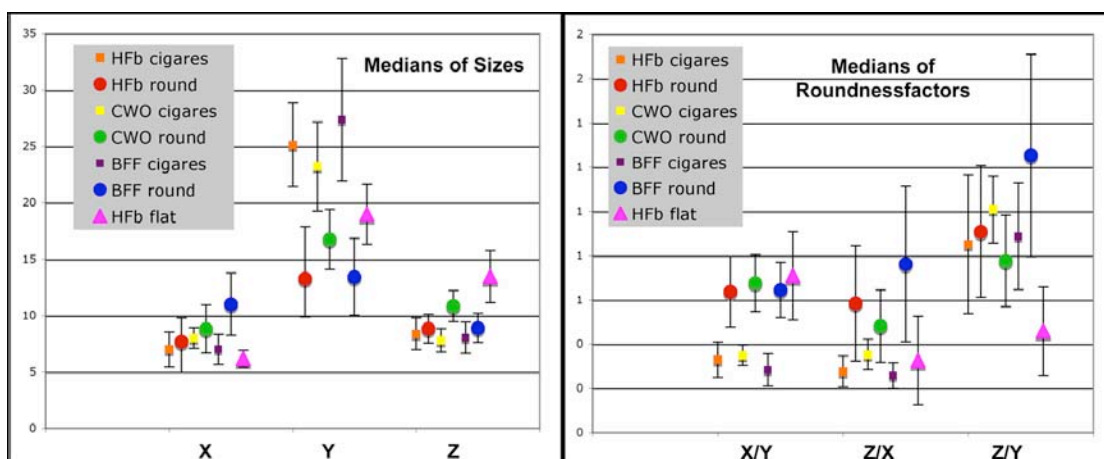


Fig. 23) Medians of size (left diagram) and roundness factors (right diagram) for fibroblasts of different species, grown on slides with micropattern;

All following experiments were evaluated with the “enhanced absolute distances to surface” (eADS) program developed in our group by T. Thormeyer (Thormeyer 2005). For evaluation of CTs several different aspects were taken into consideration. First the absolute distance of CTs in 3D to a given reference surface was measured. Therefore both, nuclear counterstain with DAPI and the nuclear lamina stained by Lamin B were chosen as reference structure. Invaginations in the surface of the nucleus are detectable with Lamin B but not with DAPI. If one of the CTs is bound more to the lamina it is detectable in that way. Additionally the evaluation with DAPI reference was done in 2D. By a comparison of 3D and 2D measurements a preferential location of CTs at the top and bottom of the nuclei should be uncovered. All evaluations were normalized for the smallest radius of nuclei. In the following short overview the evaluations were listed (Table 10):

3D : ADS – ref.: Lamin B	3D : normalized – ref.: Lamin B
3D : ADS – ref.: DAPI	3D : normalized – ref.: DAPI
2D : ADS – ref.: DAPI	2D : normalized – ref.: DAPI

For simplicity only the median of the normalized evaluations will be considered in the following results. Normalized values consider already the different sizes of nuclei and therefore emphasize the difference between distributions without taking into account the different shapes or sizes of nuclei. Note that all distances are given as percentage of the smallest nuclear radius. 0% reflects the nuclear periphery and 100% the center of the nucleus. (Note that these value presentation using the eADS software is opposite to that of the 3D-RRD software. This is because in the former the distance to the nuclear periphery is given, while in the latter the distance to the nuclear center is the basis of the values.) Results were compared statistically using the Mann-Whitney Rank Sum test (Systat program) to detect significant differences between the distributions. A summary of all results (normalized and absolute values) and statistics can be found in the appendix (7.1.2.).

4.2.2.2. Distribution of human chromosomes 18 and 19 in human fibroblast cells

4.2.2.2.1. Cigar shaped cells

Human cigar shaped fibroblasts (n=31) showed a mean length of 25.2 μ m and a mean width of 8.2 μ m, whereas the z-diameter was 7.2 μ m. The mean roundness factor (ratio of the respective diameters; the value is between 0 and 1, whereas 0 means completely elongated/stretched and 1 is a perfect circle) was 0.34 in x/y, 0.29 in z/x and 0.91 in z/y. Elongation was a typical feature of these cells. But the height was not typical for normal growing fibroblasts. (Compare to the ratios of

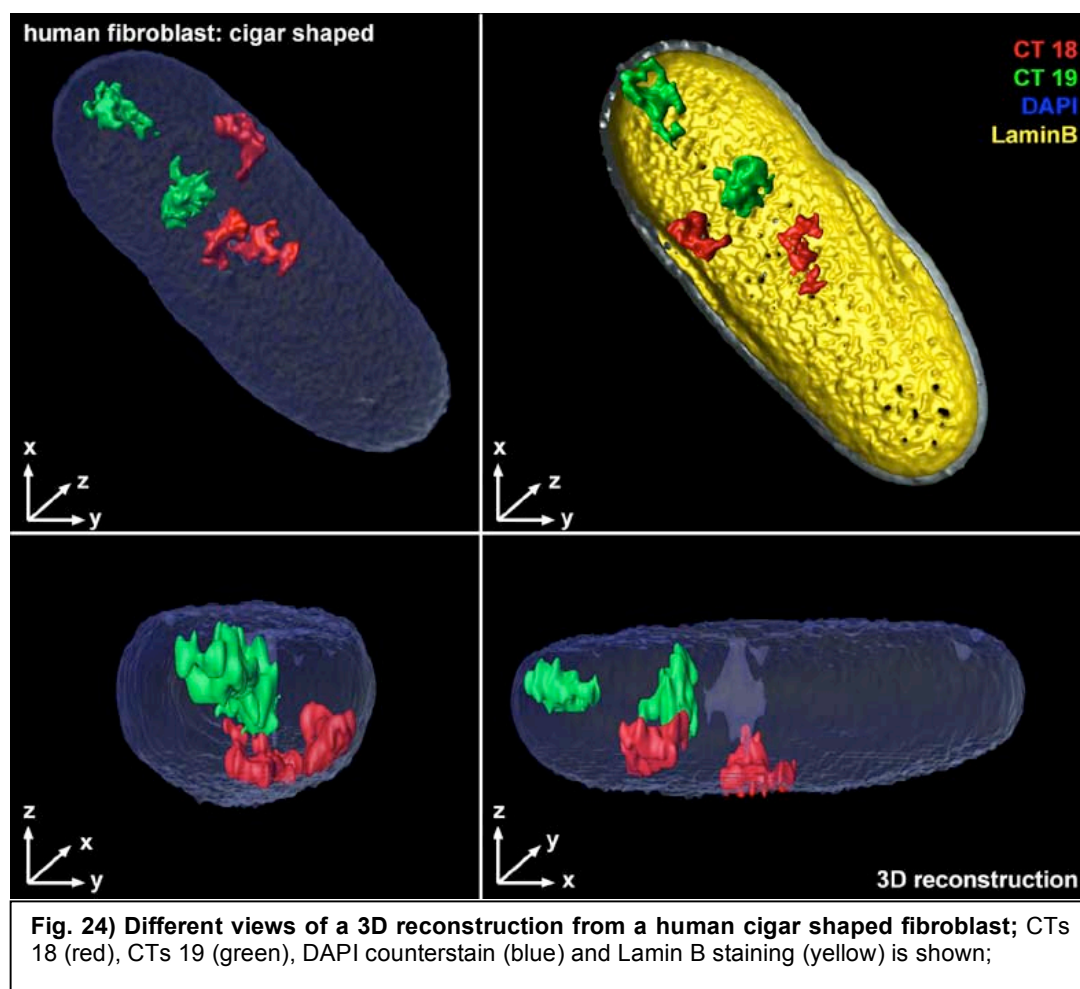
fibroblasts grown on glass coverslips, which is in x/y 0.72, in z/x 0.34 and in z/y 0.47.)

The 2D evaluation showed similar ($p=0.288$) medians for CT 18 (66%) and CT 19 (68%). For 3D evaluations the results were different:

In all cases the CTs 18 were located significantly more outside than CTs 19 ($p<0.001$, for Lamin B and DAPI as a reference structure). The median for HSA 18 was 31% with DAPI as a reference and for HSA 19 the median was 50%. For evaluations with Lamin B as a reference structure the median for CT 18 was 10% and 28% for CT 19, respectively.

All distributions, except the 3D CT 18 curve, measured against Lamin B ($p=0.314$), were significantly different from a global DNA distribution represented by the DAPI staining ($p<0.001$ and $p=0.048$ for CT 18 measured against DAPI).

Examples of cigar shaped human fibroblasts are depicted in Fig. 24. Results of eADS measurements are shown in Fig. 26 (A, C, E).



4.2.2.2.2. Round shaped cells

Nuclei of round shaped cells ($n=34$) have a mean average size of $15.1\mu\text{m}$ in x , $9.0\mu\text{m}$ in y and $8.3\mu\text{m}$ in z . The average roundness factor was 0.63 for x/y , 0.61 for z/x and 0.95 for z/y . Compared to cigar shaped nuclei the fibroblast nuclei were more spherical.

The localization of CTs 18 was more peripheral compared to CTs 19 in all investigated cases (measured in 2D and 3D for DAPI reference and in 3D with Lamin B reference). The median of the global DNA distribution stained with DAPI was 59% in 2D and 31% in 3D. The median for CTs 18 with DAPI reference was 31% for 3D and 59% for 2D evaluation. The evaluation for CTs 19 with DAPI as a reference revealed a median of 53% in 3D and 67% in 2D. With Lamin B as a reference the median for CTs 18 was 11%. CTs 19 measured against Lamin B showed a median of 28%. The radial distribution of CTs 18 and 19 were significantly different in both cases of 3D evaluations ($p<0.001$) but not for 2D evaluation ($p=0.115$). Both chromosomes were distributed significantly different ($p<0.001$) compared to the global DNA distribution while CTs 18 were distributed significantly more outside and CTs 19 more interior. Examples of round shaped human fibroblasts are depicted in Fig. 25. Graphs are shown in Fig. 26 (B, D, F).

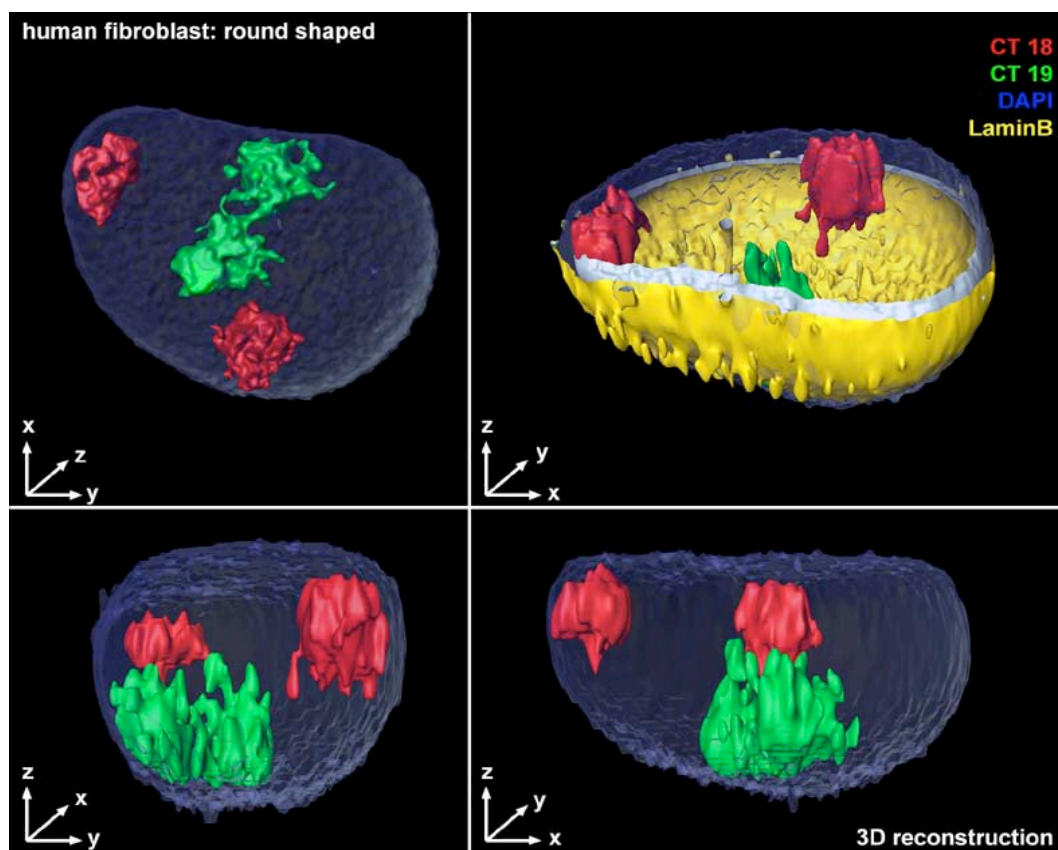


Fig. 25) Different views of a 3D reconstruction from a human round shaped fibroblast; CTs 18 (red), CTs 19 (green), DAPI counterstain (blue) and Lamin B staining (yellow) is shown;

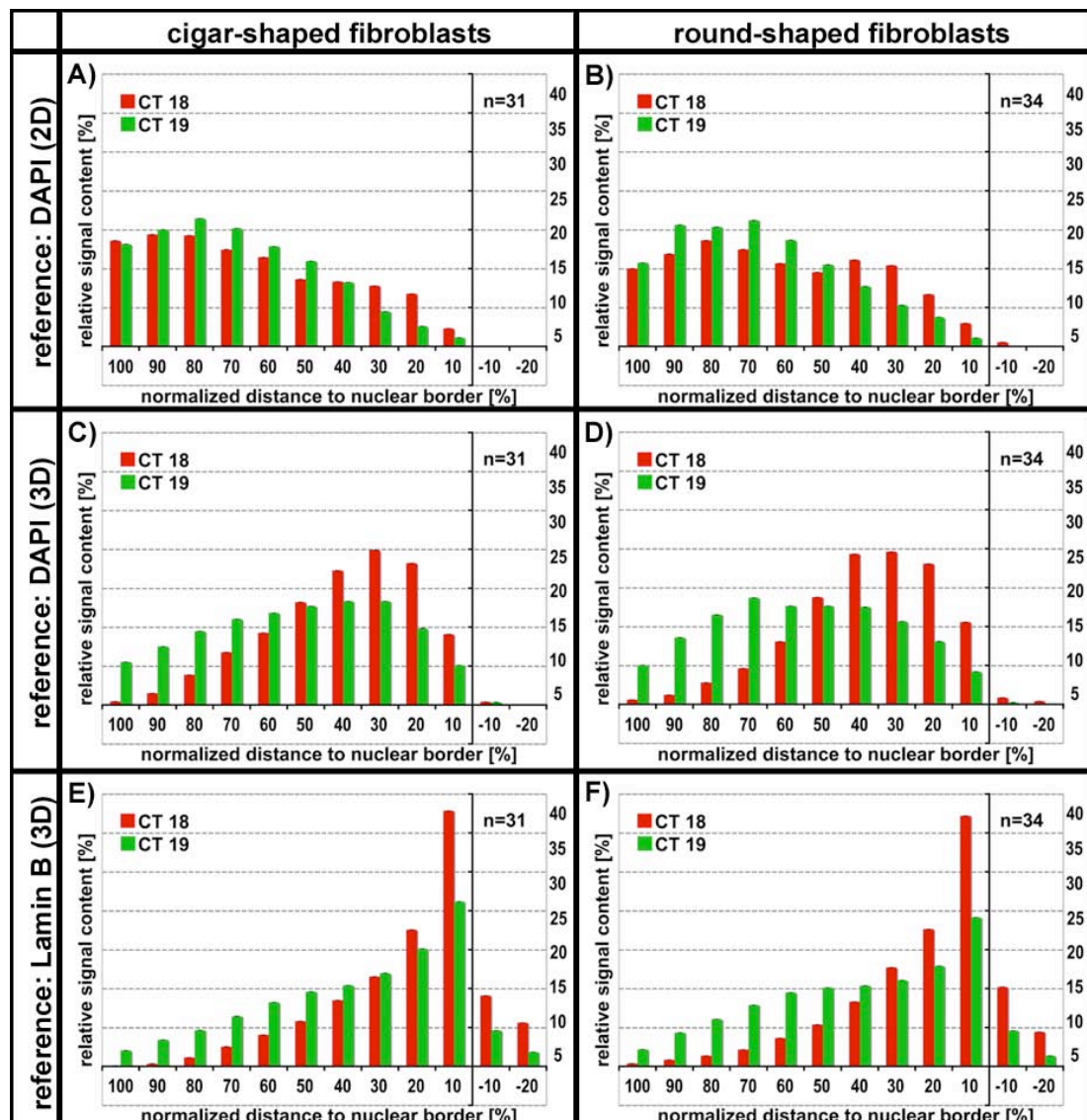


Fig. 26) Normalized eADS measurements for artificially shaped human diploid fibroblasts grown on micropattern slides: results for CT distribution of gene-poor HSA 18 CTs (red) and gene-rich HSA 19 CTs (red) in cigar shaped fibroblasts (left panel) or round shaped fibroblasts (right panel). Evaluations are performed in different ways. The reference for the 3D CT distributions was either the nuclear lamina stained with an antibody against Lamin B (A; B) or the nuclear DNA stained with DAPI (C; D). Measurements with DAPI as a reference structure were performed additionally in 2D (E; F).

4.2.2.3. Distribution of human orthologous chromosomes 18 and 19 in fibroblasts of Wolf's guenon

Chromosomes of the higher old world monkey Wolf's guenon (*Cercopithecus wolfi*) ($2n=72$) are all of a comparable size. In this species, the distribution of gene-poor and gene-rich human orthologous CTs 18 and 19 were shown to follow a gene-density related CT distribution in "normal" flat fibroblasts (Neusser et al. 2007). This was in contrast to the results found for human fibroblasts where CTs are positioned according to chromosome size.

4.2.2.3.1. Cigar shaped cells

Nuclei of 26 cigar shaped cells (see Fig. 27) with a mean length of $23.2\mu\text{m}$ in x-, $7.9\mu\text{m}$ in y- and $8.2\mu\text{m}$ in z were evaluated. The roundness factor was 0.35 in the x/y-, 0.36 in the z/x- and 1.05 in the z/y-plane. Like human fibroblasts these cells were elongated and similar to human cigar shaped fibroblasts.

For all evaluations (see Fig. 29 A, C, E) it was shown that CTs 18 were located significantly more towards the periphery than CTs 19 ($p < 0.001$ for 3D evaluations and $p = 0.002$ for 2D evaluation). In the 2D evaluation the CTs 18 median was found at 47%, while the CTs 19 median was at 68%. Both curves were significantly different from a random DNA distribution ($p = 0.001$). In 3D the median for CTs 18 in reference to DAPI was 26% and 56% for CTs 19, respectively. When Lamin B served as the reference structure the median for CTs 18 was 18%, the one for CTs 19 was 48%. In comparison to the DAPI distribution 3D curves for CTs 19 differed significantly with $p < 0.001$, but not the CTs 18 curves ($p = 0.510$ for Lamin B and $p = 0.964$ for DAPI reference).

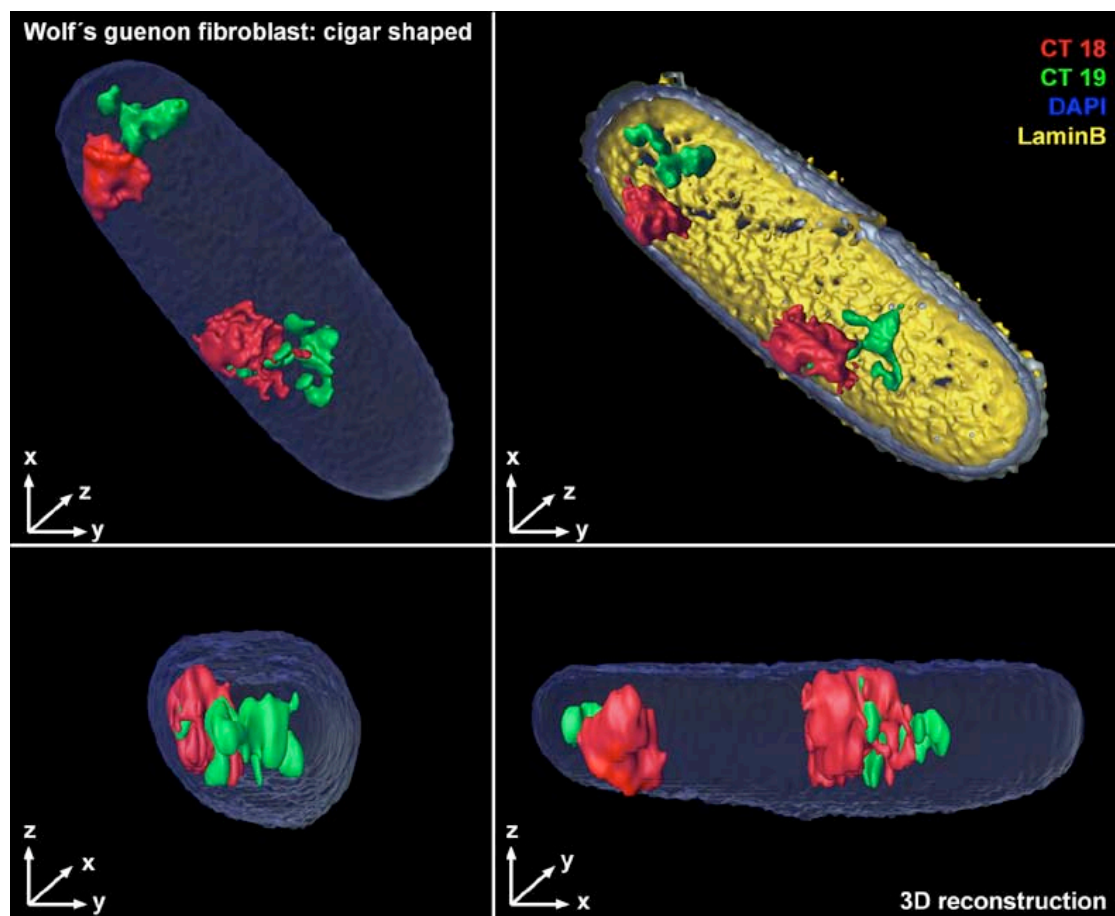


Fig. 27) Different views of a 3D reconstruction from a Wolf's guenon cigar shaped fibroblast; CTs 18 (red), CTs 19 (green), DAPI counterstain (blue) and Lamin B staining (yellow) is shown;

4.2.2.3.2. Round shaped cells

Round shaped fibroblasts of Wolf's guenon ($n=35$) have a diameter of $16.4\mu\text{m}$ in x , $11.1\mu\text{m}$ in y and $8.7\mu\text{m}$ in z . The roundness factor was 0.69 in the x/y -, 0.55 in the z/x - and 0.79 in the z/y -plane, which was very similar to human "round" shaped fibroblasts.

Again CTs 18 were always located more at the nuclear periphery than CTs 19. This difference was significant for 3D evaluation ($p<0.001$) and for 2D evaluation ($p=0.006$). In 2D the median for CTs 18 was 40%, for CTs 19 50%. In 3D using DAPI fluorescence to define the nuclear border the median for CTs 18 was found at 26% and for CTs 19 at 54%. With Lamin B as a reference the median for CTs 18 was 17% and for CTs 19 40%. In comparison to a random DNA distribution all curves, except the 3D curve for CTs 18 in Lamin B evaluation ($p=0.095$) were significantly different ($p<0.001$).

Examples of round shaped fibroblasts of Wolf's guenon are depicted in Fig. 28. Results of eADS measurements are shown in Fig. 29 (B, D, F).

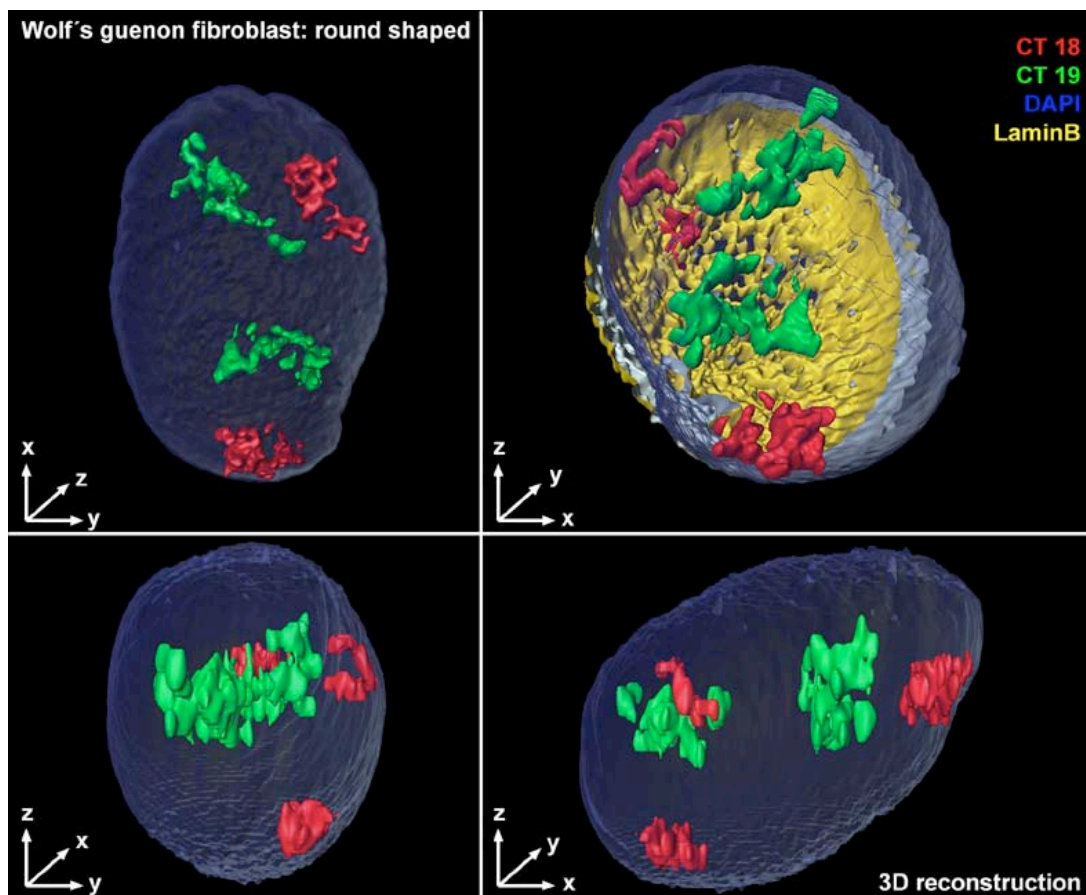


Fig. 28) Different views of a 3D reconstruction from a Wolf's guenon round shaped fibroblast; CTs 18 (red), CTs 19 (green), DAPI counterstain (blue) and Lamin B staining (yellow) is shown;

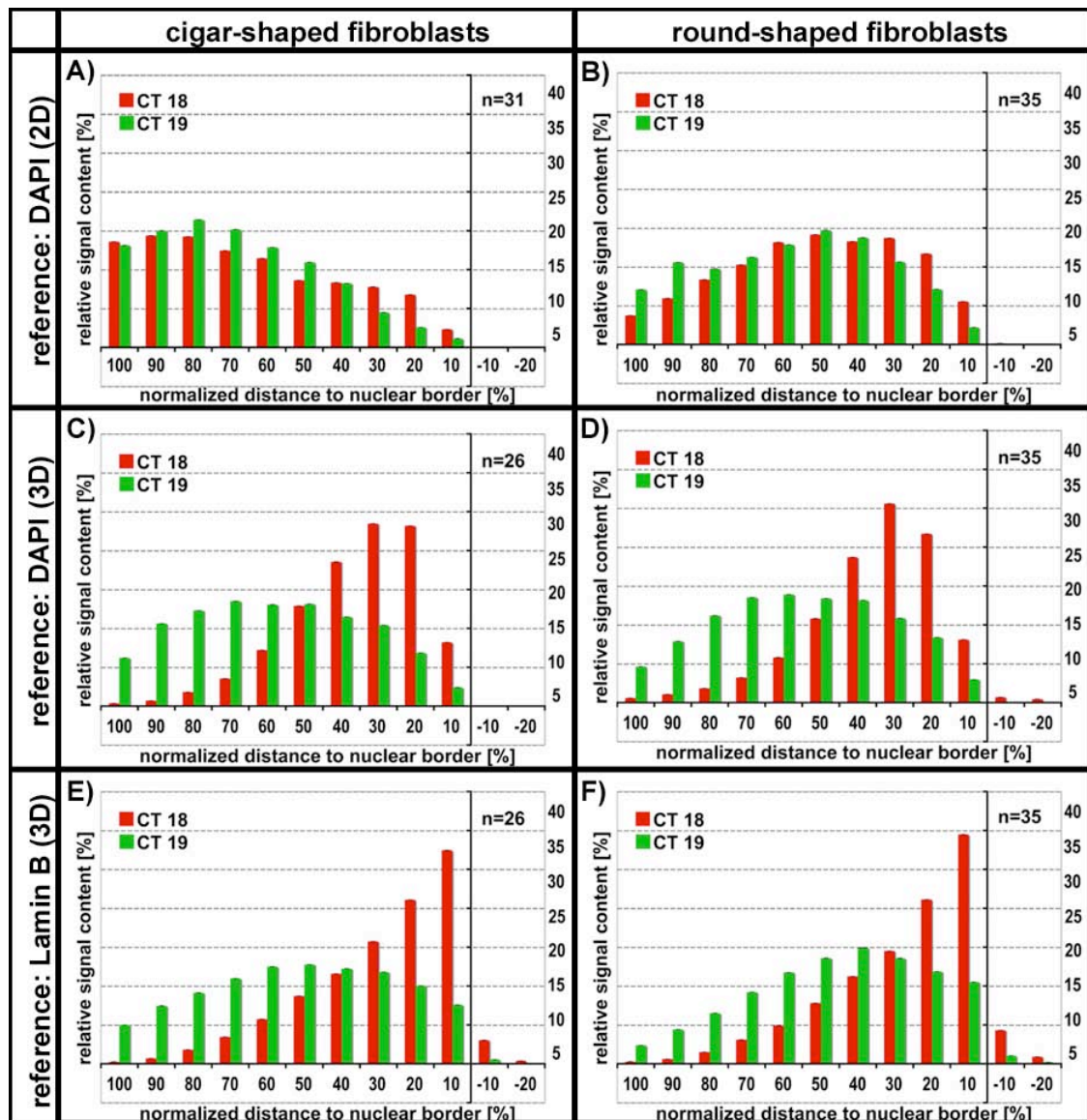


Fig. 29) Normalized eADS measurements for artificially shaped Wolf's guenon fibroblasts grown on micropattern slides: results for CT distribution of gene-poor orthologous CTs 18 (red) and gene-rich orthologous CTs 19 (red) in cigar shaped fibroblasts (left panel) or round shaped fibroblasts (right panel). Evaluations are performed in different ways. The reference for the 3D CT distributions was either the nuclear lamina stained with an antibody against Lamin B (A; B) or the nuclear DNA stained with DAPI (C; D). Measurements with DAPI as a reference structure were performed additionally in 2D (E; F).

4.2.2.4. Distribution of bovine chromosomes 19 and 20 in fibroblast nuclei of Cattle

In the bovine species (*Bos Taurus*, BTA) the chromosomes (except for the sex chromosomes) are rather similar in size (30-100Mb) compared to human chromosomes (50-250Mb). The gene-poorest chromosome is BTA 20 (69Mb; 5.2 genes/Mb), the gene-richest BTA 19 (63Mb; 19.2 genes/Mb, according to Ensembl database). All experiments in cattle concerning gene-density distributions were performed with those chromosomes.

4.2.2.4.1. Bovine fetal fibroblasts (BFF451-1): “normal” flat shape

If bovine fetal fibroblasts were grown on regular glass cover slips, the typical shape of nuclei was flat and ellipsoid. In these cells we found a significant difference in the radial distribution of CTs 19 and CTs 20. Statistical tests revealed a significant difference between CTs 19 and 20. The median for CTs 19 was 56% and for CTs 20 49% respectively (for details and diagram look chapter 4.4.3.).

4.2.2.4.2. Cigar shaped bovine fetal fibroblasts (BFF451-1)

In cigar shaped nuclei ($n=25$) the diameter was $28.2\mu\text{m}$ in x, $8.2\mu\text{m}$ in y and $7.2\mu\text{m}$ in z with a corresponding roundness factor of 0.30 in the x/y-, 0.26 in the z/x- and 0.91 in the z/y-plane.

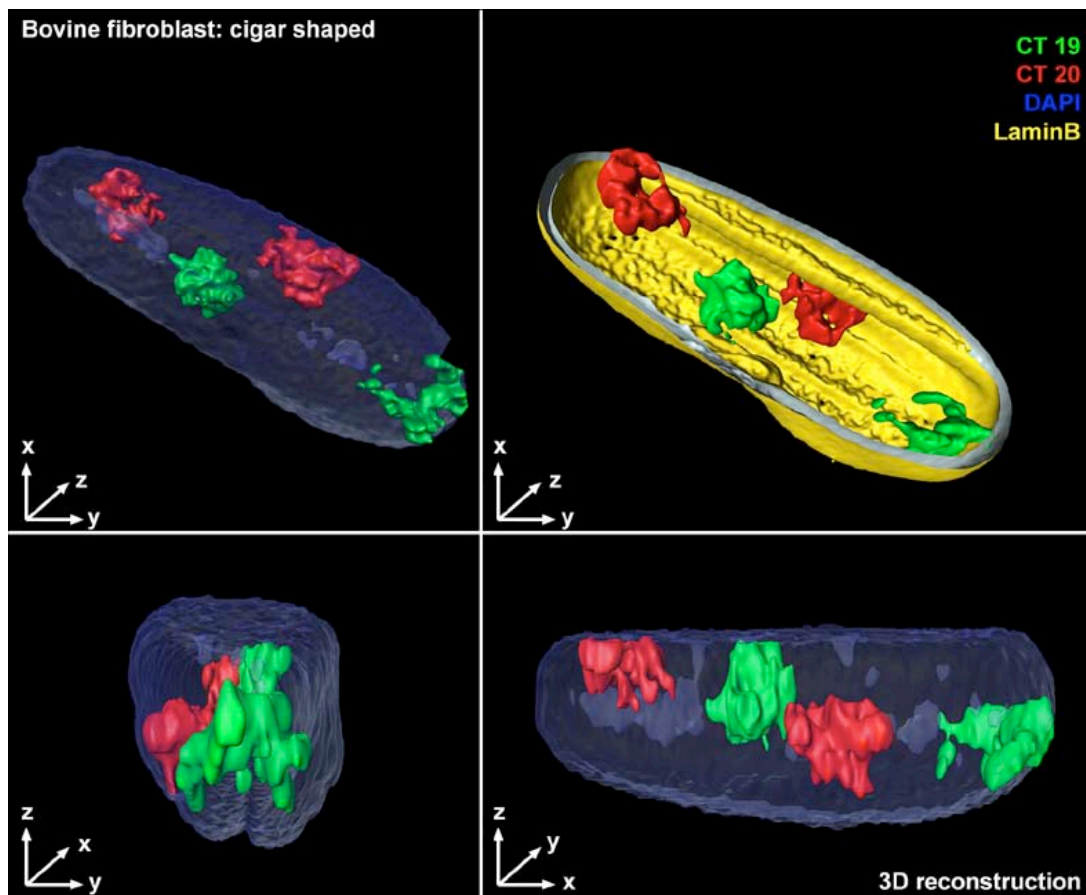


Fig. 30) Different views of a 3D reconstruction from a bovine cigar shaped fibroblast; CTs 19 (green), CTs 20 (red), DAPI counterstain (blue) and Lamin B staining (yellow) is shown;

For 2D evaluations the median was 67% for CTs 19 and 52% for CTs 20. No significant difference was found in this case ($p=0.168$). The 3D evaluation with DAPI as a reference revealed a significant difference between CTs 19 and 20 with $p<0.001$. The median for CTs 19 was 52% and for CTs 20 41%. The median for CTs 19 measured to the Lamin B reference was 22%. The corresponding median for CTs 20 was 16%. Interestingly this difference was not significant with $p=0.168$.

However all values were significantly different from a random distribution with $p < 0.001$. Examples of cigar shaped bovine fibroblasts are depicted in Fig. 30. Results of eADS measurements are shown in Fig. 32 (A, C, E).

4.2.2.4.3. Round shaped bovine fetal fibroblasts (BFF 451-1)

Nuclei of round shaped bovine fibroblasts ($n=25$) showed a diameter of $14.3\mu\text{m}$ in x , in y it was $9.0\mu\text{m}$ and $11.3\mu\text{m}$ in z respectively. The roundness factor was 0.65 in the xy -, 0.86 in the z/x - and 1.31 in the z/y -plane.

Also in these nuclei I found a statistically significant difference in the radial distribution of CTs 19 and CTs 20. In 2D the medians were 67% for CTs 19 and 52% for CTs 20. Using DAPI fluorescence to determine the nuclear surface, the medians in 3D were 52% for CTs 19 and 41% for CTs 20. Using Lamin B as reference resulted in a median of 22% for CTs 19 and 16% for CTs 20. All curves were significantly different from a random DNA distribution counterstained with DAPI ($p < 0.001$ and $p = 0.006$ for CTs 20 using Lamin B as reference).

Examples of cigar shaped human fibroblasts are depicted in Fig. 31. Results of eADS measurements are shown in Fig. 32 (B, D, F).

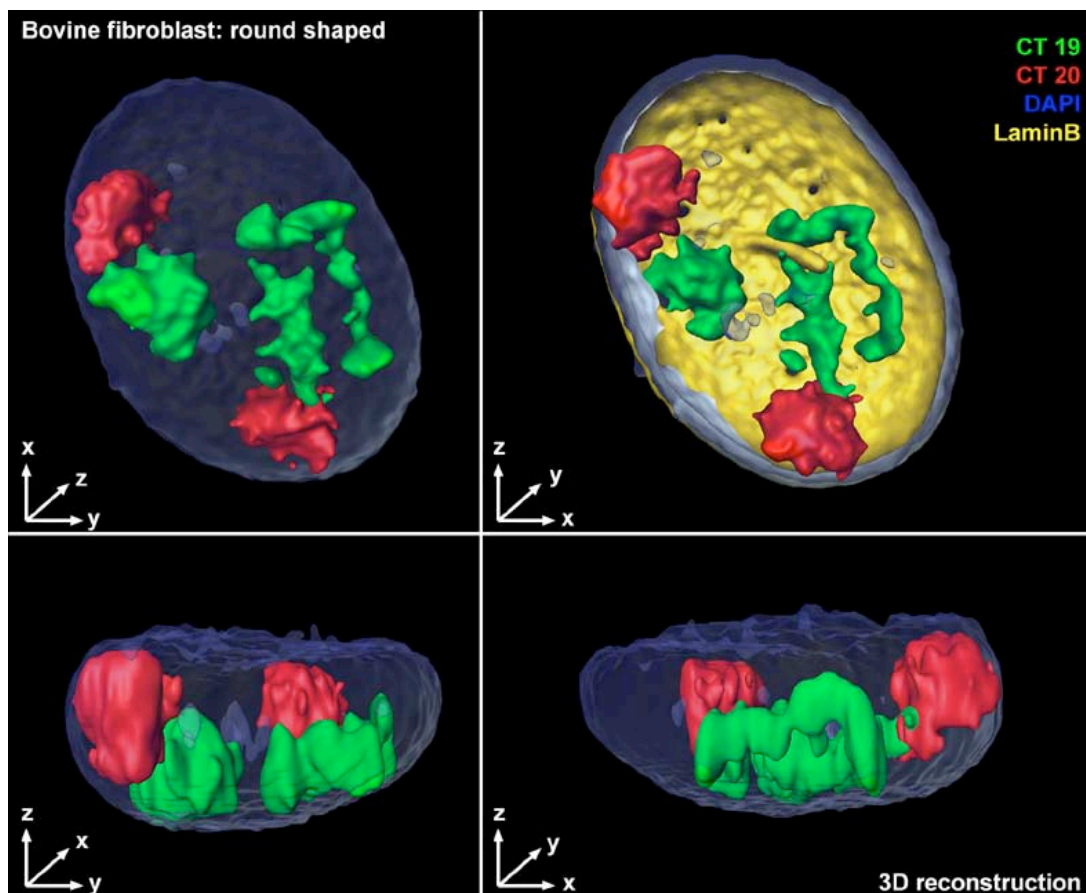


Fig. 31) Different views of a 3D reconstruction from a bovine round shaped fibroblast; CTs 19 (green), CTs 20 (red), DAPI counterstain (blue) and Lamin B staining (yellow) is shown;

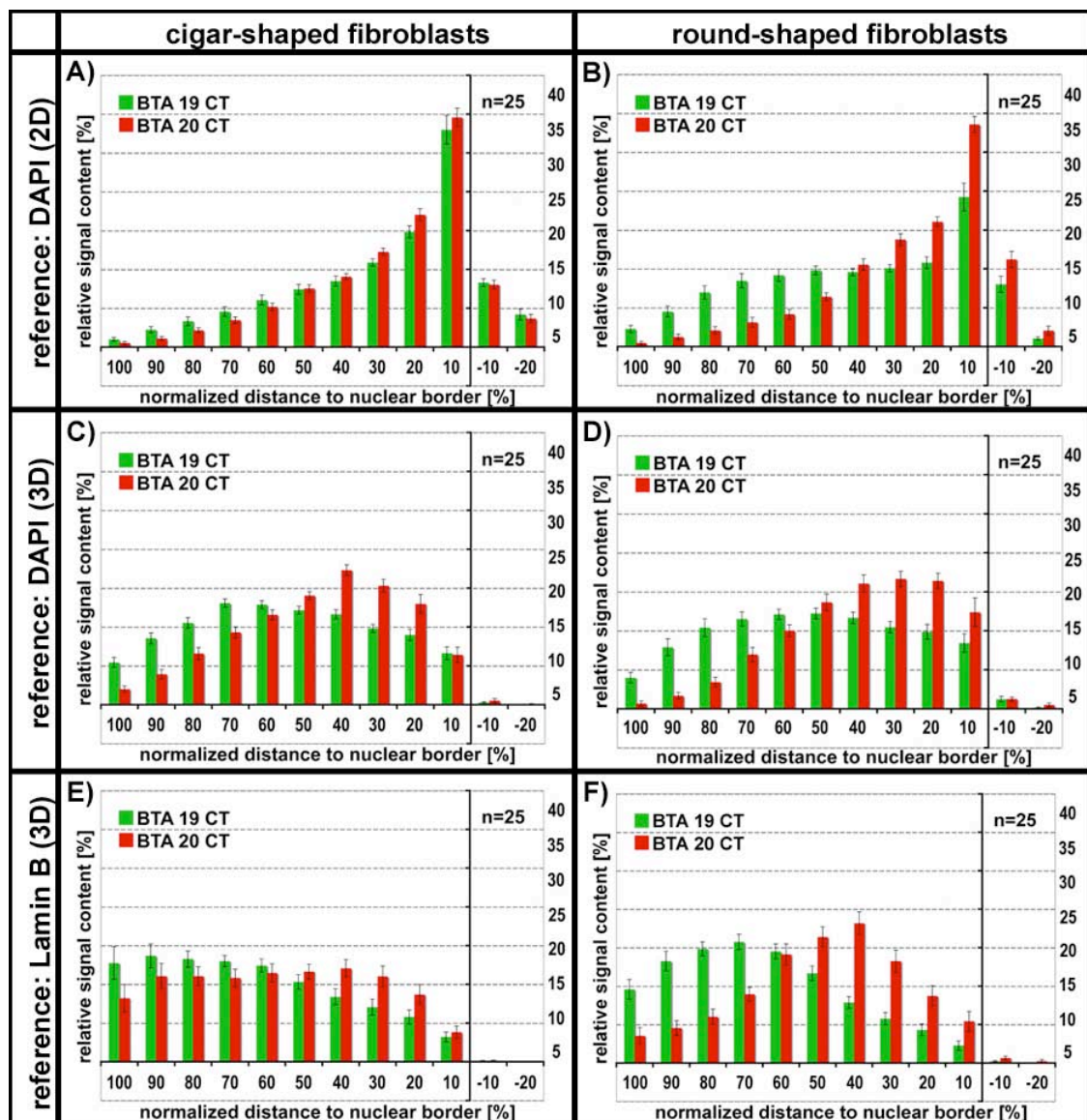


Fig. 32) Normalized eADS measurements for artificially shaped bovine diploid fibroblasts grown on micropattern slides: results for CT distribution of gene-rich BTA 19 CTs (red) and gene-poor BTA 20 CTs (red) in cigar shaped fibroblasts (left panel) or round shaped fibroblasts (right panel). Evaluations are performed in different ways. The reference for the 3D CT distributions was either the nuclear lamina stained with an antibody against Lamin B (A; B) or the nuclear DNA stained with DAPI (C; D). Measurements with DAPI as a reference structure were performed additionally in 2D (E; F).

4.3. FISH on 3D preserved bovine preimplantation embryos

This improved protocol for 3D-FISH on embryos will be included as a chapter in a volume of the *Methods in Molecular Biology* series from Humana Press presenting cutting-edge technical applications of FISH techniques. (edited by J. M. Bridger and E. Volpi) (<http://humanapress.com>).

4.3.1. Establishment of a FISH protocol on 3D preserved embryos

Starting point was the protocol for three-dimensionally (3D) preserved cells, where fixed cells had a morphology very close to the natural state. Several modifications and adjustments were necessary in order to obtain reproducibly strong signals that could be recorded by LSM and evaluated/analyzed accordingly. In the following the, including the handling of embryos, which had to be adapted for the individual fixation, hybridization and detection steps:

4.3.2. Embryo attachment

Since embryos could not be stably fixed to any surface, compared to cells growing in suspension, such as lymphocytes, which are immobilized with Poly-Lysine, embryos were handled individually, by transferring them from one liquid to another each by each. This was done, by using a transferpettor (a kind of pipette where instead of the tips a glass capillary is placed; available in different volumes; here 2µl or 5µl volume were used). Pipetting embryos was constantly controlled by using a binocular. A common problem was that embryos would eventually stick to the inner glass surface of the capillaries used. If this happened they could be removed by pipetting the solution up and down several times.

4.3.3. Choosing the best wells to securely handle embryos

For incubation steps in liquid the correct and most comfortable bin has to be chosen. There were mainly three aspects that had to be considered:

- The dilution factor: the smaller the volume of the solution wherein embryos are transferred the bigger is the dilution factor. With big dilution factors it is hard to establish the working concentration of solutions, which might cause inefficiency of the working protocols.
- Tracking of embryos: the more liquid or the bigger the space of the well, the harder it is to track all embryos.
- The depth of the wells: the working space at the binocular is limited. By using wells with a high edge, this space is further reduced. The danger is to break the

capillaries containing embryos or that embryos could not be reached within the well if they are not lying exactly in the middle of the cavity.

Another option was to work in small drops of liquids instead of using wells. Then the following aspects had to be considered:

- Drops should not dry out. Therefore heating is not possible, except a humid chamber is used.
- The surface tension should be strong enough to keep the drops in shape. This limits the application of detergents to low concentrations.
- The surface of plastic wells can be different and should be tested previously in order to minimize potential sticking of embryos, as well as to make sure that the surface tension is not influenced in a bad manner.

In general all liquids should contain BSA and a detergent (TritonX-100 or Tween 20), at least in low dilutions, to avoid embryos from sticking to any surface (plastic bins, glass pipette). This was especially necessary when the zona pellucida had been removed.

4.3.4. Modifications of the fixation protocol

By applying the standard fixation protocol used for cells except for the freezing/thawing step in liquid nitrogen no hybridization signals were obtained. The following modifications were applied then:

- An additional HCl incubation directly after formaldehyde fixation was implemented to remove the zona pellucida. This glycoprotein layer protects embryos and is important for the initiation of the acrosome reaction during fertilization. During FISH procedure it may avoid a proper permeabilization.
- Permeabilization of the embryos using the detergent TritonX-100 was prolonged to 60 minutes.
- Incubation in HCl obviously destroyed embryo morphology and the incubation time was therefore further reduced from 5 to 10min, like used for cells, to approximately 1min.

These modifications did still not result in successful hybridization signals in embryos. I finally succeeded when the embryos were treated in a repetitive way: After a complete round of fixation and a 2 day incubation in 50% formamide the embryos were incubated once more in HCl and 0.5% TritonX-100 for permeabilization.

4.3.5. Set up FISH: denaturation and hybridization

The best results for FISH on bovine somatic cells were obtained performing separate denaturation of probes (including a pre-annealing step to get rid of

repetitive sequences) and specimen DNA. This was tested for embryos as well. Embryos were denatured in 70% FA/2xSSC on a slide on the hot block. Probes were denatured at 95°C and pre-annealed for 30min at 37°C before the probe mixture was put on the embryos. However this procedure revealed no results. Success was achieved if a denaturation of both, probes and embryos together it was performed. Embryos were pipetted directly into 6µl of hybridization mixture, placed at a slide in the middle of a metal ring. Try to transfer as less liquid as possible with the embryos that the probe is not diluted too much. Everything was covered with mineral oil and equilibrated then at 37°C for 3 hours. During that time the probe could be dispersed within the embryos, which seems to be crucial for a successful hybridization. Denaturation was performed on the hotblock at 76°C for 3min.

4.3.6. Modifications and improvements for probe detection in embryos

Directly labeled probes were tested in order to shorten the detection procedure but without success. Subsequently I used indirect labeled probes but these often showed high background, in the nuclei as well as in the cytoplasm. Most probably probes and antibodies bound unspecifically to cellular and nuclear components that are present abundantly in the embryos such as lipids, proteins and RNAs.

As a compromise between intensity of signals and minimizing background signal I decided to use a two-layer detection. Some slight modifications compared to cultured cells were though necessary to improve hybridization results:

- All incubations were performed at room temperature because they need to be followed at the binocular and therefore any other stable temperature was impossible to keep.
- The second stringent washing step in 0.1% SSC was supplemented by another stringent washing step in 50% formamide. (These incubations were also done at room temperature and not at 62°C like with cells which might decrease the stringency effect of the washings.)
- Incubation of the first antibody was performed over night at 4°C.
- DAPI was added in antifade/embedding medium at a concentration of 0.05µg/µl to improve counterstaining of nuclei.
- Before adding antifade solution to the embryos they were incubated in glycerol solutions with increasing glycerol concentration (20%, 40% and 60%), in order to minimize potential damaging of embryos by the glycerol-based and therefore denser antifade solution.

4.3.7. Recording embryos at the confocal laser scanning microscope (CLSM)

Embryos were too thick to be embedded between two glass slides like commonly done for cells. I finally decided to use μ -slides (Ibidi, Martinsried), which were developed originally for living cell experiments. Those slides contain small chambers on the upper part and a thin foil instead of a glass or plastic bottom, provided a good solution for experiments with embryos. A partition of the slides into different chambers was helpful for finding the fixed embryos on the slide easily. The μ -slide (18 well, flat; <http://www.ibidi.de/products/slide18.html>) contains 18 slots that were not deeper than 2mm. For a better attachment of the embryos to the slides, the surface of the wells was covered with Poly-L-Lysine (concentration: 1mg/ml) for about 1 hour. Additional solution was shortly drained afterwards and slides were directly used. (I did not use the outer columns because they could not be reached by the objective in combination with our microscope stand.) Between 1 and 3 embryos were transferred in each well on the slides. For a better attachment of embryos on the slides, keep attention that as less liquid as possible is transferred together with them. Slides were kept over night at 4°C in a metal box (containing wet tissues to prevent embryos from drying out). In that way embryos should be glued to the slides. The next day they were covered carefully with antifade medium containing DAPI (concentration: 0.05 μ g/ml). The location of embryos in the well was registered with a binocular for a faster tracking at the microscope.

At the CLSM, embryos were first checked for their morphology and the number of nuclei was counted using DAPI staining. Only embryos with an adequate number of nuclei for their developmental age were used. For the distribution analysis individual nuclei were scanned with a vertical voxel size of 30 to 80nm. Additionally a single overview picture or a complete stack of the whole embryo was taken.

Embryos were very thick (80 to 120 μ m). Therefore frequently only nuclei from the lower part of the embryos, which was glued to the surface of the slide, could be properly focused using a 63x objective lense. Signals from the upper part were moreover much weaker.

4.4. Gene-rich and gene-poor chromosomes in bovine species

4.4.1. Bovine karyotype

The genome of cattle – *Bos taurus* (BTA) – has been sequenced partially so far and the obtained sequence data is available e.g. on the ENSEMBL database (http://www.ensembl.org/Bos_taurus/index.html; 19.06.2008). The bovine karyotype consists of 58 autosomes and 2 sex chromosomes XX or XY. Except the X chromosome all chromosomes are telocentric. The differences in chromosome sizes were less pronounced in cattle (40-146Mb in cattle) compared to human (50-250Mb). Genes annotated to individual chromosomes were used to determine the gene density, whereas protein coding and all RNA genes were counted. In cattle, chromosome 19 (19.2 genes/Mb) has the highest gene density and chromosome 20 (5.2 genes/Mb) the lowest (see Fig. 33).

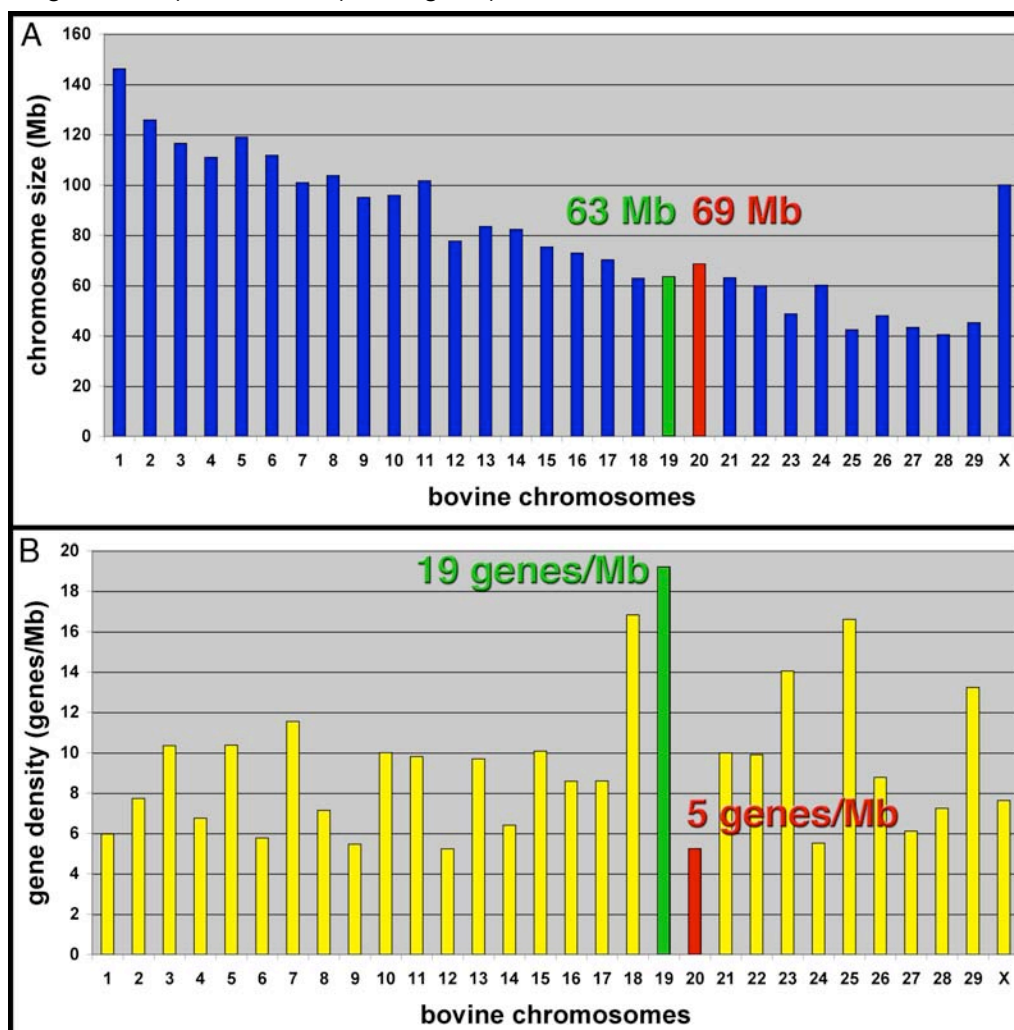
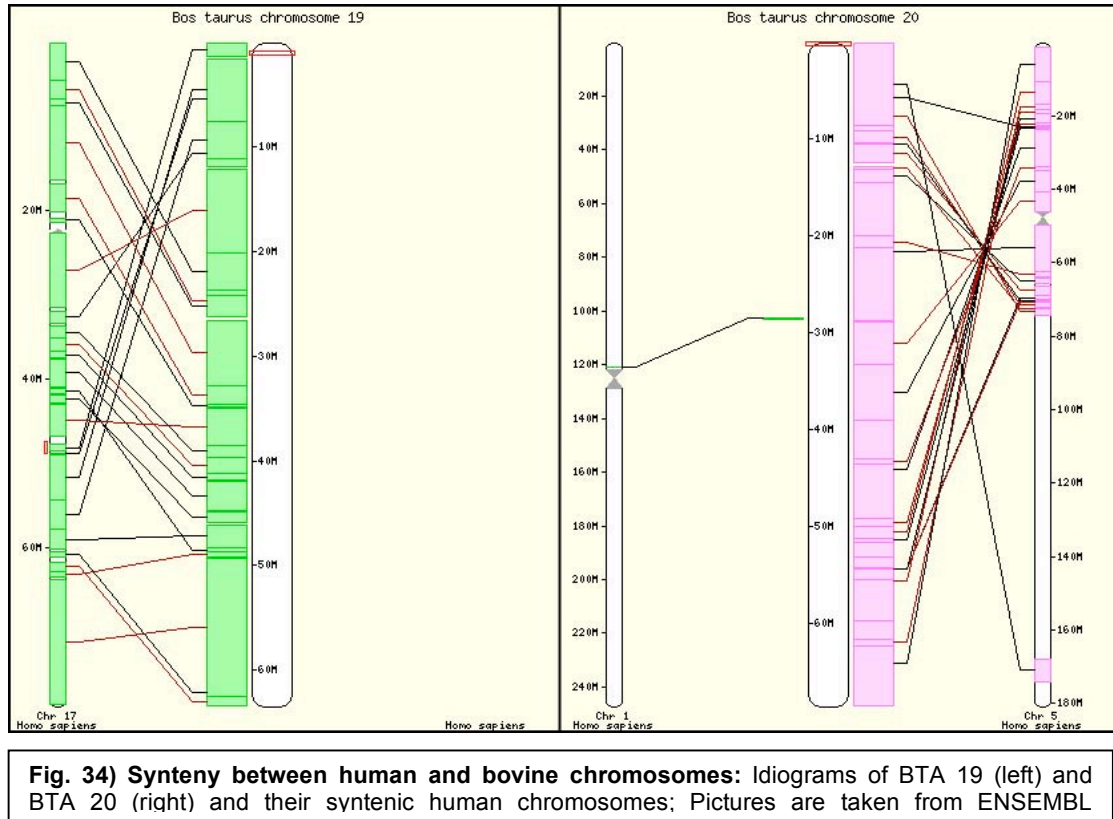


Fig. 33) Size and gene density of bovine chromosomes: Histograms show size in Mb (A) and gene density in genes/Mb (B) of bovine chromosomes, respectively. The corresponding data was extracted from the bovine Ensembl genome data base, version 48.3e (http://www.ensembl.org/Bos_taurus/index.html). For the present study we have chosen the most gene dense chromosome 19 (19 genes/Mb; green) and the similar sized most gene poor chromosome 20 (5 genes/Mb; red).

The bovine chromosome 19 has large syntenic regions to gene-rich human chromosome 17, while BTA 20 has large syntenic blocks to parts of human chromosome 5, which represents a rather gene-poor chromosome (6.4 genes/Mb). An overview is given in Fig. 34.



4.4.2. Probe optimization

Before using paint probes in 3D experiments they were all tested on bovine metaphase preparations. Conditions for stringent washings, time of pre-annealing and the amount of C_0t_1 DNA were tested in these pre-experiments to optimize probe hybridization. However, not all parameters optimized in these experiments could finally be used for the hybridization experiments with embryos, but these experimental set-up refinements were helpful to refine the conditions for 3D FISH on embryos.

It was for example impossible to use solutions at other temperatures than room temperature, because all treatments were performed under the binocular. (Our binocular model has not a stage that could be heated.) To minimize variation in temperature, though dishes with embryos were placed on a hot block during the incubation times. Pre-annealing of probes for about 30min to pre-hybridize repetitive DNA in the probe with the supplemented C_0t_1 DNA resulted in excellent FISH signals in bovine somatic cells (Fig. 35) but for embryos an equilibration with the

hybridization mixture containing the DNA probe and C₀t1 DNA was sufficient. The amount of C₀t1 DNA for successful hybridization of the probe on embryos was finally raised to 600µg for 3µg of paint probes compared to 200µg for 3µg of paint probe used in cells.

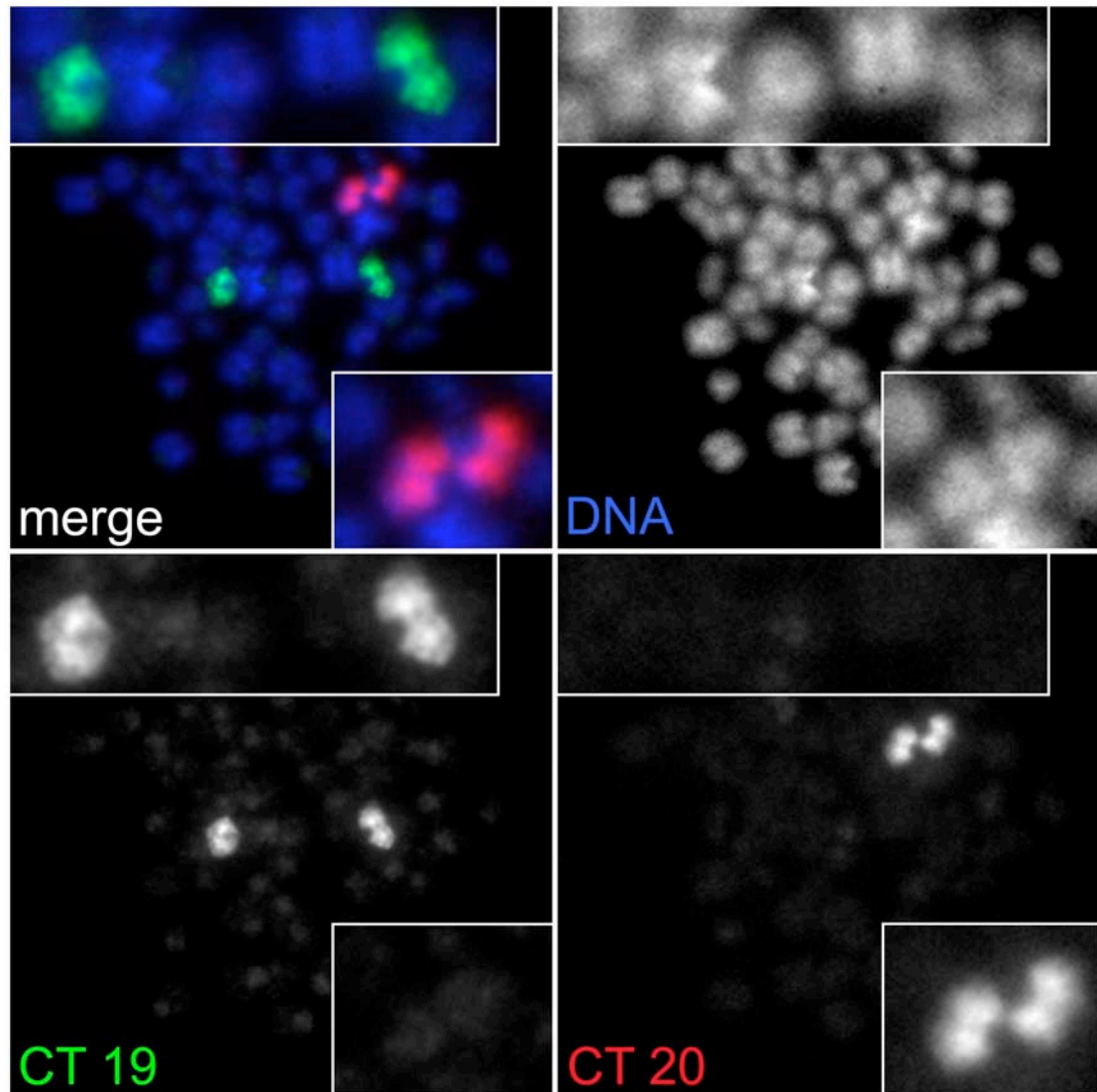


Fig. 35) Specificity of FISH probes for bovine chromosomes 19 and 20: Bovine mitotic chromosome spreads of bovine fetal fibroblasts were hybridized with chromosome specific paint probes for bovine chromosomes 19 (green) and 20 (red). DNA was counterstained using DAPI (blue).

4.4.3. 3D distribution of CTs 19 and 20 in diploid bovine fibroblast nuclei

Experiments for the radial distribution of CTs 19 and 20 in bovine fibroblast nuclei (Fig. 36) were performed by measuring the absolute distances of CTs in reference to the nuclear border (DAPI staining) with the eADS program. This experiment was performed twice. In the first set 28 nuclei were investigated. The median for CTs 19 was 51% and for CTs 20 33%. The curves for both distributions were significantly different from each other ($p < 0.001$). The differences to DAPI stained nuclear DNA were significantly different as well, with both CTs located more inside ($p < 0.001$ for CTs 19 and $p = 0.005$ for CTs 20).

In the second experiment the bovine chromosomes 19 and 20 were investigated in 25 nuclei. The median for CTs 19 was 56% and 49% for CTs 20. The difference between CTs 19 and 20 was significant ($p = 0.016$). In comparison to the nuclear DNA, stained with DAPI, both CT distributions were more inside the nuclei and differed significantly from the overall DNA distribution ($p < 0.001$).

Because there were two data sets including both the CTs 19 and 20 a comparison between the medians in both evaluations was made and revealed an equal distribution for CT 19 ($p = 0.271$) but not for CT 20 ($p < 0.001$).

(Additionally the bovine chromosomes X (1st experiment) and 18 (2nd experiment) were evaluated. The results were listed in the appendix.)

4.4.4. 3D distribution of CTs 19 and 20 in diploid bovine lymphocyte nuclei

The radial distributions of CTs 19 and 20 in 25 nuclei of bovine lymphocytes (Fig. 36) were investigated in the same way like fibroblasts (4.4.3.). Their nuclear morphology was typically spherical and thus clearly different from commonly flat shaped fibroblast nuclei. The median distribution was 61% for CTs 19 and 27% for CTs 20. The distributions for CTs 19 and 20 were highly significant ($p < 0.001$). In comparison to the DAPI stained nuclear DNA CTs 19 and 20 were significantly more interior ($p < 0.001$).

(Like in fibroblast nuclei the bovine chromosome 18 was additionally stained and evaluated. The results were listed in the appendix.)

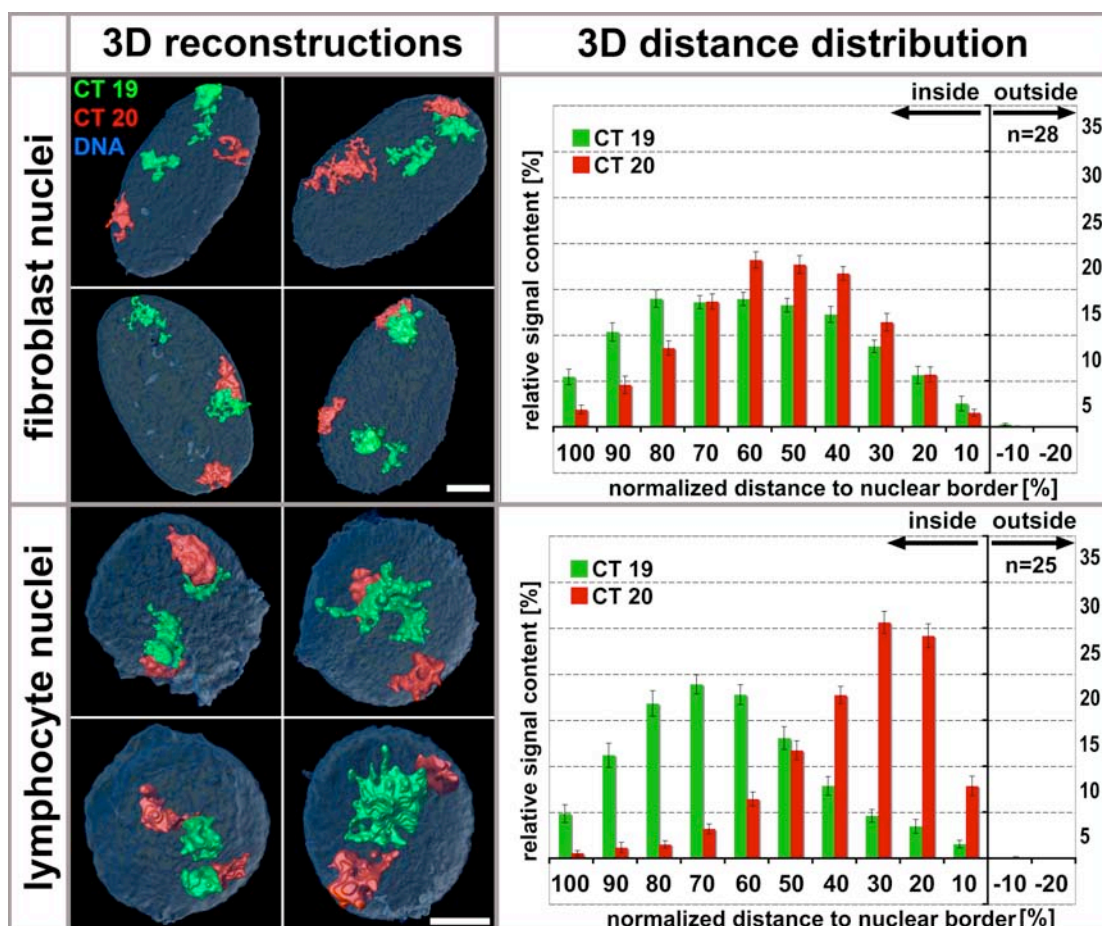


Fig. 36) Radial distributions of CTs 19 and 20 in bovine fibroblasts and lymphocytes: Images highlight 3D-reconstructions of four representative bovine fibroblast and lymphocyte nuclei, respectively. Surface renderings were performed using Amira 4.1 (Visage Imaging) software applied to confocal image stacks. Chromosomes 19 are shown in green, 20 in red, while the nucleus is represented as transparent blue shell. Scale bar: 5 μ m. In the right column the respective distance distribution plots are shown. Relative signal content of the respective CTs are plotted against the normalized distance to the nuclear surface, with the value 100% representing the nuclear center, 0% the nuclear border. Error bars indicate standard errors of the mean. Note, that for both cell types there is a significant difference in the distribution of chromosome 19 and 20 with 19 being more internal than 20, though the difference is more pronounced in bovine lymphocytes ($p < 0.001$) than in fibroblasts ($p = 0.016$). n = number of analyzed nuclei.

4.4.5. 3D radial distribution of CTs 19 and 20 in IVF embryos

The following developmental stages of IVF embryos were analyzed: zygotes and embryos with 4 to 8 cells represented stages before a major genome activation took place. It is described that the latter takes place in bovine at the 8 to 16 cell stage (Kopecny et al. 1989). Moreover, we included 10-16 cell embryos as well as blastocysts, representing embryos either during or after MGA, with the latter resembling a stage where cellular differentiation in **Trophectoderm (TE)** and **Inner Cell Mass (ICM)** has already taken place. Presence/absence of global transcription in 4-8 and 10-16 cell embryos was confirmed by incorporation and detection of the mRNA precursor BrU (data not shown). For individual stages only embryos with an adequate number of cells were used for evaluation. The four chosen classes for investigation were zygotes, each containing two pronuclei. Embryos in the 4-8 cell group showed on average 5 nuclei/embryo while 10-16 cell embryos had on average 12 nuclei/embryo. The last class comprised blastocysts with an average number of cells of more than 64 cells per embryo. Only some blastocysts were already hatched or partly hatched at the point of fixation. For evaluation I did not distinguish further between the hatched and not hatched embryos. To obtain a statistically relevant result of our analysis I have included between 8 and 45 embryos (e) per stage, corresponding to 45 to 102 nuclei (n). For the evaluation a statistical number of nuclei (n) was collected from several different embryos (e). The number of nuclei in each embryo was determined and averaged for each stage of development (n/e).

The individual stages were further subdivided, as zygotes were grouped in early, mid and late zygotes (hours post fertilization; hpf). Day 2 and day 3 embryos were subdivided according to their global DNA distribution, which could be either homogeneous or heterogeneous. Blastocysts were separated according to the origin of cells, i.e. either from **Inner Cell Mass (ICM)** or **Trophectoderm (TE)**. Zygotes and day 2 embryos (5n/e) showed no difference in the distribution of gene-rich and gene-poor chromosomes. With the onset of **Major Genome Activation (MGA)**, day 3 embryos (12n/e) and blastocysts displayed a gene-density dependent distribution as observed in somatic cells. Detailed results are given in the following:

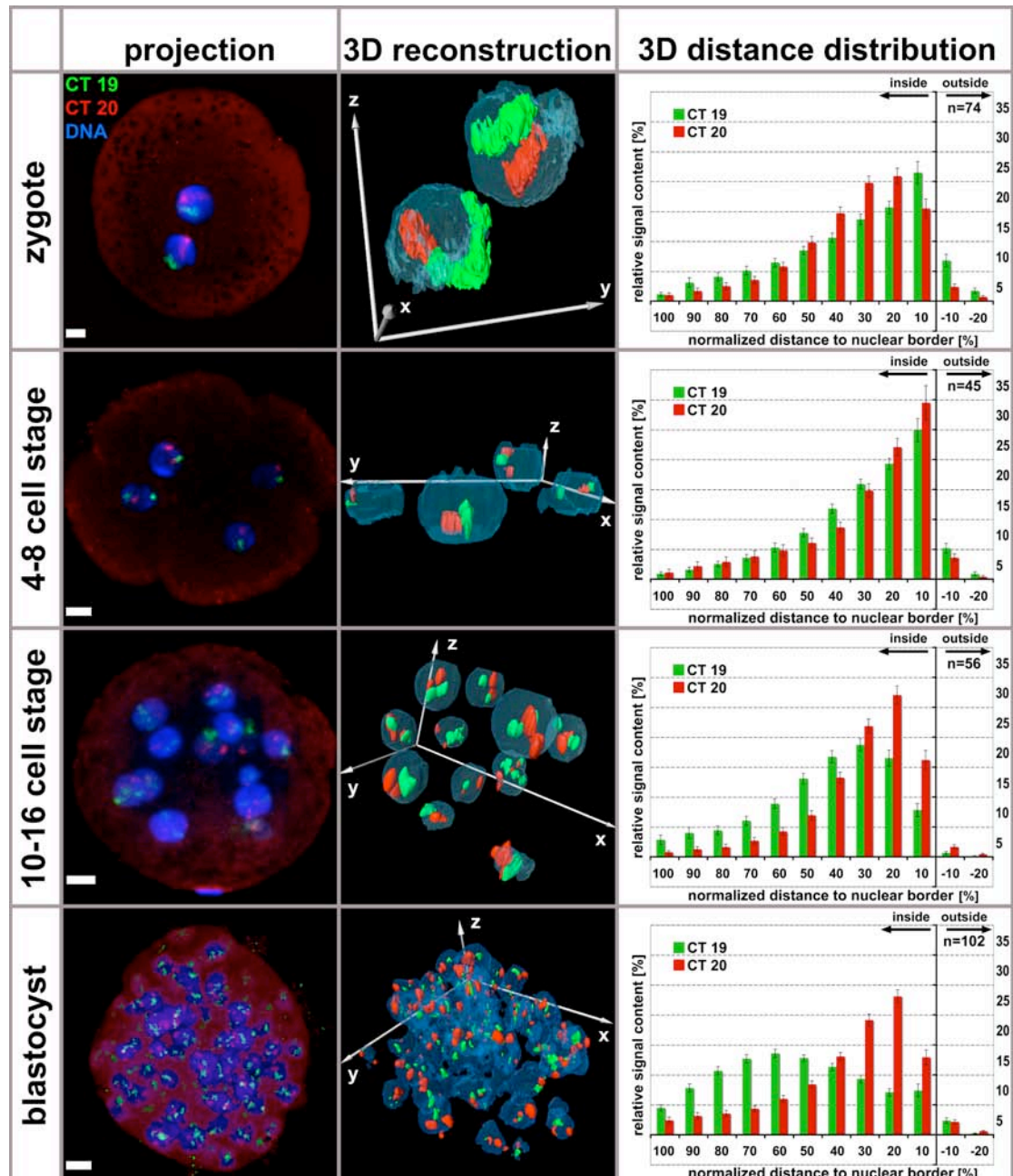


Fig. 37) Radial distributions of CTs 19 and 20 in bovine IVF embryos: Territories of bovine chromosomes 19 and 20, visualized by FISH are shown in green and red, respectively, while nuclear DNA stained by DAPI is depicted in blue. Representative embryos are shown for each of the four analyzed consecutive developmental stages. In the left column maximum intensity projections are depicted, while the middle column highlights the respective embryo as 3D reconstructions. Note that reconstructions show embryos from a different perspective. Scale bars: 10 μ m. The distance distribution plots for the respective developmental stages are shown in the right column, analogous to figure 1. Whereas CTs 19 and 20 show a similar radial distribution up to the 8 cell stage ($p>0.1$), a significant difference in their nuclear position can be observed in embryos with 10-16 cells and blastocysts ($p<0.001$), though being more pronounced in the latter.

4.4.5.1. Zygotes – early, mid and late

74 pronuclei from 45 embryos were evaluated, all of which contained 2 pronuclei. Chromosomes 19 showed a median of 22% and chromosomes 20 of 25% after eADS evaluation. No statistical difference ($p=0.322$) was detectable between the curves of these two CTs. However, CTs 20 differed from the overall DNA distribution stained by DAPI with a median more outside ($p=0.002$), but not CTs 19 ($p=0.285$).

A division into three subclasses was made according to the time after fertilization (hpf). Early zygotes were fixed 11 hpf, mid zygotes 18 hpf and late zygotes 21 hpf. From 11 early embryos 23 nuclei were evaluated. The medians for CTs 19 (23%) and for CTs 20 (27%) were not significantly different ($p=0.913$). Only CTs 20 were significantly different from the DAPI distribution with a median more outside ($p=0.048$). In contrast CTs 19 were not significantly different to the DAPI distribution ($p=0.416$).

From mid zygotes 30 nuclei from 16 different embryos were evaluated. The median was 22% for CTs 19 and 25% for CTs 20, without showing a significant difference ($p=0.363$). Again the curve for CTs 20 differed from the DAPI distribution with being more peripheral ($p=0.042$). The CTs 19 curve was not significantly different distributed in comparison to an overall DNA distribution ($p=0.569$).

For the late embryos 25 nuclei from 11 embryos were analyzed. The median for CTs 19 was 21%, for CTs 20 it was 25%. The distributions were not significantly different ($p=0.211$). CTs 20 were significantly more outside than an overall DNA distribution ($p=0.019$). CTs 19 showed a distribution that was not significantly different from the DAPI distribution ($p=0.497$).

To summarize all values for the different subclasses were similar. The comparison of curves for CTs 19 and 20 between the individual stages revealed no significant difference (p values were all >0.1). I conclude that none zygotic sub-stages revealed a difference in the radial distribution of CTs 19 and 20.

4.4.5.2. Day 2 embryos: 4-8 cells per embryo

From day 2 embryos 45 nuclei from 13 different embryos were evaluated. The average number of nuclei per embryo was 5. The median for the CTs 19 distribution was 19%, for CTs 20 it was 14%. The difference between both curves was not significant ($p=0.281$). Comparing both distributions against the DAPI distribution revealed no significant difference, neither to CTs 19 ($p=0.096$) nor to CTs 20 ($p=0.028$).

The data set was divided according to the global DNA distribution. There was found either a homogeneous DAPI distribution comparable to that in somatic cells or nuclei with large areas that appeared as DNA free or at least having a very low DNA concentration, at least as displayed by DAPI staining (compare Fig. 40 A and B). 58% nuclei belonged to the fraction with a "hollow" phenotype: 31 nuclei from 11 embryos, with a mean number of 5 nuclei per embryo were evaluated. The median of CTs 19 was 17% and 12% for CTs 20, showing no significant difference

($p=0.166$). Interestingly the difference to DAPI distribution was significant for both curves: $p=0.004$ for CTs 19 and $p=0.001$ for CTs 20, both being more external.

The 14 (42%) homogeneous nuclei, from 6 different embryos, with an average number of 5 nuclei per embryo showed also a similar radial distribution for CTs 19 and CTs 20 ($p=0.945$). The median for CTs 19 and CTs 20 were 25%, in both cases. The distributions were not different from the DAPI distribution: ($p=0.206$ and $p=0.323$, respectively).

While there was no difference in the distribution of CTs 19 between hollow and homogenous nuclei ($p=0.072$), there was a significant difference for CTs 20 ($p=0.017$). In hollow nuclei the chromatin and also the individual CTs were shifted towards the periphery. Results are shown in figure Fig. 40 D and E.

4.4.5.3. Day 3 embryos: 10-16 cells per embryo

Day 3 embryos ranging from 10 to 16 nuclei had a mean average of 12 nuclei per embryo. 56 nuclei from 8 embryos were evaluated. For CTs 19 the median was 32% and 20% for CTs 20, resembling a significant difference with $p<0.001$. Both distributions were different to the DAPI distribution with CTs 19 located more internal ($p<0.001$) and CTs 20 located more peripheral ($p=0.033$).

The data set was again split according to the appearance of the global DNA distribution. 54% which corresponds to 41 nuclei from 6 different embryos, with an average number of 6 nuclei per embryo, showed the “hollow” phenotype in their DAPI staining. The median for CTs 19 was 30% and 20% for CTs 20 showing a significant difference ($p<0.001$). Both curves were statistically different from the DAPI distribution with CTs 19 located more internal ($p<0.001$) and CTs 20 located more peripheral ($p=0.003$).

For nuclei with a homogeneous DAPI staining (46%) 19 nuclei from 2 different embryos were evaluated. The mean number of nuclei per embryo was 13. The distributions between CTs 19 and CTs 20 were significantly different ($p=0.002$) with a median value of 39% for CTs 19 and 23% for CTs 20. In comparison to the DAPI distribution CTs 19 were significantly more internal ($p<0.001$), not so CTs 20 which were located only slightly more peripheral ($p=0.884$).

Though the medians show a clear shift for both CTs in the homogeneous compared with the “hollow” nuclei, the difference was only significant for the case of CTs 20 ($p<0.001$) but not for CTs 19 ($p=0.824$). Results are shown in Fig. 40 F and G.

4.4.5.4. Blastocysts: ICM vs TE

107 nuclei from 8 different blastocysts were analyzed. The mean average of cells was not calculated because blastocysts contain too many nuclei to record them all at the CLSM. Embryos were fixed 6-7 days after fertilization and most of them were still not hatched. The difference between CTs 19 and CTs 20 was significant with $p < 0.001$. The median for CTs 19 was 52% and 22% for CTs 20. Only the curve for CTs 20 was similar to a DAPI distribution ($p = 0.936$), not the curve for CTs 19 ($p < 0.001$), which was more internal.

Blastocysts show already cellular differentiation into cells of the ICM and TE. All nuclei that could be unambiguously allocated to the ICM or TE were evaluated individually to investigate if those distinct cell types show a difference in the radial distribution of CTs 19 and 20.

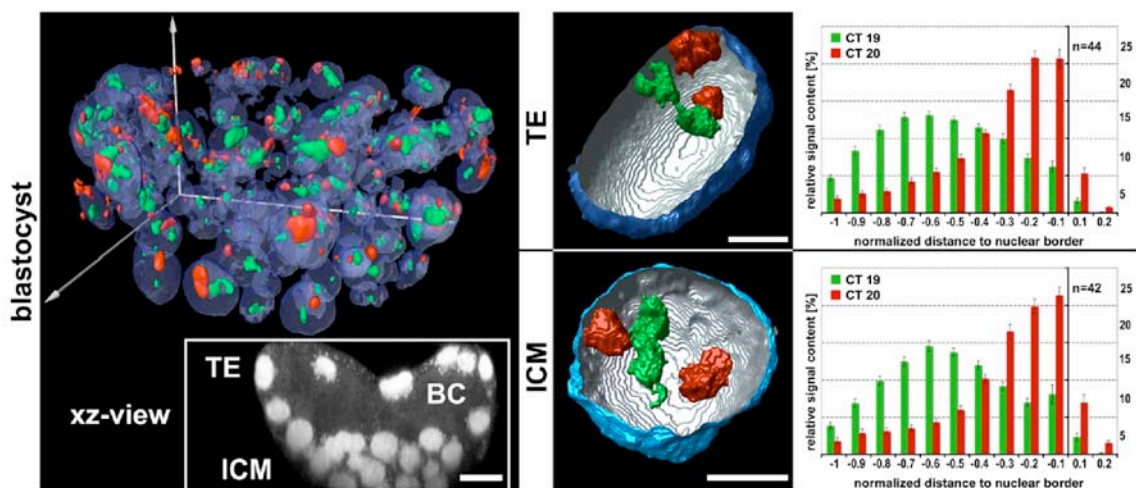


Fig. 38) Radial distributions of CTs 19 and 20 in the trophectoderm and inner cell mass: The left panel shows a 3D reconstruction of a bovine IVF day-6 blastocyst with CTs 19 highlighted in green, CTs 20 in red and nuclei counterstained by DAPI, depicted in blue. The inset shows an xz cross section of the same blastocyst visualizing only DAPI stained nuclei. Note that the blastocoel (BC) is partially collapsed, probably due to the fixation procedure. However, a clear separation of trophectoderm (TE) and inner cell mass (ICM) cells was possible in most embryos and only such were included in the analysis. Scale bar: 20 μ m In the middle column 3D reconstructions of representative TE and ICM cell nuclei are shown. Scale bars: 5 μ m. Note the difference in nuclear shape, while TE cells had typically an ellipsoid/cylindrical shape, ICM cells were mostly spherical. On the right, the respective distance distribution plots for TE and ICM cells are presented, showing similar distributions for both cell types with gene dense chromosomes 19 being significantly more interior than gene poor chromosomes 20 ($p < 0.001$).

For the ICM 42 nuclei from 5 different embryos were evaluated. The median for CTs 19 was 51%, for CTs 20 was 22%, which was significantly different with $p < 0.001$. Only the curve of CTs 20 was like the distribution for DAPI ($p = 0.879$) while that of CTs 19 showed a significantly more internal location ($p < 0.001$).

For cells of the TE 44 nuclei originating from 6 different embryos were analyzed. Again the distribution showed a significant difference between CTs 19 and CTs 20 ($p < 0.001$). The median for CTs 19 was 51%, for CTs 20 it was 21%. Only the

distribution of CTs 20 was similar to DAPI ($p=0.963$), the distribution for CTs 19 was again significantly more internal ($p<0.001$).

The distributions of CTs 19 ($p=0.473$) and CTs 20 ($p=0.592$) were not significantly different between nuclei of ICM and TE cells. Results concerning the differences between ICM and TE are shown in Fig. 38.

4.4.6. Global DNA distribution

A surprising observation when analyzing the CT distribution in bovine IVF preimplantation embryos was that nuclei frequently showed a non-homogenous distribution of DNA stained by DAPI, especially in very early stages. I often observed large areas within nuclei that were apparently free of DNA or showed at least a very low staining intensity (Fig. 39 and Fig. 40 A). The proportion of such “hollow” nuclei decreased during development. While in zygotes 90% ($n=70$, $e=45$), i.e. a majority of nuclei showed such an unequal DNA distribution, in 4-8 cell embryos it dropped to 58% ($n=60$, $e=13$), in 10-16 cell embryos it still accounted for 54% ($n=76$, $e=12$), while a minimum was reached in blastocysts, where only a minority of 17% ($n=118$, $e=8$) showed this phenomenon (see Fig. 40). Since the same phenomenon was also seen in mildly fixed embryos prepared for immunofluorescence we exclude that it represents an artifact caused by the FISH fixation procedure (see Fig. 39). Though the reason or functional implications of this unexpected DNA distribution remain completely elusive, I found that individual blastomeres in post-MGA embryos were clearly

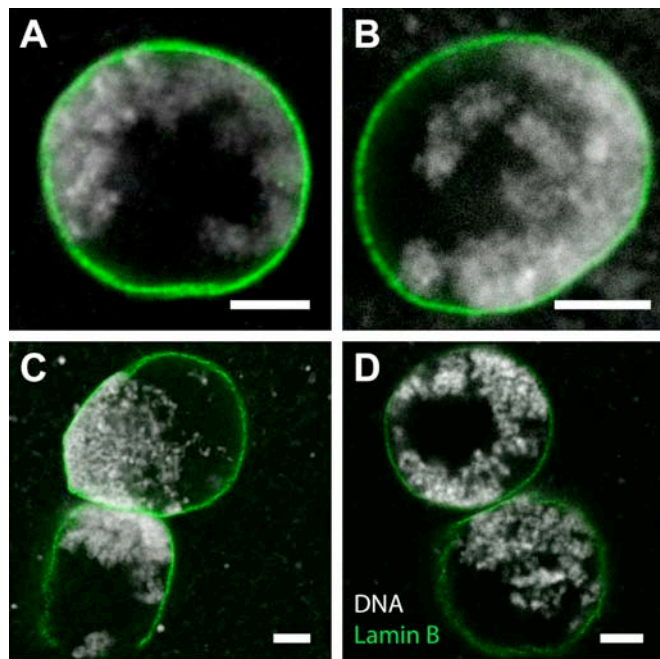


Fig. 39) Asymmetrical DNA distribution in pronuclei. A-D) Confocal midsections through pronuclei taken from four bovine IVF zygotes 22 hours post fertilization, stained with DAPI (grey) together with an anti-lamin B antibody (green) to demarcate the nuclear border. Note the large DNA poor regions typically seen in bovine pronuclei. Scale bar: 5 μ m.

transcriptionally active as shown by BrU incorporation (data not shown), arguing in favor that such nuclei represent a “normal” physiological state. To exclude the possibility that the lack of a gene density related CT distribution in embryos before MGA is due to the high proportion of “hollow” nuclei, that would simply leave less

space in the nucleus for the chromosome to arrange in a distinct manner, I subdivided 4-8 cell embryos and 8-16 cell embryos in a “hollow” and a “homogeneous” group and analyzed them separately (figure 29C-F). I found that independent of the global DNA distribution, i.e. whether the nuclei were “hollow” or not, they showed the same stage specific radial distribution, i.e. no difference between CTs 19 and 20 in 4-8 cell embryos (“hollow”: $p=0.17$; $n=31$, $e=11$ vs. “homogenous”: $p=0.95$; $n=14$, $e=6$) and a significant difference in 10-16 cell embryos (“hollow”: $p<0.001$; $n=41$, $e=6$ vs. “homogenous”: $p=0.002$; $n=19$, $e=2$). I conclude therefore that the global DNA distribution has no influence on the stage specific radial distribution of CTs 19 and 20. It should be noted however, that the distribution of CTs in general was different in “hollow” vs. “homogenous” nuclei, in that the former showed the tendency of a more peripheral distribution of both CTs, most probably caused by the large DNA free areas in the nuclear interior that constrain the DNA to the nuclear periphery (compare histograms in figure 40D vs. 40E and 40F vs. 40G).

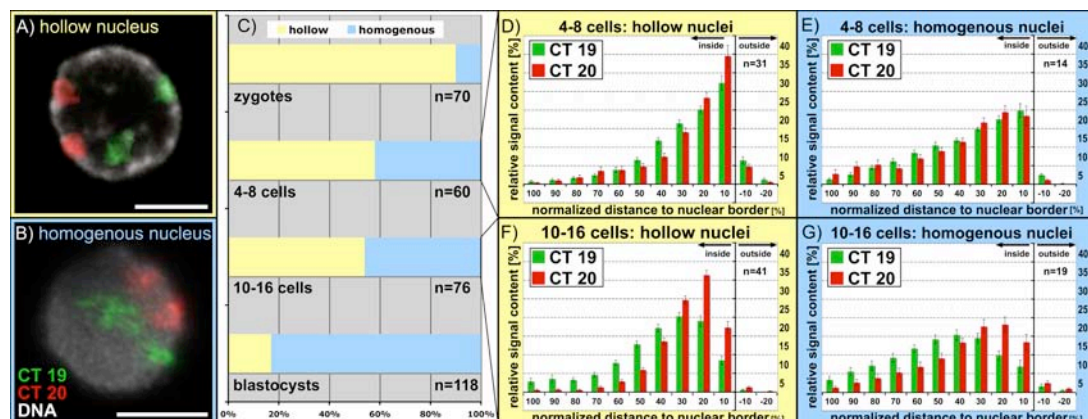


Fig. 40) Influence of the global DNA distribution on the radial distribution of CTs 19 and 20: Images shown in A and B show two typical cases of nuclei with a differing global DNA arrangement. The nucleus shown in A shows a large DNA free/poor region evoking the impression of a “hollow nucleus”, while the nucleus in B essentially resembles a DNA distribution similar to that of somatic cells with a more homogenous appearance. Nuclear DNA stained with DAPI is shown as a confocal mid section, while CTs represent superimposed maximum intensity projections. The chart in C illustrates the incidence of “hollow” nuclei in the analyzed developmental stages arguing for a reduction of this particular spatial genome organization during the course of preimplantation development. Distance distribution plots in D and E illustrate the chromosomal localization in hollow versus normal nuclei in embryos with 4-8 cells, i.e. before major genome activation, while plots depicted in F and G show the distribution in embryos with 10-16 cells, i.e. during major genome activation. While no gene density related distribution was found in embryos before major genome activation independent of the global DNA arrangement, the typical internal/peripheral localization of chromosomes 19 and 20 was visible in hollow as well as homogenous nuclei of embryos during major genome activation. Note that hollow nuclei show a generally more peripheral distribution of both chromosomes compared to homogeneous nuclei, which is consistent with the observation that the DNA free/poor regions were mostly observed in the nuclear center causing a “marginalization” of the genome.

4.4.7. Test of FISH on embryos of another species: the mouse model

FISH on 3D preserved preimplantation nuclei was tested accordingly in another species for proof of principle. Mouse preimplantation embryos were available and provide another interesting reason for further investigation: In the species mouse the major genome activation occurs during the second cell cycle of development. Consequently it represents a well suited object of investigation to test whether the establishment of a gene density related CT distribution as observed in cattle is really correlated with MGA and merely a timely coincidence. We received mouse embryos immediately when they have been washed out. We could cultivate them successfully until blastocyst stage in our lab (see Fig. 41).

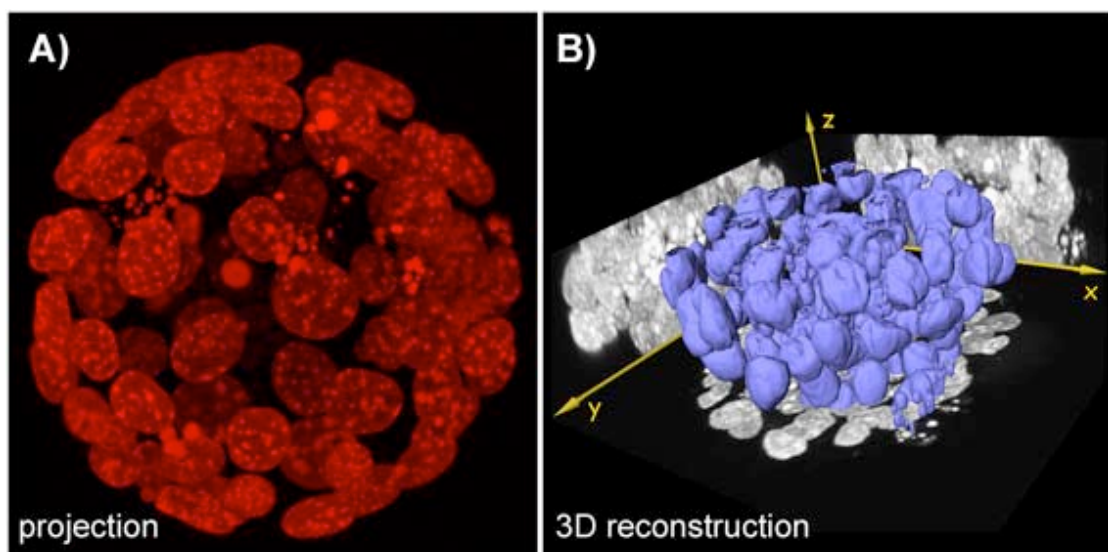


Fig. 41) Mouse blastocysts: Mouse embryos could be successfully grown up to blastocyst stage. On the left side (A) a projection of a confocal image stack is shown. DNA is shown in red by DAPI staining. On the right side (B) a 3D reconstruction of the data stack is shown.

4.4.7.1. Modifications of the FISH protocol for mouse preimplantation embryos

Fixation was performed as described for bovine embryos but with slight modifications: Embryos were much smaller and paler than bovine embryos. Since tracking of embryos in 12wells was difficult and risky to loose them they were treated in drops (except permeabilization). 4 cell stages were treated for the first time in HCl only in a concentration of 0.01N because they were extremely sensitive to this kind of treatment and tended to fall apart. In contrast the treatment in 0.1N HCl for zygotes was prolonged up to 5min because with shorter incubation time the zona pellucida could not be removed and no signals were obtained in that case.

4.4.7.2. Gene rich and gene poor chromosomes in mouse

It could be proven that in principle the protocol is working on mouse embryos as well. While zygotes showed only weak signals 4 cell stage embryos showed a strong FISH signal for CTs (see Fig. 42). Subject of investigation were CT 11, the most gene-rich chromosome (15.9 genes/Mb) and CT X, which has the third lowest gene content (7.9 genes/Mb) in mouse (Mayer et al. 2005).

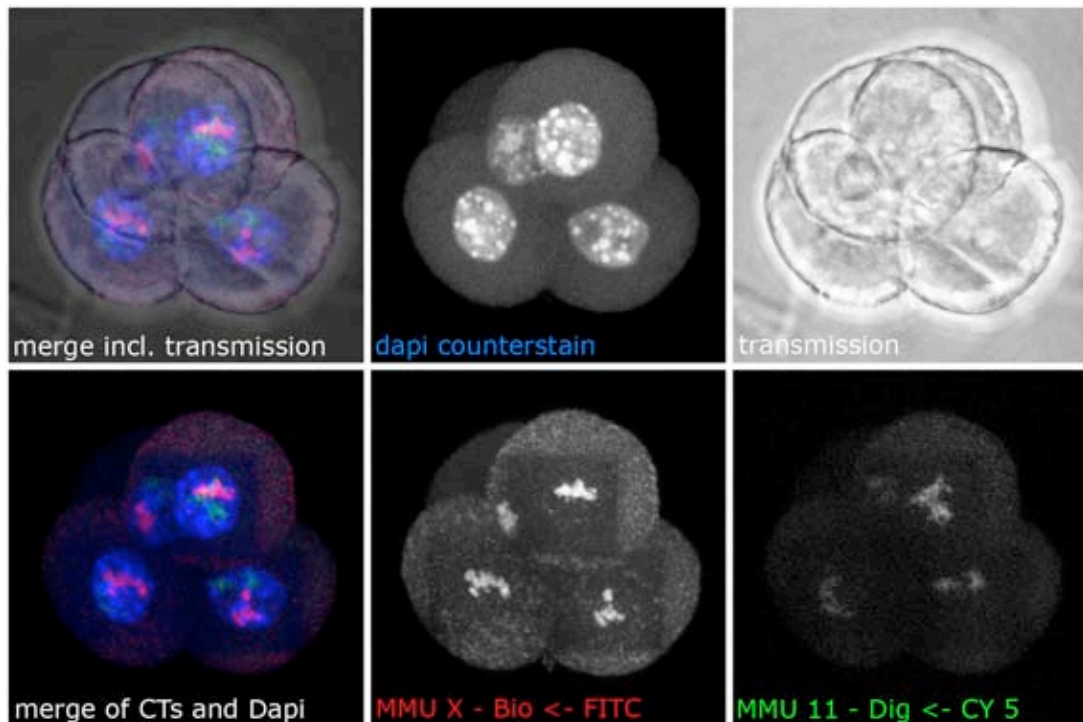


Fig. 42) FISH on mouse embryos: a mouse 4 cell stage is shown, overlays (very left panel) and according signal channels, with DNA counterstain DAPI (blue), transmission and CTs X (red) and CTs 11 (green).

4.5. Localization of an Oct4-GFP transgene in NT embryos

Genes for pluripotency are very important the beginning of embryonic development. One example is Oct4, a homeodomain transcription factor of the POU family, which is crucial for development and active throughout the preimplantation period. A loss of Oct4 expression in early mouse embryos results in a loss of pluripotency and a dedifferentiation to trophectoderm (Niwa et al. 2000; Niwa et al. 2005). Recently Oct4 resounded throughout the land as being one of the four essential pluripotency genes for the self-renewal potential of embryonic stem cells (Maherali et al. 2007; Okita et al. 2007; Wernig et al. 2007). Even if it was shown later by the group of R. Jaenisch that this is not the case for mouse somatic stem cell renewal which even requires less factors (Lengner et al. 2007; Wernig et al. 2008). However the importance is unchallenged and therefore a far interest in Oct4 and its function is

present. To study the process of early gene activation an elegant system was developed in the group of E. Wolf that allows a monitoring of the gene expression (Wuensch et al. 2007).

4.5.1. The reporter gene construct GOF18- Δ PE-EGFP

The reporter construct GOF18- Δ PE-EGFP with a length of 21.2kb contains an enhanced green fluorescent protein (EGFP) sequence as reporter. It is flanked by a 9kb fragment of the murine Pou5f1 (=Oct4, old nomenclature) with a deletion in the proximal enhancer (PE) as promoter or enhancer. On the other side it is flanked by a 9kb fragment of the structural Pou5f1 gene containing 5 exons (Kirchhof et al. 2000). A schematic drawing of the GOF18- Δ PE-EGFP reporter construct is given in Fig. 43.

In the group of E. Wolf this construct was stably integrated at a single site in a bovine fetal fibroblast cell line: Therefore they co-transfected BFF116 cells by electroporation with the GOF18- Δ PE-EGFP reporter



Fig. 43) The reporter gene construct GOF18- Δ PE-EGFP (21.2kb), which contains EGFP flanked by a 9kb fragment of the murine Pou5f1 upstream region with a deletion in the proximal enhancer (PE) and a 9kb fragment containing the (nontranscribed) structural Pou5f1 gene. Exons are represented by black boxes. The red boxes mark the target sites for the transgene-specific FISH probe. From (Wuensch et al. 2007)

construct and a neomycin resistance cassette FRT-neo-FRT. They further analyzed (FISH, genotyping, karyotyping, cryopreservation) resistant cell colonies. Then they used those transfected BFF cells (with a single-locus integration of the GOF18- Δ PE-EGFP reporter construct but without detectable EGFP expression) at passage 9-11 for first-round somatic cell nuclear transfer (SCNT). Fibroblasts obtained from transgenic fetuses (checked for positive EGFP expression on day 4-6; used for in-vitro outgrowth formation at day 7) were used at passage 4-6 for second-round SCNT. Pregnancies were terminated at day 34 after SCNT. The recovered fetuses were finally used by them to establish transgenic fetal fibroblast culture BFF451-1 (Wuensch et al. 2007). In the present project exclusively these cells were used for nuclear transfer (NT) experiments. During embryo development different stages of embryo development were investigated regarding their Oct4 activation. Expression of Oct4 was simply detectable by the expression of EGFP in blastomeres of embryos, but unfortunately not after FISH procedure. It was shown by A. Wuensch et al. that Oct4 was activated during the fourth cell cycle with increasing EGFP levels in growing stages like embryos of day 6 if development of embryos was proper. Later, in day 34 embryos the transgene was shown to be silenced like the endogenous Oct4. For detailed description of the system and all results see

(Wuensch et al. 2007). In the following text the reporter gene construct will be called GOF (transgene).

We used this system to investigate whether this developmentally regulated transgene would re-localize upon its activation during MGA (major genome activation).

4.5.2. Oct4-GFP (GOF) – the transgene and its localization

To study not only the localization of GOF in relation to the nucleus but also in relation to its harboring territory it was necessary to identify the integration site of the GOF construct in the donor cell line. Previously it was shown that there was only one integration site (Wuensch et al. 2007) but the respective chromosome had not yet been identified.

As far as bovine chromosomes were not very different in size the localization of GOF was hard to guess. I tested gradually the following paint probes for colocalization with the transgene: BTA 10, 11-29. Tests were done on metaphase spreads from BFF451-1. The same cell line that was exclusively used for all further NT experiments. It turned out that GOF was integrated in bovine chromosome number 13. Though already visible from DAPI counterstained chromosomes we used a centromeric (alpha satellite) probe together with the GOF and CT 13 probe to confirm the proximity of the integration site close to the centromeric regions. As a second line of evidence, to determine the identity of the transgene carrying chromosome I used a chromosome specific paint probe for sheep (*Ovis aries*) chromosome 13 (kindly given by S. Müller (LMU, Munich)) which is homologous to bovine chromosome 13 (Ansari et al. 1999). The results clarify the colocalization of sheep and bovine chromosome 13 as well as GOF (see Fig. 44).

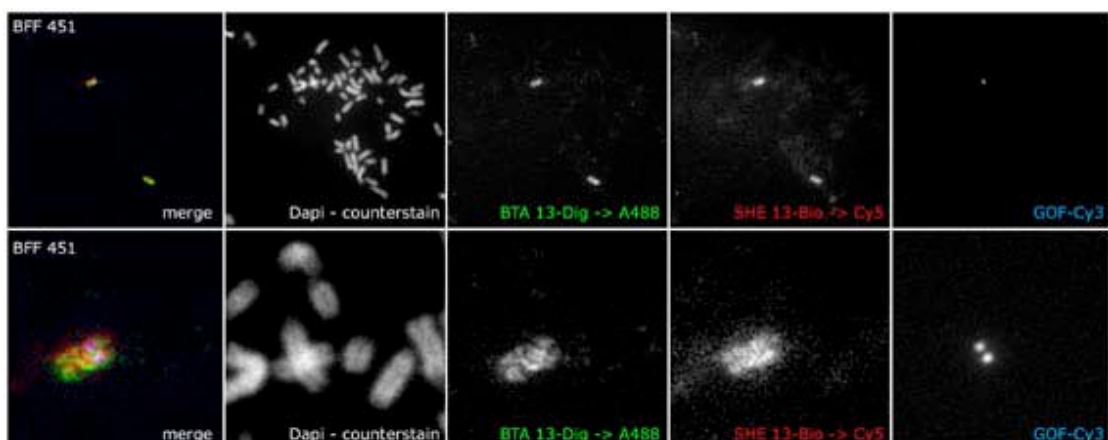


Fig. 44) Localization of GOF: the transgene GOF (blue) is integrated on bovine chromosome 13 (green); the localization was confirmed with the corresponding sheep probe (red); DNA counterstain (white) is performed with DAPI;

4.5.3. GOF distribution in BFF451-1 nuclei

As expected and according to the endogenous Oct4 gene in diploid fibroblasts BFF451-1 the transgene was not active because EGFP fluorescent signals were negative, i.e. not GFP fluorescence could be detected. In 29 fibroblasts the radial distribution of CT 13, the centromeres and GOF were evaluated with the eADS program. Again, the normalized median values were determined.

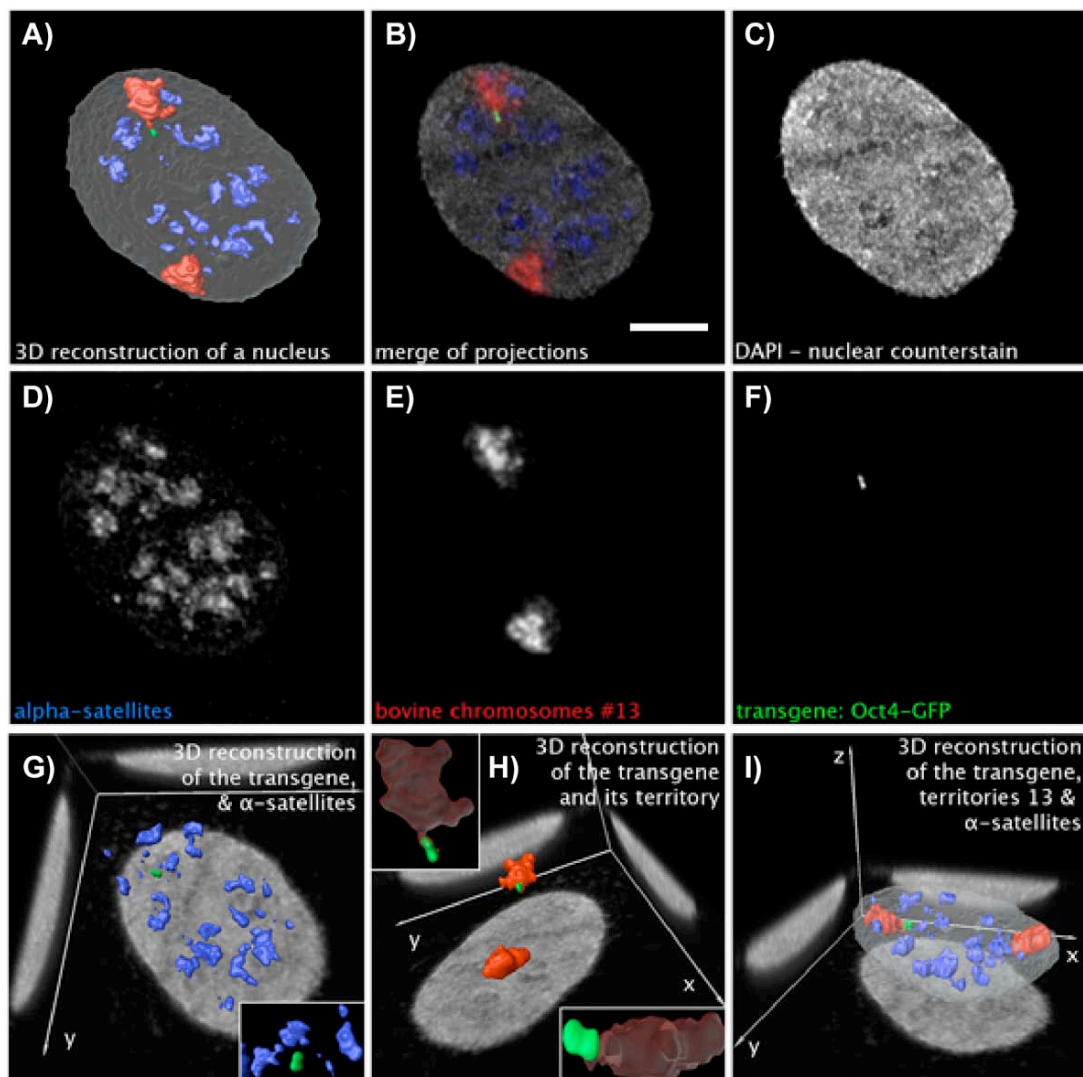


Fig. 45) Localization of GOF in bovine fibroblast nuclei: frames C) – F) show projections of the single channel; B) shows a merge of all projections with the DAPI stained whole DNA (white), GOF (green), CT 13 (red) and centromeres (blue); frame A) shows a 3D reconstruction in the same view than B); frames G) – I) show 3D reconstructions of the transgene (green) in reference to the different compartments; bar: 5 μ m;

The median for GOF with respect to the nuclear periphery was 59%. In comparison to a DAPI distribution the distribution of GOF was more internal ($p < 0.001$). In relation to the chromosome territory 13 the median value for GOF was 0%. GOF is found inside the CT but the distributions of GOF and the CT 13 were not significantly different ($p = 0.738$). As from the quantitative evaluation that distinguished between

internal and external location from the CT visual inspection confirmed that GOF was in all analyzed nuclei within the harboring CT.

The α -satellites showed a median of 43% in relation to the nuclear border, which was significantly more internal than the DAPI distribution ($p < 0.001$).

The bovine chromosome 13 has a length of 83Mb and contains 775 genes, which is equivalent to a gene density of 9.7 genes/Mb. This represents roughly the overall gene density of all bovine chromosomes, which equals 9 genes/Mb.

CT 13 showed a median of 39% with respect to the nuclear periphery. The distribution was significantly different to the DAPI distribution ($p < 0.001$). It was possible to distinguish between the two homologues of CT 13 because only one was containing a GOF signal. To exclude the possibility that GOF would have an influence on the localization of CT 13 a separation of the two homologues, in the following called "CT 13+GOF" and "CT 13-GOF", was made. The distributions of the separated CTs were not significantly different from each other ($p = 0.352$). The median of the CT 13 including the transgene was 34%, while the one for the CT 13 without GOF was 39%. Both curves were again significantly more internal than the DAPI distribution (CT 13+GOF: $p = 0.005$; CT 13-GOF: $p < 0.001$).

4.5.4. Distribution of GOF in NT embryos of different developmental stages

Stages of day 2 (4-8 nuclei; in average: 5 nuclei/embryo) and day 4 (10-16 nuclei; in average: 11 nuclei/embryo) embryos were investigated, as well as blastocysts. For evaluation only embryos with an expected number of nuclei for the respective age/stage were considered, which was generally a minority given that only few NT embryos develop properly due to incomplete or faulty reprogramming (Fig. 46).

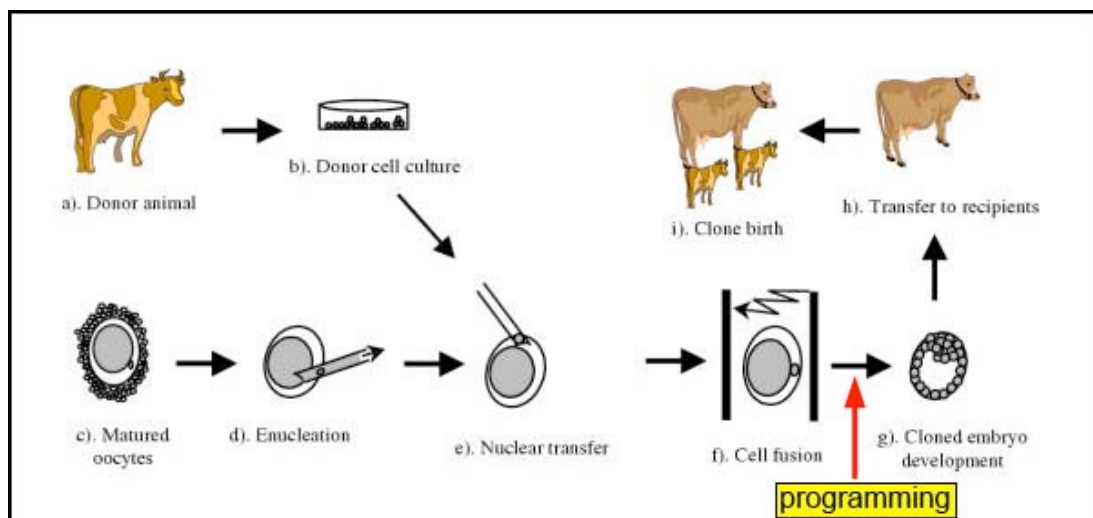


Fig. 46) Scheme of nuclear transfer: A donor cell nucleus from culture (a, b) is transferred into an enucleated oocyte (c-e). Cell fusion is induced by an electric pulse (f). Donor cell nucleus has to undergo reprogramming processes for further development to blastocyst (g) and transfer into recipient (h) which might result in healthy offspring (i) (taken from (Latham 2004)).

4.5.4.1. Distribution in day 2 embryos

33 nuclei were evaluated belonging to the group of day 2 embryos all having less than 8 nuclei per embryo. The nuclei were collected from 17 different embryos with an average size of 5 nuclei per embryo. The median for GOF in relation to the nucleus was 13%. The curve was not significantly different from the DAPI distribution ($p=0.083$). The median for GOF in relation to the CTs 13 was 16%. The distribution of GOF in respect to the CTs 13 was significantly different ($p=0.029$). The median for the distribution of CTs 13 in the nucleus was 17%. The statistical analysis revealed that it was not different from the DAPI distribution ($p=0.449$). If the homolog CTs were distinguished in transgenic and non-transgenic, the median for CT 13+GOF was 15%, the median for CT 13-GOF was 14% which revealed no significant difference ($p=0.416$). Both curves were statistically indistinguishable from the DAPI distribution (CT 13+GOF: $p=0.262$; CT 13-GOF: $p=0.770$). The intranuclear distributions of GOF and CTs 13 with respect to the nuclear periphery were not significantly different from each other ($p=0.248$). Results are depicted in Fig. 48 and 49.

4.5.4.2. Distribution in day 4 embryos

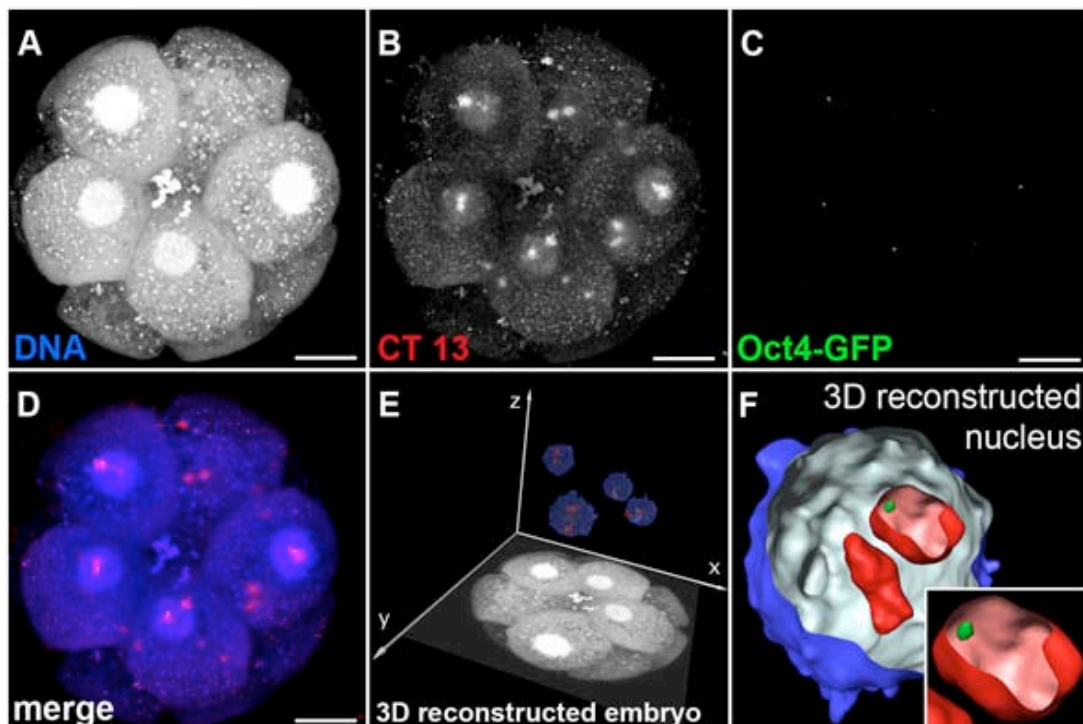


Fig. 47) Maximum intensity projections of confocal optical serial sections (A-D) and 3D-reconstructions (E-F) of a bovine NT embryo containing 12 nuclei: 3-D FISH was carried out with bovine chromosome 13 paint probe (red) and a probe for the Oct4/GFP transgene (green). Four nuclei are highlighted in E. F shows a single 3D reconstructed nucleus at a higher magnification. Scale bar: 20 μ m. Note that the Oct4/GFP locus resides more in the interior of the CT compared to the fibroblast nucleus shown in figure 45.

For this stage of development 33 nuclei were evaluated, collected from 6 different embryos with an average size of 11 nuclei per embryos. Results revealed a median of 20% for GOF and 26% for CT 13 with respect to the nuclear border. Both distributions were not significantly different from the DAPI distribution ($p=0.902$ and $p=0.078$) and they were not significantly different from each other ($p=0.222$). When evaluated individually the median of the transgenic and non-transgenic CTs were identical equaling 20%. Distributions were not different from each other ($p=0.090$) and not different from the DNA distribution ($p=0.437$ and $p=0.051$).

The evaluation with CT 13 as a reference structure showed a median value of 24% for the GOF signal. There was no statistical difference from the CT 13 distribution ($p=0.909$). For details see Fig. 47. Results and examples are depicted in Fig. 48 and 49.

4.5.4.3. Distribution in day 7 embryos

All 4 evaluated day 7 embryos were blastocyst with more than 100 cells. For the evaluation 64 nuclei were used.

The median for GOF in relation to the nucleus, visualized by DAPI was 23%. This was not significantly different from the DAPI distribution ($p=0.954$). In relation to the CT the median was 27%, not statistically different from CT 13 distribution ($p=0.364$). The median for CT 13 in the nucleus was 30%. This was significantly more interior than the DAPI distribution ($p=0.007$). The distributions of GOF and CT 13 were not significantly different from each other ($p=0.453$). If the two homologues were analyzed separately, the median was in both cases 23%. The distributions were not significantly different from each other ($p=0.220$) and CT 13-GOF was not distributed significantly different to the DAPI distribution ($p=0.858$), however CT 13+GOF was different ($p=0.046$). Results are shown in Fig. 48 (reference: DAPI) and Fig. 49 (reference: CT 13).

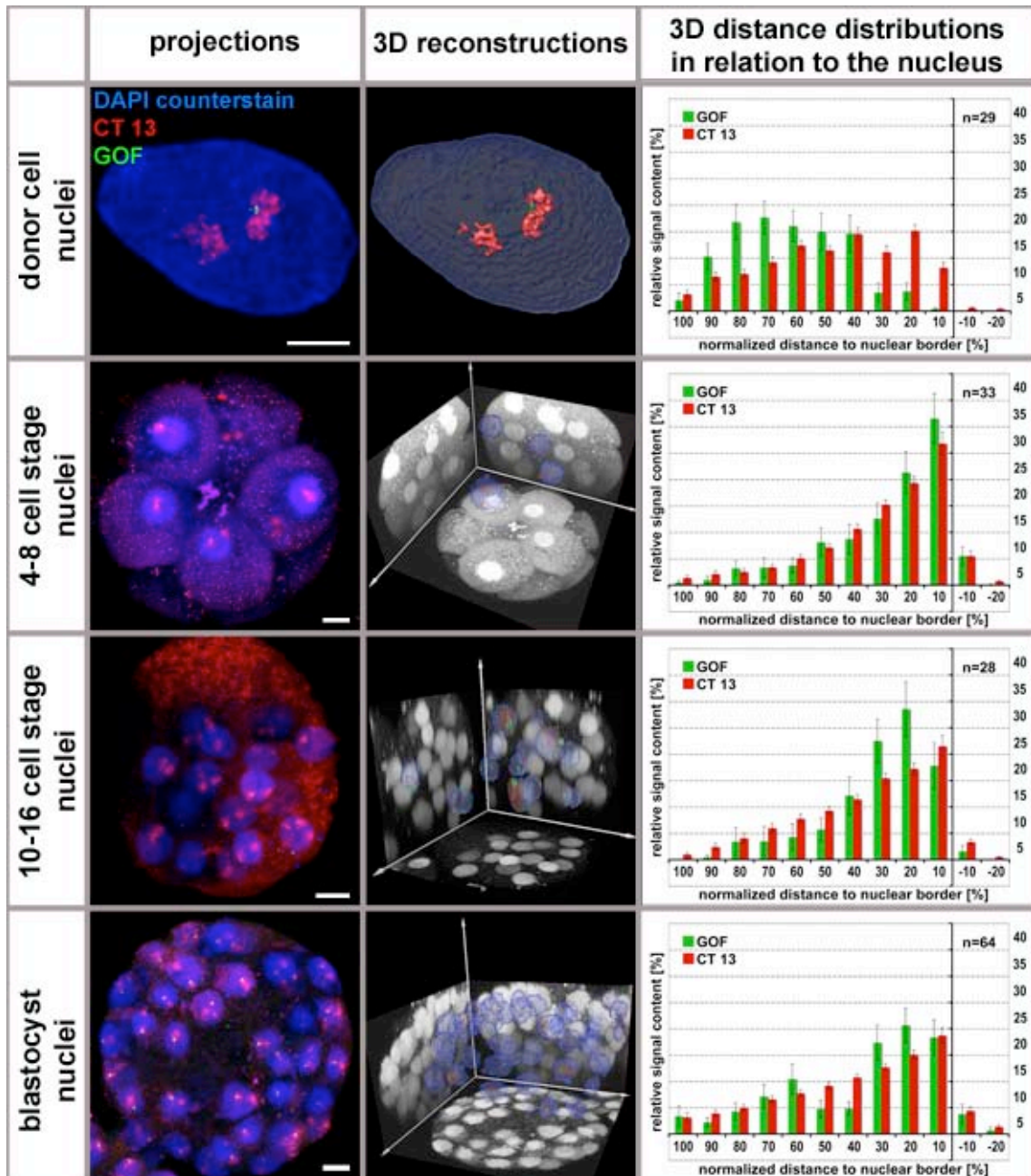


Fig. 48) Radial distributions of Oct4-GFP (GOF) and CTs 13 in bovine NT embryos: Territories of bovine chromosomes 13 and the transgene Oct4-GFP, visualized by FISH are shown in red and green, respectively, while nuclear DNA stained by DAPI is depicted in blue. Representative embryos are shown for each of the three analyzed consecutive developmental stages. In the left column maximum intensity projections are depicted, while the middle column highlights the respective embryo as 3D reconstructions. Note that reconstructions show embryos from a different perspective. Scale bars: 10 μ m. The distance distribution plots for the respective developmental stages are shown in the right column. Whereas CTs 13 and the transgene show a similar radial distribution in all embryonic stages ($p > 0.1$), a significant difference in their nuclear position can be observed in donor cells ($p < 0.001$). The distribution between donor cells and all developmental stages differs significantly ($p < 0.001$) while comparing the distributions in the different embryonic stages, only a significance between 4 cell stages and blastocysts ($p = 0.22$) is found. The radial distribution for BTA 13 CTs are significantly different ($p < 0.01$) for all comparisons between donor cells and embryonic stages as well as all embryonic stage among each other, except donor cells and blastocysts ($p = 0.083$). In general there is a re-localization of both, the transgene and CTs 13 from the inside of the nuclei found in donor cells towards the periphery if transferred into an oocyte. During early development there is again a re-localization of the transgene and CTs 13 towards the interior of nuclei found.

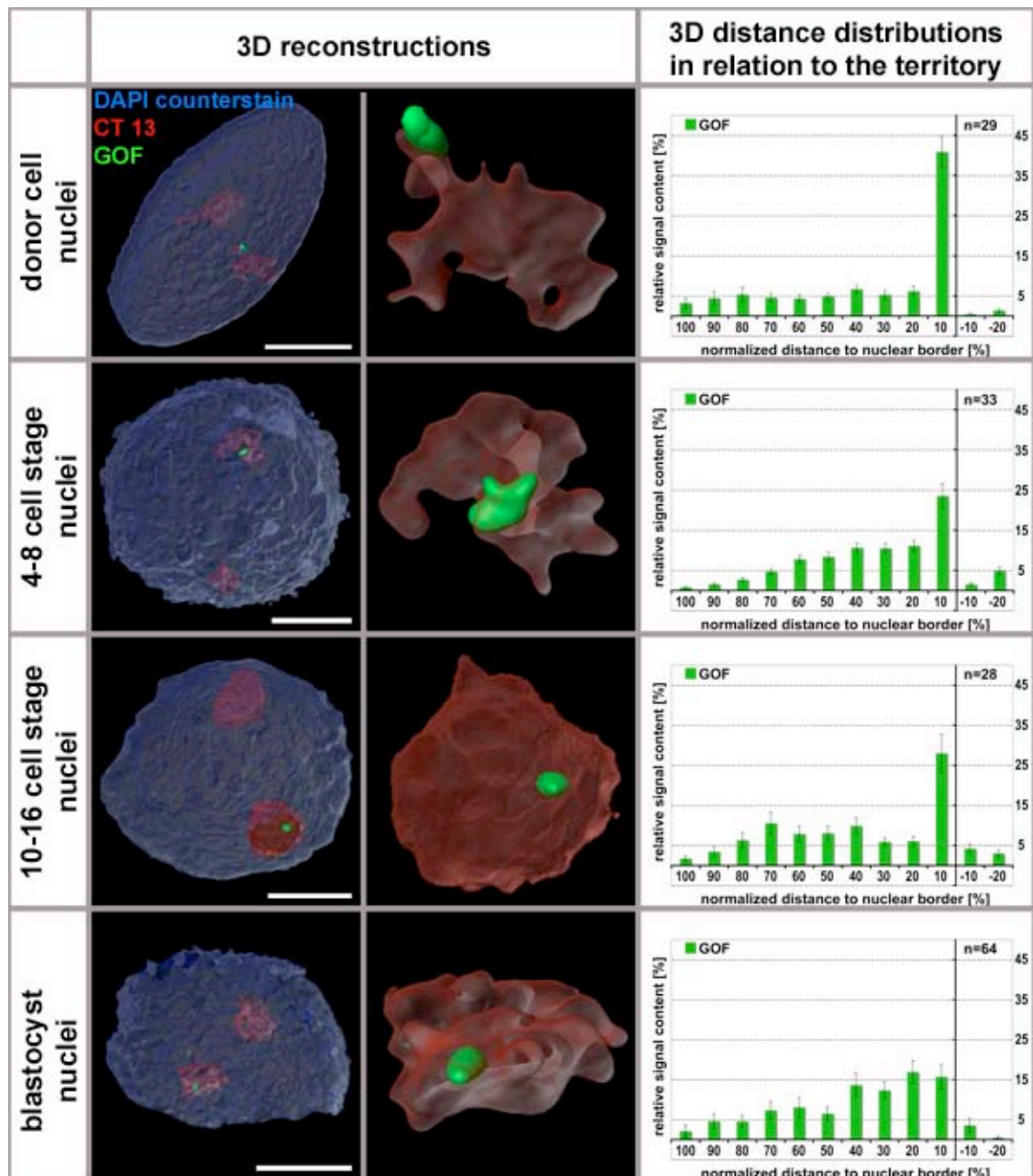


Fig. 49) Radial distributions of GOF (Oct4-GFP) in bovine NT embryos in relation to its harboring CT: Territories of bovine chromosomes 13 and the transgene Oct4-GFP, visualized by FISH are shown in red and green, respectively, while nuclear DNA stained by DAPI is depicted in blue. Representative nuclei from donor cells and embryos are shown for each of the analyzed groups. In the left column 3D reconstructions from the whole nuclei including CTs 13 and the transgenes are depicted, while the middle column highlights the respective CTs harboring the transgene as 3D reconstructions. Scale bars: 10 μ m. The distance distribution plots for the respective stages are shown in the right column. While the transgene is located at the periphery of CTs 13 in donor cells (the repressive state of the transgene) it is constantly moving inside during the different developmental stages, even upon activation which occurs with the 10-16 cell stage.

4.5.4.4. Comparing the GOF distribution in different developmental stages

To look for differences in the spatial distribution of GOF that might be correlating with the activation of the transgene all distributions between the stages were compared, i.e. the distributions of the CTs and GOF with respect to the nuclear periphery, as well as the distributions of GOF from the CT 13 periphery.

4.5.4.4.1. GOF in relation to CT 13

The localization of GOF in fibroblasts in relation to the CT was very peripheral with a median of 0%. In day 2 embryos, where the transgene was shown to still be silent the localization of the transgene was slightly but not significantly changed ($p=0.788$). However the GOF signal was now found more interior with a median value of 16%. In later embryonic stages, correlating with the transgenes transcriptional activation (day 2 to day 4) as well as with its upregulation (day 4 to day 7), the GOF signal was found more and more interior in reference to the CT. Corresponding medians were 24% (day 4) and 27% (day 7). Irrespective of the decreasing medians with further developmental stage there was only a statistically significant difference found for the comparison between fibroblasts and blastocysts ($p=0.032$) and between d2 embryos and blastocysts ($p=0.018$). All other comparisons revealed not a statistically significant difference ($p>0.5$) (see Fig. 50).

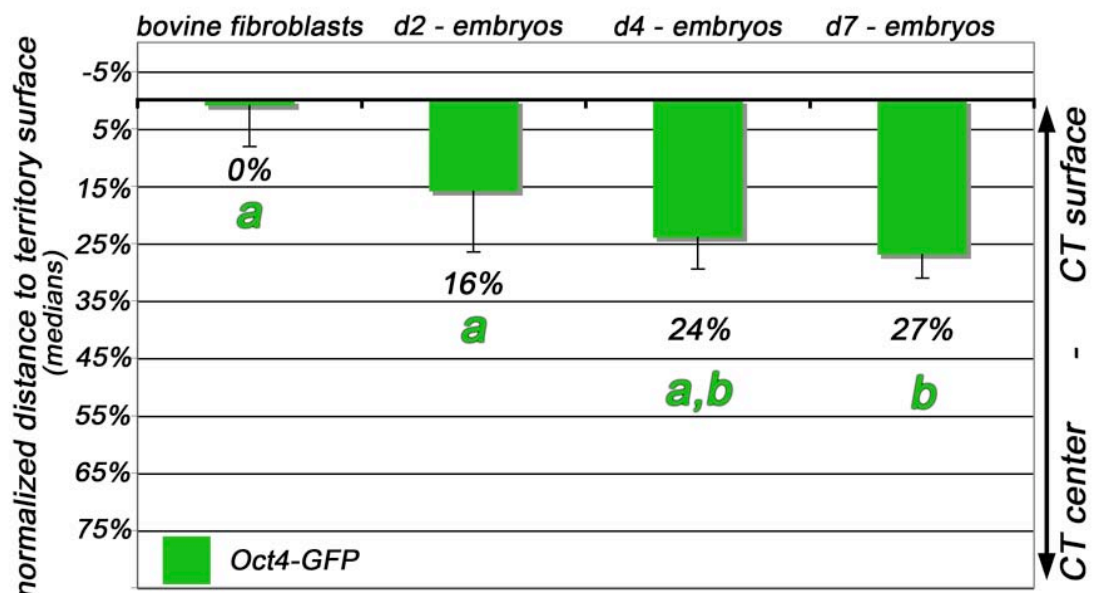


Fig. 50) Comparison of the GOF localization between different developmental stages: Shown are the medians of the radial distribution of Oct4-GFP in relation to CTs 13 in donor cells and different developmental stages, respectively. Median values are given in percent [%]. Error bars show the standard errors. Different small green letters indicate significant difference ($p>0.5$).

4.5.4.4.2. GOF in relation to the nucleus

When the localization of GOF with respect to the nuclear border was compared between the individual developmental stages I found a significant difference between fibroblasts and all embryonic stages going along with an increasing internalization of the transgene from day 2 to day 4 as well as from day 4 to day 7. In fibroblasts GOF was located most interior, showing a median of 59%. In contrast, in day 2 embryos GOF was located much more at the periphery with a median of 13%. In later stages it was again found progressively more in the nuclear interior with a median of 20% day 4 embryos and 23% in blastocysts (compare Fig. 51). The localization of GOF in the BFF cells was significantly different to all other embryonic stages ($p < 0.001$). The localization of GOF between day 2 and day 7 was significantly different ($p = 0.022$). The comparison between day 2 and day 4 as well as day 4 with day 7 revealed no significant difference ($p = 0.270$ and $p = 0.576$).

4.5.4.4.3. CT 13 in relation to the nucleus

The median localization of CT 13 (both homologues evaluated together) was 39% in BFF cells. In early embryos of day 2 it was found much more at the periphery having a median of 17%. In later developmental stages the CT 13 was found increasingly more interior with median of 26% (day 4) and 30% (day 7). The localization of CT 13 with respect to the nuclear periphery in BFF cells in comparison was significantly different to all embryonic stages ($p < 0.001$), except day 7 ($p = 0.083$). The CT 13 localization in day 2 differed significantly from day 4 and day 7 ($p = 0.004$ and $p < 0.001$) as well between day 4 and day 7 ($p = 0.008$). Results are shown in Fig. 51.

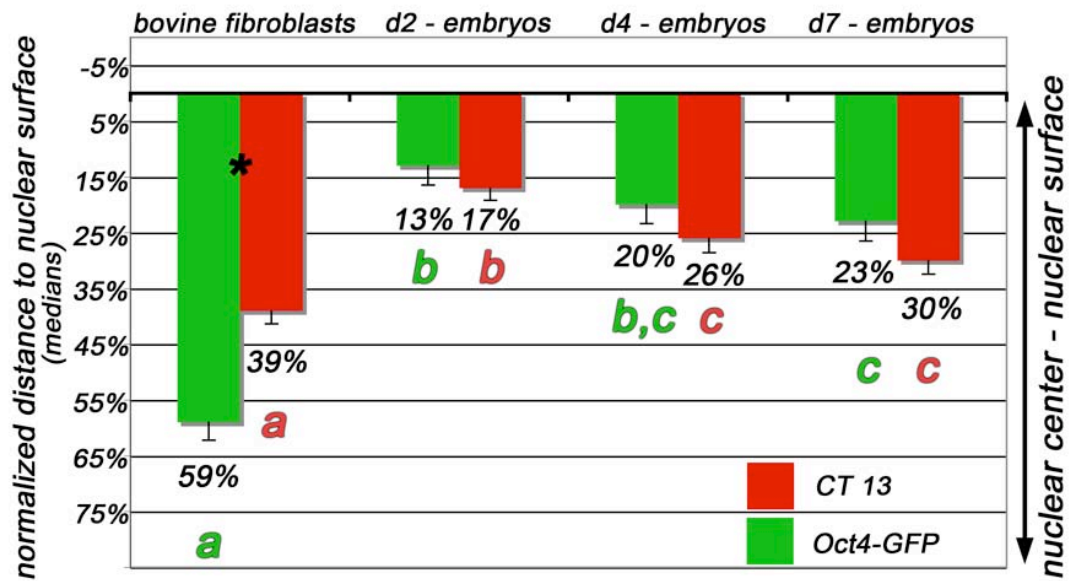


Fig. 51) Comparison of GOF & CTs 13 localization in different developmental stages: Shown are the medians of the radial distribution of CT 13 and Oct4-GFP in relation to the nuclear border in donor cells and different developmental stages, respectively. Median values are given in percent [%]. Bars indicate the standard error. Asterisk indicates a significant difference between the distribution of Oct4-GFP and CT 13. Different small green/red letters indicate significant difference ($p > 0.5$).

5. Discussion: Establishment of CT pattern during early preimplantation development and potential influences related to nuclei shape and cell cycle stage

5.1. Symmetry of sister cells

The establishment of CTs was shown to occur during early G1 (Gerlich et al. 2003; Walter et al. 2003). Thereafter movements are restricted to smaller scales (Abney et al. 1997; Edlmann et al. 2001; Gilbert et al. 2004). The neighborhood positions of CTs are depending on their positions in the metaphase plate, resulting in sister cells with a high degree of symmetry, which was already postulated 100 years ago by Theodor Boveri (Boveri, 1909).

This was confirmed previously for HeLa cells (Walter et al. 2003). In my thesis a quantitative analysis was performed, with HeLa cells, human mammary epithelial cells (HMEC) and human diploid fibroblasts. As shown in the present work the radial distribution pattern is conserved in individual cells, but not the side-by-side arrangements of CTs. While the symmetry for sister cells is very high (see Fig. 52), a high variation already in cousin cells was found. After three cell cycles the symmetry value between

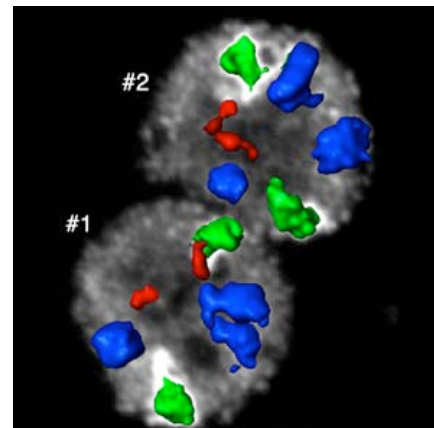


Fig. 52) 3D reconstruction of two HeLa nuclei showing a symmetrical pattern of CTs 4 (green), 7 (blue, triploid) and 21 (red). Projection (grey) is outlining the nuclear border.

cells in one clone was comparable to not related cells. Experiments with living cells enable me to define the genealogy of cells to ensure the relationships between investigated nuclei. In agreement with earlier data these findings strongly argue for the determination of CT pattern during mitosis, especially during the formation of the metaphase plate, whereas separation of sister chromatids finally leads to symmetrical daughter cells. Since this formation is established individually with each cell cycle the pattern in cousin cells are already different. Independent of this mechanism, a radial distribution according to gene-density is maintained and re-established after every cell division in all nuclei (Cremer and Cremer 2001; Cremer et al. 2006). For further discussion see attached manuscript (Köhler et. al, in preparation).

5.2. Radial CT distribution in somatic cells

Earlier studies had shown that there are apparently no fixed neighborhood positions of CTs in nuclei of different cell types, while a radial distribution of CTs was found in all cell types investigated so far (Cremer and Cremer 2001; Cremer et al. 2006; Lanctot et al. 2007). Discrepancies concerning the influence of cell cycle stage and cell shape between a number of publications have caused considerable confusion with respect to this issue (Croft et al. 1999; Bridger et al. 2000; Bolzer et al. 2005; Neusser et al. 2007). In this work the following experiments were set up to address these questions:

The location of different pairs of CTs in human fibroblasts in S-phase and in G0 phase was analyzed to look for cell stage specific changes. Fibroblast nuclei of different species were artificially re-shaped by using specially coated slides to investigate the influence on CT distributions.

5.2.1. Influence of the cell cycle

For CT positioning in flat shaped fibroblasts some discrepancies were published in the past years. The distribution motifs were described as gene-size (Bolzer et al. 2005) or gene-density dependent (Croft et al. 1999; Neusser et al. 2007). The point of the respective CT distribution was concordantly found to be during early G1 (Croft et al. 1999; Walter et al. 2003). However changes in radial CT arrangement between quiescent and senescent cells were described (Bridger et al. 2000).

Subjects of investigation were the equally sized human chromosomes 18 and 19, typically known for their low and high gene content, respectively. The Bickmore group did not find a significant difference in the distribution of both CTs in cells that were serum starved and had exited the cell cycle, i.e. were quiescent, while in proliferating fibroblasts the difference was very pronounced (Bridger et al. 2000). Since a recent M-FISH analysis, visualizing all human chromosomes in fibroblasts at the same time, revealed no difference between the localization of CTs 18 and 19, an investigation concerning cell cycle stages was undertaken in a subsequent experiment described in this work. The results for both, G0 and cycling cells showed that CT 18 was slightly shifted towards the nuclear periphery but not significantly. This difference in nuclear distribution in both CTs was slightly but not significantly more pronounced in S-phase cells using an evaluation methods called 3D-RRD which determines the relative distance of fluorescent objects from the nuclear center (Bolzer et al. 2005). As compared to the eADS software which is measuring absolute distances from the segmented nuclear border to each signal voxel the 3D-RRD program is measuring relative distances in shells based on the nuclear center.

To confirm the data as obtained for CTs 18 and 19, other chromosomes were investigated to uncover a potentially cell cycle dependence of CT arrangements. All small chromosomes, like Y, 17, 18, 19, 20, were located towards the interior in comparison to the global DNA distribution, visualized by TOPRO staining. Only the large chromosome 1 was located at the periphery, but again without a significant difference between G0 and cycling cells. The differences between CT 1 and 20, which have both the same overall gene content, but differ in size, were significant in G0 and S-phase cells. This again indicated an overall size dependent distribution independent from the cell cycle stage. The only shift in CT distribution between different cell cycle stages was found for CT Y, which moved towards the interior in cycling cells (Bolzer et al. 2005). Moreover the distribution between CTs Y and 17 was significantly different in cycling cells but not in G0 cells, besides their similar small size being 58Mb and 79Mb. The results were the same for nuclei evaluated in 2D and 3D.

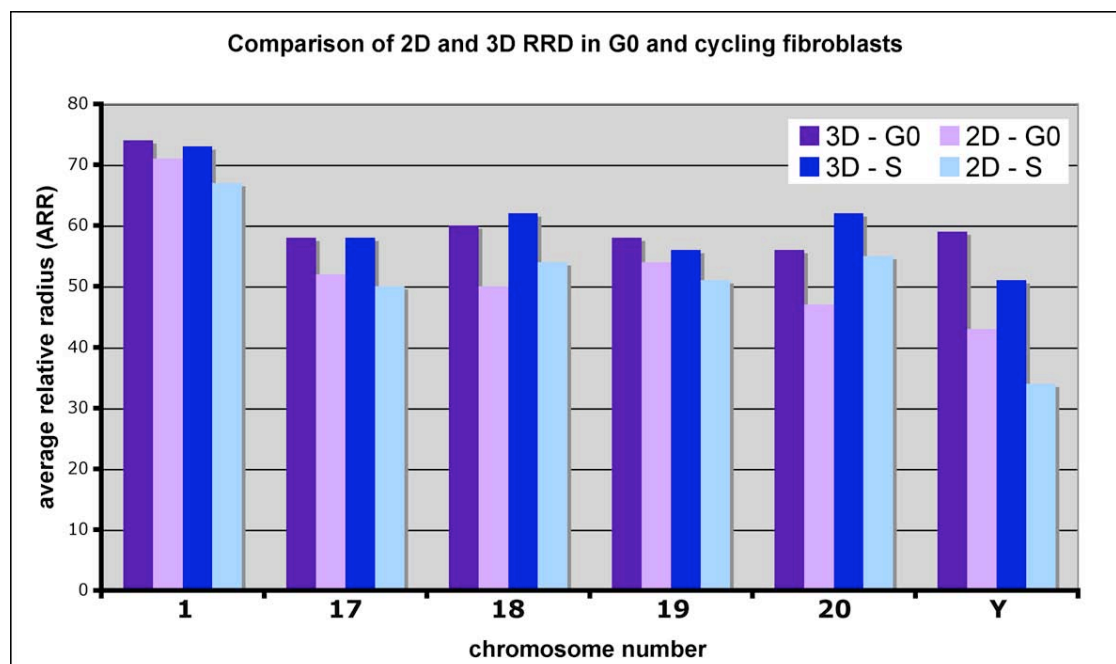


Fig. 53) ARR of different CTs in G0 and cycling human diploid fibroblasts: evaluated in 3D- and 2D-RRD.

Notably the experimental set-ups were different in the groups of W. Bickmore and T. Cremer. While in the Bickmore group fibroblasts were serum-starved and senescent cells were at a very late passage (p38) (Bridger et al. 2000), fibroblasts analyzed in the Cremer group were all taken from the same semi-confluent culture whereas the cell cycle stage was defined by replication labeling and staining of their cell cycle marker Ki67 (Bolzer et al. 2005). An influence due to the age and culture conditions of fibroblasts cannot be excluded. With increasing age further changes cannot be excluded. Therefore the fibroblast nuclei in our

experiments were not as old as the once used by the Bickmore group (passage ~12 vs. passage 38). Anyway G0 cells in a semiconfluent culture are most probably different from G0 cells obtained by serum starvation and therefore might show a different nuclear organization.

5.2.2. Implications of evaluation methods

Evaluations of CTs reveal similar tendencies in different cell cycle stages. However results from different groups showed considerable differences with respect to the significance of the observed differences. Because all groups use their own modified FISH protocols and different evaluation methods it appears probable that differences arise from the distinct experimental approaches.

The quantitative evaluations performed in the Bickmore group were mainly based on the evaluation of flattened specimen, which results from the FISH procedure that includes a fixation in methanol/acetic acid and air drying of specimen. Even if they write that they can confirm their results in 3D, they do not use 3D preserved cells for the whole evaluation procedure but only in parts. The nucleus, determined by DAPI staining, was divided into 5 concentric shells (or rings). Shell 1 reflected the core of the nucleus and shell 5 the periphery. The proportion of FISH signal for each CT in the according shells was then determined (Croft et al. 1999).

In the Cremer group two different softwares are used for evaluation: The program RRD can be used in 2D or 3D, which means that either projections (which corresponds to flattened specimen) or morphology preserved 3D objects can be used. In either case the nucleus was divided into 25 concentric shells (3D) or rings (2D). These shells were defined by dividing the x-, y- and z- radii of the nucleus into 25 nuclear shells/rings of equal thickness. As a consequence, the innermost shell (0% of the radius) provides the smallest volume or area, while the outermost shell (100% of radius) has the biggest volume or area. All voxels attributed to a given CT were located into one of the shells/rings (Cremer et al. 2001). CTs were defined by a manually set threshold, whereas subjectivity may influence the outcome. We could show that a potential bias in the evaluation by choosing such a threshold value manually was neglectable, at least within a reasonable range of threshold. As shown in a test analysis where different thresholds for the same data set are use, tendencies and significances of the results remain the same (see Table 11).

Table 11: ARR of CTs 4, 7 and 21 in 22 HeLa nuclei, measured in 2D with the RRD program. Evaluations were performed 3 times, with a minimum, optimum and maximum threshold respectively. Distributions among each other revealed no significant difference ($p>0.8$).

	DAPI	CT 4	CT 7	CT 21
minimum	60.61	58.98	61.98	41.87
optimum	62.19	60.33	63.58	43.30
maximum	64.47	62.83	65.99	45.61

The RRD program represents a well-suited evaluation method for round/spherical shaped nuclei. When nuclei show a flat, ellipsoidal or irregular shape a division into concentric shells is inaccurate. Therefore another program, that measures the shortest absolute distances (ADS) from each voxels of a signal to a given surface, was developed, described in detail in (Albiez et al. 2006; Kupper et al. 2007). The segmentation of the object of interest as well of the reference object is again threshold dependent. Distances that describe an internal location within the reference object were given as negative values, the once located outside are given as positive values. Normalization is done by setting the maximum distance for each nucleus to 1, which corresponds to the smallest radius. All other distance values were then given as the proportion to this maximal value (between 0 and 1). Results were grouped into ten classes of frequency distribution. Voxels at the very periphery were accordingly assigned to the group having a distance of 0% of the largest possible distance and the ones in the center were assigned to 100%. For a detailed description and comparison of the RRD program with the ADS program see (von Hase et al. submitted).

For accuracy the evaluations concerning the radial distribution of CTs 18 and 19 on human diploid fibroblasts, originally performed with the RRD program (see Fig. 18 and published in (Bolzer et al. 2005)), were repeated with the ADS program (see Fig. 19). This time a significant difference comparing the location of CTs 18 to 19 was found in the case of cycling cells for absolute distances. If the distance values were normalized the radial distribution of CTs 18 and 19 were significantly different in cycling **and** G0 cells. One should note that a chromosome size dependent distribution pattern is not excluding that CTs are simultaneously arranged according to their gene-density. Investigations in species with similar-sized chromosomes revealed that a gene-density correlated pattern is decisive (Neusser et al. 2007). Most probably a gene-density dependent distribution is masked by gene-size in the case of flat human fibroblasts. The flatness of fibroblast nuclei results in a nearly 2D shape of nuclei. The center of the nuclei and the top and bottom of cells (in z direction) come very close together but not the center and the borders in xy-direction. This is why a 2D evaluation might be appropriate with flat shaped fibroblasts. Any attachment of the CTs to the nuclear lamina that might be involved in a real peripheral location cannot be seen in flat nuclei. This leads us to the idea of artificially shaped nuclei.

5.2.3. Positions in xy- and z-dimension

Fixation protocols that helped to preserve the shape of nuclei and using image acquisition with increased axial resolution, such as CLSM, provide information in all 3 dimensions. To consider the distances to the reference surface/center correctly it was necessary to measure distance values in all 3 dimensions. In 2D evaluations maximum intensity projections of the nuclei were used. Consequently signals at a considerable distance that lie on top of each other might be projected to the same position in 2D and their distance is therefore underestimated.

In flat fibroblast nuclei their z-dimension was very small (see Fig. 54), therefore a 2D evaluation was considered to be sufficient if comparing 2D and 3D evaluations (see 5.2.2.). In 3D all CTs revealed a location close to the border because they often reach the top or bottom of the nucleus due to short expansion in z.

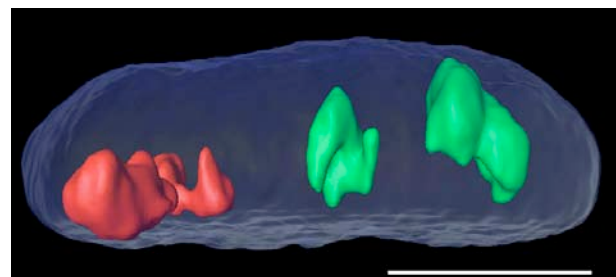


Fig. 54) Flat shaped human fibroblast: grown on normal substrate, note that CTs (CT 18, red; CT 19, green) often reach the top or bottom of the nucleus. Scale bar: 5 μ m.

For each experiment considering the cell cycle stage dependent radial distributions a 2D **and** a 3D evaluation was performed, without any significant differences between both evaluation methods. This suggests that even in flat cells the majority of voxels closely related to lamin were distributed along the nuclear rim, while interior CTs really have all of their voxels concentrated in the innermost part, without touching the nuclear border. For flat shaped cells it seems sufficient to evaluate CTs in 2D. Nevertheless there are no contrary results and therefore no argues against a 3D evaluation.

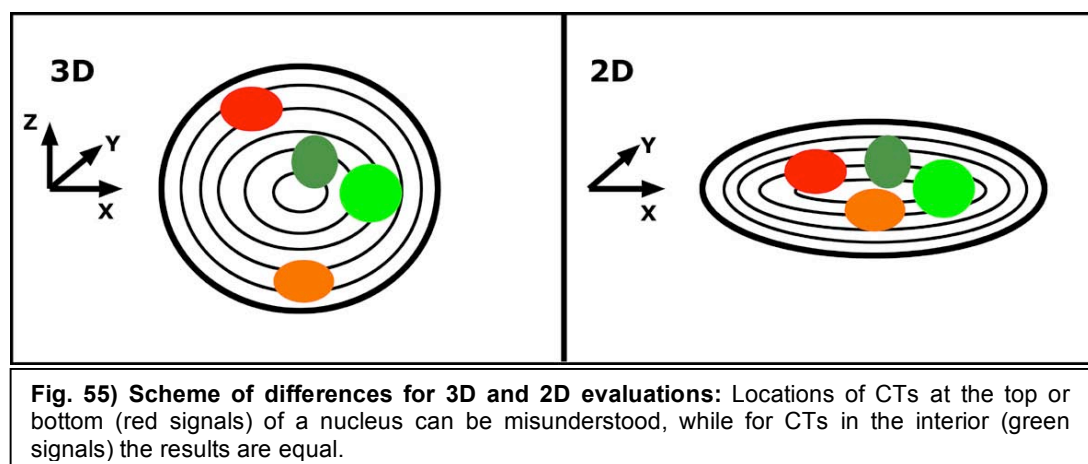


Fig. 55) Scheme of differences for 3D and 2D evaluations: Locations of CTs at the top or bottom (red signals) of a nucleus can be misunderstood, while for CTs in the interior (green signals) the results are equal.

Comparing 2D and 3D evaluations applied on spherical cells might provide another possibility for an accurate relocation of CTs. For 2D evaluations maximum intensity projections were used as described for fibroblasts. If there were differences in the results compared to the 3D spatial evaluations one might speculate about 3D positions at the top or bottom of the nuclei. For example if in 2D there was no difference between two CTs, but it was uncovered in 3D evaluations this might indicate that the one with the smaller distance to the border in 3D was located at the top or bottom of a nucleus. Interpretations of 2D results could be misleading then concerning a location of CTs along the nuclear rim and the attachment to the lamina (see Fig. 55).

5.2.4. Changes in shape: “blown up” fibroblasts

Experiments investigating gene-rich and gene-poor chromosome pools in the old world monkey Wolf’s guenon (*Cercopithecus wolfi*) revealed a gene-density dependent distribution in flat shaped fibroblasts (Neusser et al. 2007). In contrast to humans all chromosomes in Wolf’s guenon are equally sized (Neusser et al. 2007). To find out if the similarity in the distribution of human CTs 18 and 19 was due to the flat shape of the nucleus, i.e. because the difference between nuclear interior and periphery was starkly reduced, fibroblasts were artificially re-shaped by the use of special micropatterned coverslips.

So called “round” nuclei were not perfectly spherical after growing on those slides but z-dimension was much larger, which meant the ratio between x-/y- and z- plane was closer to 1, thereby resulting in a rounder overall shape. The other type of cells grown on micropattern slides was called “cigar” shaped. These cells were typically elongated like fibroblasts but the z diameter was bigger, resulting in a rather round shape in yz-diameter. In both cases a shift of CTs 18 towards the top or bottom was detectable. 3D evaluations revealed a significant difference of the distributions of CTs 18 and 19. This clearly argues for shape dependent positioning of CTs in nuclei. CTs 18 are closer attached to the lamina and are therefore located in the periphery. In flat nuclei they can come close to the center because z-dimension is highly compressed.

These changes in the morphology of nuclei were detectable in fibroblasts of different species. Differences in the distribution of the respective CTs to flat shaped fibroblasts in Wolf’s guenon and cattle were not as pronounced as in human, because the flat fibroblasts already showed a difference according to the gene-density correlated CT distribution.

For human artificially shaped round and cigar like nuclei the distributions between CTs 18 and 19 was different in all 3D evaluations, but not the 2D evaluations. This argues in favor of the idea of a preferred localization of CTs 18 at the top or bottom of the nucleus. The equatorial plane of the nucleus is occupied with the big chromosomes. The smaller chromosomes locate according to their gene-density only in axial direction (Neusser et al. 2007). Accordingly there was no evidence for a gene-density distribution in 2D, as already published by the Bickmore group (Croft et al. 1999; Bridger et al. 2000).

Geometrical constraints have major influences on the localization of CTs in flat shaped cells. In the equatorial plane there is most space provided for large chromosomes to distribute in an appropriate way (Bolzer et al. 2005). Otherwise they would not fit into the space of a flat nucleus. The rules for a gene-density dependent distribution can be considered only for smaller CTs since they distribute according to their gene-density along the axial axis, which is very small in the case of flat nuclei. Therefore one can consider a gene-density correlated CT distribution is masked by a gene-size correlated one in flat nuclei.

5.2.5. Invaginations of the nuclear lamina

The nuclear lamina is not smooth and uniformly shaped like a shell around the nucleus as one might conclude from a DAPI counterstaining. Especially for artificially shaped nuclei the general morphology includes more invaginations of the nuclear lamina into the interior of the nucleus than normally seen in fibroblasts. By staining the lamina using anti-Lamin B antibodies invaginations can readily be detected and associations between CTs and the lamina can be discovered. The lamina was suggested to anchor chromatin indicating a close connection of peripheral located CTs to the Lamin B (Dechat et al. 2008). Deep invaginations might provide an environment as typically observed for silent regions at the peripheral compartments (Lanctot et al. 2007). Therefore an object attached to an invaginated lamin stretch and by that defined as peripheral, might appear internal if nuclear DNA was used as a reference.

Indeed in cattle fibroblasts the differences between CTs 19 and 20 were abrogated if Lamin B served as a reference for evaluations. This indicates that both chromosomes were attached to the lamina. In nuclei with an artificially spherical shape the invaginations seemed to become more and to reach deeper into the nuclear space, thereby building a larger surface for potential CT attachments.

In general in round and cigar shaped nuclei many invaginations were found. With extended invaginations the surface of a nucleus is enlarged. Maybe the transport

out of the nucleus into the cytoplasm is enhanced by this spatial organization. Under usual cell culture conditions fibroblasts are very flat and from anywhere in the nucleus the way to the nuclear rim is very short. By “blowing up” the nuclei distances were expanded in the z-dimension (about 2-5 times). The increase in invaginations might represent a compensation for the enlarged, which again shortens the distances of certain CTs to the nuclear periphery. Therefore these invaginations might be a reaction of cells on the altered conditions, meaning the different 3D shape.

The analysis using Lamin B as reference structure revealed a very close connection of CTs 18 to the lamina. The distance of CTs 19 to Lamin B was also smaller than measured for DAPI but not as much as for CTs 18. But of course Lamin B staining was expected to be underneath the nuclear border, but looking at the distribution graphs, it is obvious that Lamin B was also found inside the nuclei, which implements the existence of invaginations (see Fig. 31, upper, right picture).

5.2.6. Comparison between different species

In Wolf's guenon the CT distributions for all 2D and 3D evaluations, independent of the nuclear shape, were exactly the same: in comparison to DAPI and to Lamin B as reference structures CTs 18 were located at the periphery while CTs 19 were located in the centre of the nucleus. Observing a significant difference in the 2D evaluations indicates that the overall distribution in all dimensions was gene-density dependent and not only along z-dimension.

In bovine species the situation for round fibroblasts was as expected and equal to those of Wolf's guenon. Bovine chromosomes were of similar size as well, and flat shaped fibroblasts as well as lymphocytes showed a gene-density dependent distribution of CTs 19 and CTs 20. A difference was also found in cigar shaped bovine fibroblasts where the distribution with respect to DAPI was as expected. For the 2D DAPI distribution however, no difference was found as well as for the distribution with respect to Lamin B. For both chromosomes irrespectively of their different gene content the attachment to the lamina can be considered equal. One should note however, that even if this difference was not significant and standard deviation were high, a clear tendency could be observed for a more internal distribution as revealed by the median value.

5.3. Early bovine embryos

In this paragraph two main results that provide insight into the nuclear organization during early bovine embryonic development will be discussed:

- A gene-density related CT distribution is established during major genome activation (MGA).
- A developmentally regulated Oct4-GFP transgene and its harboring CT is reorganized upon nuclear transfer.

5.3.1. Gene-density correlated distribution pattern of CTs in adult bovine cells

In the present study we could show that a gene density related distribution of chromosome territories (CTs) as described in many other species (Croft et al. 1999; Cremer et al. 2001; Habermann et al. 2001; Mayer et al. 2005; Neusser et al. 2007) is also present in bovine cells. Not only could I demonstrate a more internal positioning of chromosome 19 and a more peripheral of chromosome 20, I could also show that the extent of this differential distribution is more pronounced in lymphocytes than in fibroblasts. Very similar results have been presented for the respective human and mouse cell types (Cremer et al. 2001; Mayer et al. 2005). In fact in those species the distribution of gene dense and poor chromosomes in fibroblasts though showing the same tendency as in lymphocytes failed to meet the significance level, i.e. were distributed statistically the same. A possible reason for this cell type specific difference has been attributed to nuclear shape. In flat fibroblasts nuclei gene poor chromatin/chromosomes that contact the nuclear periphery protrude much further into the nuclear interior as compared to spherical lymphocyte nuclei, or in other words in flat shaped nuclei there is less “internal” space than in spherical nuclei. From the other point of view, internally located chromosomes/chromatin could get easily into contact with the upper and lower nuclear surface due to a reduced height. Interestingly, if a flat human fibroblast nucleus is artificially remodeled to adapt a spherical shape, the distribution of gene dense and gene poor chromosomes changes significantly, becoming similar to that of a lymphocyte nucleus (see chapter 5.2.4.). Apart from gene density, also gene size has been shown to play a role in the distribution of chromosomes (Sun et al. 2000; Cremer et al. 2001; Bolzer et al. 2005; Neusser et al. 2007), though mainly in flat shaped nuclei. This size dependent distribution is hypothesized to reflect the mechanism of sister-chromatid separation during mitosis (discussed in (Sun et al. 2000) and (Habermann et al. 2001)).

Since a gene density related distribution has also been shown for cells in tissues (Cremer et al. 2003) one can exclude the possibility that it represents an artificial phenomenon of cultured cells only. Recently, we could show that gene density as a distributional motif applies in fact not only to complete chromosomes but also to sub-chromosomal regions (Kupper et al. 2007). This finding confirmed previous observations where a gene density correlated distribution was also found for chromosomal portions belonging to human chromosome 18 and 19 involved in multiple structural chromosomal rearrangements in cancerous human cells as well as in cells from various primate species (Cremer et al. 2001; Tanabe et al. 2002). While several genes or gene cluster have been shown to change their intranuclear localization as a function of transcriptional activity (reviewed e.g. in (Heard and Bickmore 2007; Lanctot et al. 2007; Sexton et al. 2007)), the radial distribution of larger sub-chromosomal regions appears to be independent from transcriptional activity and solely arrange according to their gene density (Kupper et al. 2007).

5.3.2. FISH on 3D preserved early bovine embryos

The establishment of FISH on 3D preserved embryos was essential for determining distances and positions of CTs and smaller nuclear (sub-) compartments in nuclei of embryos.

Publications concerning the localizations of CTs in embryos so far only presented data from flattened embryos caused by the specifically used fixation procedures, that maximize hybridization efficiency, but severely affect morphology of nuclei (Hepperger et al. 2007): Embryos were fixed in methanol/acetic acid (MAA), dehydrated by an ethanol series and air-dried (McKenzie et al. 2004; Diblik et al. 2005; Diblik et al. 2007; Finch et al. 2008). Consequently, such analyses represent only 2D evaluations with all limitations as discussed above (see 5.2.2. and in (Finch et al. 2008)). Accordingly, chromatin domains positioned at a considerable distance in axial direction of the native embryonic nuclei may come into close proximity after embryo flattening, thus 2D distances recognized by these authors likely underestimated the true 3D distances present in the native embryos. In contrast, I fixed bovine embryos under conditions, which maintained the 3D shape of nuclei using buffered formaldehyde as a cross-linking fixation agent. Air-drying was strictly avoided throughout the whole fixation and 3D-FISH procedure.

For their FISH experiments they used commercially available paint probes paints for CTs (Diblik et al. 2005; Diblik et al. 2007) or centromeres, respectively (McKenzie et al. 2004; Finch et al. 2008). In all studies only small specific regions were stained, but never the complete territory. Consequently results and conclusions should be

interpreted with caution as they might represent specifically the distribution of the specific regions only and not be representative for the complete CT.

5.3.3. Distribution of gene-rich and gene-poor CTs in nuclei of early bovine embryos

An important question of the present thesis was to investigate at which time point during development a gene density dependent radial distribution would be established. To address this issue I investigated the radial distribution of bovine chromosomes 19 and 20 in 4 different preimplantation stages of *in vitro* fertilized (IVF) embryos. Crucial for the investigation of embryos was the establishment of an appropriate fluorescence in situ hybridization protocol to visualize CTs in three-dimensionally preserved embryos (3D-FISH). Our protocols currently used for cells (Cremer et al. 2007) had to be modified by several essential steps in order to achieve sufficient permeability of the specimen for the DNA probes (see Material and Methods). To our knowledge our group is the first to present a protocol that allows the visualization of specific DNA sequences in morphologically preserved embryos.

A first important observation in the present study was that chromosomes in pronuclei of zygotes are arranged as non-overlapping territories, just as in somatic cells. This could not be anticipated *a priori*, given that haploid pronuclei have first to be remodeled, from a gametic conformation, which is especially dramatic in the case of the sperm chromatin where protamines have to be exchanged for histone proteins in order to decondense the highly compacted DNA. Moreover, chromatin of pronuclei seems to be in general differently organized as compared to blastomere chromatin or chromatin in somatic cells. In mouse pronuclei for example pericentric heterochromatin is visualized in confocal midsections as a narrow ring around nucleolar precursor bodies (Martin et al. 2006; Merico et al. 2007) and not arranged as in somatic cells where they often build spherical objects attached to the nuclear periphery and/or the nucleoli (Mayer et al. 2005). In bovine pronuclei an asymmetrical distribution of DNA was often observed during the course of the present study with a pronounced concentration at one pole of the pronucleus and large DNA free spaces (see Fig. 39). The finding that chromosomes in zygotes are arranged as individual non-intermingling territories confirms a previous observation by Brandriff et al. who showed the existence of compact pronuclear chromosome “domains” (Brandriff and Gordon 1992) in human decondensing sperm nuclei that had been artificially fused with hamster oocytes. However unlike in the present study the authors used a heterologous system and applied a fixation method that is known

to severely affect embryo and nuclear morphology. Nevertheless, their conclusion fits well with the observation made in bovine IVF zygotes.

My finding that that a gene density correlated distribution of CTs is only established during MGA, but is not present in pre-MGA embryos, poses the possibility that transcriptional activity is involved in the establishment of this specific spatial organization of chromosomes. The maintenance of such a differential chromosome distribution however, could be independent of transcription, at least in the short term. This was concluded in a study by Croft et al. (1999), who showed that reversible and irreversible inhibition of transcription, applied several hours before fixation of human lymphoblasts and fibroblasts, had no effect on the gene density related distribution of CTs (Croft et al. 1999). Moreover, a gene density correlated distribution of human chromosomes 18 and 19 was demonstrated in non-stimulated, quiescent lymphocytes as well as in stimulated, cycling lymphocytes (compare (Cremer et al. 2001) with (Croft et al. 1999) and (Cremer et al. 2003)) though the former show a reduced transcriptional activity as compared to the latter (Cooke and Kay 1973). Similarly, the Cremer group could show recently that on a sub-chromosomal scale a gene density related distribution of chromatin was present in both cycling and quiescent human lymphocytes as well as fibroblasts (Kupper et al. 2007).

We know of only one study providing an argument for the possible influence of transcriptional activity *per se* on the radial distribution of chromatin (Bridger et al. 2000). Bridger and coworkers found that quiescent or senescent human fibroblasts did not exhibit a gene-density correlated radial distribution of HAS 18 and 19 CTs, whereas such a distribution was re-established after re-entry of quiescent fibroblasts into the cell cycle (Bridger et al. 2000). Whether this change is causally related with the reduced level of transcription in quiescent/senescent compared with cycling fibroblasts remains unclear. It should be noted that in the study by Kupper et al. (2007) a gene-density correlated distribution of subchromosomal regions was found in human fibroblasts independently of the cell cycle stage, i.e. in S- as well as in G0-phase cells (Kupper et al. 2007). The data for human G0 and cycling fibroblasts were used for further evaluation and comparison of the RRD and ADS program by J. v. Hase. There was no significant difference obtained for both evaluation methods, neither in 2D nor in 3D. CTs 18 and 19 were distributed equally. Additionally an evaluation in 1D was performed showing that all distributions were equally distributed around the center (for further discussion of the programs see (von Hase et al. submitted)).

The reason for the contradictory results between the findings of Bridger et al., Kupper et al. and Hase et al. is not known, but a possible effect might be that in the study by Bridger *et al.* quiescent fibroblasts were induced by serum starvation, while in the other two studies G0 cells were identified with the help of cell cycle markers within a growing culture, which might represent cells that though being *de facto* non-cycling are functionally different to serum starved cells.

Whether activation of the embryonic genome is a prerequisite of the observed chromosome-specific distribution or a consequence or a mere temporal coincidence has still to be clarified. We are currently trying to assess this problem by suppressing MGA to test the impact on the establishment of CT distribution. An observable difference would argue that the radial distribution of CTs is a downstream event of transcription rather than a preceding one.

Recently a number of studies have addressed the question how chromosomes are spatially distributed in early human embryos (McKenzie et al. 2004; Diblik et al. 2005; Diblik et al. 2007; Finch et al. 2008). In all these studies locus specific or chromosome specific satellite probes for several or all of the following chromosomes were used: 13, 15, 16, 18, 21, 22, X and Y. The distributions of these sub-chromosomal regions were analyzed asking 1) whether they differed among each other (McKenzie et al. 2004), 2) whether they were different to a “random” distribution resembled by global DNA staining (Diblik et al. 2005; Diblik et al. 2007; Finch et al. 2008) or 3) whether they would differ between eu- and aneuploid blastomeres (McKenzie et al. 2004; Diblik et al. 2005; Diblik et al. 2007; Finch et al. 2008). In all studies 3-4 days old embryos were analyzed, comprising at least 6 blastomeres. Since MGA in human embryos was described to take place at the 4-8 cell stage (Braude et al. 1988) the embryos used in all the above studies should be considered transcriptionally active. All studies found a difference in the distribution of one or several chromosomes in euploid compared to aneuploid nuclei. However, in the studies by Diblik et al. and Finch et al. no significant difference in the distribution of any of the analyzed chromosomes to the global DNA distribution could be shown. This is contradictory to the results in the present study since the CT distribution in my data set differed significantly from the global DNA distribution, most notably for CTs 19 in post-MGA embryos, which were located significantly more in the interior than DAPI stained DNA. In the study by McKenzie et al. all analyzed chromosome regions (13, 16, 18, 21, 22, X and Y) showed a similar radial arrangement not differing between each other. This result is also in contrast to the observation presented here as one would expect to see a difference in the radial distribution between the gene dense human chromosome 22 and the other mostly gene poor

human chromosomes, as has been described in lymphoblastoid cells (Boyle et al. 2001). A number of differences in the experimental approaches might account for the observed discrepancy between their and my findings. First of all, it should be noted that all these studies utilized embryos that were generated by assisted fertilization and which were screened for chromosomal aneuploidies in the course of preimplantation diagnosis. Therefore embryos, or blastomeres were fixed according to established protocols that maximize hybridization efficiency, but which were shown previously to severely affect the native morphology of nuclei (Hepperger et al. 2007), a fact that is also discussed in one of these studies (Finch et al. 2008). These fixation procedures included hypotonic treatment and fixation by denaturation instead of cross-linking as in the present study. Moreover, in all these studies embryos were air-dried, which leads to a flattening of the embryo, losing the information from the third dimension, so that a 2D-evaluation only could be performed. Objects lying on top of each other at a considerable distance in the native embryo can get into close proximity after embryo flattening, thus underestimating their actual distance in the evaluation. Moreover, in all analyses commercial probe sets were used comprising probes that were either locus specific or specific for sub-chromosomal satellite regions, i.e. were not visualizing the complete CTs. Though in general such probes could detect a non-random radial distribution of CTs, as has been shown in the study of Sun et al. (Sun et al. 2000), the utilization of such probes in combination with a fixation approach with only poor morphological preservation might finally distort the spatial information on the native CT arrangement.

The observation that nuclei especially of early preimplantation stages contain large spaces devoid of DNA or at least with a very low DNA concentration is intriguing. Though it cannot be completely ruled out that these nuclei represent dying or early apoptotic stages, it appears improbable, given that in zygotes, 4-8 cell and 10-16 cell embryos they represent the majority of all nuclei. Moreover, within the same post-MGA embryos “hollow” nuclei showed transcriptional activity just as nuclei with a conventional DNA distribution. A possible explanation is that these DNA free spaces represent enlarged areas of an inter-chromatin domain (ICD) space (reviewed in (Cremer et al. 2006)) that in somatic cells is spatially reduced to a level that is hardly visible by conventional light microscopy. In the Cremer group it could be shown previously that such an ICD compartment can be artificially enlarged and visualized by increasing the intra-nuclear calcium levels, thereby inducing chromatin condensation (Albiez et al. 2006). In the present work it could be shown that these DNA free spaces that are often found in an internal nuclear compartment do have

an influence on the global distribution of DNA in that it gets concentrated towards the nuclear periphery. However, this spatial arrangement does not influence the relative distribution of gene dense and poor chromosomes with respect to each other (see Fig. 40). In other words, the lack or presence of a gene density related distribution in pre- and post-MGA embryos is unaffected by these DNA free/poor regions.

Our finding that in bovine blastocysts both trophectoderm and inner cell mass cells showed a very similar gene density related distribution (see Fig. 38), despite their different cellular functions fits well with the idea of gene density acts as a general spatial organizational principle, independent of the cell type.

In conclusion, I could show with this series of experiments that a gene-density related distribution of CTs as described for several other species is also present in cattle. Utilizing a newly developed protocol for 3D-FISH on preimplantation embryos I provide evidence that this gene-density related CT distribution is established during MGA and extended at the blastocyst stage but absent in earlier pre-MGA stages. It remains to be elucidated though, if the establishment of a non-random higher order radial chromatin arrangement during MGA are functionally and/or mechanistically interconnected or if they represent only chance coincidence.

5.3.4. Localization of a developmentally regulated Oct4-GFP transgene

The spatial organization of the nucleus is considered to be involved as an epigenetic regulator of nuclear function. For several genes it has been shown that transcriptional activity correlates with their spatial positioning within the nucleus and relative to its harboring chromosome. In this work I have analyzed the distribution of a mouse Oct4-GFP transgene integrated into chromosome 13 of a bovine fibroblast cell line that was used as nuclear donor cell line in NT experiments. The transgene and CT 13 differed significantly in their nuclear distribution in

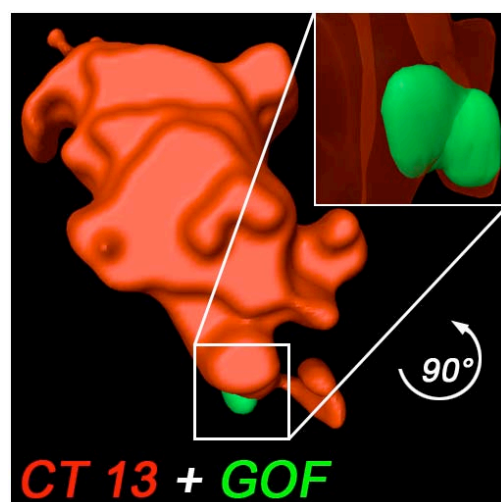


Fig. 56) 3D reconstruction of GOF – detailed view: GOF (green) is located at the border of CT 13 (blue) in fibroblast nuclei, in distance to α -satellite sequences (red):

donor fibroblasts, with the transgene being more interior and CT 13 more peripheral in comparison to each other. Hence in a switched off state in flat fibroblasts the transgene is found in the nuclear interior.

In comparison to CT 13 the transgene is located at the very periphery of the territory (see Fig. 56), even if the distribution of the CT and the transgene are not significantly different.

Studies investigating stable integrated transgenes in cultured hamster and mouse cells showed an expression dependent nuclear positioning: active transgenes were found located more towards the nuclear interior than inactive genes, e.g. targeting the VP16 acidic activation domain to a peripheral chromosome site via a lac-repressor fusion protein or using an inducible pPALZ8.8 plasmid, which consists of lac operator repeats and a β -globin regulatory sequence (Tumbar and Belmont 2001; Dietzel et al. 2004; Chuang et al. 2006). This is in agreement with the findings presented here where I observed a more internal position of the transgene in comparison to the nucleus upon activation, even if those findings were not significant. In the case of bovine fibroblasts the transgene for Oct-4 is silent, but becomes activated in NT embryos during MGA (Wuensch et al. 2007). A re-positioning of gene localization can be with respect to various nuclear compartments like peripherally located heterochromatin (Kosak et al. 2002; Zink et al. 2004; Williams et al. 2006) or pericentric regions (Brown et al. 1997). In several studies gene have been described to loop out of their host chromosome, when actively transcribed, like the Major Histocompatibility Complex (MHC) locus on chromosome 4p21 (Volpi et al. 2000) or the HoxB cluster on chromosome 17q21-q22 (Chambeyron and Bickmore 2004). In the present study no loops were detected, not in the silent state nuclei of fibroblasts, nor upon activation in blastocysts. Quiet the contrary was the case as upon activation of the transgene a more and more internal location of the transgene was found. Anyway the localization of the transgene in silent fibroblasts was found to be at the very periphery of the nuclei but without looping out. The localization can be rather described as a protrusion like extension (see Fig. 56) such as described for active genes in other publications of the Cremer group (Albiez et al. 2006; Kupper et al. 2007).

The location of genes or subchromosomal regions was described to be mainly dependent on the gene-density of the region (Kupper et al. 2007). The influence of transcriptional activity, R- or G-band assignment as well as replication timing had a minor influence (Kupper et al. 2007). In mouse a correlation between the GC content and the presence of certain repetitive elements for the positioning of subchromosomal regions was shown (Hepperger et al 08). A positioning in relation

to the nucleus (interior or periphery) seems to be more decisive than a certain location in relation to each CT (Kupper et al. 2007). Usually as a typical silencing compartment within the nucleus serves the peripheral heterochromatin along the nuclear lamina (Chubb et al. 2002; Lanctot et al. 2007). However there were also genes described to be active while positioned at the nuclear lamina (Ragoczy et al. 2006), i.e. in drosophila a repositioning of a subtelomeric gene towards the NPCs is described upon its activation (Taddei et al. 2006). In another study it was recently shown that a transgene tethered to the lamina can maintain its transcriptional activity (Kumaran and Spector 2008). So one can conclude that the zones of active and inactive gene transcription come very close together at the nuclear periphery (Brown and Silver 2007). Interestingly the silenced transgene in the present study was not found in a classical silenced compartment like the nuclear periphery, but was found located in the interior of the nucleus and furthermore at the border of the harboring CT where one would rather expect actively transcribed genes.

5.3.5. Remodeling of the Oct4-GFP transgene during nuclear transfer

Nuclear transfer experiments provide a proper model to reprogram cells back to a totipotent state. This allows the analysis of the spatial distribution of re-activated pluripotency associated genes if they are properly switched on in NT embryos. In this work the distribution of an Oct4-GFP transgene integrated in chromosome 13 of a bovine fibroblast cell line was analyzed comparing the 3-dimensional distribution of the transgene and CT 13 in the fibroblast donor cell line and in day-2 embryos where it is silent with day-4 and day-7 embryos when the transgene is activated and reaches its highest expression levels, respectively.

The presented results provide evidence for a large scale, spatial reorganization of the Oct4-GFP transgene as well as of its harboring chromosome upon transfer of a somatic nucleus into an enucleated oocyte. Moreover, a redistribution of this developmentally regulated transgene from the CT periphery towards the interior accompanying its expression upon major genome activation was observed:

- Both the transgene and CTs 13 are located significantly more towards the nuclear periphery in NT embryos compared to donor cells (**Table 12**).
- Transgene and CTs 13 differ significantly in their nuclear distribution in donor fibroblasts, with the transgene being more interior, CTs 13 more peripheral. No significant difference was found in NT embryos (**Table 12**).
- There is no detectable difference in the CT distribution between the transgene harboring CT 13 and the homolog without GOF (see appendix 7.1.4.).

- Both transgene and CT 13 move towards the nuclear interior during pre-implantation development (Table 12).
- The transgene is located at the CT 13 surface in donor fibroblasts and gets increasingly internalized during pre-implantation development (Table 12).

Developmental Stage	transgene median	CT 13 median	
Bovine fibroblasts (donor cells)	59 % ^{1,a}	39 % ^{2,a}	internal location
day-2 embryos	13 % ^{1,b}	17 % ^{1,b}	peripheral location
day-4 embryos	20 % ^{1,b,c}	26 % ^{1,c}	↓ internal location
day-7 embryos	23 % ^{1,c}	30 % ^{1,c}	

Table xx: Median distances of the transgene and CT 13 from the nuclear surface. 0 % represents the very border of the nucleus, 100% the very center.

a,b,c Values within the same column with different alphabetical superscripts differ significantly (P<0.05).

1,2 Values within the same row with different numerical superscripts differ significantly (P<0.05).

When comparing the location of the transgene and the CT between the donor cells and the embryonic stages a significant difference was found in all cases. In fibroblasts a distinct internal location was found for both, while in embryos both signals were found more towards the nuclear periphery. This indicated a remodeling of donor cells during NT. During MGA a movement of both, the transgene and the CT towards the interior of the nucleus is found.

Despite the fact that the transgene is inactive in fibroblasts it was found more internal in fibroblasts than in the active states of embryos. Since CT 13 is of average size and gene density an “intermediate” location between the interior and the periphery should be anticipated (Croft et al. 1999; Cremer et al. 2001; Bolzer et al. 2005; Neusser et al. 2007), which was indeed the case with a median value of 39%. Anyway the transgene with a median of 59% showed a very internal localization in comparison to the active embryonic stages. That was contrary to what we expected. The localization of the transgene with respect to the territory is not random but polarized towards the interior of the nucleus. It cannot be excluded that fibroblast specific genes are located close to the transgene that might be responsible for the observed internal location.

The shape of the transgenic fibroblast donor nuclei is flat and ellipsoid in contrast to the nuclei in preimplantation embryos. All comparisons of CT and transgene distributions between donor cells and embryonic stages revealed a significant difference, which may be due to a different shape between both cell types.

The overall chromatin distribution in nuclei of early preimplantation embryos was heterogeneous in the majority of embryos. DNA free/poor spaces in the nuclear interior apparently caused a concentration of DNA at the nuclear periphery. This was described in detail (see Fig 39 and chapter 4.4.6.) for IVF embryos and was seen to a lesser extent in NT embryos (Ketterl 2008). This global distribution of DNA might explain the observed peripheral distribution of CT 13 and GOF in day 2 embryos compared to fibroblasts. GFP expression was described to start with the fourth cell cycle, which yields the 16 cell stage (Wuensch et al. 2007) which is when we observe a shift of the transgene towards the interior. Active genes and CTs containing gene dense areas were described several times to be located in the interior of nuclei (Tumbar and Belmont 2001; Chambeyron and Bickmore 2004; Zink et al. 2004; Chuang et al. 2006; Ragooczy et al. 2006; Kupper et al. 2007; Hepperger et al. 2008). In the present study the transgene and the harboring territory show a tendency to be located more towards the interior upon activation. Anyway the location is not as much inside as it is found in fibroblasts where the transgene is completely silent. Like previously reported the overall gene density is most decisive for the positioning of CTs (Kupper et al. 2007). This is in accordance with the finding that there is no difference between the CT 13 homolog that harbors the transgene and the one that has no inserted transgene. These findings lead to the conclusion the role of Oct4-GFP for the location of the CT 13 is diminished. But the transgene itself is always more interior than the CT, which supports the idea of a polarized organization of CTs (Croft et al. 1999; Sadoni et al. 1999; Kupper et al. 2007). It would be interesting to look for the subchromosomal organization of the CT 13 in terms of a comparison between the homologues including the transgene and the one without. There might be an influence of the transgene insertion on the subchromosomal organization of the CT 13 that leads to a polarization of the CT with the transgene and being located more interior with respect to the nuclear counterstain.

Developmental Stage	transgene median
Bovine fibroblasts (donor cells)	0% ^a
day-2 embryos	16% ^a
day-4 embryos	24% ^{a,b}
day-7 embryos	27% ^b

location at CT border
↓
location inside CT

Table xx: Median distances of the transgene in respect to its harboring CT 13. 0 % represents the very border of the CT, 100% the very center.
a,b Values with different alphabetical superscripts differ significantly (P<0.05).

With respect to the CT 13 surface the Oct4 transgene is distributed without significant difference in donor cells and day 2 embryos in both cases reflecting the situation in the silent state. Upon activation an increased internal localization was observed that was however not significant in case of day 4 embryos where the transgene is expressed only poorly (Wuensch et al. 2007) while it was significant in day 7 embryos when compared to the silent state in fibroblasts and day 2 embryos. This observation is in contrast to what has been described in the literature, where for some genes a reorganization in the opposite direction is described (Volpi et al. 2000; Chubb and Bickmore 2003). They found expressed genes not only at the border of the CT but also looping out further away from the territory surface into the interior of the nucleus (Volpi et al. 2000). However, expressed genes (Mahy et al. 2002; Stadler et al. 2004) as well as active transcription sites (Verschure et al. 1999) have also been described to reside within CTs. Although the transgene is localized near the centromere of CT 13 and centromeres were generally shown to be at the CT border in humans (Weierich et al. 2003) the transgene is found internal in bovine nuclei and is even further internalized upon activation.

Most strikingly, the transgene together with the territory is generally found much more outside in early preimplantation embryos if compared to the donor cells, which are silent. A possible explanation therefore could be the overall DNA distribution found in nuclei of preimplantation embryos, which is described for IVF embryos in the present work (see chapter 4.4.6. and Fig. 39) but was found as well, even to a lesser extent, in NT embryos (Ketterl 2008). A certain portion of nuclei in early

embryos showed a “hollow” formation with respect to its DNA staining in DAPI. Therefore a general shift of all CTs towards the nuclear periphery seems to be likely. Noticeable the polarized organization of the CTs gets lost if comparing fibroblasts and preimplantation embryos. While in fibroblasts there is a considerable alignment of the CT with the transgene being interior of the nucleus, the latter show a territorial internal localization of the transgene. Maybe this reorganization goes along with the overall reorganization of DNA in the nucleus with the CTs generally located more at the periphery.

The location of actively transcribed genes in relation to the CT was described to be less important in comparison to the relative position in the nucleus (Kupper et al. 2007). According to the CT-IC model a locus within the territory can be reached by deep lacunas and transcription is not restricted to the CT surface (Albiez et al. 2006). There are many possible influences that may influence the location of GOF, like the gene density surrounding the integration site of the transgene (Kupper et al. 2007) as well as the replication timing (Grasser et al. 2008).

5.3.6. Remodeling during early differentiation events

The endogenous Oct4 in mouse and human was described to be expressed in ICM cells, loss of Oct4 causes a differentiation into trophoblast cells (Koestenbauer et al. 2006). A study, comparing human ES and lymphoblastoid cells revealed that Oct4 is outside the territory in ES cells but found within the CT margins in differentiated lymphoblastoid cells (Wiblin et al. 2005). In a similar study Oct4 loci were found on extended chromatin loops, away from the harboring territory, in 70% of all investigated human ES cells while in differentiated ES cells Oct4 was found only at the periphery of its CT (Bartova et al. 2008). In mouse ES cells and macrophages contrasting results were published by Hepperger et al. who showed that 85% of all Oct4 signals were localized within the territory border (Hepperger et al. 2008). No significant differences were found between mouse ES cells and mouse macrophages (Hepperger et al. 2008).

In the present study I was able to comparatively analyze an Oct4-GFP transgene in fibroblasts as a differentiated somatic cell type where the transgene was silent as well as bovine preimplantation embryos as undifferentiated stages. Furthermore an investigation of the first differentiation stages in blastocysts, where cells of ICM can be distinguished from TE cells, was possible.

The intranuclear localization of the transgene and CT 13 was identical in cells of ICM and TE. When the transgene is switched off it may take several cell cycles until a repositioning of Oct4-GFP occurs because it is maybe a rather slow process in

nuclear re-organization. For the endogenous loci of Oct4 it was shown that it is silent only in 50% of the NT embryos (Wuensch et al. 2007), which might be the same for the transgene. Maybe there is no difference between nuclei from ICM and TE because the transgene is still active in most of the TE cells. A switch off might be detectable at single cell level or with increased age of embryos. Our “oldest” preimplantation embryos were fixed at day 7, where differentiation just started and therefore Oct4 is most probably still active. On the other hand one cannot exclude that a mouse transgene for Oct4 is behaving differently from a bovine endogenous Oct4 gene because of its foreign origin and their competition.

5.3.7. Future perspectives/outlook

Although I could describe several interesting dynamic changes in the higher order chromatin organization in bovine IVF and NT embryos several concrete questions remain to be elucidated, i.e.:

- Is the gene-density related CT distribution really correlating with the onset of transcription/MGA?
- What is first – distribution of CTs or onset of transcription?
- Show all chromosomes a gene-density correlated distribution?
- What is the situation in other species?
- The heterogenous distribution in early nuclei: is it also found in other species and of what consists the “holes”?
- What is the distribution of the endogenous Oct4 gene? How are other developmentally regulated genes distributed? Is there a difference for the active and inactive states and in different species?

In an ongoing diploma thesis N. Ketterl is currently investigating the distribution of bovine chromosomes 19 and 20 in NT embryos (Ketterl 2008). The distribution in donor fibroblasts has been described in the present project to be gene-density related, whereas in early preimplantation embryos up to the 8 cell stage an equal distribution of both chromosomes was found. Studies in NT embryos provide a model to look to what extent the radial distribution of CTs represents a reprogrammable parameter. In this context our major questions are whether fibroblasts will be reprogrammed according to the situation in the early zygotes, i.e. if the gene density related distribution will be erased. If yes, at which stage will it be erased and when will it be re-established compared to IVF embryos.

To confirm that the establishment of a higher-order CT arrangement correlates indeed with MGA and not with the time period elapsed after fertilization or with the number of cell divisions, we would like to confirm our finding in *mouse* in vivo

embryos. We anticipate that if MGA is indeed the correlating parameter the transition from a random CT distribution to a gene density related one should take place already at the 2 cell stage, i.e. when MGA takes place during murine development.

Another unsolved question is whether transcription is causally involved in the establishment of CT distribution. To approach this N. Ketterl will inhibit major genome activation by applying transcription inhibitors such as α -amanitin. She will analyze such embryos in which MGA has been artificially suppressed at a developmental stage where IVF control embryos already show a gene density related CT distribution. The presence of such a distribution would argue that CT arrangement is a transcription-independent event, possibly anticipating transcriptional activation of the embryonic genome. Absence of a gene density correlated CT distribution on the other hand would intimately link both events, arguing for a causal involvement of transcription in the establishment of this higher-order chromatin arrangement.

Concerning the localization of genes it would be interesting to study the localization of the endogenous Oct4 gene in NT and IVF embryos as well as the spatial distribution of other genes during reprogramming, development and differentiation. Interesting candidates could be the genes Sox2, Nanog, Klf4 or c-myc, which have the potential to induce a stem cell like phenotype if ectopically expressed in differentiated cells (Takahashi and Yamanaka 2006; Takahashi et al. 2007; Wernig et al. 2007; Yu et al. 2007).

6. References:

- Abney, J. R., B. Cutler, et al. (1997). "Chromatin dynamics in interphase nuclei and its implications for nuclear structure." *J Cell Biol* **137**(7): 1459-68.
- Agarwal, N., T. Hardt, et al. (2007). "MeCP2 interacts with HP1 and modulates its heterochromatin association during myogenic differentiation." *Nucleic Acids Res* **35**(16): 5402-8.
- Albiez, H., M. Cremer, et al. (2006). "Chromatin domains and the interchromatin compartment form structurally defined and functionally interacting nuclear networks." *Chromosome Res* **14**(7): 707-33.
- Albiez, H., R. Zinner, et al. (in preparation). "Deconvolution of 3D confocal microscope data sets improves image quality."
- Allison, D. C. and A. L. Nestor (1999). "Evidence for a relatively random array of human chromosomes on the mitotic ring." *J Cell Biol* **145**(1): 1-14.
- Ansari, H. A., A. A. Bosma, et al. (1999). "Standard G-, Q-, and R-banded ideograms of the domestic sheep (*Ovis aries*): homology with cattle (*Bos taurus*). Report of the committee for the standardization of the sheep karyotype." *Cytogenet Cell Genet* **87**(1-2): 134-42.
- Arnold, M., E. A. Cavalcanti-Adam, et al. (2004). "Activation of integrin function by nanopatterned adhesive interfaces." *Chemphyschem* **5**(3): 383-8.
- Aston, K. I., G. P. Li, et al. (2006). "The developmental competence of bovine nuclear transfer embryos derived from cow versus heifer cytoplasts." *Anim Reprod Sci* **95**(3-4): 234-43.
- Bartova, E., J. Krejci, et al. (2008). "Differentiation of human embryonic stem cells induces condensation of chromosome territories and formation of heterochromatin protein 1 foci." *Differentiation* **76**(1): 24-32.
- Berg, U. and G. Brehm (1989). "In vitro production of bovine blastocysts by in vitro maturation and fertilization of oocytes and subsequent in vitro culture." *Zuchthygiene* **24**(3): 134-139.
- Bernstein, E. and C. D. Allis (2005). "RNA meets chromatin." *Genes Dev* **19**(14): 1635-55.
- Bickmore, W. A. and P. Teague (2002). "Influences of chromosome size, gene density and nuclear position on the frequency of constitutional translocations in the human population." *Chromosome Res* **10**(8): 707-15.
- Blobel, G. (1985). "Gene gating: a hypothesis." *Proc Natl Acad Sci U S A* **82**(24): 8527-9.
- Bolzer, A., G. Kreth, et al. (2005). "Three-dimensional maps of all chromosomes in human male fibroblast nuclei and prometaphase rosettes." *PLoS Biol* **3**(5): e157.
- Boveri, T. (1909). "Die Blastomerenkerne von *Ascaris megaloccephala* und die Theorie der Chromosomenindividualität." *Arch Zellforsch* **3**: 181-268.
- Boyle, S., S. Gilchrist, et al. (2001). "The spatial organization of human chromosomes within the nuclei of normal and emerin-mutant cells." *Hum Mol Genet* **10**(3): 211-9.
- Branco, M. R. and A. Pombo (2006). "Intermingling of chromosome territories in interphase suggests role in translocations and transcription-dependent associations." *PLoS Biol* **4**(5): e138.
- Brandriff, B. F. and L. A. Gordon (1992). "Spatial distribution of sperm-derived chromatin in zygotes determined by fluorescence in situ hybridization." *Mutat Res* **296**(1-2): 33-42.
- Braude, P., V. Bolton, et al. (1988). "Human gene expression first occurs between the four- and eight-cell stages of preimplantation development." *Nature* **332**(6163): 459-61.
- Brero, A., H. P. Easwaran, et al. (2005). "Methyl CpG-binding proteins induce large-scale chromatin reorganization during terminal differentiation." *J Cell Biol* **169**(5): 733-43.
- Bridger, J. M., S. Boyle, et al. (2000). "Re-modelling of nuclear architecture in quiescent and senescent human fibroblasts." *Curr Biol* **10**(3): 149-52.
- Bridger, J. M., I. R. Kill, et al. (1998). "Association of pKi-67 with satellite DNA of the human genome in early G1 cells." *Chromosome Res* **6**(1): 13-24.

- Brown, C. R. and P. A. Silver (2007). "Transcriptional regulation at the nuclear pore complex." Curr Opin Genet Dev **17**(2): 100-6.
- Brown, K. E., S. S. Guest, et al. (1997). "Association of transcriptionally silent genes with Ikaros complexes at centromeric heterochromatin." Cell **91**(6): 845-54.
- Brownell, J. E., J. Zhou, et al. (1996). "Tetrahymena histone acetyltransferase A: a homolog to yeast Gcn5p linking histone acetylation to gene activation." Cell **84**(6): 843-51.
- Bruggerhoff, K., V. Zakhartchenko, et al. (2002). "Bovine somatic cell nuclear transfer using recipient oocytes recovered by ovum pick-up: effect of maternal lineage of oocyte donors." Biol Reprod **66**(2): 367-73.
- Campbell, K. H., R. Alberio, et al. (2005). "Cloning: eight years after Dolly." Reprod Domest Anim **40**(4): 256-68.
- Campbell, N. A. (1997). Biology. Heidelberg, Spektrum Verlag.
- Chakalova, L., E. Debrand, et al. (2005). "Replication and transcription: shaping the landscape of the genome." Nat Rev Genet **6**(9): 669-77.
- Chambeyron, S. and W. A. Bickmore (2004). "Chromatin decondensation and nuclear reorganization of the HoxB locus upon induction of transcription." Genes Dev **18**(10): 1119-30.
- Chen, C. S., M. Mrksich, et al. (1997). "Geometric control of cell life and death." Science **276**(5317): 1425-8.
- Cheutin, T., A. J. McNairn, et al. (2003). "Maintenance of stable heterochromatin domains by dynamic HP1 binding." Science **299**(5607): 721-5.
- Christova, R., T. Jones, et al. (2007). "P-STAT1 mediates higher-order chromatin remodelling of the human MHC in response to IFN γ ." J Cell Sci **120**(Pt 18): 3262-70.
- Chuang, C. H., A. E. Carpenter, et al. (2006). "Long-range directional movement of an interphase chromosome site." Curr Biol **16**(8): 825-31.
- Chubb, J. R. and W. A. Bickmore (2003). "Considering nuclear compartmentalization in the light of nuclear dynamics." Cell **112**(4): 403-6.
- Chubb, J. R., S. Boyle, et al. (2002). "Chromatin motion is constrained by association with nuclear compartments in human cells." Curr Biol **12**(6): 439-45.
- Clark, R. J. and G. Felsenfeld (1971). "Structure of chromatin." Nat New Biol **229**(4): 101-6.
- Conchello, J. A. and J. W. Lichtman (2005). "Optical sectioning microscopy." Nat Methods **2**(12): 920-31.
- Cook, P. R. (1999). "The organization of replication and transcription." Science **284**(5421): 1790-5.
- Cooke, A. and J. E. Kay (1973). "Effect of phytohaemagglutinin on the nuclear RNA polymerase activity of human lymphocytes." Exp Cell Res **79**(1): 179-85.
- Cornforth, M. N., K. M. Greulich-Bode, et al. (2002). "Chromosomes are predominantly located randomly with respect to each other in interphase human cells." J Cell Biol **159**(2): 237-44.
- Cremer, C., T. Cremer, et al. (1980). "Detection of laser-UV microirradiation-induced DNA photolesions by immunofluorescent staining." Hum Genet **54**(1): 107-10.
- Cremer, M., K. Kupper, et al. (2003). "Inheritance of gene density-related higher order chromatin arrangements in normal and tumor cell nuclei." J Cell Biol **162**(5): 809-20.
- Cremer, M., S. Müller, et al. (2007). "Cell Preparation and Multicolor FISH in 3D Preserved Cultured Mammalian Cells." CSH Protocols **(10)**.
- Cremer, M., J. von Hase, et al. (2001). "Non-random radial higher-order chromatin arrangements in nuclei of diploid human cells." Chromosome Res **9**(7): 541-67.
- Cremer, T. (1985).
- Cremer, T. and C. Cremer (2001). "Chromosome territories, nuclear architecture and gene regulation in mammalian cells." Nat Rev Genet **2**(4): 292-301.
- Cremer, T., C. Cremer, et al. (1982). "Rabl's model of the interphase chromosome arrangement tested in Chinese hamster cells by premature chromosome condensation and laser-UV-microbeam experiments." Hum Genet **60**(1): 46-56.

- Cremer, T., C. Cremer, et al. (1982). "Analysis of chromosome positions in the interphase nucleus of Chinese hamster cells by laser-UV-microirradiation experiments." *Hum Genet* **62**(3): 201-9.
- Cremer, T., M. Cremer, et al. (2006). "Chromosome territories--a functional nuclear landscape." *Curr Opin Cell Biol* **18**(3): 307-16.
- Cremer, T., A. Kurz, et al. (1993). "Role of chromosome territories in the functional compartmentalization of the cell nucleus." *Cold Spring Harb Symp Quant Biol* **58**: 777-92.
- Cremer, T., P. Lichter, et al. (1988). "Detection of chromosome aberrations in metaphase and interphase tumor cells by in situ hybridization using chromosome-specific library probes." *Hum Genet* **80**(3): 235-46.
- Croft, J. A., J. M. Bridger, et al. (1999). "Differences in the localization and morphology of chromosomes in the human nucleus." *J Cell Biol* **145**(6): 1119-31.
- Dechat, T., K. Pflieger, et al. (2008). "Nuclear lamins: major factors in the structural organization and function of the nucleus and chromatin." *Genes Dev* **22**(7): 832-53.
- Deng, W., S. W. Tsao, et al. (2003). "A new method for improving metaphase chromosome spreading." *Cytometry A* **51**(1): 46-51.
- Diblik, J., M. Macek, Sr., et al. (2005). "Topology of chromosomes 18 and X in human blastomeres from 3- to 4-day-old embryos." *J Histochem Cytochem* **53**(3): 273-6.
- Diblik, J., M. Macek, Sr., et al. (2007). "Chromosome topology in normal and aneuploid blastomeres from human embryos." *Prenat Diagn* **27**(12): 1091-9.
- Dietzel, S., K. Zolghadr, et al. (2004). "Differential large-scale chromatin compaction and intranuclear positioning of transcribed versus non-transcribed transgene arrays containing beta-globin regulatory sequences." *J Cell Sci* **117**(Pt 19): 4603-14.
- Dillon, N. and R. Festenstein (2002). "Unravelling heterochromatin: competition between positive and negative factors regulates accessibility." *Trends Genet* **18**(5): 252-8.
- Durrin, L. K., R. K. Mann, et al. (1991). "Yeast histone H4 N-terminal sequence is required for promoter activation in vivo." *Cell* **65**(6): 1023-31.
- Dyer, K. A., T. K. Canfield, et al. (1989). "Molecular cytological differentiation of active from inactive X domains in interphase: implications for X chromosome inactivation." *Cytogenet Cell Genet* **50**(2-3): 116-20.
- Edelmann, P., H. Bornfleth, et al. (2001). "Morphology and dynamics of chromosome territories in living cells." *Biochim Biophys Acta* **1551**(1): M29-39.
- Finch, K. A., G. Fonseka, et al. (2008). "Nuclear organisation in totipotent human nuclei and its relationship to chromosomal abnormality." *J Cell Sci* **121**(Pt 5): 655-63.
- Finch, K. A., K. G. Fonseka, et al. (2008). "Nuclear organization in human sperm: preliminary evidence for altered sex chromosome centromere position in infertile males." *Hum Reprod* **23**(6): 1263-70.
- Foster, H. A. and J. M. Bridger (2005). "The genome and the nucleus: a marriage made by evolution. Genome organisation and nuclear architecture." *Chromosoma* **114**(4): 212-29.
- Fraser, P. and W. Bickmore (2007). "Nuclear organization of the genome and the potential for gene regulation." *Nature* **447**(7143): 413-7.
- Furukawa, K., H. Inagaki, et al. (1994). "Identification and cloning of an mRNA coding for a germ cell-specific A-type lamin in mice." *Exp Cell Res* **212**(2): 426-30.
- Gasser, S. M. and U. K. Laemmli (1986). "The organisation of chromatin loops: characterization of a scaffold attachment site." *Embo J* **5**(3): 511-518.
- Gerlich, D., J. Beaudouin, et al. (2003). "Global chromosome positions are transmitted through mitosis in mammalian cells." *Cell* **112**(6): 751-64.
- Gilbert, N., S. Boyle, et al. (2004). "Chromatin architecture of the human genome: gene-rich domains are enriched in open chromatin fibers." *Cell* **118**(5): 555-66.
- Goldberg, A. D., C. D. Allis, et al. (2007). "Epigenetics: a landscape takes shape." *Cell* **128**(4): 635-8.
- Goldman, R. D., Y. Gruenbaum, et al. (2002). "Nuclear lamins: building blocks of nuclear architecture." *Genes Dev* **16**(5): 533-47.

- Grasser, F., M. Neusser, et al. (2008). "Replication-timing-correlated spatial chromatin arrangements in cancer and in primate interphase nuclei." J Cell Sci **121**(Pt 11): 1876-86.
- Gray, J. W., D. Peters, et al. (1979). "Slit-scan flow cytometry of mammalian chromosomes." J Histochem Cytochem **27**(1): 441-4.
- Greaves, I. K., M. Svartman, et al. (2001). "Chromosomal painting detects non-random chromosome arrangement in dasyurid marsupial sperm." Chromosome Res **9**(3): 251-9.
- Grosse-Hovest, L., S. Muller, et al. (2004). "Cloned transgenic farm animals produce a bispecific antibody for T cell-mediated tumor cell killing." Proc Natl Acad Sci U S A **101**(18): 6858-63.
- Gruenbaum, Y., R. D. Goldman, et al. (2003). "The nuclear lamina and its functions in the nucleus." Int Rev Cytol **226**: 1-62.
- Haaf, T. and M. Schmid (1991). "Chromosome topology in mammalian interphase nuclei." Exp Cell Res **192**(2): 325-32.
- Habermann, F. A., M. Cremer, et al. (2001). "Arrangements of macro- and microchromosomes in chicken cells." Chromosome Res **9**(7): 569-84.
- Hake, S. B., A. Xiao, et al. (2007). "Linking the epigenetic 'language' of covalent histone modifications to cancer." Br J Cancer **96** **Suppl**: R31-9.
- Heard, E. and W. Bickmore (2007). "The ins and outs of gene regulation and chromosome territory organisation." Curr Opin Cell Biol **19**(3): 311-6.
- Hepperger, C., A. Mannes, et al. (2008). "Three-dimensional positioning of genes in mouse cell nuclei." Chromosoma.
- Hepperger, C., S. Otten, et al. (2007). "Preservation of large-scale chromatin structure in FISH experiments." Chromosoma **116**(2): 117-33.
- Hiendleder, S., D. Bebbere, et al. (2004). "Maternal-fetal transplacental leakage of mitochondrial DNA in bovine nuclear transfer pregnancies: potential implications for offspring and recipients." Cloning Stem Cells **6**(2): 150-6.
- Hiendleder, S., C. Mund, et al. (2004). "Tissue-specific elevated genomic cytosine methylation levels are associated with an overgrowth phenotype of bovine fetuses derived by in vitro techniques." Biol Reprod **71**(1): 217-23.
- Hiendleder, S., K. Prelle, et al. (2004). "Nuclear-cytoplasmic interactions affect in utero developmental capacity, phenotype, and cellular metabolism of bovine nuclear transfer fetuses." Biol Reprod **70**(4): 1196-205.
- Hiendleder, S., V. Zakhartchenko, et al. (2003). "Heteroplasmy in bovine fetuses produced by intra- and inter-subspecific somatic cell nuclear transfer: neutral segregation of nuclear donor mitochondrial DNA in various tissues and evidence for recipient cow mitochondria in fetal blood." Biol Reprod **68**(1): 159-66.
- Houdebine, L. M. (2005). "Use of transgenic animals to improve human health and animal production." Reprod Domest Anim **40**(4): 269-81.
- Ingber, D. E. (2003). "Mechanosensation through integrins: cells act locally but think globally." Proc Natl Acad Sci U S A **100**(4): 1472-4.
- Jackson, D. A. and A. Pombo (1998). "Replicon clusters are stable units of chromosome structure: evidence that nuclear organization contributes to the efficient activation and propagation of S phase in human cells." J Cell Biol **140**(6): 1285-95.
- Jenuwein, T. and C. D. Allis (2001). "Translating the histone code." Science **293**(5532): 1074-80.
- Joffe, B. I., I. V. Solovei, et al. (1998). "Ordered arrangement and rearrangement of chromosomes during spermatogenesis in two species of planarians (Plathelminthes)." Chromosoma **107**(3): 173-83.
- Ketterl, N. (2008). Untersuchungen zur gendichteabhängigen Verteilung von Chromosomen in frühen Rinderembryonen nach Kerntransfer. Institut für Humangenetik, Department II. München, LMU.
- Kim, S. H., P. G. McQueen, et al. (2004). "Spatial genome organization during T-cell differentiation." Cytogenet Genome Res **105**(2-4): 292-301.

- Kirchhof, N., J. W. Carnwath, et al. (2000). "Expression pattern of Oct-4 in preimplantation embryos of different species." *Biol Reprod* **63**(6): 1698-705.
- Koestenbauer, S., N. H. Zech, et al. (2006). "Embryonic stem cells: similarities and differences between human and murine embryonic stem cells." *Am J Reprod Immunol* **55**(3): 169-80.
- Kopečný, V., J. E. Flechon, et al. (1989). "Nucleologenesis and the onset of transcription in the eight-cell bovine embryo: fine-structural autoradiographic study." *Mol Reprod Dev* **1**(2): 79-90.
- Kornberg, R. D. (1974). "Chromatin structure: a repeating unit of histones and DNA." *Science* **184**(139): 868-71.
- Kosak, S. T., D. Scalzo, et al. (2007). "Coordinate gene regulation during hematopoiesis is related to genomic organization." *PLoS Biol* **5**(11): e309.
- Kosak, S. T., J. A. Skok, et al. (2002). "Subnuclear compartmentalization of immunoglobulin loci during lymphocyte development." *Science* **296**(5565): 158-62.
- Koss, L. G. (1998). "Characteristics of chromosomes in polarized normal human bronchial cells provide a blueprint for nuclear organization." *Cytogenet Cell Genet* **82**(3-4): 230-7.
- Kozubek, S., E. Lukasova, et al. (1997). "Distribution of ABL and BCR genes in cell nuclei of normal and irradiated lymphocytes." *Blood* **89**(12): 4537-45.
- Kreth, G., P. Edelmann, et al. (2001). "Towards a dynamical approach for the simulation of large scale, cancer correlated chromatin structures." *Ital J Anat Embryol* **106**(2 Suppl 1): 21-30.
- Kreth, G., J. Finsterle, et al. (2004). "Radial arrangement of chromosome territories in human cell nuclei: a computer model approach based on gene density indicates a probabilistic global positioning code." *Biophys J* **86**(5): 2803-12.
- Kues, W. A., J. W. Carnwath, et al. (2005). "From fibroblasts and stem cells: implications for cell therapies and somatic cloning." *Reprod Fertil Dev* **17**(1-2): 125-34.
- Kumaran, R. I. and D. L. Spector (2008). "A genetic locus targeted to the nuclear periphery in living cells maintains its transcriptional competence." *J Cell Biol* **180**(1): 51-65.
- Kupper, K., A. Kolbl, et al. (2007). "Radial chromatin positioning is shaped by local gene density, not by gene expression." *Chromosoma* **116**(3): 285-306.
- Lamond, A. I. and D. L. Spector (2003). "Nuclear speckles: a model for nuclear organelles." *Nat Rev Mol Cell Biol* **4**(8): 605-12.
- Lanctot, C., T. Cheutin, et al. (2007). "Dynamic genome architecture in the nuclear space: regulation of gene expression in three dimensions." *Nat Rev Genet* **8**(2): 104-15.
- Latham, K. E. (2004). "Cloning: questions answered and unsolved." *Differentiation* **72**(1): 11-22.
- Lengner, C. J., F. D. Camargo, et al. (2007). "Oct4 expression is not required for mouse somatic stem cell self-renewal." *Cell Stem Cell* **1**(4): 403-15.
- Lesko, S. A., D. E. Callahan, et al. (1995). "The experimental homologous and heterologous separation distance histograms for the centromeres of chromosomes 7, 11, and 17 in interphase human T-lymphocytes." *Exp Cell Res* **219**(2): 499-506.
- Lichter, P., T. Cremer, et al. (1988). "Delineation of individual human chromosomes in metaphase and interphase cells by in situ suppression hybridization using recombinant DNA libraries." *Hum Genet* **80**(3): 224-34.
- Luetjens, C. M., C. Payne, et al. (1999). "Non-random chromosome positioning in human sperm and sex chromosome anomalies following intracytoplasmic sperm injection." *Lancet* **353**(9160): 1240.
- Luger, K., A. W. Mader, et al. (1997). "Crystal structure of the nucleosome core particle at 2.8 Å resolution." *Nature* **389**(6648): 251-60.
- Lukasova, E., S. Kozubek, et al. (1997). "Localisation and distance between ABL and BCR genes in interphase nuclei of bone marrow cells of control donors and patients with chronic myeloid leukaemia." *Hum Genet* **100**(5-6): 525-35.
- Maherali, N., R. Sridharan, et al. (2007). "Directly Reprogrammed Fibroblasts Show Global Epigenetic Remodeling and Widespread Tissue Contribution." *Cell Stem Cell* **1**(1): 55-70.

- Mahy, N. L., P. E. Perry, et al. (2002). "Gene density and transcription influence the localization of chromatin outside of chromosome territories detectable by FISH." *J Cell Biol* **159**(5): 753-63.
- Mahy, N. L., P. E. Perry, et al. (2002). "Spatial organization of active and inactive genes and noncoding DNA within chromosome territories." *J Cell Biol* **157**(4): 579-89.
- Malhas, A., C. F. Lee, et al. (2007). "Defects in lamin B1 expression or processing affect interphase chromosome position and gene expression." *J Cell Biol* **176**(5): 593-603.
- Maniotis, A. J., C. S. Chen, et al. (1997). "Demonstration of mechanical connections between integrins, cytoskeletal filaments, and nucleoplasm that stabilize nuclear structure." *Proc Natl Acad Sci U S A* **94**(3): 849-54.
- Manuelidis, L. (1985). "Individual interphase chromosome domains revealed by in situ hybridization." *Hum Genet* **71**(4): 288-93.
- Martin, C., N. Beaujean, et al. (2006). "Genome restructuring in mouse embryos during reprogramming and early development." *Dev Biol* **292**(2): 317-32.
- Martin, C., V. Brochard, et al. (2006). "Architectural reorganization of the nuclei upon transfer into oocytes accompanies genome reprogramming." *Mol Reprod Dev* **73**(9): 1102-11.
- Mateos-Langerak, J., S. Goetze, et al. (2007). "Nuclear architecture: Is it important for genome function and can we prove it?" *J Cell Biochem* **102**(5): 1067-75.
- Mayer, R., A. Brero, et al. (2005). "Common themes and cell type specific variations of higher order chromatin arrangements in the mouse." *BMC Cell Biol* **6**: 44.
- McKenzie, L. J., S. A. Carson, et al. (2004). "Nuclear chromosomal localization in human preimplantation embryos: correlation with aneuploidy and embryo morphology." *Hum Reprod* **19**(10): 2231-7.
- Meaburn, K. J., E. Cabuy, et al. (2007). "Primary laminopathy fibroblasts display altered genome organization and apoptosis." *Aging Cell* **6**(2): 139-53.
- Meaburn, K. J. and T. Misteli (2007). "Cell biology: chromosome territories." *Nature* **445**(7126): 379-781.
- Meaburn, K. J., T. Misteli, et al. (2007). "Spatial genome organization in the formation of chromosomal translocations." *Semin Cancer Biol* **17**(1): 80-90.
- Merico, V., J. Barbieri, et al. (2007). "Epigenomic differentiation in mouse preimplantation nuclei of biparental, parthenote and cloned embryos." *Chromosome Res* **15**(3): 341-60.
- Meyer-Ficca, M., J. Muller-Navia, et al. (1998). "Clustering of pericentromeres initiates in step 9 of spermiogenesis of the rat (*Rattus norvegicus*) and contributes to a well defined genome architecture in the sperm nucleus." *J Cell Sci* **111** (Pt 10): 1363-70.
- Misteli, T. (2007). "Beyond the sequence: cellular organization of genome function." *Cell* **128**(4): 787-800.
- Misteli, T. (2008). "Physiological importance of RNA and protein mobility in the cell nucleus." *Histochem Cell Biol* **129**(1): 5-11.
- Misteli, T., J. F. Caceres, et al. (1997). "The dynamics of a pre-mRNA splicing factor in living cells." *Nature* **387**(6632): 523-7.
- Mitelman, F. (2000). "Recurrent chromosome aberrations in cancer." *Mutat Res* **462**(2-3): 247-53.
- Moen, P. T., Jr., C. V. Johnson, et al. (2004). "Repositioning of muscle-specific genes relative to the periphery of SC-35 domains during skeletal myogenesis." *Mol Biol Cell* **15**(1): 197-206.
- Morgan, H. D., F. Santos, et al. (2005). "Epigenetic reprogramming in mammals." *Hum Mol Genet* **14 Spec No 1**: R47-58.
- Müller, S., M. Neusser, et al. (2007). "Preparation of Complex DNA Probe Sets for 3D FISH with up to Six Different Fluorochromes." *CSH Protocols* (10).
- Muller, S. and J. Wienberg (2001). ""Bar-coding" primate chromosomes: molecular cytogenetic screening for the ancestral hominoid karyotype." *Hum Genet* **109**(1): 85-94.
- Munkel, C., R. Eils, et al. (1999). "Compartmentalization of interphase chromosomes observed in simulation and experiment." *J Mol Biol* **285**(3): 1053-65.

- Munne, S., J. Cohen, et al. (2002). "Preimplantation genetic diagnosis for advanced maternal age and other indications." *Fertil Steril* **78**(2): 234-6.
- Munne, S., C. Magli, et al. (1999). "Positive outcome after preimplantation diagnosis of aneuploidy in human embryos." *Hum Reprod* **14**(9): 2191-9.
- Nagele, R., T. Freeman, et al. (1995). "Precise spatial positioning of chromosomes during prometaphase: evidence for chromosomal order." *Science* **270**(5243): 1831-5.
- Nagele, R. G., T. Freeman, et al. (1998). "Chromosome spatial order in human cells: evidence for early origin and faithful propagation." *Chromosoma* **107**(5): 330-8.
- Nagele, R. G., T. Freeman, et al. (1999). "Chromosomes exhibit preferential positioning in nuclei of quiescent human cells." *J Cell Sci* **112** (Pt 4): 525-35.
- Nagele, R. G., A. Q. Velasco, et al. (2001). "Telomere associations in interphase nuclei: possible role in maintenance of interphase chromosome topology." *J Cell Sci* **114**(Pt 2): 377-88.
- Neusser, M., V. Schubel, et al. (2007). "Evolutionarily conserved, cell type and species-specific higher order chromatin arrangements in interphase nuclei of primates." *Chromosoma* **116**(3): 307-20.
- Nichols, J., B. Zevnik, et al. (1998). "Formation of pluripotent stem cells in the mammalian embryo depends on the POU transcription factor Oct4." *Cell* **95**(3): 379-91.
- Niwa, H., J. Miyazaki, et al. (2000). "Quantitative expression of Oct-3/4 defines differentiation, dedifferentiation or self-renewal of ES cells." *Nat Genet* **24**(4): 372-6.
- Niwa, H., Y. Toyooka, et al. (2005). "Interaction between Oct3/4 and Cdx2 determines trophoblast differentiation." *Cell* **123**(5): 917-29.
- Okita, K., T. Ichisaka, et al. (2007). "Generation of germline-competent induced pluripotent stem cells." *Nature* **448**(7151): 313-7.
- Olins, A. L. and D. E. Olins (1974). "Spheroid chromatin units (v bodies)." *Science* **183**(122): 330-2.
- Ottaviani, D., E. Lever, et al. (2008). "Anchoring the genome." *Genome Biol* **9**(1): 201.
- Pajeroski, J. D., K. N. Dahl, et al. (2007). "Physical plasticity of the nucleus in stem cell differentiation." *Proc Natl Acad Sci U S A* **104**(40): 15619-24.
- Parada, L. and T. Misteli (2002). "Chromosome positioning in the interphase nucleus." *Trends Cell Biol* **12**(9): 425-32.
- Parada, L. A., P. G. McQueen, et al. (2004). "Tissue-specific spatial organization of genomes." *Genome Biol* **5**(7): R44.
- Parada, L. A., P. G. McQueen, et al. (2002). "Conservation of relative chromosome positioning in normal and cancer cells." *Curr Biol* **12**(19): 1692-7.
- Paterson, L., P. DeSousa, et al. (2003). "Application of reproductive biotechnology in animals: implications and potentials. Applications of reproductive cloning." *Anim Reprod Sci* **79**(3-4): 137-43.
- Paulson, J. R. and U. K. Laemmli (1977). "The structure of histone-depleted metaphase chromosomes." *Cell* **12**(3): 817-28.
- Postberg, J., O. Alexandrova, et al. (2005). "Exploiting nuclear duality of ciliates to analyse topological requirements for DNA replication and transcription." *J Cell Sci* **118**(Pt 17): 3973-83.
- Probst, A. V., F. Santos, et al. (2007). "Structural differences in centromeric heterochromatin are spatially reconciled on fertilisation in the mouse zygote." *Chromosoma* **116**(4): 403-15.
- Rabl, C. (1885). Über Zelltheilung. *Morphologisches Jahrbuch*. C. Gegenbaur. **10**: 214-330.
- Ragoczy, T., M. A. Bender, et al. (2006). "The locus control region is required for association of the murine beta-globin locus with engaged transcription factories during erythroid maturation." *Genes Dev* **20**(11): 1447-57.
- Richmond, T. J., J. T. Finch, et al. (1984). "Structure of the nucleosome core particle at 7 Å resolution." *Nature* **311**(5986): 532-7.
- Roix, J. J., P. G. McQueen, et al. (2003). "Spatial proximity of translocation-prone gene loci in human lymphomas." *Nat Genet* **34**(3): 287-91.
- Sachs, R. K., G. van den Engh, et al. (1995). "A random-walk/giant-loop model for interphase chromosomes." *Proc Natl Acad Sci U S A* **92**(7): 2710-4.

- Sadoni, N., S. Langer, et al. (1999). "Nuclear organization of mammalian genomes. Polar chromosome territories build up functionally distinct higher order compartments." J Cell Biol **146**(6): 1211-26.
- Santos, F. and W. Dean (2004). "Epigenetic reprogramming during early development in mammals." Reproduction **127**(6): 643-51.
- Santos, F., A. H. Peters, et al. (2005). "Dynamic chromatin modifications characterise the first cell cycle in mouse embryos." Dev Biol **280**(1): 225-36.
- Santos, F., V. Zakhartchenko, et al. (2003). "Epigenetic marking correlates with developmental potential in cloned bovine preimplantation embryos." Curr Biol **13**(13): 1116-21.
- Satzinger, H. (2008). "Theodor and Marcella Boveri: chromosomes and cytoplasm in heredity and development." Nat Rev Genet **9**(3): 231-8.
- Scaffidi, P. and T. Misteli (2005). "Reversal of the cellular phenotype in the premature aging disease Hutchinson-Gilford progeria syndrome." Nat Med **11**(4): 440-5.
- Schardin, M., T. Cremer, et al. (1985). "Specific staining of human chromosomes in Chinese hamster x man hybrid cell lines demonstrates interphase chromosome territories." Hum Genet **71**(4): 281-7.
- Schermelleh, L., P. M. Carlton, et al. (2008). "Subdiffraction multicolor imaging of the nuclear periphery with 3D structured illumination microscopy." Science **320**(5881): 1332-6.
- Sedat, J. and L. Manuelidis (1978). "A direct approach to the structure of eukaryotic chromosomes." Cold Spring Harb Symp Quant Biol **42 Pt 1**: 331-50.
- Sexton, T., H. Schober, et al. (2007). "Gene regulation through nuclear organization." Nat Struct Mol Biol **14**(11): 1049-1055.
- Shi, W., V. Zakhartchenko, et al. (2003). "Epigenetic reprogramming in mammalian nuclear transfer." Differentiation **71**(2): 91-113.
- Shumaker, D. K., T. Dechat, et al. (2006). "Mutant nuclear lamin A leads to progressive alterations of epigenetic control in premature aging." Proc Natl Acad Sci U S A **103**(23): 8703-8.
- Solovei, I., A. Cavallo, et al. (2002). "Spatial preservation of nuclear chromatin architecture during three-dimensional fluorescence in situ hybridization (3D-FISH)." Exp Cell Res **276**(1): 10-23.
- Solovei, I., L. Schermelleh, et al. (2006). Detection of Cell Cycle Stages in situ in Growing Cell Populations. Cell Biology, Elsevier Science, USA: 291- 299.
- Solovei, I. V., B. I. Joffe, et al. (1998). "Unordered arrangement of chromosomes in the nuclei of chicken spermatozoa." Chromosoma **107**(3): 184-8.
- Spector, D. L. (1990). "Higher order nuclear organization: three-dimensional distribution of small nuclear ribonucleoprotein particles." Proc Natl Acad Sci U S A **87**(1): 147-51.
- Spector, D. L. (2001). "Nuclear domains." J Cell Sci **114**(Pt 16): 2891-3.
- Stadler, S., V. Schnapp, et al. (2004). "The architecture of chicken chromosome territories changes during differentiation." BMC Cell Biol **5**(1): 44.
- Starborg, M., K. Gell, et al. (1996). "The murine Ki-67 cell proliferation antigen accumulates in the nucleolar and heterochromatic regions of interphase cells and at the periphery of the mitotic chromosomes in a process essential for cell cycle progression." J Cell Sci **109 (Pt 1)**: 143-53.
- Stewart, C. and B. Burke (1987). "Teratocarcinoma stem cells and early mouse embryos contain only a single major lamin polypeptide closely resembling lamin B." Cell **51**(3): 383-92.
- Sun, H. B., J. Shen, et al. (2000). "Size-dependent positioning of human chromosomes in interphase nuclei." Biophys J **79**(1): 184-90.
- Sun, H. B. and H. Yokota (1999). "Correlated positioning of homologous chromosomes in daughter fibroblast cells." Chromosome Res **7**(8): 603-10.
- Taddei, A., G. Van Houwe, et al. (2006). "Nuclear pore association confers optimal expression levels for an inducible yeast gene." Nature **441**(7094): 774-8.
- Takahashi, K., K. Tanabe, et al. (2007). "Induction of pluripotent stem cells from adult human fibroblasts by defined factors." Cell **131**(5): 861-72.

- Takahashi, K. and S. Yamanaka (2006). "Induction of pluripotent stem cells from mouse embryonic and adult fibroblast cultures by defined factors." Cell **126**(4): 663-76.
- Tanabe, H., S. Muller, et al. (2002). "Evolutionary conservation of chromosome territory arrangements in cell nuclei from higher primates." Proc Natl Acad Sci U S A **99**(7): 4424-9.
- Telenius, H., A. H. Pelmeur, et al. (1992). "Cytogenetic analysis by chromosome painting using DOP-PCR amplified flow-sorted chromosomes." Genes Chromosomes Cancer **4**(3): 257-63.
- Thomson, I., S. Gilchrist, et al. (2004). "The radial positioning of chromatin is not inherited through mitosis but is established de novo in early G1." Curr Biol **14**(2): 166-72.
- Thormeyer, T. (2005). Untersuchungen zur Lokalisation der nukleären Matrix in Zellkernen nach induzierter Chromatinkondensation. Institut für Humangenetik, Department II. München, LMU.
- Tremethick, D. J. (2007). "Higher-order structures of chromatin: the elusive 30 nm fiber." Cell **128**(4): 651-4.
- Trinkle-Mulcahy, L. and A. I. Lamond (2008). "Nuclear functions in space and time: Gene expression in a dynamic, constrained environment." FEBS Lett **582**(14): 1960-70.
- Tumbar, T. and A. S. Belmont (2001). "Interphase movements of a DNA chromosome region modulated by VP16 transcriptional activator." Nat Cell Biol **3**(2): 134-9.
- Turner, B. M. (2005). "Reading signals on the nucleosome with a new nomenclature for modified histones." Nat Struct Mol Biol **12**(2): 110-2.
- Vazquez, J., A. S. Belmont, et al. (2001). "Multiple regimes of constrained chromosome motion are regulated in the interphase Drosophila nucleus." Curr Biol **11**(16): 1227-39.
- Verschure, P. J., I. van Der Kraan, et al. (1999). "Spatial relationship between transcription sites and chromosome territories." J Cell Biol **147**(1): 13-24.
- Volpi, E. V., E. Chevret, et al. (2000). "Large-scale chromatin organization of the major histocompatibility complex and other regions of human chromosome 6 and its response to interferon in interphase nuclei." J Cell Sci **113** (Pt 9): 1565-76.
- von Hase, J., D. Koehler, et al. (submitted). "High precision measurements of absolute distance distributions from intranuclear surfaces (ADS) in 3D confocal microscopy images." Chromosome Res.
- Wade, P. A. and N. Kikyo (2002). "Chromatin remodeling in nuclear cloning." Eur J Biochem **269**(9): 2284-7.
- Wallis, J. W., L. Hereford, et al. (1980). "Histone H2B genes of yeast encode two different proteins." Cell **22**(3): 799-805.
- Walter, J., B. Joffe, et al. (2006). "Towards many colors in FISH on 3D-preserved interphase nuclei." Cytogenet Genome Res **114**(3-4): 367-78.
- Walter, J., L. Schermelleh, et al. (2003). "Chromosome order in HeLa cells changes during mitosis and early G1, but is stably maintained during subsequent interphase stages." J Cell Biol **160**(5): 685-97.
- Wang, G. G., C. D. Allis, et al. (2007). "Chromatin remodeling and cancer, Part I: Covalent histone modifications." Trends Mol Med **13**(9): 363-72.
- Wansink, D. G., W. Schul, et al. (1993). "Fluorescent labeling of nascent RNA reveals transcription by RNA polymerase II in domains scattered throughout the nucleus." J Cell Biol **122**(2): 283-93.
- Watson, J. M., J. Meyne, et al. (1996). "Ordered tandem arrangement of chromosomes in the sperm heads of monotreme mammals." Proc Natl Acad Sci U S A **93**(19): 10200-5.
- Weierich, C., A. Brero, et al. (2003). "Three-dimensional arrangements of centromeres and telomeres in nuclei of human and murine lymphocytes." Chromosome Res **11**(5): 485-502.
- Wernig, M., A. Meissner, et al. (2008). "c-Myc is dispensable for direct reprogramming of mouse fibroblasts." Cell Stem Cell **2**(1): 10-2.
- Wernig, M., A. Meissner, et al. (2007). "In vitro reprogramming of fibroblasts into a pluripotent ES-cell-like state." Nature.

- Wiblin, A. E., W. Cui, et al. (2005). "Distinctive nuclear organisation of centromeres and regions involved in pluripotency in human embryonic stem cells." J Cell Sci **118**(Pt 17): 3861-8.
- Williams, R. R., V. Azuara, et al. (2006). "Neural induction promotes large-scale chromatin reorganisation of the Mash1 locus." J Cell Sci **119**(Pt 1): 132-40.
- Wischnitzer, S. (1973). "The submicroscopic morphology of the interphase nucleus." Int Rev Cytol **34**: 1-48.
- Wolf, E., V. Zakhartchenko, et al. (1998). "Nuclear transfer in mammals: recent developments and future perspectives." J Biotechnol **65**(2-3): 99-110.
- Wuensch, A., F. A. Habermann, et al. (2007). "Quantitative Monitoring of Pluripotency Gene Activation after Somatic Cloning in Cattle." Biol Reprod.
- Ye, Q., I. Callebaut, et al. (1997). "Domain-specific interactions of human HP1-type chromodomain proteins and inner nuclear membrane protein LBR." J Biol Chem **272**(23): 14983-9.
- Ye, Q. and H. J. Worman (1996). "Interaction between an integral protein of the nuclear envelope inner membrane and human chromodomain proteins homologous to Drosophila HP1." J Biol Chem **271**(25): 14653-6.
- Yoshimizu, T., N. Sugiyama, et al. (1999). "Germline-specific expression of the Oct-4/green fluorescent protein (GFP) transgene in mice." Dev Growth Differ **41**(6): 675-84.
- Yu, J., M. A. Vodyanik, et al. (2007). "Induced pluripotent stem cell lines derived from human somatic cells." Science **318**(5858): 1917-20.
- Zakhartchenko, V., G. Durcova-Hills, et al. (1999). "Potential of fetal germ cells for nuclear transfer in cattle." Mol Reprod Dev **52**(4): 421-6.
- Zakhartchenko, V., G. Durcova-Hills, et al. (1999). "Effects of serum starvation and re-cloning on the efficiency of nuclear transfer using bovine fetal fibroblasts." J Reprod Fertil **115**(2): 325-31.
- Zakhartchenko, V., M. Stojkovic, et al. (1997). "Karyoplast-cytoplast volume ratio in bovine nuclear transfer embryos: effect on developmental potential." Mol Reprod Dev **48**(3): 332-8.
- Zink, D., M. D. Amaral, et al. (2004). "Transcription-dependent spatial arrangements of CFTR and adjacent genes in human cell nuclei." J Cell Biol **166**(6): 815-25.
- Zirbel, R. M., U. R. Mathieu, et al. (1993). "Evidence for a nuclear compartment of transcription and splicing located at chromosome domain boundaries." Chromosome Res **1**(2): 93-106.
- Zorn, C., C. Cremer, et al. (1979). "Unscheduled DNA synthesis after partial UV irradiation of the cell nucleus. Distribution in interphase and metaphase." Exp Cell Res **124**(1): 111-9.

7. Appendix

7.1. Tables of results and statistics

As a brief overview all results the performed experiments are summarized in the following. Note that besides the normalized data, already discussed in the text, the absolute distance to surface (ADS) values are shown. Characteristically the median value is representing the curve, additionally the mean standard errors are listed and the number of nuclei and embryos counted for evaluation.

To decide if distributions are equal or different, a Mann-Whitney-Rank Sum was performed. Values that are below 0.05 indicate a significant difference between two curves. Those values are spelled in thick red letters.

7.1.1. Distribution of CTs 18 & 19 in human fibroblasts during cell cycle

Relative radial distribution of CTs 1 and 20 in human fibroblasts during cell cycle:

HFb G0 n=20	Relative Radial Distribution (RRD)		
3D	HSA 1	HSA 20	DAPI
ARR %	74	56	69
SDM %	37	60	7
2D	HSA 1	HSA 20	DAPI
ARR %	71	47	63
SDM %	40	75	7

Mann-Whitney Rank Sum test	Relative Radial Distribution (RRD)		
3D		HSA 20	DAPI
	HSA 1	p<0.001	p<0.001
2D	HSA 20		p<0.001
	HSA 1	p<0.001	p<0.001
2D	HSA 20		p<0.001
	HSA 1	p<0.001	p<0.001

HFb S n=20	Relative Radial Distribution (RRD)		
3D	HSA 1	HSA 20	DAPI
ARR %	73	62	68
SDM %	41	61	6
2D	HSA 1	HSA 20	DAPI
ARR %	67	55	62
SDM %	53	80	5

Mann-Whitney Rank Sum test	Relative Radial Distribution (RRD)		
3D		HSA 20	DAPI
	HSA 1	p<0.001	p<0.001
2D	HSA 20		p<0.001
	HSA 1	p=0.006	p<0.001
2D	HSA 20		p<0.001
	HSA 1	p=0.006	p<0.001

Mann-Whitney Rank Sum test	Relative Radial Distribution (RRD)		
3D	G0/S	HSA 1	HSA 20
	HSA 1	p=0.957	
	HSA 20		p=0.086
2D	G0/S	HSA 1	HSA 20
	HSA 1	p=0.579	
	HSA 20		p=0.086

Relative radial distribution of CTs 17 and Y in human fibroblasts during cell cycle:

HFb G0 n=20	Relative Radial Distribution (RRD)		
3D	HSA Y	HSA 17	DAPI
ARR %	59	58	69
SDM %	75	59	8
2D	HSA Y	HSA 17	DAPI
ARR %	43	52	63
SDM %	118	67	8

Mann-Whitney Rank Sum test	Relative Radial Distribution (RRD)		
3D		HSA 17	DAPI
	HSA Y	p=0.860	p<0.001
2D	HSA 17		p<0.001
		HSA 17	DAPI
2D	HSA Y	p=0.108	p<0.001
	HSA 17		p<0.001

HFb S n=20	Relative Radial Distribution (RRD)		
3D	HSA Y	HSA 17	DAPI
ARR %	51	58	68
SDM %	78	59	5
2D	HSA Y	HSA 17	DAPI
ARR %	34	50	62
SDM %	5	130	59

Mann-Whitney Rank Sum test	Relative Radial Distribution (RRD)		
3D		HSA 17	DAPI
	HSA Y	p=0.021	p<0.001
2D	HSA 17		p<0.001
		HSA 17	DAPI
2D	HSA Y	p=0.005	p<0.001
	HSA 17		p<0.001

Mann-Whitney Rank Sum test	Relative Radial Distribution (RRD)		
3D	G0/S	HSA Y	HSA 17
	HSA Y	p=0.016	
	HSA 17		p=0.648
2D	G0/S	HSA Y	HSA 17
	HSA Y	p=0.062	
	HSA 17		p=0.279

Relative radial distribution of CTs 18 and 19 in human fibroblasts during cell cycle:

HFb G0 n=20	Relative Radial Distribution (RRD)		
3D	HSA 18	HSA 19	DAPI
ARR %	60	58	68
SDM %	67	67	7
2D	HSA 18	HSA 19	DAPI
ARR %	50	54	62
SDM %	87	86	6

Mann-Whitney Rank Sum test	Relative Radial Distribution (RRD)		
3D		HSA 19	DAPI
	HSA 18	p=0.675	p<0.001
2D	HSA 19		p<0.001
		HSA 19	DAPI
2D	HSA 18	p=0.457	p<0.001
	HSA 19		p<0.001

HFb S n=20	Relative Radial Distribution (RRD)		
3D	HSA 18	HSA 19	DAPI
ARR %	62	56	68
SDM %	65	70	4
2D	HSA 18	HSA 19	DAPI
ARR %	54	51	62
SDM %	110	99	5

Mann-Whitney Rank Sum test	Relative Radial Distribution (RRD)		
3D		HSA 19	DAPI
	HSA 18	p=0.126	p<0.001
2D	HSA 19		p<0.001
		HSA 19	DAPI
2D	HSA 18	p=0.757	p<0.001
	HSA 19		p<0.001

Mann-Whitney Rank Sum test	Relative Radial Distribution (RRD)		
3D	G0/S	HSA 18	HSA 19
	HSA 18	p=0.482	
	HSA 19		p=0.617
2D	G0/S	HSA 18	HSA 19
	HSA 18	p=0.448	
	HSA 19		p=0.146

Absolute distances to surface of CTs 18 and 19 in human fibroblasts during cell cycle:

HFb G0 n=20	ADS: medians [in nm]			ADS: normalized medians [in %]		
3D	HSA 18	HSA 19	DAPI	HSA 18	HSA 19	DAPI
Median	-1015	-1321	-742	46	58	31
STABWN	689	678	253	20	22	2

HFb S n=20	ADS: medians [in nm]			ADS: normalized medians [in %]		
3D	HSA 18	HSA 19	DAPI	HSA 18	HSA 19	DAPI
Median	-1015	-1366	-771	46	51	29
STABWN	341	419	94	13	15	1

HFb G0+S n=40	ADS: medians [in nm]			ADS: normalized medians [in %]		
3D	HSA 18	HSA 19	DAPI	HSA 18	HSA 19	DAPI
Median	-1015	-1339	-744	46	56	30
STABWN	549	588	191	17	19	2

Mann-Whitney Rank Sum test	ADS: medians			ADS: normalized medians		
3D		HSA 19	DAPI		HSA 19	DAPI
	HSA 18	p=0.058	p<0.001	HSA 18	p=0.039	p<0.001
	HSA 19		p<0.001	HSA 19		p<0.001

Mann-Whitney Rank Sum test	ADS: medians			ADS: normalized medians		
3D		HSA 19	DAPI		HSA 19	DAPI
	HSA 18	p=0.007	p<0.001	HSA 18	p=0.014	p<0.001
	HSA 19		p<0.001	HSA 19		p<0.001

Mann-Whitney Rank Sum test	ADS: medians			ADS: normalized medians		
3D		HSA 19	DAPI		HSA 19	DAPI
	HSA 18	p<0.001	p<0.001	HSA 18	p<0.001	p<0.001
	HSA 19		p<0.001	HSA 19		p<0.001

Mann-Whitney Rank Sum test	ADS: medians			ADS: normalized medians		
3D	G0/S	HSA 18	HSA 19		HSA 18	HSA 19
	HSA 18	p=0.925		HSA 18	p=0.465	
	HSA 19		p=0.117	HSA 19		p=0.860

Mann-Whitney Rank Sum test	ADS: medians			ADS: normalized medians		
3D	G0/G0+S	HSA 18	HSA 19		HSA 18	HSA 19
	HSA 18	p=0.956		HSA 18	p=0.672	
	HSA 19		p=0.363	HSA 19		p=0.919

Mann-Whitney Rank Sum test	ADS: medians			ADS: normalized medians		
3D	S/G0+S	HSA 18	HSA 19		HSA 18	HSA 19
	HSA 18	p=0.956		HSA 18	p=0.672	
	HSA 19		p=0.363	HSA 19		p=0.919

7.1.2. Distribution of gene poor and gene rich chromosomes in artificially shaped fibroblasts from different species

Distribution of CTs 18 and 19 in human artificially shaped fibroblasts:

HFb "cigars" n=31	ADS: medians [in nm]		ADS: normalized medians [in %]	
ref: LaminB	HSA 18	LaminB	HSA 18	LaminB
Median	-170	-430	10	29
STABWN	220	277	12	14
ref: Dapi 3D	HSA 18	HSA 19	HSA 18	HSA 19
Median	-800	-1301	31	50
STABWN	413	533	12	15
ref: Dapi 2D	HSA 18	HSA 19	HSA 18	HSA 19
Median	-2479	-2587	66	68
STABWN	904	688	19	14

HFb "round" n=34	ADS: medians [in nm]		ADS: normalized medians [in %]	
ref: LaminB	HSA 18	LaminB	HSA 18	LaminB
Median	-200	143	11	28
STABWN	256	19	13	16
ref: Dapi 3D	HSA 18	LaminB	HSA 18	LaminB
Median	-900	-1425	31	53
STABWN	335	421	12	14
ref: Dapi 2D	HSA 18	LaminB	HSA 18	LaminB
Median	-2288	-2522	59	67
STABWN	886	757	18	14

Mann-Whitney Rank Sum test	ADS: medians		ADS: normalized medians	
ref: LaminB	HSA 19	DAPI	HSA 19	DAPI
	HSA 18	p=0.314	HSA 18	p=0.314
ref: Dapi 3D	HSA 19	DAPI	HSA 19	DAPI
	HSA 18	p<0.001	HSA 18	p<0.001
ref: Dapi 2D	HSA 19	DAPI	HSA 19	DAPI
	HSA 18	p=0.360	HSA 18	p=0.288

Mann-Whitney Rank Sum test	ADS: medians		ADS: normalized medians	
ref: LaminB	HSA 19	DAPI	HSA 19	DAPI
	HSA 18	p<0.001	HSA 18	p=0.859
ref: Dapi 3D	HSA 19	DAPI	HSA 19	DAPI
	HSA 18	p<0.001	HSA 18	p<0.001
ref: Dapi 2D	HSA 19	DAPI	HSA 19	DAPI
	HSA 18	p=0.104	HSA 18	p=0.115

Distribution of CTs 18 and 19 in Wolf's guenon artificially shaped fibroblasts:

Mann-Whitney Rank Sum test	ADS: medians	ADS: normalized medians
ref: LaminB	HSA 19	HSA 19
	HSA 18	HSA 18
	HSA 19	HSA 19
ref: Dapi 3D	HSA 18	HSA 18
	HSA 19	HSA 19
	HSA 19	HSA 19
ref: Dapi 2D	HSA 18	HSA 18
	HSA 19	HSA 19
	HSA 19	HSA 19

CWO "cigars" n=26	ADS: medians [in nm]	ADS: normalized medians [in %]
ref: LaminB	HSA 18	HSA 18
Median	-317	18
STABWN	99	7
ref: Dapi 3D	HSA 18	HSA 18
Median	-819	26
STABWN	283	8
ref: Dapi 2D	HSA 18	HSA 18
Median	-1693	47
STABWN	730	19

Mann-Whitney Rank Sum test	ADS: medians	ADS: normalized medians
ref: LaminB	HSA 19	HSA 19
	HSA 18	HSA 18
	HSA 19	HSA 19
ref: Dapi 3D	HSA 18	HSA 18
	HSA 19	HSA 19
	HSA 19	HSA 19
ref: Dapi 2D	HSA 18	HSA 18
	HSA 19	HSA 19
	HSA 19	HSA 19

CWO "round" n=35	ADS: medians [in nm]	ADS: normalized medians [in %]
ref: LaminB	HSA 18	HSA 18
Median	-241	17
STABWN	103	9
ref: Dapi 3D	HSA 18	HSA 18
Median	-836	26
STABWN	349	11
ref: Dapi 2D	HSA 18	HSA 18
Median	-2044	40
STABWN	896	14

Distribution of CTs 19 and 20 in bovine artificially shaped fibroblasts:

BFF "cigars" n=25	ADS: medians [in nm]			ADS: normalized medians [in %]				
ref: LaminB	BTA 19	BTA 20	LaminB	DAPI	BTA 19	BTA 20	LaminB	DAPI
Median	-320	-253	140	-120	22	16	9	8
STABWN	235	105	33	80	12	7	3	5
ref: Dapi 3D	BTA 19	BTA 20	LaminB	DAPI	BTA 19	BTA 20	LaminB	DAPI
Median	-1400	-1000	-216	-632	52	41	9	26
STABWN	295	271	99	75	10	10	4	2
ref: Dapi 2D	BTA 19	BTA 20	LaminB	DAPI	BTA 19	BTA 20	LaminB	DAPI
Median	-2240	-1924	-	0	67	52	-	0
STABWN	870	870	-	0	17	17	-	0

BFF "round" n=25	ADS: medians [in nm]			ADS: normalized medians [in %]				
ref: LaminB	BTA 19	BTA 20	LaminB	DAPI	BTA 19	BTA 20	LaminB	DAPI
Median	-582	-336	160	-200	31	14	7	9
STABWN	435	213	21	85	18	9	2	3
ref: Dapi 3D	BTA 19	BTA 20	LaminB	DAPI	BTA 19	BTA 20	LaminB	DAPI
Median	-1268	-973	-180	-747	48	31	7	24
STABWN	572	334	95	111	16	10	3	2
ref: Dapi 2D	BTA 19	BTA 20	LaminB	DAPI	BTA 19	BTA 20	LaminB	DAPI
Median	-2467	-1697	-	0	62	40	-	0
STABWN	664	600	-	206	13	15	-	5

Mann-Whitney Rank Sum test	ADS: medians		ADS: normalized medians	
ref: LaminB	BTA 19	BTA 20	BTA 19	BTA 20
	p=0.160	p=0.003	p=0.168	p=0.002
ref: Dapi 3D	BTA 19	BTA 20	BTA 19	BTA 20
	p<0.001	p<0.001	p<0.001	p<0.001
ref: Dapi 2D	BTA 19	BTA 20	BTA 19	BTA 20
	p=0.157	p<0.001	p=0.168	p<0.001

Mann-Whitney Rank Sum test	ADS: medians		ADS: normalized medians	
ref: LaminB	BTA 19	BTA 20	BTA 19	BTA 20
	p=0.002	p<0.001	p<0.001	p=0.006
ref: Dapi 3D	BTA 19	BTA 20	BTA 19	BTA 20
	p=0.003	p<0.001	p<0.001	p<0.001
ref: Dapi 2D	BTA 19	BTA 20	BTA 19	BTA 20
	p<0.001	p<0.001	p<0.001	p<0.001

7.1.3. Distribution of gene rich and gene poor chromosomes in bovine preimplantation embryos

Results of ADS measurements for bovine fibroblast control nuclei:

bovine cells	ADS: medians [in nm]				ADS: normalized medians [in %]			
fibroblasts	BTA 18	BTA 19	BTA 20	DAPI	BTA 18	BTA 19	BTA 20	DAPI
Median	-755	-969	-816	-506	43	56	49	29
STABWN	212	264	220	81	11	11	9	2
n	28	28	28	28	28	28	28	28
fibroblasts	BTA X	BTA 19	BTA 20	DAPI	BTA X	BTA 19	BTA 20	DAPI
Median	-570	-866	-573	-285	28	51	33	17
STABWN	398	291	166	319	8	16	10	15
n	28	28	28	28	28	28	28	28
lymphocytes	BTA 18	BTA 19	BTA 20	DAPI	BTA 18	BTA 19	BTA 20	DAPI
Median	-874	-1953	-884	-683	28	61	27	22
STABWN	455	379	242	77	13	11	6	0
n	25	25	25	25	25	25	25	25

Mann-Whitney Rank Sum test	ADS: medians				ADS: normalized medians			
fibroblasts		BTA 19	BTA 20	DAPI		BTA 19	BTA 20	DAPI
	BTA 18	p<0.001	p=0.088	p<0.001	BTA 18	p<0.001	p=0.046	p<0.001
	BTA 19		p<0.001	p<0.001	BTA 19		p=0.016	p<0.001
fibroblasts		BTA 19	BTA 20	DAPI		BTA 19	BTA 20	DAPI
	BTA X	p<0.001	p=0.005	p=0.007	BTA X	p<0.001	p=0.002	p=0.012
	BTA 19		p<0.001	p<0.001	BTA 19		p<0.001	p<0.001
lymphocytes		BTA 19	BTA 20	DAPI		BTA 19	BTA 20	DAPI
	BTA 18	p<0.001	p=0.684	p=0.040	BTA 18	p<0.001	p=0.684	p=0.133
	BTA 19		p<0.001	p<0.001	BTA 19		p<0.001	p<0.001
	BTA 20			p=0.001	BTA 20			p<0.001

Results of ADS measurements for bovine zygote nuclei:

bovine embryos	ADS: medians [in nm]			ADS: normalized medians [in %]			Mann-Whitney Rank Sum test	ADS: medians			ADS: normalized medians		
	BTA 19	BTA 20	DAPI	BTA 19	BTA 20	DAPI		BTA 19	BTA 20	DAPI	BTA 19	BTA 20	DAPI
zygotes	BTA 19	BTA 20	DAPI	BTA 19	BTA 20	DAPI		BTA 20	DAPI		BTA 20	DAPI	
Median	-858	-881	-771	22	25	20							
STABWN	929	688	255	23	18	2							
n	74	74	74	74	74	74							
e	45	45	45	45	45	45							
n/e	2	2	2	2	2	2							
early	BTA 19	BTA 20	DAPI	BTA 19	BTA 20	DAPI		BTA 20	DAPI		BTA 20	DAPI	
Median	-924	-946	-765	23	27	21							
STABWN	978	627	244	26	19	3							
n	23	23	23	23	23	23							
e	11	11	11	11	11	11							
n/e	2	2	2	2	2	2							
mid	BTA 19	BTA 20	DAPI	BTA 19	BTA 20	DAPI		BTA 20	DAPI		BTA 20	DAPI	
Median	-813	-861	-731	22	25	20							
STABWN	961	705	244	26	22	2							
n	30	30	30	30	30	30							
e	16	16	16	16	16	16							
n/e	2	2	2	2	2	2							
late	BTA 19	BTA 20	DAPI	BTA 19	BTA 20	DAPI		BTA 20	DAPI		BTA 20	DAPI	
Median	-865	-1076	-780	21	25	19							
STABWN	733	695	275	16	19	3							
n	25	25	25	25	25	25							
e	11	11	11	11	11	11							
n/e	2	2	2	2	2	2							

zygotes		BTA 20	DAPI		BTA 20	DAPI						
	BTA 19	p=0.340	p=0.662	BTA 19	p=0.322	p=0.285						
	BTA 20		p=0.035	BTA 20		p=0.002						
early		BTA 20	DAPI		BTA 20	DAPI						
	BTA 19	p=0.878	p=0.380	BTA 19	p=0.913	p=0.416						
	BTA 20		p=0.253	BTA 20		p=0.048						
mid		BTA 20	DAPI		BTA 20	DAPI						
	BTA 19	p=0.271	p=0.877	BTA 19	p=0.363	p=0.569						
	BTA 20		p=0.139	BTA 20		p=0.042						
late		BTA 20	DAPI		BTA 20	DAPI						
	BTA 19	p=0.207	p=0.684	BTA 19	p=0.211	p=0.497						
	BTA 20		p=0.018	BTA 20		p=0.019						

Results of ADS measurements for bovine embryos containing 4-8 nuclei:

bovine embryos	ADS: medians [in nm]			ADS: normalized medians [in %]			Mann-Whitney Rank Sum test	ADS: medians			ADS: normalized medians		
	BTA 19	BTA 20	DAPI	BTA 19	BTA 20	DAPI		BTA 19	BTA 20	DAPI	BTA 19	BTA 20	DAPI
4-8 cell stage	BTA 19	BTA 20	DAPI	BTA 19	BTA 20	DAPI		BTA 20	DAPI		BTA 20	DAPI	
Median	-892	-747	-1063	19	14	21							
STABWN	675	733	266	13	20	1							
n	45	45	45	45	45	45							
e	13	13	13	13	13	13							
n/e	5	5	5	5	5	5							
hollow	BTA 19	BTA 20	DAPI	BTA 19	BTA 20	DAPI		BTA 20	DAPI		BTA 20	DAPI	
Median	-823	-650	-1180	17	12	21							
STABWN	700	684	255	12	17	1							
n	31	31	31	31	31	31							
e	11	11	11	11	11	11							
n/e	5	5	5	5	5	5							
homogeneous	BTA 19	BTA 20	DAPI	BTA 19	BTA 20	DAPI		BTA 20	DAPI		BTA 20	DAPI	
Median	-1078	-1107	-943	24	25	21							
STABWN	573	722	272	12	22	1							
n	14	14	14	14	14	14							
e	6	6	6	6	6	6							
n/e	5	5	5	5	5	5							

4-8 cell stage		BTA 20	DAPI		BTA 20	DAPI						
	BTA 19	p=0.313	p=0.234	BTA 19	p=0.281	p=0.096						
	BTA 20		p=0.063	BTA 20		p=0.028						
hollow		BTA 20	DAPI		BTA 20	DAPI						
	BTA 19	p=0.229	p=0.041	BTA 19	p=0.166	p=0.004						
	BTA 20		p=0.006	BTA 20		p=0.001						
homogeneous		BTA 20	DAPI		BTA 20	DAPI						
	BTA 19	p=0.982	p=0.094	BTA 19	p=0.945	p=0.206						
	BTA 20		p=0.301	BTA 20		p=0.323						
hollow / homogeneous		BTA 19	BTA 20		BTA 19	BTA 20						
	BTA 19	p=0.017		BTA 19	p=0.017							
	BTA 20		p=0.161	BTA 20		p=0.161						

Results of ADS measurements for bovine embryos containing 10-16 nuclei:

bovine embryos	ADS: medians [in nm]			ADS: normalized medians [in %]			Mann-Whitney Rank Sum test	ADS: medians			ADS: normalized medians		
	BTA 19	BTA 20	DAPI	BTA 19	BTA 20	DAPI		BTA 20	DAPI	BTA 20	DAPI	BTA 20	DAPI
10-16 cell stage													
Median	-1811	-1155	-1281	32	20	23							
STABWN	968	2316	217	17	58	2							
n	56	56	56	56	56	56							
e	8	8	8	8	8	8							
n/e	12	12	12	12	12	12							
hollow													
Median	-1771	-1158	-1304	30	20	23							
STABWN	1014	509	143	18	9	1							
n	41	41	41	41	41	41							
e	6	6	6	6	6	6							
n/e	12	12	12	12	12	12							
homogeneous													
Median	-2109	-991	-1140	39	23	22							
STABWN	908	3807	234	16	97	2							
n	19	19	19	19	19	19							
e	2	2	2	2	2	2							
n/e	13	13	13	13	13	13							
hollow / homogeneous													
Median													
STABWN													
n													
e													
n/e													

Results of ADS measurements for bovine blastocyst nuclei:

bovine embryos	ADS: medians [in nm]			ADS: normalized medians [in %]			Mann-Whitney Rank Sum test	ADS: medians			ADS: normalized medians		
	BTA 19	BTA 20	DAPI	BTA 19	BTA 20	DAPI		BTA 20	DAPI	BTA 20	DAPI	BTA 20	DAPI
blastocysts													
Median	-1731	-803	-864	52	22	22							
STABWN	758	792	287	18	18	4							
n	107	107	107	107	107	107							
e	8	8	8	8	8	8							
n/e													
ICM													
Median	-1827	-865	-894	51	22	22							
STABWN	822	861	298	17	20	3							
n	42	42	42	42	42	42							
e	5	5	5	5	5	5							
n/e													
TE													
Median	-1680	-652	-803	51	21	22							
STABWN	640	724	280	17	15	4							
n	44	44	44	44	44	44							
e	6	6	6	6	6	6							
n/e	>50	>50	>50	>50	>50	>50							
ICM / TE													
Median													
STABWN													
n													
e													
n/e													

Statistical values for comparison of results between different stages:

Absolute medians (measured in reference to DAPI):

BTA 19	lymphocytes	zygotes	4-8 cell stage	10-16 cell stage	blastocysts
fibroblasts	p<0.001	p=0.254	p=0.347	p<0.001	p<0.001
lymphocytes		p<0.001	p<0.001	p=0.274	p=0.241
zygotes			p=0.495	p<0.001	p<0.001
4-8 cell stage				p<0.001	p<0.001
10-16 cell stage					p=0.754

BTA 20	lymphocytes	zygotes	4-8 cell stage	10-16 cell stage	blastocysts
fibroblasts	p=0.007	p=0.003	p=0.545	p<0.001	p=0.471
lymphocytes		p=0.708	p=0.364	p=0.026	p=0.261
zygotes			p=0.273	p=0.185	p=0.098
4-8 cell stage				p=0.061	p=0.834
10-16 cell stage					p=0.009

Normalized medians (measured in reference to DAPI):

BTA 19	lymphocytes	zygotes	4-8 cell stage	10-16 cell stage	blastocysts
fibroblasts	p=0.020	p<0.001	p<0.001	p<0.001	p=0.140
lymphocytes		p<0.001	p<0.001	p<0.001	p=0.002
zygotes			p=0.616	p<0.001	p<0.001
4-8 cell stage				p<0.001	p<0.001
10-16 cell stage					p<0.001

BTA 20	lymphocytes	zygotes	4-8 cell stage	10-16 cell stage	blastocysts
fibroblasts	p<0.001	p<0.001	p<0.001	p<0.001	p<0.001
lymphocytes		p=0.254	p=0.003	p<0.001	p=0.046
zygotes			p=0.014	p=0.026	p=0.312
4-8 cell stage				p=0.343	p=0.083
10-16 cell stage					p=0.237

7.1.4. Distribution of the transgene GOF and its harboring CT during nuclear transfer and early development

ADS results for bovine donor cells:

bovine transgenic donor cells	ADS: medians [in nm]					ADS: normalized medians [in %]				
	GOF	BTA 13	Dapi	α -sat.		GOF	BTA 13	Dapi	α -sat.	
ref.: DAPI	-1102	-700	-600	-900		59	39	28	43	
Median	382	304	85	290		17	13	13	13	
STABWN	29	29	29	29		29	29	29	29	
n										

ref.: DAPI	BTA 13 +GOF		BTA 13 -GOF		Dapi	
	GOF		-GOF			
Median	-719	-857	-600		59	34
STABWN	370	446	85		17	16
n	29	28	29		29	16

ref.: CT	BTA 13		Dapi		α -sat.	
	GOF					
Median	0	-50	-	-	0	16
STABWN	144	42	-	-	38	10
n	29	29	-	-	29	29

Mann-Whitney Rank Sum test	ADS: medians					ADS: normalized medians				
	GOF	BTA 13	Dapi	α -sat.		GOF	BTA 13	Dapi	α -sat.	
transgenic fibroblasts; ref.: DAPI	p=0.002	p=0.002	p=0.010	p<0.001	p=0.419	p<0.001	p<0.001	p<0.001	p<0.001	p=0.560
	α -sat.									

transgenic fibroblasts; ref.: DAPI	BTA 13 +GOF		BTA 13 -GOF		Dapi	
	GOF		-GOF			
transgenic fibroblasts; ref.: DAPI	p=0.005	p=0.039	p=0.002	p=0.030	p=0.352	p=0.005

transgenic fibroblasts; ref.: CT	BTA 13		Dapi		α -sat.	
	GOF					
transgenic fibroblasts; ref.: CT	p=0.414	p=0.738				

ADS results for the distribution of GOF and CT 13 in bovine NT embryos with nuclear border as reference:

bovine embryos	ADS: medians [in nm]			ADS: normalized medians [in %]		
	GOF	BTA 13	Dapi	GOF	BTA 13	Dapi
4 cell stages						
Median	-711	-868	-922	13	17	20
STABWN	881	571	234	20	12	2
n	33	33	33	33	33	33
e	17	17	17	17	17	17
n/e	5	5	5	5	5	5
16 cell stages						
Median	-760	-973	-824	20	26	20
STABWN	677	562	117	17	14	2
n	28	28	28	28	28	28
e	6	6	6	6	6	6
n/e	11	11	11	11	11	11
blastocysts						
Median	-698	-969	-763	23	30	22
STABWN	1237	737	191	28	20	3
n	65	65	65	64	64	64
e	4	4	4	4	4	4
n/e	>50	>50	>50	>50	>50	>50
ICM						
Median	-1185	-934	-909	30	22	24
STABWN	968	382	84	26	11	1
n	8	8	8	8	8	8
e	2	2	2	2	2	2
n/e	>50	>50	>50	>50	>50	>50
TE						
Median	-695	-1000	-752	18	28	21
STABWN	1316	812	199	43	22	3
n	51	51	51	51	51	51
e	3	3	3	3	3	3
n/e	>50	>50	>50	>50	>50	>50

Mann-Whitney Rank Sum test	ADS: medians			ADS: normalized medians		
	GOF	BTA 13	Dapi	GOF	BTA 13	Dapi
4 cell stages						
		BTA 13	Dapi		BTA 13	Dapi
	GOF	p=0.311	p=0.233	GOF	p=0.248	p=0.083
	BTA 13		p=0.644	BTA 13		p=0.449
16 cell stages						
		BTA 13	Dapi		BTA 13	Dapi
	GOF	p=0.225	p=0.676	GOF	p=0.222	p=0.902
	BTA 13		p=0.159	BTA 13		p=0.078
blastocysts						
		BTA 13	Dapi		BTA 13	Dapi
	GOF	p=0.339	p=0.800	GOF	p=0.453	p=0.954
	BTA 13		p=0.006	BTA 13		p=0.007
ICM						
		BTA 13	Dapi		BTA 13	Dapi
	GOF	p=1.000	p=0.645	GOF	p=0.878	p=0.878
	BTA 13		p=0.798	BTA 13		p=0.645
TE						
		BTA 13	Dapi		BTA 13	Dapi
	GOF	p=0.354	p=0.618	GOF	p=0.430	p=0.807
	BTA 13		p=0.028	BTA 13		p=0.030
ICM/TE						
	GOF	p=0.406		GOF	p=0.618	
	BTA 13		p=0.782	BTA 13		p=0.974

ADS results for the distribution of GOF, CT 13 harboring GOF and CT 13 without GOF in bovine NT embryos with nuclear border as reference:

bovine embryos	ADS: medians [in nm]				ADS: normalized medians [in %]			
	GOF	BTA 13 +GOF	BTA 13 -GOF	Dapi	GOF	BTA 13 +GOF	BTA 13 -GOF	Dapi
4 cell stages								
Median	-711	-671	-631	-922	13	15	14	20
STABWN	881	884	698	234	20	17	16	2
n	33	28	19	33	33	28	19	33
e	17	17	17	17	17	17	17	17
n/e	5	5	5	5	5	5	5	5
16 cell stages								
Median	-760	-836	-836	-824	20	20	20	20
STABWN	677	697	697	117	17	18	18	2
n	28	26	26	28	28	26	26	28
e	6	6	6	6	6	6	6	6
n/e	11	11	11	11	11	11	11	11
blastocysts								
Median	-698	-763	-733	-763	23	23	23	22
STABWN	1237	870	870	191	28	23	23	3
n	65	43	44	65	64	42	44	64
e	4	4	4	4	4	4	4	4
n/e	>50	>50	>50	>50	>50	>50	>50	>50

Mann-Whitney Rank Sum test	ADS: medians				ADS: normalized medians			
	GOF	BTA 13 +GOF	BTA 13 -GOF	Dapi	GOF	BTA 13 +GOF	BTA 13 -GOF	Dapi
4 cell stages								
		p=0.799	p=0.397	p=0.233				
					p=0.787	p=0.335	p=0.083	
16 cell stages								
blastocysts								

ADS results for the distribution of GOF in bovine NT embryos with CT 13 as reference:

bovine embryos	ADS: medians [in nm]		ADS: normalized medians [in %]		Mann-Whitney Rank Sum test	ADS: medians		ADS: normalized medians	
	GOF	BTA 13	GOF	BTA 13		GOF	BTA 13	GOF	BTA 13
4 cell stages	GOF	BTA 13	GOF	BTA 13	4 cell stages		BTA 13		BTA 13
Median	-129	-227	16	32		GOF	p=0.029	GOF	p=0.029
STABWN	197	109	60	10					
n	34	34	34	34					
e	17	17	17	17					
n/e	5	5	5	5					
16 cell stages	GOF	BTA 13	GOF	BTA 13		16 cell stages		BTA 13	
Median	-170	-235	24	32	GOF		p=0.737	GOF	p=0.909
STABWN	249	116	29	12					
n	28	28	28	28					
e	6	6	6	6					
n/e	11	11	11	11					
blastocysts	GOF	BTA 13	GOF	BTA 13	blastocysts			BTA 13	
Median	-696	-984	27	30		GOF	p=0.222	GOF	p=0.364
STABWN	1241	736	32	18					
n	64	64	64	64					
e	4	4	4	4					
n/e	>50	>50	>50	>50					
ICM	GOF	BTA 13	GOF	BTA 13		ICM		BTA 13	
Median	-1185	-1098	40	33	GOF		p=0.734	GOF	p=0.970
STABWN	934	870	26	18					
n	10	10	10	10					
e	2	2	2	2					
n/e	>50	>50	>50	>50					
TE	GOF	BTA 13	GOF	BTA 13	TE			BTA 13	
Median	-695	-969	75	82		GOF	p=0.252	GOF	p=0.365
STABWN	1278	780	33	19					
n	55	55	55	55					
e	3	3	3	3					
n/e	>50	>50	>50	>50					
ICM/TE		GOF		GOF		ICM/TE	GOF	p=0.279	GOF

Statistical comparison between all stages:

Absolute Medians in reference to DAPI:

GOF	4 cell stage	16 cell stage	blastocyst
BFF 451-1	p=0.020	p=0.036	p=0.102
4 cell stage		p=0.816	p=0.484
16 cell stage			p=0.565

Normalized medians in reference to DAPI:

GOF	4 cell stage	16 cell stage	blastocyst
BFF 451-1	p<0.001	p<0.001	p<0.001
4 cell stage		p=0.116	p=0.036
16 cell stage			p=0.678

BTA 13	4 cell stage	16 cell stage	blastocyst
BFF 451-1	p=0.327	p=0.083	p<0.001
4 cell stage		p=0.099	p=0.005
16 cell stage			p=0.025

BTA 13	4 cell stage	16 cell stage	blastocyst
BFF 451-1	p<0.001	p<0.001	p=0.001
4 cell stage		p=0.041	p=0.009
16 cell stage			p=0.497

BTA 13+GOF	4 cell stage	16 cell stage	blastocyst
BFF 451-1	p=0.658	p=0.749	p=0.066
4 cell stage		p=0.671	p=0.094
16 cell stage			p=0.213

BTA 13+GOF	4 cell stage	16 cell stage	blastocyst
BFF 451-1	p<0.001	p=0.002	p=0.083
4 cell stage		p=0.287	p=0.004
16 cell stage			p=0.059

BTA 13-	4 cell stage	16 cell stage	blastocyst
BFF 451-1	p=0.234	p=0.804	p=0.967
4 cell stage		p=0.179	p=0.899
16 cell stage			p=0.124

BTA 13-	4 cell stage	16 cell stage	blastocyst
BFF 451-1	p=0.004	p=0.023	p=0.007
4 cell stage		p=0.121	p=0.515
16 cell stage			p=0.359

Absolute Medians in reference to CT 13:

GOF	4 cell stage	16 cell stage	blastocyst
BFF 451-1	p<0.001	p=0.041	p<0.001
4 cell stage		p=0.290	p=0.652
16 cell stage			p=0.451

Normalized medians in reference to CT 13:

GOF	4 cell stage	16 cell stage	blastocyst
BFF 451-1	p=0.788	p=0.267	p=0.032
4 cell stage		p=0.134	p=0.018
16 cell stage			p=0.460

7.2. Material and technical equipment

7.2.1. Chemicals, enzymes and reagents

Chemicals

7—amino-actinomycin D (7-AAD)	Molecular Probes, Leiden NL
Acetic acid (100%)	Merck, Darmstadt
Agarose SEAKEM ME	Cambrex Bioscience, Rockland, ME, USA
Antifade-Medium (Vectashield)	Vector, Burlingame
β-Mercaptoethanol	Merck, Darmstadt
bicarbonate buffer (NaHCO ₃)	
Bovine Serum Albumin (BSA) for PBS solutions	Sigma-Aldrich, Deisenhofen
Bovine Serum Albumin (BSA) for SSC solutions	MP Biomedicals, Solon, OH, USA
CaCl ₂	Merck, Darmstadt
Cetus II buffer	Roche, Mannheim
Colcemide (10µg/ml)	Biochrom AG, Berlin
4',6-Diamino-2-phenylindole (DAPI)	Sigma-Aldrich, Deisenhofen
Dimethyl-sulfoxid (DMSO)	Sigma-Aldrich, Deisenhofen
Dextranulphate	Amersham Biosciences, Freiburg
EDTA (Titriplex III)	Merck, Darmstadt
Ethanol absolute (type 642, 510)	Merck, Darmstadt
Ethidium bromide	Sigma-Aldrich, Deisenhofen
Fetal calf serum (FCS)	Biochrom AG, Berlin
Ficoll-Paque PLUS	GE Healthcare, München
Formaldehyde (37%)	Sigma-Aldrich, Deisenhofen
Formamide	Merck, Darmstadt
Gel-loading-buffer (6x)	Sigma-Aldrich, Deisenhofen
Glacial acetic acid	Merck, Darmstadt

Glycine	
Glycerol	Merck, Darmstadt
HCl 1N	Merck, Darmstadt
Heparin	Braun, Melsungen
HEPES	Merck, Darmstadt
Immersionoil (Immersol 518)	Zeiss, Jena
Isopropanol	Merck, Darmstadt
KCl	Merck, Darmstadt
Methanol	Merck, Darmstadt
MgCl ₂	Merck, Darmstadt
NaCl	Merck, Darmstadt
NaOH	Merck, Darmstadt
Nick-translation buffer (10x)	Roche, Mannheim
Nitrogen (liquid)	Messer Griesheim GmbH, Krefeld
Paraformaldehyde	Merck, Darmstadt
Penicillin/Streptomycine	Biochrom AG, Berlin
PCR buffer (10x)	Perkin Elmer, Wellesley, USA
Phytohaemagglutinin (PHA-E)	Biochrom AG, Berlin
Poly-L-Lysine	Sigma-Aldrich, Deisenhofen
Sodiumchloride	Merck, Darmstadt
Sodium citrate dihydrate	Merck, Darmstadt
Solution 3	Roche, Mannheim
TO-PRO-3 iodide	Molecular Probes, Leiden NL
Tris-HCl 1M, pH 7.8	Sigma-Aldrich, Deisenhofen
Triton X-100	Sigma-Aldrich, Deisenhofen
Trolox	Sigma-Aldrich, Deisenhofen
Tween 20	Calbiochem, San Diego, CA, USA

Cell Culture Materials

Dulbeccos MEM (DMEM)	Gibco Invitrogen, Karlsruhe
Fetal calf serum (FCS)	Seromed Biochrom, Berlin
Penicillin/Streptomycin (10000 I.E./10000 µg/ml)	Seromed Biochrom, Berlin
RPMI 1640 media	Seromed Biochrom, Berlin
Meliseptol	B.Braun Biotech International, Melsungen
10xTrypsin/EDTA	Biochrom AG, Berlin

Enzymes

DNA Polymerase I (Kornberg Polymerase)	Roche, Mannheim
DNase I	Roche, Mannheim
Nuclease S1	Roche, Mannheim
Pepsin (10% in H ₂ O)	Sigma-Aldrich, Deisenhofen
Proteinase K	Roche, Mannheim
10xTrypsin/EDTA	Biochrom AG, Berlin
Taq-Polymerase	Invitrogen GmbH, Karlsruhe

Nucleotides & DNA

5-Bromo-2'-deoxyuridine	Sigma-Aldrich, Taufkirchen
6MW -primer	MWG-Biotech, Ebersberg
Aminoallyl-dUTP	Sigma-Aldrich, Taufkirchen
Biotin-16-dUTP	Roche, Mannheim
Biotin (succinimidyl ester)	Molecular Probes, Leiden NL
Bovine calf thymus DNA	Invitrogen GmbH, Karlsruhe
BrUTP	Sigma-Aldrich, Deisenhofen
C ₀ t-1 DNA (human)	Invitrogen GmbH, Karlsruhe
C ₀ t-1 DNA (mouse)	Invitrogen GmbH, Karlsruhe
Cy3 (succinimidyl ester)	Amersham Biosciences, Freiburg
Cy5 (succinimidyl ester)	Amersham Biosciences, Freiburg
dATP, dCTP, dGTP, dTTP	Amersham Biosciences, Freiburg
Digoxigenin-11-dUTP	Roche, Mannheim

Digoxigenin (succinimidyl ester)	Molecular Probes, Leiden NL
DNP-11-dUTP	NEN Life Science Products Boston, MA, USA
DNP (succinimidyl ester)	Molecular Probes, Leiden NL
FITC (succinimidyl ester)	Molecular Probes, Leiden NL
GenomiPhi DNA Amplification Kit	GE Healthcare,
Lamda/HindIII marker	Frementas, St. Leon-Rot
Mouse C ₀ t-1 DNA	Invitrogen GmbH, Karlsruhe
Salmon Sperm DNA	Invitrogen GmbH, Karlsruhe
TAMRA (succinimidyl ester)	Molecular Probes, Leiden NL
TexasRed (succinimidyl ester)	Molecular Probes, Leiden NL

Antibodies

Primary antibodies

Avidin-Alexa488 (1:200)	Molecular Probes, Leiden NL
Avidin-Cy5 (1:100)	Jackson Immunoresearch, Baltimore
Avidin-FITC (1:200)	Vector, Burlingame CA, USA
Goat-anti-Lamin B (1:50)	Santa Cruz Biotechnology Inc., USA
Goat-anti-DNP (1:250)	Sigma-Aldrich, Deisenhofen
Rabbit-anti-DNP (1:200)	Sigma-Aldrich, Deisenhofen
Mouse-anti-Dig (1:500)	Sigma-Aldrich, Deisenhofen
Mouse-anti-BrdU (1:200)	Roche, Mannheim
Mouse-anti-BrdU/IdU (1:1000)	Caltag, Hamburg
Mouse-anti-Digoxigenin	Sigma-Aldrich, Deisenhofen
Mouse-anti-Digoxigenin-Cy3 (1:100)	Jackson Immunoresearch, Baltimore
Mouse-anti-Digoxigenin-Cy5 (1:100)	Jackson Immunoresearch, Baltimore
Mouse-anti-Lamin A/C (1:50)	Santa Cruz Biotechnology Inc., USA
Mouse-anti-Ki67 (1:100)	Dako, Glostrup, Denmark
Rabbit-anti-Ki67 (1:100)	Roche, Mannheim
Rat-anti-BrdU/CldU (1:50)	abcam, Cambridge, UK
Sheep-anti-Dig-FITC (1:100)	Roche, Mannheim
Streptavidin-Cy3 (1:100)	Jackson Immunoresearch, Baltimore
Streptavidin-Cy5 (1:100)	Jackson Immunoresearch, Baltimore
Streptavidin-Alexa488 (1:100)	Molecular Probes, Leiden NL

Secondary antibodies

Donkey anti-mouse-Cy3 (1:200)	Jackson Immunoresearch, Baltimore
Donkey anti-goat-alexa488 (1:500)	Molecular Probes, Leiden NL
Goat anti-Avidin-Biotin (1:200)	Vector, Burlingame CA, USA
Goat anti-Avidin-FITC (1:100)	Vector, Burlingame CA, USA
Goat-anti-mouse-alexa488 h.c.a. (1:200)	Molecular Probes, Leiden NL
Goat anti-mouse-Biotin (1:200)	Vector, Burlingame CA, USA
Goat anti-mouse-Cy3 (1:100)	Jackson Immunoresearch, Baltimore
Goat anti-mouse-Cy5 (1:100)	Jackson Immunoresearch, Baltimore
Goat anti-mouse-AMCA (1:100)	Molecular Probes, Leiden NL
Goat anti-rabbit-alexa488 h.c.a. (1:200)	Molecular Probes, Leiden NL
Goat anti-rabbit-Biotin (1:100)	Biosource, Camarillo
Goat anti-rabbit-Cy3 (1:200)	Amersham Biosciences, Freiburg
Goat anti-rabbit-Cy3-Fab (1:200)	Jackson Immunoresearch, Baltimore
Goat anti-rabbit-FITC (1:200)	Biosource, Camarillo
Goat anti-rabbit-TexasRed (1:500)	Jackson Immunoresearch, Baltimore
Goat anti-Streptavidin-FITC (1:200)	Vector, Burlingame CA, USA
Goat anti-Streptavidin-Biotin (1:200)	Vector, Burlingame CA, USA
Rabbit anti-goat-FITC (1:200)	Sigma-Aldrich, Deisenhofen
Sheep anti-Digoxigenin-FITC (1:50)	Roche, Penzberg
Sheep anti-mouse-Cy3 (1:500)	Jackson Immunoresearch, Baltimore
Sheep anti-mouse-FITC (1:200)	Sigma-Aldrich, Deisenhofen

7.2.2. Media, buffers and solutions

Buffers/Solutions	Constituents	Annotations
4xSSCT	0.2% Tween 20 in 4xSSC	10µl of dATP, dCTP and dGTP (each 100mM) + 470µl H ₂ O bidest store at -20°C
ACG-Mix for label DOP-PCR	2mM dATP, dCTP and dGTP	10µl of dATP, dCTP and dGTP (each 100mM) + 470µl H ₂ O bidest store at -20°C
Agarose gel	1% agarose in TAE buffer	5g in 500ml, warm up in microwave, sway every 3 to 4 minutes. Until solution is clear, cool down before pouring:
Blocking solution	4% BSA in PBST 4% BSA in 4xSSCT	4g BSA → ad 100ml PBST 4g BSA → ad 100ml PBST
DAPI stock solution	2mg/ml dd H ₂ O	steril filtered
DNase I stock solution	1mg/ml DNase I (2000 U/mg)	2 U/µl DNaseI in 0,03 M NaCl and 50% Glycerin
DMEM full media	450ml DMEM 50ml FCS (10%) 5ml Penicillin/Streptomycine (100 I.E./100 µg/ml)	Constituents DMEM: 3,7g/l NaHCO ₃ 4,5g/l D-Glucose Stable Glutamine, Na-pyruvate
dNTP-Mix for DOP-PCR	je 2,5mM dATP, dGTP, dCTP, dTTP; H ₂ O bidest.	20µl dATP + 20µl dGTP + 20µl dCTP + 20µl dTTP + 720µl H ₂ O bidest.
dTTP for label DOP-PCR	1mM dTTP	10µl dTTP+990µl H ₂ O bidest store at -20°C
Ethanol (70%, 90% and 100%)	Ethanol (type 642)	70, 90 or 100ml EtOH→ad 100ml Using H ₂ O bidest
Fixative (for 2D metaphase preparation)	Methanol/acetic acid (3:1)	cool to -20°C before use
Fixative for post-fixation	1% Formaldehyde in PBS or 1% Paraformaldehyde in PBS	dilute Formaldehyde 37% about 1:40 in PBS or dilute 1g Paraformaldehyde in 100ml PBS and dissolve by heating and steaming; always freshly made!
Fixative (for 3D preserved cells)	3,7% Formaldehyde in PBS or 4% Paraformaldehyde in PBS	dilute Formaldehyde 37% 1:10 in PBS or dilute 4g Paraformaldehyde in 100ml PBS and dissolve by heating and steaming; always freshly made!
Formamide/2xSSC (storing and denaturation solution)	70% formamide in 2xSSC	50ml 20xSSC + 350ml formamide + 100ml H ₂ O bidest. adjust to pH 7.0 with 1M HCl, store at -20°C
Freezing medium	50% FCS 10% DMSO (appropriate medium)	50ml FCS + 10ml DMSO + 40ml appropriate medium
Glycerol (20%)	20% glycerol in 1xPBS	100ml glycerol + 400ml 1xPBS
HCl (0,1M)		50ml HCl (1M) + 450ml H ₂ O bidest.
HCl (0.05M)		25ml HCl (1M) + 475ml H ₂ O bidest.
Hybridization mastermix	20% Dextran sulphate in 2xSSC	Dissolve 8g Dextran sulphate in 40ml 2xSSC, vortex, filter using 0,45µm filter, aliquot, store at -20°C
KCl solution, hypotone (0.56%)	75mM KCl in H ₂ O bidest.	Dissolve 0,56g in 100ml H ₂ O bidest.
NaOH (1N)	1 N NaOH in H ₂ O	4g NaOH ad 100ml H ₂ O bidest.
Nick translation stop mix	0.1% Bromophenol Blue, 0.5% Dextran Blue, 0.1M NaCl, 20mM EDTA, 20mM Tris-HCl pH 7.5	40mg Bromophenol Blue + 200mg Dextran Blue + 800µl 5M NaCl + 1.6ml 0.5M EDTA + 800µl 1M Tris-HCl pH 7.5
PBS (pH 7,4)	140 mM NaCl 2.7 mM KCl 6.5 mM Na ₂ HPO ₄ 1.5 mM KH ₂ PO ₄	20xPBS: 160g NaCl + 4g KCl + 36g Na ₂ HPO ₄ * 2H ₂ O + 4.8g KH ₂ PO ₄ ; ad 1l H ₂ O bidest.; adjust pH to 7.4 (with 1M HCl); dilute to 1xPBS; autoclave for cell culture use; add 4g Na-Azide to 10l of 1xPBS (→0.04%) for laboratory

PBS (pH 7,4)	140 mM NaCl 2.7 mM KCl 6.5 mM Na ₂ HPO ₄ 1.5 mM KH ₂ PO ₄	20xPBS: 160g NaCl + 4g KCl + 36g Na ₂ HPO ₄ * 2H ₂ O + 4.8g KH ₂ PO ₄ ; ad 1l H ₂ O bidest.; adjust pH to 7.4 (with 1M HCl); dilute to 1xPBS; autoclave for cell culture use; add 4g Na-Azide to 10l of 1xPBS (→0.04%) for laboratory use;
PBST Pepsinization solution	0.02% Tween 20 in 1xPBS 0.005% pepsin in 0,01 M HCl	200µl Tween 20 in 1l PBS 50µl Pepsin (10%) + 10ml 0.1M HCl; ad 100ml H ₂ O bidest.; prewarm to 37°C before use
RPMI 1640 full media	450ml RPMI 1640 50ml FCS (10%) 5ml Penicillin/Streptomycin (100 I.E./100 µg/ml)	Constituents RPMI 1640: 25mM HEPES, 5,5g/l NaCl, 2,0g NaHCO ₃ , 5mg/l Phenolred, 0,5g/l N-Acetyl-L-alanyl-L-glutamin; prewarm to 37°C before use
SSC (Standard Saline Citrate) pH 7.0	150mM NaCl, 15mM Na-citrate dihydrate and H ₂ O	20xSSC: 175.3g NaCl + 88.2g Na-citrate → ad 1l H ₂ O bidest; adjust to pH 7.0 with NaOH; dilute to 4x, 2x oder 0.1SSC; add 4g Na-Azide to 10l SSC (→0.004%) for laboratory use;
Storing solution for fixed cells	50% formamide in 1xSSC	250ml formamide + 250ml 2xSSC; adjust pH to 7.4
TAE buffer (pH 8.0)	40mM Tris-Acetat, 1mM EDTA	50xTAE: 242g Tris + 8.6g EDTA + 57.1ml glacial acetic acid; ad 1l H ₂ O bidest. adjust pH to 7.0 with glacial acetic acid; dilute to 1xTAE;
TE buffer	10mM Tris; 1mM EDTA	20µl 1M Tris/HCl pH 7.8 + 4µl 0.5M EDTA + 1978µl H ₂ O bidest.

7.2.3. Equipment and instrumentation

Glass, plastic ware and other implements

Items	Company
4 well plates	Nunc GmbH & Co. KG, Langensfeld
6 well plates	Greiner bio-one, Frickenhausen
12 well plates	Greiner bio-one, Frickenhausen
60 well microtest plate	Greiner bio-one, Frickenhausen
Automatic pipette	Gilson, Inc., Middleton
Canula	Braun, Melsungen
Cell culture flasks (75cm ² , 25cm ²)	Falcon/Becton Dickinson, S. Jose Greiner bio-one, Frickenhausen
Coverslips 15x15mm	Menzel-Gläser
Coverslips 18x18mm	Marienfild, Lauda-Königshofen
Coverslips 20x20mm	Marienfild, Lauda-Königshofen
Coverslips 24x24mm	Marienfild, Lauda-Königshofen
Coverslips 24x60mm	Menzel-Gläser, Braunschweig
Coverslips, photoetched 23x23mm	Bellco Glass, Inc., Vineland
Culture dishes	Falcon/Becton Dickinson, S. Jose
Cuvettes	Schubert Medizinprodukte GmbH
Cryo vials 2ml	Greinerbio-one, Frickenhausen
Falcon tube (15ml; 50ml)	Falcon/Becton Dickinson, S. Jose
Fixogum	Marabu, Tamm
Forceps	Dumont, Montignez
Glass marker diamond	Kraus & Winter, Hamburg
Glass bottles 100ml, 250ml, 500ml	Schott, Stafford UK
Glass capillaries	Neolab, Heidelberg
Glass capillaries (for transferpettor)	Brand GmbH, Wertheim
Gloves Nitril	Ansell, Richmond Meditrade, Kiefersfelden
Gloves Latex	Ansell, Richmond Meditrade, Kiefersfelden

Isopropanol box	Nalgene, Rochester
Immersion oil	Zeiss, Jena
Immersion oil	Leica, Wetzlar
Injection needles (Sterican 0.90x40mm)	Rose GmbH, Trier
Injection needles (Sterican 0.45x25mm)	Braun Melsungen, Melsungen
Kim wipes	Kimberly-Clark
Leucosep (30ml)	Greiner bio-one, Frickenhausen
Liquid nitrogen tank with racks	Messer, Griesheim
Metal box with lid	Schubert Medizinprodukte GmbH
Mikro-Pipette tips	Greiner bio-one, Frickenhausen
Mikro-Pipettes (2µl, 10µl, 200µl, 1000µl)	Gilson, Inc., Middleton
Mineral oil	Sigma-Aldrich, Deisenhofen
Nail polish	Manhattan, Müller GmbH & Co. KG, Ulm- v Jungingen
Parafilm-M®	Pechiney Plastic Packaging, Inc., Neenah
PCR tubes 0.5 ml	Molecular probes, San Diego
Pipette tips for PCR	Molecular Bio Products
Plastic dishes, different sizes, round and square	Falcon/Becton, Greiner bio-one
Quadriperms (4 well plates)	VivaScience AG, Hannover
Rubber cement	Marabu, Tamm
Reaction tubes 1,5ml	Eppendorf, Hamburg
Safety pipette filler	Deutsch und Neumann
Slides	Langenbrinck, Teningen
Slide briefcases and boxes	Schubert Medizinprodukte GmbH
Slides with metalring	Brunel, Microscopes LTd., Chippenham, UK
µ-slides	Ibidi, Martinsried
Staining Jars acc. to Coplin Staining Jars acc. to Hellendahl	Hecht Assistant, Sondheim
Serological pipettes 2ml, 5ml, 10ml, 25ml	Sarstedt, Nümbrecht
Sterile plastic pipettes 1ml, 2ml, 5ml, 10ml, 25ml	Falcon/Becton Dickinson, S. Jose
Sterile tubes 50ml/15ml	Falcon/Becton Dickinson, S. Jose
Test tubes 1.5ml/2ml	Eppendorf, Hamburg
Transferpettor	Brand GmbH, Wertheim
Tweezers	Dumont, Montignez
Waste container	Biochrom, Berlin

Technical equipment

Items	Company
Autoclave (steam) "Varioklav"	H+P Labortechnik GmbH, Oberschleissheim
Bunsenburner with foot switch	WLD-Tec GmbH, Göttingen
Centrifuge/Biofuge pico	Kendro, Langenselbold
Centrifuge/Rotana/S	Hettich, Tuttlingen
CO ₂ incubator/BB6220 CU	Kendro, Langenselbold
CO ₂ incubator/Hera Cell	Kendro, Langenselbold
Drying stove	Heraeus, Hanau
Freezer (-80°C)/6485	GFL, Burgwedel
Freezers/various types (-20°C)	Privileg/Quelle, Fürth
Fridge (+4°C)	AEG, Frankfurt a. M.
Gel eletrophoresis chamber & equipment, various sizes	Bosch, Gerlingen-Schillerhöhe
Gel imager	Owl Scientific Inc., Portsmouth
Hot block/DB 2-D	MWG-Biotech, Ebersberg
Ice machine/AF-10	Techne, Cambridge
Incubator/Certomat HK	Scotsman, Bettolino di Pogliano
Laminar air flow cabinet	B.Braun Biotech international, Melsungen
Living cell chamber including temperature controller	Biohit Helsinki
Magnetic stirrer/IkaMag RH	Biotechs, Beck Rd. Butler
Magnetic stirrer/RCT basic	Ika Labortechnik, Staufen
Minicentrifuge	Ika Labortechnik, Staufen
pH-meter/pH538	National Labnet, Woodbridge
Reflex camera / Ricoh XR/KR 10-M	WTW, Weilheim
PS-speck microscope point-source-kit	Ricoh, Frankfurt a. M.
Sterile workbench "Herasafe"	Molecular probes, San Diego
Test tube rotator/34528	Heraeus, Hanau
Thermocycler/Techne Progene	Snijders, Tilburg
Vacuum centrifuge/BaVaco-M Mini-30	Techne, Cambridge
	Bachhofer, Reutlingen

Vortexing machine
 Water baths/1004
 Water baths/5
 Water baths/M12
 Weighing machine/ 2254

Ika Labortechnik, Staufen
 GFL, Burgwedel
 Julabo, Seelbach
 Lauda, Lauda-Königshofen
 Sartorius, Göttingen

Software

Programs	Company
Evaluation	
Absolute distance to surface (ADS)	Developed by J. von Hase, KIP Heidelberg
Enhanced absolute distance to surface (eADS)	Developed by T. Thormeyer, LMU Munich
Relative radial distribution (2D/3D-RRD)	Developed by J. von Hase, KIP Heidelberg
Imaging	
Adobe Photoshop® 7.0 – CS2	Adobe Systems, Inc., S. Jose
Amira version 4.0 – 4.1.1.	TGS Europe, Merignac Cedex
Cytovision	Applied Imaging International Ltd, Newcastle Upon Tyne
Image J (v1.29 – v.1.35k)	National Institute of Health, USA
Leica-TCS-SP2 software	Leica, Heidelberg
LSM 410 software version 3.95	Zeiss, Jena
Zeiss Image Browser	Zeiss, Jena
Other	
Adobe Acrobat version 5.0 – 7.0	Adobe Systems, Inc., S. Jose
Endnote version 6.0 - X	Thomson/ISI Researchsoft, Carlsbad
Microsoft Office 2004 for Mac	Microsoft, USA
Systat	

Optics

Microscopes and accessories	Specifications
Phase contrast microscope	Axiophot 25 C (Carl Zeiss, Jena)
Objectives	CP Achromat, 5x/0,12 CP Achromat, 10x/0,25 Ph1 LD Achrostigmat, 20x/0,3 Ph1 Achrostigmat, 40x/0,55 Ph2
Digital camera	Canon G5 (5 Mpixel resolution)
Fluorescence microscope	Axiophot 2 (Carl Zeiss, Jena)
objectives	Plan-Neofluar 16x/0,5 Fluor 40x/1,3 Oil, Ph 3 Plan- Neofluar 40x/1,3 Oil Plan-Apochromat 63x/1,4 Oil Plan-Neofluar 100x/1,3 Oil
dichroic filter sets	DAPI (BP 365; FT 395; LP 450-490) FITC (BP 450-490; FT 510; LP 515-565) Cy3 (BP 546; FT 580; LP 590) Cy5 (BP 575-625; FT 645; BP 660-710) Triple Filter (TBP400/495/570; FT410/505/585; TBP460/530/610)
Camera	Coolview CCD-Camera System

Leica Confocal Laser Scanning Microscope	SP 2 (Leica, Heidelberg)
objectives	Plan-Apochromat 63×/1,4 Oil
Laser	Argon: 458nm(5mW)/476nm(5mW)/488nm(20mW) / 496nm (5mW)/514nm(20mW) laser lines Helium/Neon 594 nm laser line, 2,5mW 633 nm laser line, 10mW DPSS: 561nm laser line, 10mW UV-laser: 405nm laser line, 50mW
Beam splitters	RSP 525: emission spectrum red RSP 650: emission spectrum infrared TD 488/568/647: for emission spectrum green and for green red combinations
Emission filters	AOBS: A cousto O ptical B eam S plitter
Software	TCS-SP5 software
Leica Confocal Laser Scanning Microscope	SP 5 (Leica, Heidelberg)
objectives	Plan-Apochromat 63×/1,4 Oil
Laser	Argon: 458nm(5mW)/476nm(5mW)/488nm(20mW) / 496nm (5mW)/514nm(20mW) laser lines Helium/Neon 594 nm laser line, 2,5mW 633 nm laser line, 10mW DPSS: 561nm laser line, 10mW UV-laser: 405nm laser line, 50mW
Beam splitters	RSP 525: emission spectrum red RSP 650: emission spectrum infrared TD 488/568/647: for emission spectrum green and for green red combinations
Emission filters	AOTF: A cousto O ptical T unable F ilter
Software	TCS-SP2 software
Software	LSM 410 software, Version 3.95

7.3. Manuscript: Similarity of chromosome arrangement is lost after two cell cycles in HeLa and normal diploid cells

List of authors: D.Koehler¹, J.Mattes^{2§}, J.Gao^{2§§}, B.Joffe¹, T.Cremer¹, R.Eils^{2,3}, I.Solovei¹

¹ Chair of Anthropology and Human Genetics, Department of Biology II, Ludwig-Maximilians-University, Grosshadernerstrasse 2, D-82152, Martinsried

² Theoretical Bioinformatics, German Cancer Research Center (DKFZ), Im Neuenheimer Feld 580, 69120 Heidelberg, Germany

³ Bioinformatics and Functional Genomics, Institute of Pharmacy and Molecular Biotechnology, University of Heidelberg, Im Neuenheimer Feld 364, 69120 Heidelberg, Germany

§ Current address: Software Competence Center Hagenberg GmbH, Softwarepark 21, A-4232 Hagenberg, Austria

§§ Current address: Stowers Institute for Medical Research, 1000 E50th street, Kansas City 64110, MO, USA

ABSTRACT

Chromosomes occupy non-random tissue-specific positions in the interphase nucleus that correlate with the chromosome size and gene richness; they can also have probabilistically preferred neighbors. Earlier studies reached opposite conclusions about the degree of the transmission through mitosis of chromosome arrangement present in a given cell. None of these studies, however, analyzed more than one cell cycle and used sufficiently rigorous measures for quantitatively assessing similarity of chromosome arrangement. We studied the arrangement of 6-7 chromosomes in clones of up to 32 cells (5 divisions). Nuclear positions of chromosomes were visualized using FISH and the similarity in chromosome arrangements between cells of a clone was quantified using 3 different measures employing landmark based registration. Both in HeLa and normal diploid cells the similarity in chromosome arrangement was lost after only two cell cycles, implying a low level of transmission through mitosis. In a discussion of factors affecting the degree of the transmission we partially reconcile the contradicting results of earlier studies.

INTRODUCTION

In the interphase nucleus, chromosomes occupy distinct regions¹⁻³ referred to as chromosome territories (CTs). Their structure and spatial arrangement (relative positions in a nucleus) are the structural basis of the functional landscape for nuclear processes such as transcription and transcriptional regulation^{4,5}. Recent studies demonstrated the importance of spatial interactions between numerous chromatin regions from different CTs⁶⁻¹¹. Spatial interactions raise the question of how chromatin regions from distant CTs establish transient contacts; alternatively, they require a constant cell type specific proximity of such regions^{12,13}.

Two types of ordered CT arrangement have been found. First, CTs can occupy more central or more peripheral nuclear positions depending on gene density and chromosome size (referred to as the global radial order)¹⁴⁻¹⁷. Second, cell type specific, probabilistically preferred proximities between individual CTs were observed (referred to as neighborhood order)¹⁸⁻²². An important question is when these two types of order are established and how they are maintained in cycling cells. Two different concepts were proposed based on

photobleaching experiments of fluorescent protein tagged chromatin in living cells^{23,24}. Both groups agree that major changes of chromosome neighborhood occur during prometaphase. According to Gerlich et al (2003)²³ a chromosome specific segregation timing mechanism restores the CT arrangement present in the mother nucleus in the two daughter nuclei. A computational model for inheritance of chromosomal positions through mitosis predicted that chromosome arrangement should be lost gradually over many cell cycles. By contrast, Walter et al (2003)²⁴ argued that prometaphase changes of chromosome neighborhoods cause major changes of CT arrangement from one cell cycle to the next.

This controversy has not been settled²⁵. A strong change in chromosome arrangement after mitosis was supported by a live cell study of labeled chromosomal loci in sister cells²⁶, while another group published live cell observations supporting faithful restoration of the CT arrangement after mitosis²⁷. Here, we present a novel combined experimental and computational approach that allowed a rigorous quantitative analysis of chromosomal pattern transmission over several cell generations. We show that the maternal CT arrangement is entirely lost after only two cell cycles, implying a low level of transmission through mitosis.

RESULTS

A new experimental and computational approach to study changes in chromosome arrangement.

The contradictions between the conclusions of the earlier studies on the degree of inheritance of chromosome arrangement seem to a great degree result from methodical reasons. Therefore a step crucial for our work was to design a methodical approach assuring robust conclusions. The two core elements of our approach are (1) the analysis of several successive mitoses and (2) direct quantitative estimation of differences between CT arrangements.

To study several successive mitoses we analyzed the degree of change in CT arrangements that accumulated in a number of successive divisions. In *in vivo* studies, recovery of fluorescence prevents tracking of chromosomal regions differentially visualized by partial histone-GFP/YFP photobleaching over more than one mitosis. The degree of pattern inheritance over several generations had therefore to be extrapolated from observations of one cell cycle^{23,24,27}. In contrast to these studies, we traced inheritance of CT arrangement over up to 5 cell cycles by observing descendants of a single mother cell in cell clones. Seeding cells on gridded coverslips and monitoring selected clones by repeated imaging, first, assured that for further studies we used only true clones and, second, allowed us to trace the genealogy of cells within clones (for details see the Material and Methods section). In the cells of studied clones, CTs 4, 7, and 21 were visualized using 3D-FISH and confocal microscopy (Fig. 1, Fig. S1).

The other core element of our approach was direct quantitative estimation of differences in CT arrangement between cells. While all earlier studies were based either on qualitative comparisons or on indirect measures (distance and angle measurements, signal intensity distributions) we developed a novel approach for direct quantification of difference between CT arrangements using landmark based registration²⁸⁻³⁰. A landmark is a point that may be identified in each cell. We used as landmarks the estimated geometrical centers of individual CTs and applied three variants of registration that allowed the CT arrangement different degrees of plasticity (Fig. 2): rigid registration is sensitive to any changes in size or shape, similarity registration corrects for size only, while elastic bending energy based registration²⁸ corrects for all kinds of global and local continuous deformations. Each variant of registration provides its own measure of dissimilarity between CT arrangements in two nuclei (Fig. 2, for details see the Material and Methods section). Since it remains unknown which changes in chromosome arrangement are reversible and which are not, using three measures, very different in this respect, assured robustness of our final conclusions.

CT arrangement patterns quickly diversify in growing clones.

Using the approach described above, we assessed the dissimilarity of chromosome arrangement accumulated in HeLa cells after 1 to 5 divisions of a mother cell, i.e. in 2 to approx. 32 cell clones. To exclude the influence of chromatin movements associated with mitosis, only clones in which all cells were in interphase were used for quantitative analysis. Such clones with 2, 4, 8, and even 16-cell clones could be found easily. We also analyzed several clones with 27-38 cells, again chosen because they satisfied the above condition. The dissimilarity of CT arrangement was calculated for each possible pair of cells within a given clone. The overall dissimilarity of CT arrangement for this clone was defined as the median of the dissimilarities for cell pairs (for details see Material and Methods).

The differences in CT arrangement between cells of a clone accumulated with size of clones and reached the level of unrelated cells in 4 or 8 cell clones, depending on the considered dissimilarity measure (Fig. 3a). The dissimilarity in CT arrangement for 8-cell clones and beyond was very much comparable (Fig. S2). For clones with 2, 4, and more than 8 (8+) cells (49, 32, and 37 clones, respectively), dependence of dissimilarity on the clone size was highly significant (Kruskal-Wallis test, $P < 0.001$ for all measures, followed by Dunn's test for pairwise comparisons at the cutoff confidence level of 0.05). Importantly, sisters (i.e., cells in 2-cell clones) were significantly more similar, than cells in the 4 cell clones. The difference between the 4-cell and 8+ clones was not statistically significant except for the bending energy based dissimilarity measure, which probably depended on the measure itself. Note that in 4 cell clones some cells are sisters (share the mother) while some are cousins and share only the grandmother (Fig. 1). The proportion of cousins to sister pairs is 2:1, and therefore the similarity for cousin cells may be estimated based on the values for 2 and 4 cell clones. The estimated dissimilarity for cousin cells reached the level of unrelated cells (Fig. 3b) for all measures. A further parameter characterizing clones of a given size is the distribution of dissimilarity values for pairs of cells within clones of this age. These distributions showed a clear difference between 2-, 4- and 8+ cell clones, whereas the 8+ clones was indistinguishable from unrelated cells (Fig. 3d).

Hence, our data suggested strongly that the dissimilarity level of unrelated cells is reached by cousin cells. To confirm this conclusion, we analyzed 28 4-cell clones for which the genealogy of cells was traced. Indeed, cousin cells did not reveal any higher degree of similarity in chromosome positioning than genealogically unrelated cells (Fig. 3c), whereas sister cells were significantly more similar than cousin cells (Wilcoxon Signed Rank test, $P < 0.001$).

A computer simulation based on chromosome arrangements in unrelated cells (one from each clone: 196 in total) showed that dissimilarities between sister cells corresponded to shift of all CTs in random direction at 2.4 - 3.5 μm (depending on the registration). Dissimilarities between cousins corresponded to a shift of 3.6 - 5.4 μm (data not shown). Though the difference between shifts characteristic of sisters and cousins does not look dramatic, an important border is crossed. In line with earlier observations^{14,31}, in unrelated cells the studied chromosomes follow size-dependent radial distribution, but move freely and independently along the respective orbits. They are situated at the average distance of ca. 4.4 μm from the nuclear center (3.3, 4.5 and 5.1 μm for HSA 21, 4 and 7, respectively; Fig. S3). Being shifted by 4-5 μm , homologous CTs can partially "swap" their neighbors, and our model shows that this should indeed happens very often. Taken together, our simulation data suggest that sisters shared *the same* chromosome arrangement in 50-70% of sister pairs, while cousins nearly always had *qualitatively different* arrangements.

Pattern transmission in normal diploid cells is similar to HeLa cells.

To exclude the possibility that the quick loss of similarity in CT arrangement in HeLa cells was related to the malignant nature of these cells, we performed the same analysis for normal diploid cells. Several normal cell types tested do not form compact clones when grown *in vitro*. Human mammary epithelial cells (HMEC) grow as compact clones until 4-cell stage; thereafter the clones start to move as a whole and fuse with other clones (Fig. S4). As in the case of HeLa cells, the similarity in 2 cell HMEC (sister cells) clones was significantly higher than in 4-cell clones (Fig. 3e; n=16 and n=24 clones, respectively; Mann-Whitney Rank Sum test, $P < 0.001$ for all measures). The estimated dissimilarity in CT arrangement for cousin cells was again at the same level as that between unrelated cells (Fig. 3f). In addition, we analyzed human normal diploid fibroblasts which have been intensively used in chromosome arrangement studies^{14,16,32-34}. Fibroblasts move up to a few hundreds of micrometers a day hampering the identification of sister cells after cell division. To compare chromosome arrangement in sister nuclei we generated binucleated fibroblasts by treatment of cells with Cytochalasin B, an inhibitor of cytoplasmic division (Fig. S5). In accordance with the above findings for HeLa and HMEC, the dissimilarity in CT arrangement for sister nuclei was clearly below the level of unrelated cells (Fig. 3g). Hence, normal diploid cells did not show a higher degree of inheritance of interphase CT arrangement than HeLa.

Interphase chromatin arrangement is modified by changes in nuclear shape, but remains stable otherwise.

The above findings indicate clearly that maternal chromosomal order was entirely lost after only two cell cycles. We went on to study, at which stage of the cell cycle the observed loss of chromosomal order took place (c.f. Walter et al. (2003); Thomson et al (2004)^{24,26}). To study chromosomal rearrangements in mid interphase we labeled chromatin in HeLa cells by replication labeling and studied *in vivo* 38 nuclei. In each nucleus, we traced 10-18 foci distributed throughout the whole volume of the nucleus for 5-12 hours during interphase using *in vivo* confocal microscopy followed by 3D reconstruction (Fig. S6). Dissimilarity between the initial and final arrangement of replication foci was then estimated for all possible combinations of 7 foci in the same way as it was done for 7 chromosomes of HeLa cells. Median of these values was used as the measure of dissimilarity between initial and final arrangements.

We tested several parameters that might affect rearrangement of foci: accumulated linear displacement of the nucleus along the substrate surface, change of the area of the nuclear projection to the substrate plane, change in the roundness of this projection, as well as the rate of change of these parameters per hour. In accordance with our own preliminary findings³⁵, the degree of rearrangement correlated with the change in the nuclear shape. Other parameters studied showed no effect on chromosome arrangement. Interestingly, rearrangement correlated equally well with mean deformation over all observation period and with maximal deformation observed within a single one-hour window over the same period (Table S1). This finding suggests that chromatin rearrangement was caused by quick strong single deformations, rather than by cumulative effect of small ones. Indeed, the most pronounced rearrangements were observed when two cells collided causing a high degree of nuclear deformation (Fig. 4). In 4 nuclei interphase rearrangement of replication foci resulted in dissimilarity comparable to the dissimilarity of CT positions in sister cells, and two of these nuclei came in a temporary contact with another nucleus.

In accordance with the reported low mobility of chromatin in interphase^{24,36}, only relatively small displacements of foci took place in the majority of cells. Median dissimilarity accumulated over interphase was 3 to 6 times smaller (depending on the registration), than the respective values for sister cells. The median displacement for replication foci over mid interphase was 0.97 μm , that is, 3 and 4 times less than in sister cells and unrelated cells, respectively. As revealed by our computer simulations, chromosomal patterns are mostly retained in interphase with this low dissimilarity level. We conclude that (1) overall changes in nuclear shape were the major cause of chromatin rearrangement in interphase and (2) that

pronounced chromosomal rearrangements only rarely occurred in interphase in our experiment.

DISCUSSION

To analyze the degree of preservation of CT arrangements during clonal growth through up to 5 cell divisions, we quantified the accumulating differences using 3 different measures. We found for both HeLa and normal diploid cells that the similarity in CT arrangements between cells of a clone was lost after two cell cycles. Major repositioning of chromatin regions during interphase occurred only in a small proportion of nuclei and was caused by strong changes in the shape of the nucleus. Below we discuss which phases of mitosis affect the degree of pattern transmission and compare our results with those of earlier publications.

Changes of chromosome neighborhood arrangements during prometaphase congression of chromosomes.

Gerlich et al (2003) formally described formation of the metaphase chromosome arrangement as projection of their interphase positions onto the plane defined by the corresponding metaphase plate. Although this assumption simplifies chromosome movements occurring in living cells – e.g., due to the asymmetry of spindle formation³⁷ and the effect of delayed biorientation³⁸ – this model is a useful tool for the analysis of changes in chromosomal neighborhood arrangements induced by congression. It is however important to take in account that spindle formation during early prometaphase³⁹ can be initiated in any direction³⁷. Later the spindle rotates and achieves its final orientation only with the onset of the metaphase^{40,41}. After completion of kinetochore attachment to the spindle, the spindle and the condensed chromosomes rotate together. Since the primary orientation of the spindle determines the plane onto which chromosomes will congress, it also determines which chromosomes will become neighbors in the metaphase plate.

For most of the possible primary orientations of the spindle, widely separated chromosomes (e.g., at the opposite poles of the forming spindle) congress to the same region of the metaphase plate (Fig. 5). An accurate transmission of the neighborhood pattern of prophase chromosomes to the ensuing metaphase plate is only possible if (1) nuclei are flat and (2) the spindle is initially oriented perpendicularly to the substratum (Fig. 5d). Such a primary spindle orientation is not common, e.g., it was only observed in 15% of HeLa prometaphase cells³⁷ (and our own observations). Even if sister cells have an identical CT arrangement, spindles of the next division are formed independently and will transform this arrangement differently (Fig. 5). For two HeLa cell cousin, the probability to have a similar CT neighborhood arrangement is only 0.023 ($0,15^2$). This explains convincingly why the similarity in chromosome arrangement is lost already by cousin cells. The CT arrangement of the founder cell of a clone should therefore be lost after two mitoses. This mechanism also conforms well to the observations by Walter and collaborators²⁴ (Fig. S7). It was suggested²³ that chromosome-specific difference in timing of chromatid separation restores the maternal arrangement in daughter cell nuclei nearly completely. This restoration effect was not observed in our experiments with both HeLa and normal diploid cells.

Preservation of chromosome order during cell cycle progression from the metaphase plate to the formation of sister nuclei.

The average dissimilarity between sisters remained statistically significantly below the level of unrelated cells and cousins. Yet, only in about 15% of sister nuclei CT neighborhood arrangements looked clearly similar at face value, while in 12-23% of sister cell pairs (depending on the registration method) the dissimilarity of neighborhood CT arrangements exceeded the respective median value for cousin cells. Previous studies suggested that dissimilarity between sisters mainly depends on G1^{24,26}. Metaphase plates and early anaphase plates are typically oriented vertically to the substratum, while at late anaphase-telophase plates re-align parallel to the surface. It was suggested^{31,42} that anaphase plates rotate without major deformation, thus transmitting the chromosome arrangement and size-dependent radial distribution from the metaphase to the interphase nuclei. On the other

hand, in line with our live cell observations, the similarity of CT arrangements between sister nuclei was lost in a sarcoma cell line because these nuclei attained different shapes during early G1²⁶. In contrast to sparse cultures we used for our experiments, in sub-confluent HeLa cultures we observed that after division cells were forced to move between the neighboring cells to establish contact with the substratum. These movements were accompanied by diverse major deformations of nuclei which likely strongly reduced the similarity in chromosome arrangement between sister cells.

Concluding remark.

In summary, our and other results imply that major changes of CT proximity patterns occur during prometaphase and early G1. Remarkably, changes of chromosome arrangements during prometaphase were first described one hundred years ago by Theodor Boveri in a study of the cleavage in the nematode *Parascaris equorum* (for review see⁴³). In some tissues, the final orientation of the spindle is inherently related to differentiation^{44,45} and determines the fate of daughter cells. The primary orientation of the spindle, however, has not been studied. Our data suggest that transmission of chromosome arrangement through mitosis cannot serve as effective epigenetic mechanism. When chromosomes take specific interphase positions depending on gene content^{15,33} or have preferred neighbors^{18,19,21,22}, special mechanisms should exist to establish these specific features in each cell individually and independently from the particular arrangement in the mother cell.

ACKNOWLEDGEMENTS

The authors thank J.Fieres for C++ codes for the first version of Bending Energy calculation program used in this project; J.Walter (Till Photonics, Munich) for helpful discussions; C.Fauth (Technical University of Munich) for MFISH analysis of the used HeLa cells, R.Hessing (University of Munich) for help with illustrations. RE received support by the EU (3DHumanGenome) and the HFSP. RE also acknowledges support on multi-dimensional imaging from Leica Microsystems CMS GmbH, Mannheim, Germany. TC was supported by DFG grant Cr59/20 and BMBF NGFN II-EP grant 0213377A.

METHODS

Cell lines and growth of clones. HeLa cells⁴⁶ (kindly donated by K.Sullivan, The Scripps Research Institute), human mammary epithelial cells (HMEC, kindly donated by T. D. Tilsty, University of California), and normal human diploid fibroblasts were routinely cultured in RPMI (HeLa) or DMEM (HMEC, fibroblasts) supplemented with 10% fetal calf serum. Cells were seeded sparsely on gridded coverslips (Bellco, USA) and after 5 h, phase contrast images of appropriate areas with single cells were recorded; afterwards cells were observed and imaged every 24 h to monitor the growth of clones. HeLa cells, that have a very low mobility, were allowed to grow for up to 6 days to pass up to 5 divisions (Fig. S1). We used for analysis 118 clones (2 cell: 49; 4 cell: 32; 8 cell: 19; 16 cell:11, one clone of 20 cells, 5 clones of 27-32 cells, and one 38 cell clone) and 78 single cells.

Clones of HMEC cells could be followed reliably only up to 4 cell clones: single epithelial cells have a low mobility, however, groups of 4 and more cells moves along the substrate and fuse with one another (Fig. S4). We used for analysis 40 HMEC clones (2 cell: 16; 4 cell: 24). Fibroblasts do not form clones and move along substrate for hundreds microns per day. To observe sister nuclei, binucleated cells were induced by incubation with cytochalasin B (5 µg/ml) for 9 h; cells were transferred to fresh medium for 5 h prior fixation (Fig. S5); 22 binucleated cells were used for analysis.

To grow 4-cell clones with completely traced genealogy, HeLa cells were seeded as described above, allowed to attach, and images of a number of appropriate view fields were recorded. Then cells were allowed to grow in live cell chamber as described²⁴. In one experiment cells were placed in the live cell chamber immediately after imaging their positions and clones were monitored starting from single cells. In another experiment cells were grown for 16 h in Petri dishes to allow them to pass the 1st mitosis and then placed in

the live cell chamber. After placing coverslips to the microscope stage, the initially selected and recorded view fields were found and imaged every 20 minutes for a period of 18 h that allowed cells to pass the second division. 28 clones with traced genealogy were used for analysis.

In vivo observations on interphase rearrangement of replication foci. The HeLa cell line used for clone study stably expresses H2B-GFP was also used for *in vivo* observations. Cells were scratch-replication-labeled with Cy3-dUTP⁴⁷, cultured for about 2 cell cycles to allow labeled chromatids to segregate, and then observed in live cell chamber under confocal microscope for a period of 5-12 hours. In each of the 8 experiments carried out, a field of view was selected at low magnification. Then 3 smaller view fields containing several nuclei with well-separated easily identifiable replication foci were chosen within this area and image stacks were collected with high magnification every hour, so that the chamber itself did not move during observations²⁴. These experimental conditions allowed cells to cycle normally: viability of cells was confirmed by the fact that in more than 60% of monitored regions of interest one or more cells underwent mitosis during observations time and cell divisions remained common at the end of the observations.

FISH and microscopy. Karyotype of the used HeLa cell line was examined by M-FISH⁴⁸ and three chromosomes not involved in any re-arrangements were chosen: diploid HSA 4 and 21 and triploid HSA 7 (Fig. S8). Tested cells were frozen and all experiments were then carried out with subcultures grown from this stock to avoid any further changes in the karyotype. Cocktail of chromosome paint probes labeled with different haptens (biotin, digoxigenin, and DNP for HSA 4, 7, and 21, respectively) was used for hybridization on all three cell types. Cells were fixed and 3D-FISH was performed as previously described⁴⁹. Briefly, cells were fixed in 4% paraformaldehyde in 1x PBS for 10min, permeabilized with 0.5% Triton-X100 for 20min, incubated in 20% glycerol for at least 1 h, repeatedly frozen in liquid nitrogen, and finally incubated in 0.1N HCl for 5 min. Prior hybridization, coverslips with fixed and pretreated cells were stored in 50% formamid/SSC at 4°C for about one week. Labeled paint probes were dissolved in a hybridization mix (50% formamide, 10% dextran sulfate, 1x SSC) together with Cot 1 DNA, applied to cells; DNA-probes and cellular DNA were denatured simultaneously on a hot block at 75°C for 3 min. Hybridization was performed for 2-3 days at 37°C in humid boxes. Post-hybridization washes were performed with 2xSSC at 37°C and 0.1xSSC at 60°C. Digoxigenin was detected with mouse-anti-dig (Sigma) and Cy3-conjugated sheep-anti-mouse antibodies (Jackson ImmunoResearch Laboratories); biotin was detected with Streptavidin-Cy5 (Vector Laboratories); DNP was detected with rabbit-anti-DNP (Sigma) and goat-anti-rabbit conjugated to Alexa488 (Invitrogen). Nuclei were counterstained with DAPI (Sigma) and mounted in Vectashield antifade (Vector Laboratories). After FISH, clones recorded during growth were re-found based on their position on the gridded coverslips and series of light optical sections through whole nuclei with voxel size of 100x100x300 nm (X,Y,Z) were collected using a Leica TCS SP1 confocal microscope.

Data evaluation. Chromosome territories (CTs) and replication foci were segmented using Amira 2.3 TGS software. Tracing the positions of replication foci was carried out manually: 3D reconstructions corresponding to 3-4 successive time points were observed together, which allowed step-wise reconstruction of the trajectories (Fig. S6) For further analysis, surfaces obtained from Amira reconstructions were exported as inventor (.iv) files, and the coordinates of the centers of volume of CTs were calculated using a program (GAQ) developed in-house. Dissimilarity between CT configurations was calculated based on geometrical centers of signals. Rigid registration was implemented according to Dryden and Mardia (1998)²⁹; similarity registration was performed using the same program after size normalization; in both cases reflection was allowed. Bending energy registration²⁸ was done using the program described earlier³⁰. For size independence, bending energy was used after normalization of the size of point configurations. The smaller of the two reciprocal bending energy values was used as dissimilarity measure to exclude the effect of rare very

high values. Since homologous chromosomes could not be distinguished in our data, for all 3 registration variants all possible pairwise associations of homologous chromosomes from 2 cells were tested and the minimal dissimilarity value found was used as respective dissimilarity measure. Calculation of intra- and cross-clone dissimilarities was performed using a program (Nuclear Nightingale) developed in-house. Our data evaluation software is available on request.

Statistical analysis. The same kind of statistical data evaluation was performed for all 3 dissimilarity measures. Because of the strong asymmetry of the distribution of dissimilarity in the case of bending energy based measure, each clone was characterized by clone median, i.e. the median dissimilarity for all possible pairs of cells in this clone. These medians were used to compare clones of different size (stages). The distributions of medians remained asymmetric for clones of smaller size. Therefore all comparisons were made using non-parametric tests (as implemented in SigmaStat software, Systat Software incorporated). Kruskal-Wallis one-way ANOVA on Ranks followed by Dunn's test for pairwise comparisons at the cutoff confidence level of 0.05 was used to compare stages; Wilcoxon Signed Rank test was applied to compare sisters and cousins in clones with traced genealogy. Calculation of dissimilarity for unrelated cells was performed using cross-clone dissimilarity values and bootstrap on clones using the Nuclear Nightingale program (for details see Fig. S9). The distributions of individual dissimilarity values (Fig. 3d) were processed ("smoothed") using naive estimator with bin size 2 (rigid and bending energy based registration) and 0.2 (similarity registration), respectively. Since estimation of cousin dissimilarities from data on 2 and 4 cells clones is only possible with means, all values shown in Figure 3b,f were recalculated for this purpose based on clone and stage means, as described above for clone and stage medians.

REFERENCES

1. □ Cremer, T. & Cremer, C. Chromosome territories, nuclear architecture and gene regulation in mammalian cells. *Nat Rev Genet* **2**, 292-301 (2001).
2. □ Misteli, T. Spatial positioning; a new dimension in genome function. *Cell* **119**, 153-6 (2004).
3. □ Misteli, T. Beyond the sequence: cellular organization of genome function. *Cell* **128**, 787-800 (2007).
4. □ Chakalova, L., Debrand, E., Mitchell, J.A., Osborne, C.S. & Fraser, P. Replication and transcription: shaping the landscape of the genome. *Nat Rev Genet* **6**, 669-77 (2005).
5. □ Cremer, T. et al. Chromosome territories--a functional nuclear landscape. *Curr Opin Cell Biol* **18**, 307-16 (2006).
6. □ Bacher, C.P. et al. Transient colocalization of X-inactivation centres accompanies the initiation of X inactivation. *Nat Cell Biol* **8**, 293-9 (2006).
7. □ Chuang, C.H. et al. Long-range directional movement of an interphase chromosome site. *Curr Biol* **16**, 825-31 (2006).
8. □ Lanctôt, C., Cheutin, T., Cremer, M., Cavalli, G. & Cremer, T. Dynamic genome architecture in the nuclear space: regulation of gene expression in three dimensions. *Nat Rev Genet* **8**, 104-115 (2007).
9. □ Ling, J.Q. et al. CTCF mediates interchromosomal colocalization between Igf2/H19 and Wsb1/Nf1. *Science* **312**, 269-72 (2006).
10. Lomvardas, S. et al. Interchromosomal interactions and olfactory receptor choice. *Cell* **126**, 403-13 (2006).
11. Spilianakis, C.G., Lalioti, M.D., Town, T., Lee, G.R. & Flavell, R.A. Interchromosomal associations between alternatively expressed loci. *Nature* **435**, 637-45 (2005).
12. Fraser, P. & Bickmore, W. Nuclear organization of the genome and the potential for gene regulation. *Nature* **447**, 413-7 (2007).
13. Teller, K., Solovei, I., Buiting, K., Horsthemke, B. & Cremer, T. Maintenance of imprinting and nuclear architecture in cycling cells. *Proc Natl Acad Sci U S A* **in press**(2007).
14. Bolzer, A. et al. Three-Dimensional Maps of All Chromosomes in Human Male Fibroblast Nuclei and Prometaphase Rosettes. *PLoS Biol* **3**, e157 (2005).
15. Boyle, S. et al. The spatial organization of human chromosomes within the nuclei of normal and emerlin-mutant cells. *Hum Mol Genet* **10**, 211-219 (2001).

16. Croft, J.A. et al. Differences in the localization and morphology of chromosomes in the human nucleus. *J Cell Biol* **145**, 1119-31 (1999).
17. Neusser, M., Schubel, V., Koch, A., Cremer, T. & Muller, S. Evolutionarily conserved, cell type and species-specific higher order chromatin arrangements in interphase nuclei of primates. *Chromosoma* **116**, 307-320 (2007).
18. Cornforth, M.N. et al. Chromosomes are predominantly located randomly with respect to each other in interphase human cells. *J Cell Biol* **159**(2002).
19. Meaburn, K.J. & Misteli, T. Cell biology: chromosome territories. *Nature* **445**, 379-781 (2007).
20. Parada, L.A., McQueen, P.G. & Misteli, T. Tissue-specific spatial organization of genomes. *Genome Biol* **5**, R44 (2004).
21. Parada, L.A., Roix, J.J. & Misteli, T. An uncertainty principle in chromosome positioning. *Trends Cell Biol* **13**, 393-6 (2003).
22. Roix, J.J., McQueen, P.G., Munson, P.J., Parada, L.A. & Misteli, T. Spatial proximity of translocation-prone gene loci in human lymphomas. *Nat Genet* **34**, 287-91 (2003).
23. Gerlich, D. et al. Global chromosome positions are transmitted through mitosis in mammalian cells. *Cell* **112**, 751-764 (2003).
24. Walter, J., Schermelleh, L., Cremer, M., Tashiro, S. & Cremer, T. Chromosome order in HeLa cells changes during mitosis and early G1, but is stably maintained during subsequent interphase stages. *J Cell Biol* **160**, 685-697 (2003).
25. Williams, R.R. & Fisher, A.G. Chromosomes, positions please! *Nat Cell Biol* **5**, 388-90 (2003).
26. Thomson, I., Gilchrist, S., Bickmore, W.A. & Chubb, J.R. The radial positioning of chromatin is not inherited through mitosis but is established de novo in early G1. *Curr Biol* **14**, 166-72 (2004).
27. Essers, J. et al. Dynamics of relative chromosome position during the cell cycle. *Mol Biol Cell* **16**, 769-75 (2005).
28. Bookstein, F.L. *Morphometric tools for landmark data. Geometry and biology.*, (Cambridge University Press, Cambridge, 1991).
29. Dryden, I. & Mardia, K.V. *Statistical shape analysis.*, (Wiley, London, 1998).
30. Mattes, J., Fieres, J. & Eils, R. A Shape Adapted Motion Model for Non-Rigid Registration. in *SPIE Medical Imaging* Vol. SPIE 4684 518-527 (San Diego, 2002).
31. Habermann, F.A. et al. Arrangements of macro- and microchromosomes in chicken cells. *Chromosome Res* **9**, 569-84 (2001).
32. Allison, D.C. & Nestor, A.L. Evidence for a relatively random array of human chromosomes on the mitotic ring. *J Cell Biol* **145**, 1-14 (1999).
33. Cremer, M. et al. Non-random radial higher-order chromatin arrangements in nuclei of diploid human cells. *Chromosome Res* **9**, 541-67 (2001).
34. Nagele, R.G., Freeman, T., McMorro, L. & Lee, H.Y. Precise spatial positioning of chromosomes during prometaphase: evidence for chromosomal order. *Science* **270**, 1831-5 (1995).
35. Yang, S. et al. Non-rigid registration of 3D multi-channel microscopy images of cell nuclei. in *Proc. 9th Internat. Conf. on Medical Image Computing and Computer-Assisted Intervention (MICCAI'06)* Vol. Lecture Notes in Computer Science 4190 (eds Larsen, R., Nielsen, L. & Sporring, J.) 907-914 (Springer-Verlag Berlin Heidelberg, Copenhagen, 2006).
36. Gasser, S.M. Visualizing chromatin dynamics in interphase nuclei. *Science* **296**, 1412-6 (2002).
37. Chaly, N. & Brown, D.L. The prometaphase configuration and chromosome order in early mitosis. *J Cell Sci* **91** (Pt 3), 325-35 (1988).
38. Kapoor, T.M. et al. Chromosomes can congress to the metaphase plate before biorientation. *Science* **311**, 388-91 (2006).
39. Khodjakov, A., Copenagle, L., Gordon, M.B., Compton, D.A. & Kapoor, T.M. Minus-end capture of preformed kinetochore fibers contributes to spindle morphogenesis. *J Cell Biol* **160**, 671-83 (2003).
40. Haydar, T.F., Ang, E., Jr. & Rakic, P. Mitotic spindle rotation and mode of cell division in the developing telencephalon. *Proc Natl Acad Sci U S A* **100**, 2890-5 (2003).
41. O'Connell, C.B. & Wang, Y.L. Mammalian spindle orientation and position respond to changes in cell shape in a dynein-dependent fashion. *Mol Biol Cell* **11**, 1765-74 (2000).
42. Solovei, I. et al. Differences in centromere positioning of cycling and postmitotic human cell types. *Chromosoma* **112**, 410-423 (2004).
43. Cremer, T. & Cremer, C. Rise, fall and resurrection of chromosome territories: a historical perspective. Part I. The rise of chromosome territories. *Eur J Histochem* **50**, 161-76 (2006).
44. Lechler, T. & Fuchs, E. Asymmetric cell divisions promote stratification and differentiation of mammalian skin. *Nature* **437**, 275-80 (2005).
45. Lee, C.Y., Robinson, K.J. & Doe, C.Q. Lgl, Pins and aPKC regulate neuroblast self-renewal versus differentiation. *Nature* **439**, 594-8 (2006).

46. Kanda, T., Sullivan, K.F. & Wahl, G.M. Histone-GFP fusion protein enables sensitive analysis of chromosome dynamics in living mammalian cells. *Curr Biol* **8**, 377-85. (1998).
47. Schermelleh, L. In vivo DNA replication labeling. in *Cell Biology Handbook: A Laboratory Manual, 3rd Edition*, Vol. 1 (ed. Celis, J.) 301-303 (Elsevier Academic Press, Amsterdam, 2006).
48. Saracoglu, K. et al. New concepts to improve resolution and sensitivity of molecular cytogenetic diagnostics by multicolor fluorescence in situ hybridization. *Cytometry* **44**, 7-15 (2001).
49. Solovej, I. et al. FISH on three-dimensionally preserved nuclei. in *FISH, A Practical Approach*, Vol. 260 (ed. Beatty B., S.M., J. Squire) 119-157 (Oxford University Press, Oxford, 2002).

FIGURES

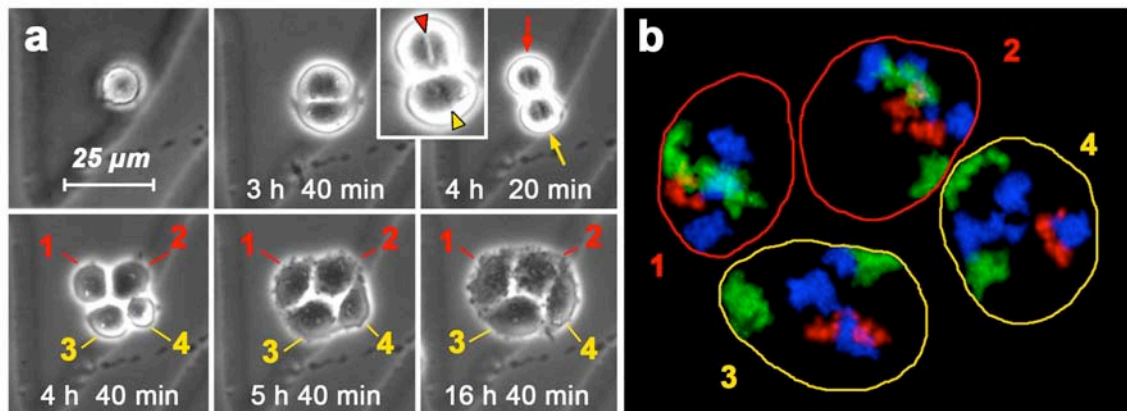
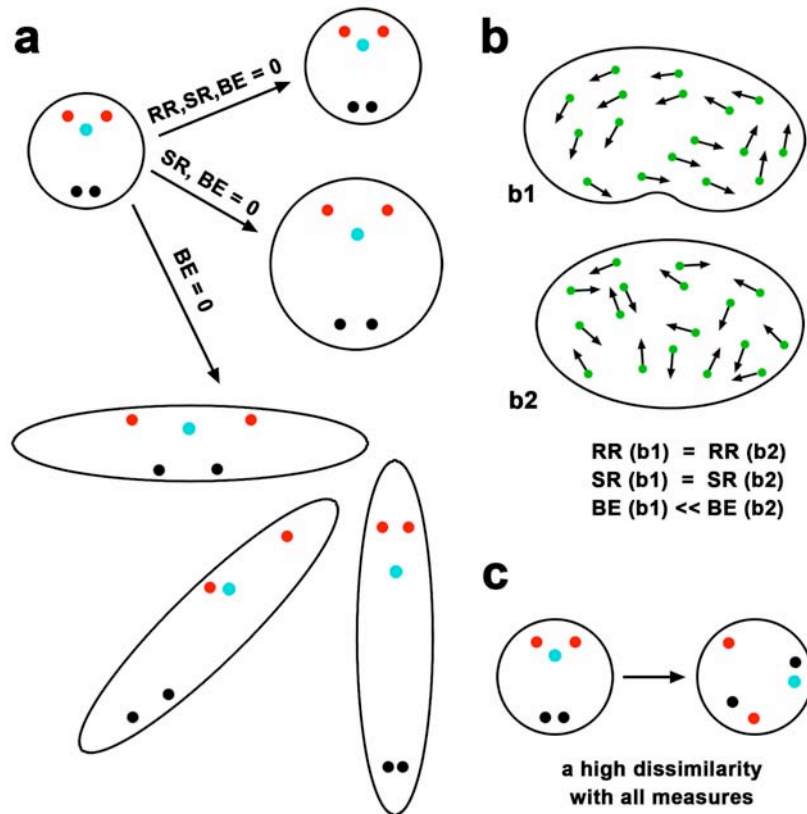


Figure 1. *In vivo* tracing of clone growth, genealogy of cells (a) and results of FISH on the same clone (b).

a, HeLa cells were seeded on gridded coverslip and the first image was taken 1 h after seeding; positions of imaged cells were recorded and cells were allowed to grow for 16 h. Then coverslips were placed in an *in vivo* cell chamber mounted on the microscope and images were taken every 20 min. The cell shown in the first image divided and formed a 2-cell clone. At the time point 4.00 h (insert) both sister cells synchronously formed metaphases. Metaphase planes in two cells are marked by red and yellow arrowheads and descendants of each cell are marked in images made at later time points with red and yellow, respectively. After the end of mitosis, relative positions of cells in the 4-cell clone remained constant (typical for HeLa). **b**, Cells were fixed 18 h after placing in live chamber and 3D-FISH with paints for chromosomes 4 (green), 7 (blue), and 21 (red) was performed. Clone was re-found and cells were identified based on their relative positions.



RR - rigid registration, SR - similarity registration, BE - Bending Energy

Figure 2. Comparison of three different methods for estimating dissimilarity of landmark patterns

a, Differences between landmark configurations that have a dissimilarity value of zero, i.e. no change of pattern: configuration shifts as a whole (all three measures); proportional change in size (RR, rigid registration; SR, similarity registration); proportional stretching/squeezing in any direction or directions (BE, elastic registration using Bending Energy).

b, The effect of coordination in displacements between individual landmark. In b1 and b2, all landmark have the same positions and shift with the same distance (arrows); the directions of shifts are coordinated (b1) or not coordinated (b2). RR and SR do not take coordination in account and assign to transformations shown in b1 and b2 the same dissimilarity value. BE strongly depends on coordination, it assigns a much smaller dissimilarity to b1 than to b2.

c, When directions of displacements are not coordinated and the displacement lengths are considerably large, landmarks are shuffled: displacement of a landmark carries no information about the displacement of the neighboring landmarks. In this case all three methods produce a high dissimilarity value.

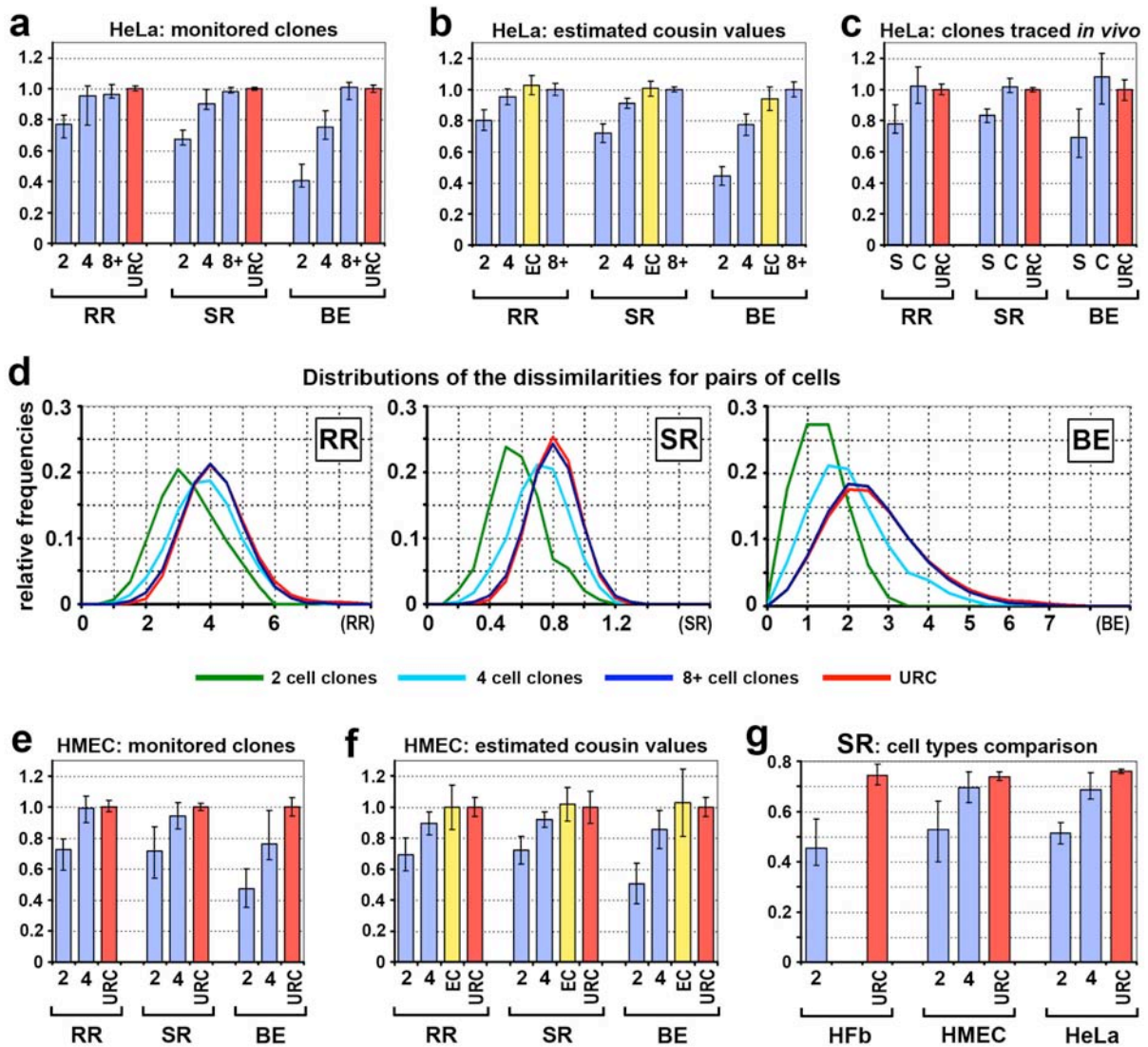


Figure 3. Dissimilarities between cells in clones of different size (age) in comparison to unrelated cells (URC)

a-d, HeLa cell clones. **a**, Dissimilarities between cells in 2-, 4-cell, and 8+ clones ($n=49$, 32 , 37 , respectively; see Material and Methods for more details). Values for 8+ clones reach the dissimilarity of URC with all measures. **b**, Dissimilarity between cousins estimated from clone data: cousins reach the 8+/URC level. **c**, Dissimilarities between sisters and cousins in 4-cell clones ($n=28$) with traced genealogy. The cousin values reach the URC level. **d**, Distributions of dissimilarities for individual pairs of cells. The distribution for 8+ clones is almost identical to that for URC. RR: rigid registration; SR: similarity registration; BE: elastic registration using Bending Energy. **e,f**, HMEC clones. Dissimilarities between HMEC in 2- and 4-cell clones (**e**) and estimated cousin dissimilarities (**f**). Note that data for HMEC are similar to HeLa data (compare to **a,b**). **g**, Comparison of HfB, HMEC and HeLa cells. Dissimilarity values estimated by similarity registration (SR) are shown because only they may be compared directly. Note the same trend and similar values for HeLa and normal cells. **S**, sister cells; **C**, cousin cells; **2, 4, 8+**, clones with 2, 4, and 8 or more cells; **EC** estimated cousin dissimilarity. **a, b, e, g** show stage medians. **c** and **f** show stage means. Error bars show 95% confidence intervals. For comparison, data on **a-c, e, f** are scaled so that dissimilarity for URC (**a,c,e**) and for 8+ (**b,f**) equals 1 for all measures.

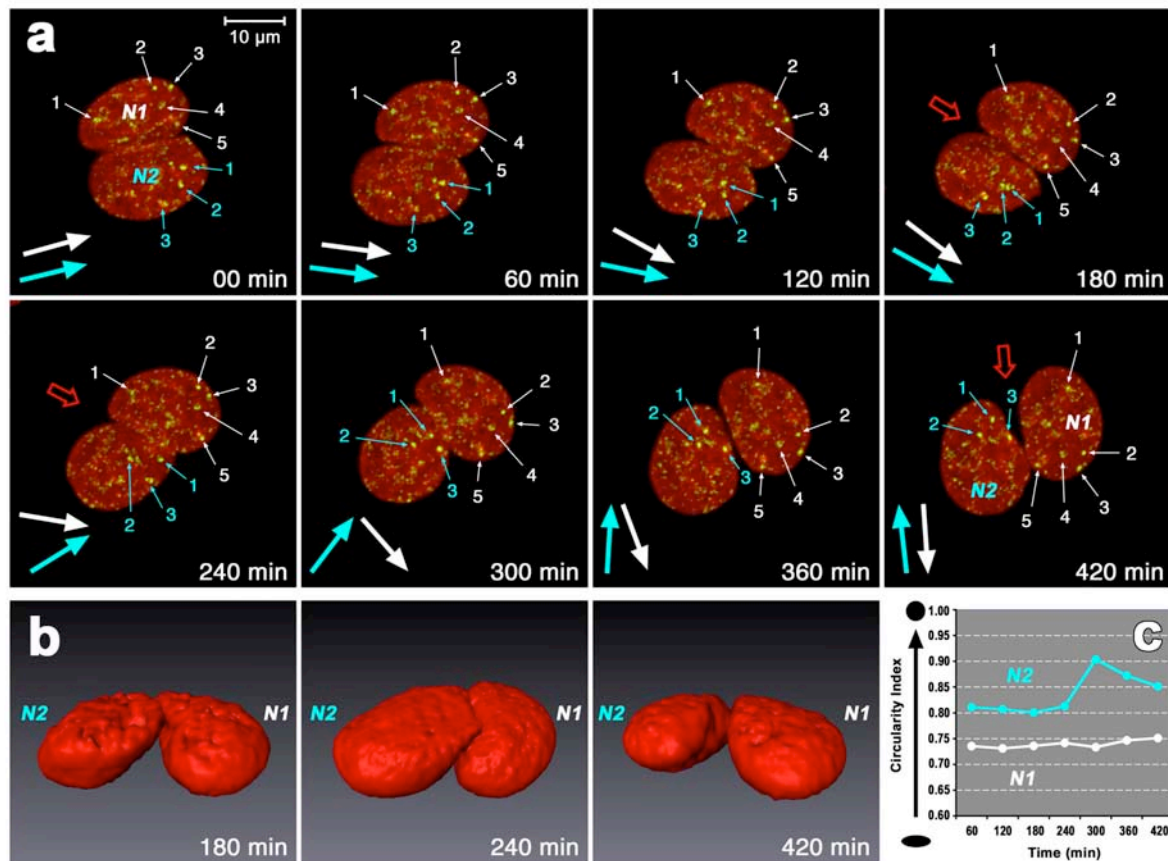


Figure 4. Shuffling of interphase positions of replication foci due to “collision” of two nuclei *in vivo*

a, Maximum intensity projections of confocal image stacks of two HeLa cell nuclei with H2B-GFP (red) and replication labeled chromatin foci (green). Image stacks were taken every 60 min for 7 h. White and blue arrows show long axes of the projections of nuclei N1 and N2, respectively. **b**, Amira based reconstructions for 3 time points, view direction as shown by red arrows in projections of the respective time points. **c**, Change of the circularity index of the projections of the same nuclei. Approx. 200 min after start of observation nucleus N2 changed the direction of its movement and a portion of the nucleus started to move over nucleus N1 (**b**). Collision was accompanied by pronounced change in the shape of nucleus N2 (**c**). Collision lasted over approx. 90 min. During this time period, orientation of the nuclei with respect to each other changed by 180°. Tracking foci in the nucleus N2 before and after the collision was readily done, but only 3 large foci could be tracked through the collision phase, since displacements of foci between consecutive time points were too large and not concerted. In contrast, the shape of nucleus N1 did not change dramatically and 13 positions of 13 foci were tracked over the observation period (five of them are marked by numbers 1-5).

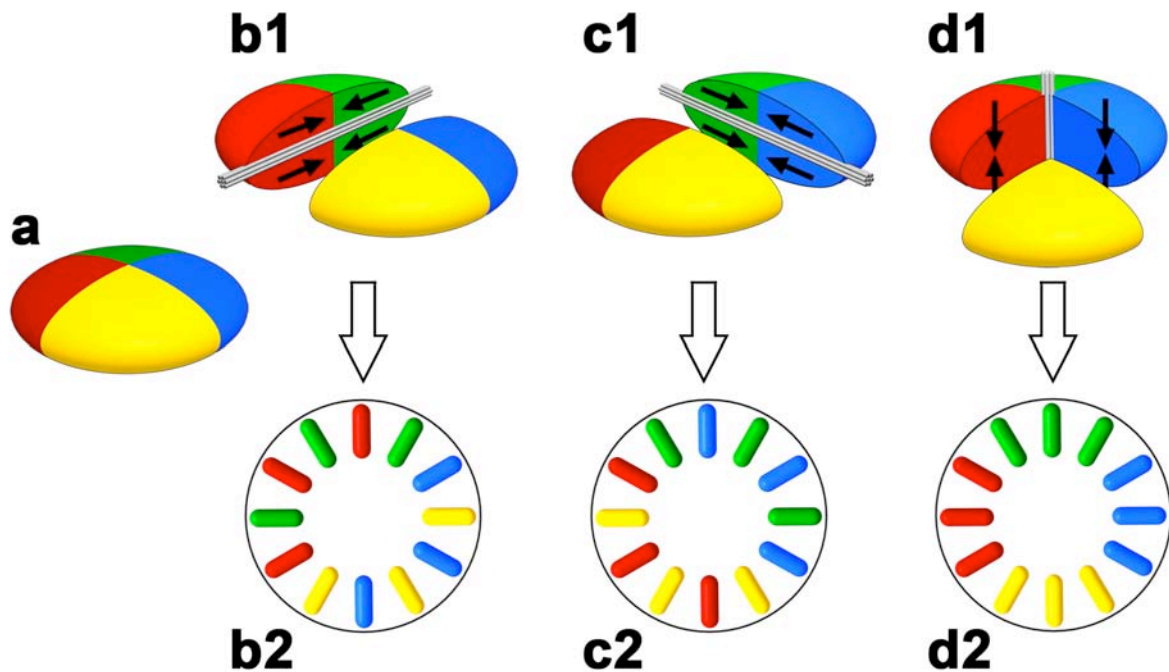
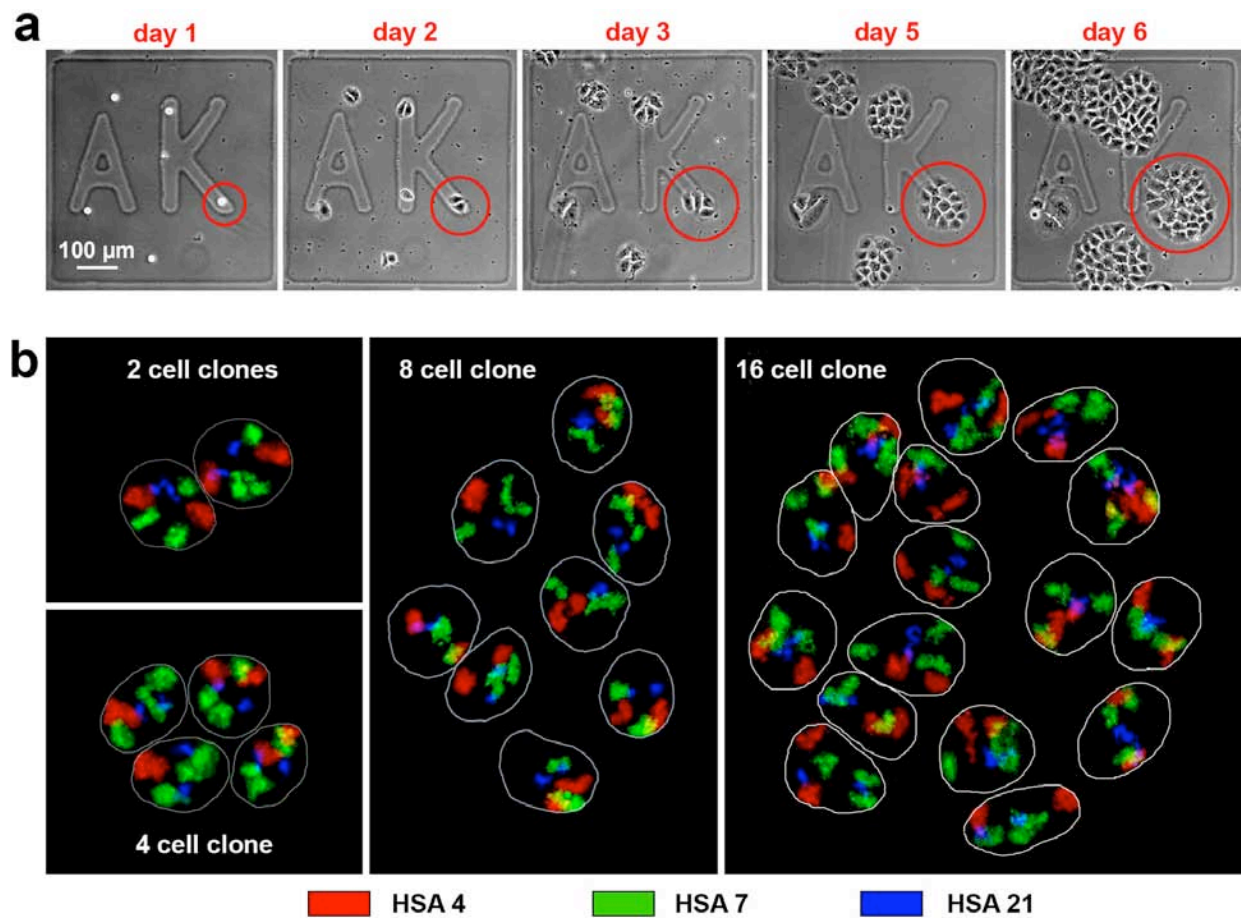


Figure 5. Primary orientation of the spindle and positioning of chromosomes in metaphase.

a, A flat nucleus with 4 arbitrarily chosen quadrants marked in different colors. **b1-d1**, Three primary orientations of the mitotic spindle (gray rods) with all three orientations being mutually perpendicular. Black arrows show the directions of chromosome congression. **b2-d2**, Every primary orientation of the spindle leads to a specific pattern of chromosome shuffling (c.f. b1-d1 and b2-d2). When the mitotic spindle is primarily oriented perpendicular to the substratum (d1), interphase chromosome arrangement is by and large transmitted to metaphase (d2).

SUPPLEMENTARY INFORMATION

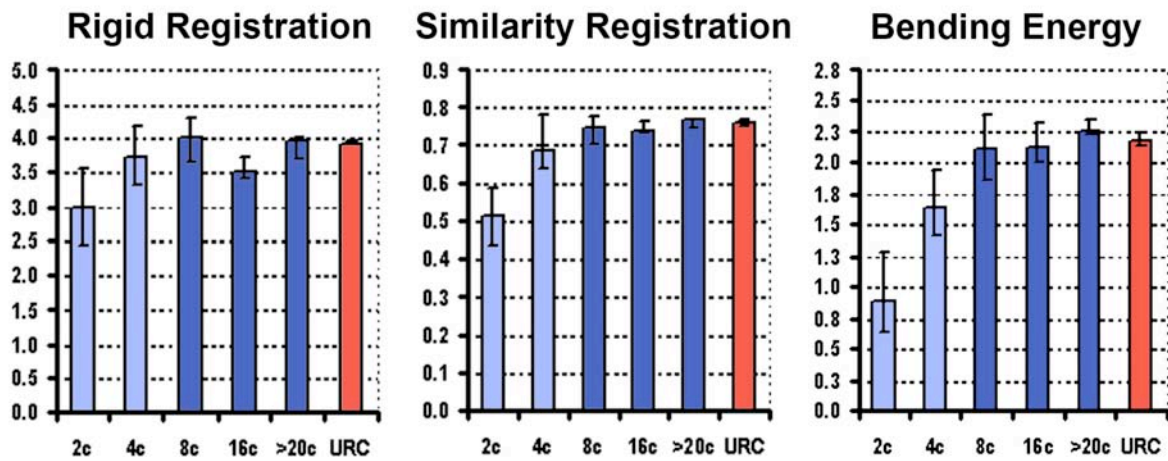
Supplementary Figure S1

**Growth of HeLa clones.**

a, phase contrast images of HeLa cells taken in 6 sequential days. One cell clone is marked by red circle.

b, maximum intensity projections of confocal stacks exemplifying 2-, 4-, 8-, and 16-cell clones monitored during growth and re-found after 3D-FISH. Visualized CTs 4, 7, and 21 are shown in red, green, and blue, respectively. Note that the used HeLa cell line has triploid chromosome 7 (c.f. Supplementary Information, Fig. S8).

Supplementary Figure S2

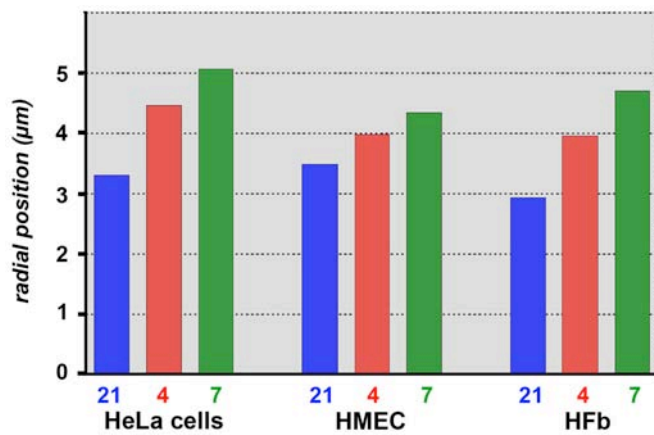
**Dissimilarities observed for clones of different size (age).**

Clones of 8 or more cells (dark blue) show the same dissimilarity level. Medians for clones of respective size are shown, error bars show 95% confidence intervals. ">20", clones of 20 or more cells; URC, unrelated cells.

Supplementary Figure S3

Median radial position of CTs 21, 4, and 7 in HeLa cells and two normal diploid cell types

Radial position is the distance between the center of the nucleus and that of a CT. Distinct size-correlated (correspondingly, chromosome number-correlated) radial distribution of the



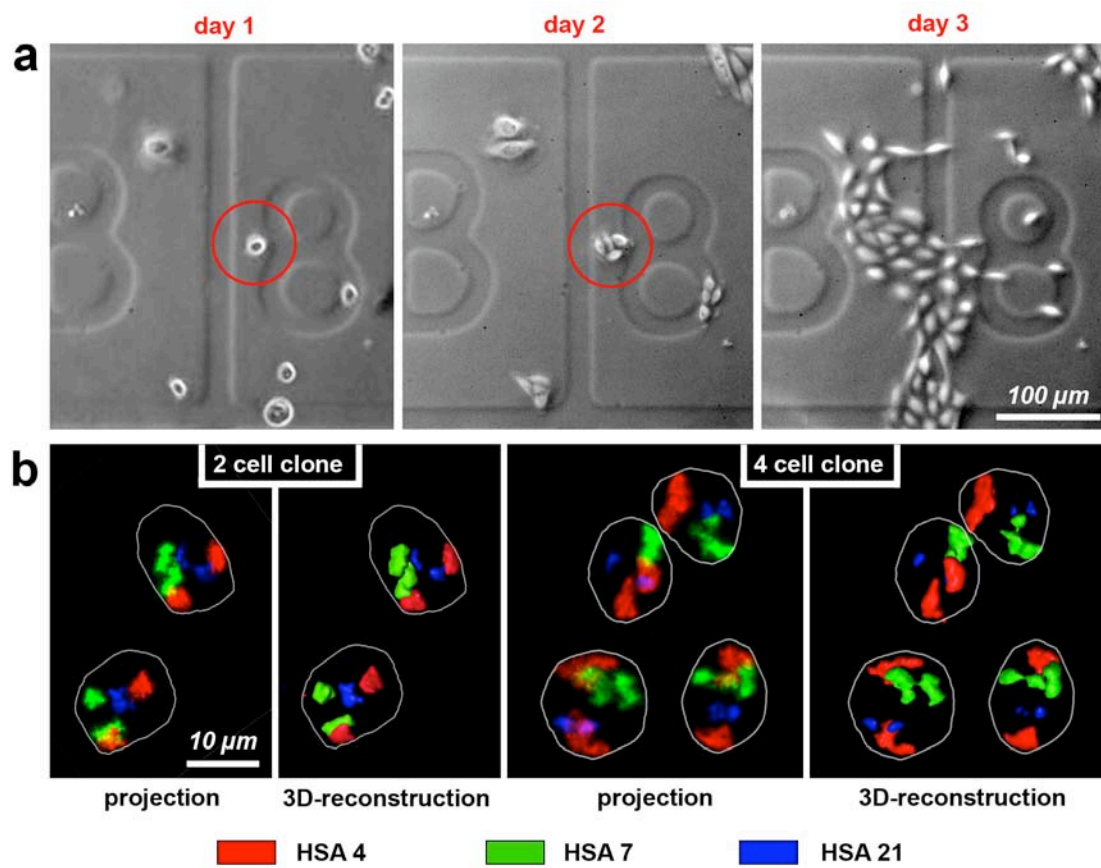
	HeLa	HMEC	HFb
KW test	P < 0.001	P < 0.009	P < 0.001
pairwise differences (Dunn's test)			
21 vs 7	P < 0.05	P < 0.05	P < 0.05
21 vs 4	P < 0.05	ns	P < 0.05
4 vs 7	ns	ns	P < 0.05

studied CTs in the nucleus is clearly manifested in all three cell types. The small HSA21 has a central position; the large HSA4 and HSA7 are situated at greater distance from the center. Why HSA7 is consistently more peripheral than HSA4 remains unknown. Relation between chromosome size (number) and position is highly statistically significant as shown by Kruskal-Wallis (KW) test (bright green cells); subsequent Dunn's test shows that radial positions of individual chromosomes are also significantly different from one another for most CT pairs (light green cells).

By contrast, positions of chromosomes on the "orbits" determined by their radial positions are random. To illustrate this we show 2D angles between homologous chromosomes in HeLa cells. In line with the assumption of random orbital positioning, for HSA4 and HSA7 the distribution of these angles was not different from a random uniform distribution and, correspondingly, the mean angle was approximately 90°. For HSA 21 the distribution of angles showed a slightly inferior fit to the random uniform model. This might be explained e.g., by a certain degree of clustering (note that HSA21 is one of the several pairs of chromosomes bearing nucleolar organizer, which tend to cluster in the nucleus). Furthermore, central positioning of a CT shifts the estimate of the homologous angles to a smaller value, since angles close to 180° are much less probable than for peripheral positions.

Chromosome	Mean 2D homologue angle	Difference from random uniform distribution, chi-square test
#4	92.18°	not significant (P > 0.1)
#7	90.11°	not significant (P > 0.1)
#21	68.77°	not significant (P > 0.05)

Supplementary Figure S4

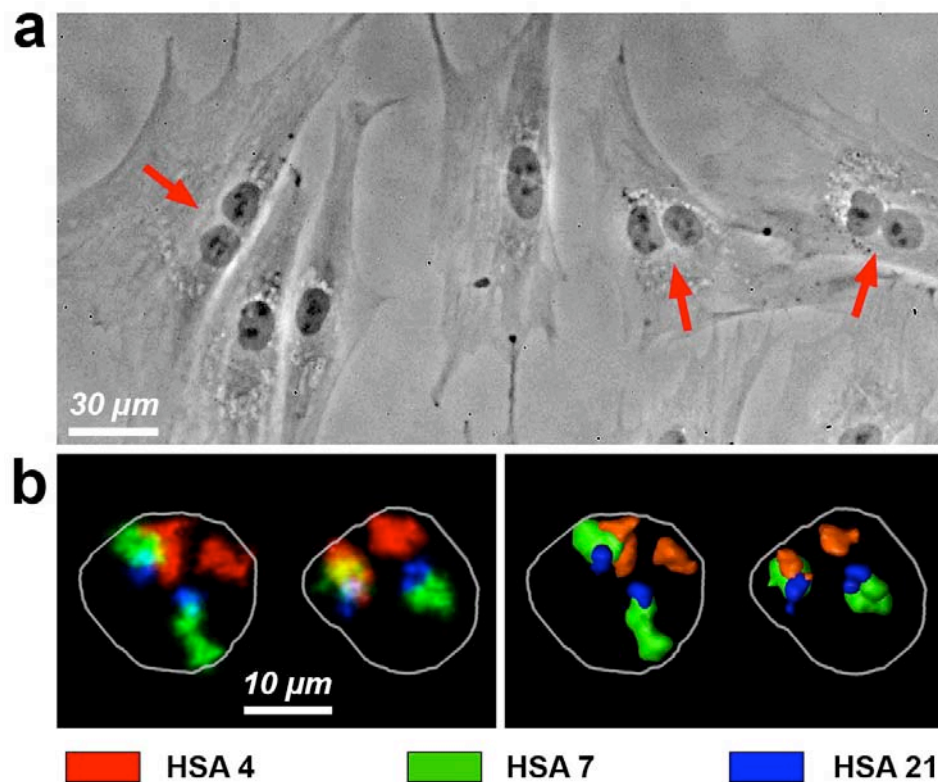


Growth of HMEC clones

a, phase contrast images of HMEC taken on 3 sequential days. One clone is marked by red circle.

b, maximum intensity projections and Amira based 3D reconstructions of confocal stacks exemplifying 2 and 4 cell clones monitored during growth and re-found after 3D-FISH. Visualized chromosome territories 4, 7, and 21 are shown in red, green, and blue, respectively.

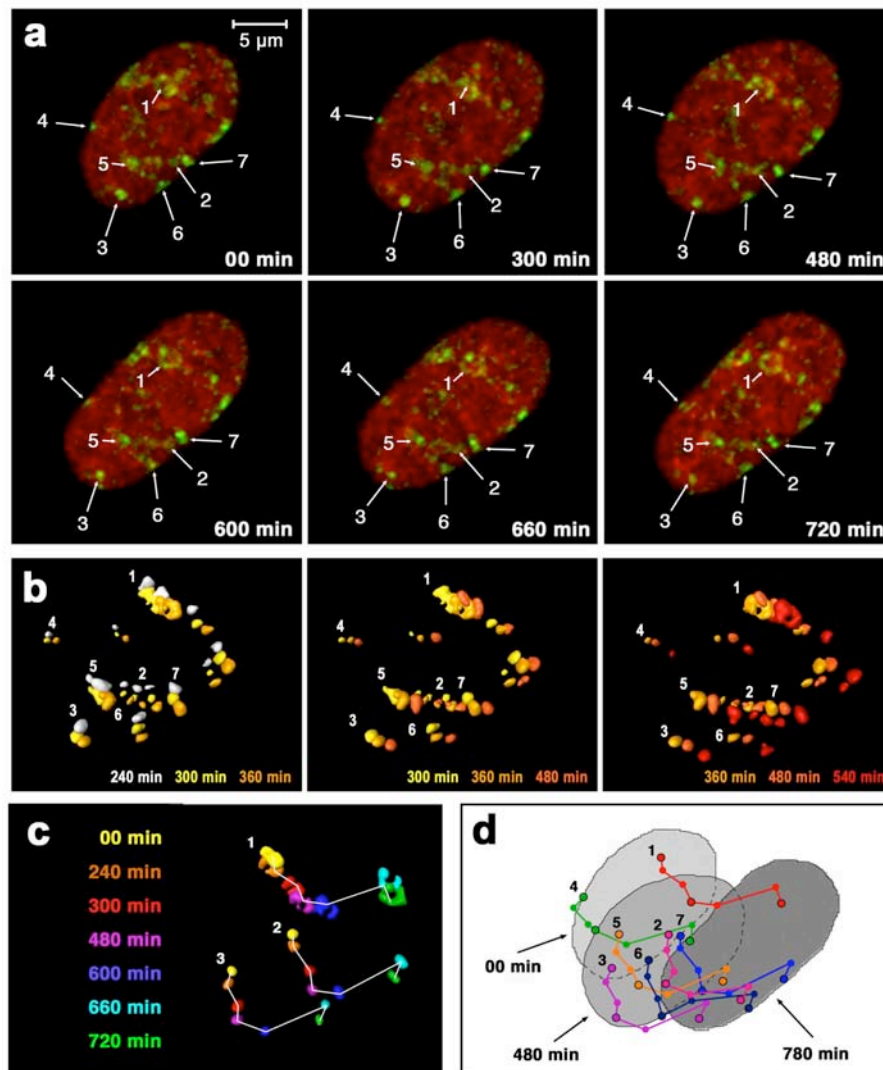
Supplementary Figure S5

**Growth of HMEC clones**

a, phase contrast image showing 3 binucleated (arrows) and several mononucleated diploid fibroblasts.

b, maximum intensity projections (left) and Amira based 3D reconstructions (right) of confocal stacks exemplifying nuclei of a binucleated fibroblast. Visualized chromosome territories 4, 7, and 21 are shown in red, green, and blue, respectively.

Supplementary Figure S6

Tracking positions of replication foci in interphase cell nuclei *in vivo*.

a, maximum intensity projections of confocal image stacks of HeLa nuclei with H2B-GFP (red) and replication labeled chromatin foci (green). Image stacks were taken every hour; only 6 time points are shown. The numbers 1 - 7 mark 7 out of 9 replication foci tracked in this nucleus.

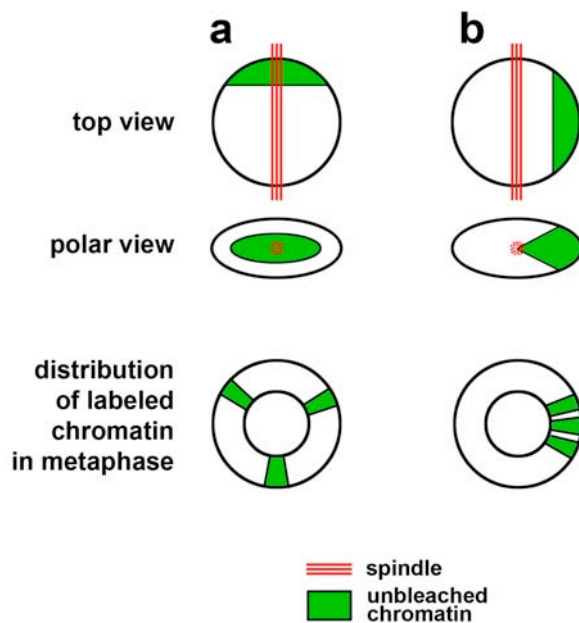
b, To trace interphase movements of individual foci, 3D reconstructions of foci were performed at each time point. Numbers mark the same replication foci, as in **a**. Five time points are shown in respective colors. Tracing the positions of individual foci was carried out manually, by placing 3-4 consecutive time points in the same Amira based reconstruction.

c, **d**, trajectories of three foci over a 12 h observation period; changes in shape and position of nuclei are shown in **d**. The 1st, 5th, and 7th positions in the trajectory belong to the time points (0, 480, and 780 min), for which projections of nuclei are shown (outlined with black circles).

Supplementary Figure S7

Retention of continuity for a small stripe of unbleached chromatin.

In the experiments by Walter and collaborators (2003) only a small stripe at the pole of the nucleus was left unbleached (green) before mitosis. Therefore, their results do not necessarily reflect transmission of chromosome arrangement, but rather retention of continuity of this small unbleached area. It was retained in 42% of cells, while in 27% of cells smaller patches of labeled chromatin were dispersed throughout the nucleus; the remaining 31% of cells showed an intermediate case.



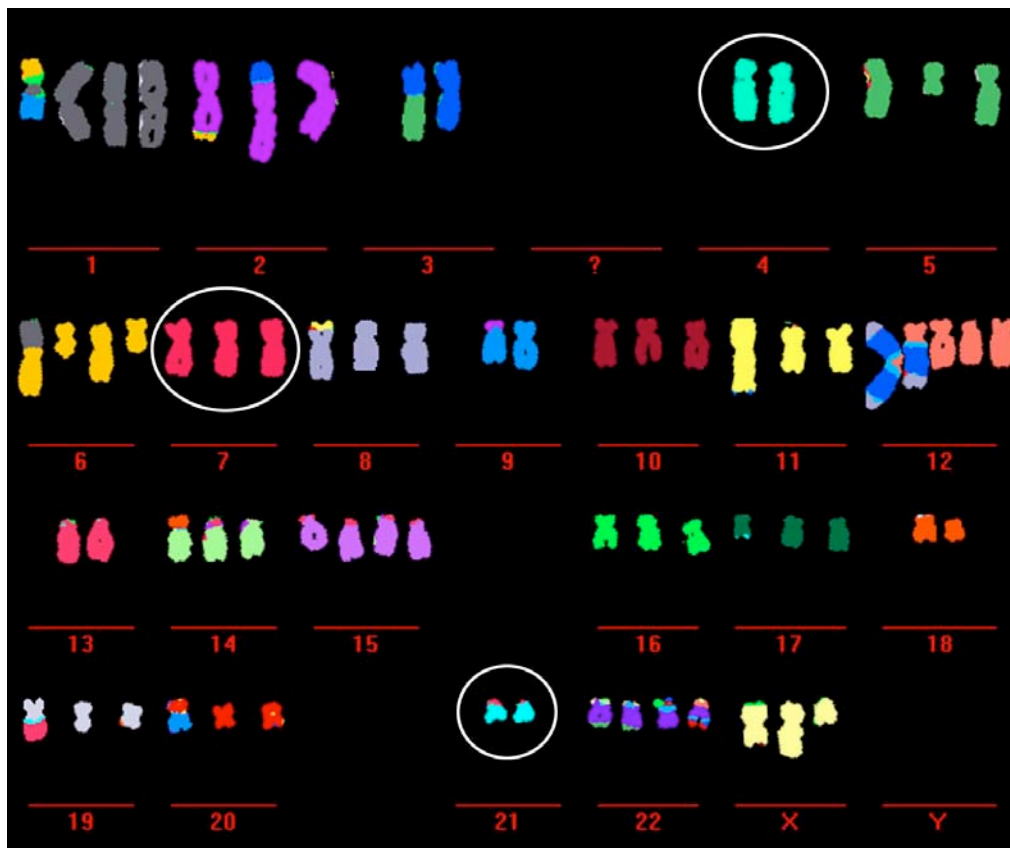
If spindle (red) is parallel to the substratum, but perpendicular to the longitudinal axis of the unbleached stripe (a), labeled chromosomes will congress to different zones of the metaphase. By contrast, if the spindle is parallel to the longitudinal axis of the unbleached stripe (b), labeled chromosomes will congress to the same portion of the metaphase. If the spindle is oriented parallel to substratum, its direction may be parallel to the unbleached stripe, perpendicular to it, or any intermediate orientations. The associated probabilities are 0.25, 0.25, and 0.50, respectively, reflecting the spatial proportionalities of these three cases. In this case continuity of a small unbleached stripe should be well retained in ca. 25% of mitoses with spindles oriented parallel to the substratum.

In another 25% continuity should be lost and in the remaining 50% there should be an intermediate situation.

As mentioned in the main text, the spindle is oriented more or less perpendicular to the substratum in 15% of HeLa cells, which increases the probability for retention of continuity of unbleached stripes ($0.15 + 0.85 \times 0.25 = 0.36$). Rough considerations made on this basis correspond reasonably well to estimates by Walter and collaborators based on visual evaluation of continuity.

	Continuity retained	Continuity <i>partially</i> retained	Continuity lost
Predictions	36%	43%	21%
Observations	42%	31%	27%

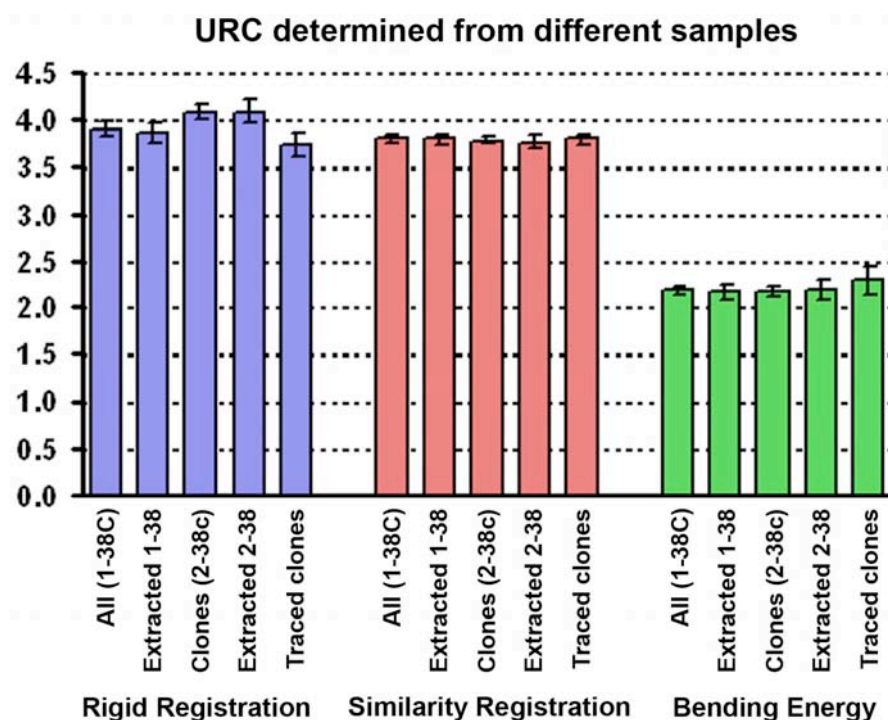
Supplementary Figure S8

**Karyotype of the used HeLa cell line.**

Multicolor classified karyogram of a HeLa cell metaphase spread obtained by M-FISH with 7 fluorochromes. Each chromosome in this metaphase was identified and false colored to visualize chromosome rearrangements. Comparison of numerous metaphase spreads showed that only three chromosomes (diploid 4 and 21, and triploid 7) were not involved in interchromosome re-arrangements or marker chromosomes formation. These 3 chromosomes were therefore chosen for the present study.

Supplementary Fig S9

Calculation of dissimilarity of chromosome arrangements between unrelated cells (URC)



A statistically robust calculation of dissimilarity between unrelated cells (URC) demands a high number of comparisons between cells. Due to the limited number of observed cells in our present study, we used the following strategy for calculation of dissimilarity of URC.

1) For each pair of clones (single HeLa cells were interpreted for this purpose as 1 cell clones) cross-clone dissimilarity was calculated as the median for all possible pairs of cells from two clones. 2) Cross-clone values were calculated for all possible pairs of clones and their median was used as the estimate of the URC dissimilarity. 3) The 95% confidence interval for this URC value was estimated by bootstrap on clones. Similar results obtained with this approach based on 3 independent samples supported the reliability of our approach.

All: all clones (78 single cells and 118 clones of different size): this value was used for comparison with clones. **Extracted 1-38:** 78 single cells and 118 single cells randomly chosen from each clone, one per clone: this sample was used to calculate distribution of individual dissimilarity values for unrelated cells in Fig 3d. **Clones 2-38:** 118 clones only. **Extracted 2-38:** 118 single cells randomly chosen from each clone. **Traced:** 28 clones with traced genealogy. This value was used for comparison with other results in the same experiment. For display convenience, values for similarity registration are multiplied by 5. Error bars show 95% confidence interval.

Supplementary Table S1

Correlation between change in the shape of the nucleus and dissimilarity in arrangement of replication foci

	Registration type					
	Rigid		Similarity		Bending Energy	
	r	P	r	P	r	P
Mean absolute change per time step	0.359	0.029	0.466	0.003	0.515	0.001
Maximal change in a single time step	0.343	0.038	0.491	0.002	0.520	0.001

Changes in the shape of the nuclei were quantified with circularity index

$$CI = \left(\sqrt{4S/\pi} \right) D$$

where S and D are area and maximal diameter (feret) of the nuclear projection.

Mean absolute change of circularity index is mean absolute value of differences between the circularity values in the beginning and at the end of each time step. r, Pearson correlation coefficient, P, significance level, number of cells: 38.

8. Abbreviations

2D	2-dimensional
3D	3-dimensional
Ab	Antibody
BAC	Bacterial Artificial Chromosome
Bp	Base pair
BrdU	5-bromo-2'-deoxyuridine
BrU	5-bromo-uridine
BSA	Bovine Serum Albumine
CCD	Charge-Coupled Device
cm	centimeter
CT	Chromosome Territory
DAPI	4',6-diamidino-2-phenylindole
Dig	Digoxigenine
d H ₂ O	de-ionized water
dd H ₂ O	ultrapure water
DMEM	Dulbecco's Modified Eagle Medium
DNA	Deoxyribo-Nucleic Acid
DNase	Deoxyribo-nuclease
DOP-PCR	Degenerate Oligonucleotid Primer-Polymerase Chain Reaction
dUTP	deoxyuridine-triphosphate
EDTA	Ethylendiamintetraacetat
EGFP	Enhanced Green Fluorescent Protein
EtOH	Ethanol
FA	Formaldehyde
FCS	Fetal Calf Serum
FISH	Fluorescence In Situ Hybridization
FITC	Fluorescein-isothiocyanat
GFP	green fluorescent protein
GOF	Oct4-GFP construct
h.c.a.	highly cross adsorbed
HEPES	N-2-hydroxyethylpiperazin-N'-2-ethanesulfonic acid
HFb	Human Fibroblasts
HSA	Homo Sapiens Autosome
HP-1	Heterochromatin Protein-1
ICM	Inner Cell Mass
IF	Immunofluorescence
IVF	in-vitro Fertilization
Kb	kilobase
LINE	Long Interspersed Nuclear Element
Mb	Megabase
NT	Nuclear Transfer
O/N	Over Night
PBS	Phosphate-Buffered Saline
PCR	Polymerase Chain Reaction
PFA	Paraformaldehyde
PSF	Point Spread Function
RNA	Ribonucleic Acid
RPMI	cell culture medium (Roswell Park Memorial Institute)
rpm	Rotations per minute
RT	Room Temperature
SINE	Short Interspersed Nuclear Element
SSC	Sodium chloride Sodium Citrate
TE	Trophectoderm
Tris	Tri(hydroxymethyl)aminomethane
Triton X-100	Octylphenoldecaethylenglycolether
Tween 20	Polyoxyethylensorbitanmonolaurat

9. Table of figures

Fig. 1	Historical drawing by Theodor Boveri	- 4-
Fig. 2	Chromosome arrangements in blastomere nuclei of <i>P. equorum</i>	- 6-
Fig. 3	Update of the chromosome territory-interchromatin compartment (CT-IC) model	- 8-
Fig. 4	Bovine oocytes	-28-
Fig. 5	Scheme of development of bovine IVF embryos	-29-
Fig. 6	Nuclear Transfer (NT)	-30-
Fig. 7	Embryo “work station”	-34-
Fig. 8	Tools for pipetting embryos	-30-
Fig. 9	Plastic stuff used for work with embryos	-35-
Fig. 10	Bovine embryos before and after fixation	-35-
Fig. 11	2D FISH of C ₀ t-1 DNA	-44-
Fig. 12	Glass slide with metal ring	-48-
Fig. 13	Plastic stuff for detection of embryos	-50-
Fig. 14	Schematic drawing of a μ -slide	-50-
Fig. 15	Processing of the DAPI channel	-55-
Fig. 16	2D/3D Relative Radial Distribution (RRD) of chromosomes 1/20 and TOPRO	-60-
Fig. 17	2D/3D Relative Radial Distribution (RRD) of chromosomes Y/17 and TOPRO	-61-
Fig. 18	2D/3D Relative Radial Distribution (RRD) of chromosomes 18/19 and TOPRO	-63-
Fig. 19	Normalized and enhanced absolute distance to surface measurements (eADS) of CTs 18 and 19	-64-
Fig. 20	Scheme and image of a slide with “micropattern”	-65-
Fig. 21	Images of human fibroblasts grown on different areas of micropattern slides	-66-
Fig. 22	Shape of cells and nuclei is depending on the substrate pattern	-67-
Fig. 23	Medians of size and roundness factors	-67-
Fig. 24	Different views of a 3D reconstruction from a human cigar shaped fibroblast	-69-
Fig. 25	Different views of a 3D reconstruction from a human round shaped fibroblast	-70-
Fig. 26	Normalized eADS measurements for artificially shaped human diploid fibroblasts grown on micropattern slides	-71-
Fig. 27	Different views of a 3D reconstruction from a Wolf’s guenon cigar shaped fibroblast	-72-
Fig. 28	Different views of a 3D reconstruction from a Wolf’s guenon round shaped fibroblast	-73-
Fig. 29	Normalized eADS measurements for artificially shaped Wolf’s guenon diploid fibroblasts grown on micropattern slides	-74-
Fig. 30	Different views of a 3D reconstruction from a bovine cigar shaped fibroblast	-75-
Fig. 31	Different views of a 3D reconstruction from a bovine round shaped fibroblast	-76-
Fig. 32	Normalized eADS measurements for artificially shaped bovine fibroblasts grown on micropattern slides	-77-
Fig. 33	Size and gene density of bovine chromosomes	-82-
Fig. 34	Synteny between human and bovine chromosomes	-83-
Fig. 35	Specificity of FISH probes for bovine chromosomes 19 and 20	-84-
Fig. 36	Radial distributions of CTs 19 and 20 in bovine fibroblasts and lymphocytes	-86-
Fig. 37	Radial distributions of CTs 19 and 20 in bovine IVF embryos	-88-
Fig. 38	Radial distributions of CTs 19 and 20 in the trophectoderm and inner cell mass	-91-
Fig. 39	Asymmetrical DNA distribution in pronuclei	-92-
Fig. 40	Influence of the global DNA distribution on the radial distribution of CTs 19 and 20	-93-
Fig. 41	Mouse blastocysts	-94-
Fig. 42	FISH on mouse embryos	-95-
Fig. 43	The reporter gene construct GOF18- Δ PE-EGFP	-96-
Fig. 44	Localization of GOF	-97-
Fig. 45	Localization of GOF in bovine fibroblast nuclei	-98-
Fig. 46	Scheme of nuclear transfer	-99-
Fig. 47	Maximum intensity projections of confocal optical serial sections and 3D reconstructions of a bovine NT embryo containing 12 nuclei	-100-
Fig. 48	Radial distributions of Oct4-GFP (GOF) and CTs 13 in bovine NT embryos	-102-
Fig. 49	Radial distributions of GOF in bovine NT embryos in relation to its harboring CT	-103-
Fig. 50	Comparison of the GOF localization between different developmental stages	-104-
Fig. 51	Comparison of the GOF&CTs 13 localization in different developmental stages	-105-
Fig. 52	3D reconstruction of two HeLa nuclei	-106-
Fig. 53	ARR of different CTs in G0 and cycling human diploid fibroblasts	-108-
Fig. 54	3D reconstruction of a flat shaped human fibroblast	-111-
Fig. 55	Scheme of differences for 3D and 2D evaluations	-111-
Fig. 56	3D reconstruction of GOF – detailed view	-121-

10. Publications

10.1. Publications:

Gao J., D. Köhler, R. Eils, I. Solovei, T. Cremer and J. Mattes. "Assessing The Similarity of Spatial Configurations Using Distance Differences and Bending Energy: Application To Chromosomal Interphase Arrangements In HeLa Cell Clones". IEEE ISBI 2004: 1400-1403 (Proceedings of the 2004 IEEE International Symposium on Biomedical Imaging: From Nano to Macro, Arlington, VA, USA, 15-18 April 2004.)

Bolzer, A., G. Kreth, I. Solovei, D. Koehler, K. Saracoglu, C. Fauth, S. Müller, R. Eils, C. Cremer, M.R. Speicher, T. Cremer (2005). "Three-Dimensional Maps of All Chromosomes in Human Male Fibroblast Nuclei and Prometaphase Rosettes." PLoS Biology 3(5): e157.

Yang, S., D. Köhler, K. Teller, T. Cremer, P. Le Baccon, E. Heard, R. Eils, K. Rohr (2006). "Non-rigid Registration of 3D Multi-channel Microscopy Images of Cell Nuclei." Med Image Comput Comput Assist Interv Int Conf Med Image Comput Comput Assist Interv 9(Pt 1): 907-14.

Cremer, M., S. Muller, D. Köhler, A. Brero, I. Solovei (2007). "Cell Preparation and Multicolor FISH in 3D Preserved Cultured Mammalian Cells. CSH Protocols doi: 10.1101/pdb.prot4723.

Muller S., M. Neusser, D. Köhler, M. Cremer (2007). "Preparation of Complex DNA Probe Sets for 3D FISH with up to Six Different Fluorochromes." CSH Protocols doi:10.1101/pdb.prot4730.

Yang, S., D. Köhler, K. Teller, T. Cremer, P. Le Baccon, E. Heard, R. Eils, K. Rohr (2008). "Nonrigid Registration of 3-D Multichannel Microscopy Images of Cell Nuclei." IEEE Transaction on Image Processing 17(4): 493-9

Hase, J.v., D. Koehler, K. Kuepper, H. Albiez, C. Weierich, G. Kreth, C. Cremer (in prep.). "High Precision Measurements of Absolute Distance Distributions from Intranuclear Surfaces (ADS) in 3D Confocal Microscopy."

Koehler, D., J. Gao, J. Mattes, T. Cremer, B. Joffe, R. Eils and I. Solovei (in prep.). "Inheritance and Diversification of Spatial Chromosome Arrangement in Growing Cell Clones of Human Cells."

Koehler, D., J. Pendse, M. Neusser, S. Muller, I. Solovei, D. Ingber and T. Cremer (in prep.). "Differences in nuclear shape enforce different spatial arrangements of chromosome territories."

Koehler, D., T. Cremer, E. Wolf, V. Zakhartchenko and A. Brero (submitted). "Changes of Higher Order Chromatin Arrangements During Bovine Major Genome Activation."

Koehler, D., V. Zakhartchenko, N. Ketterl, E. Wolf, T. Cremer, A. Brero (in prep.) "FISH on 3D preserved preimplantation embryos" (bookchapter) Methods in Molecular Biology, Humana Press (edited by J. M. Bridger and E. Volpi)

10.2. Posters/Oral Presentations:

Koehler D., J. Gao, J. Mattes, R. Eils, T. Cremer and I. Solovei: "Arrangement of chromosome territories in human cell clones." Poster, Jahrestagung der Deutschen Gesellschaft für Zellbiologie, Berlin, Germany, EJCB, Vol. 83, Suppl. 54, ISSN 0171-9335, March 24–27, 2004.

Koehler D., J. Gao, J. Mattes, R. Eils, T. Cremer and I. Solovei: "Changes in the arrangement of chromosome territories in human cell clones." Oral presentation, Gordon Research Conferences, Molecular Cytogenetics, The Queen's College, Oxford University, Oxford, United Kingdom, July 18–23, 2004.

Koehler D., J. Gao, J. Mattes, R. Eils, T. Cremer and I. Solovei: "Changes in the arrangement of chromosome territories in human cell clones." Oral presentation, ICC XV, The 15th International Chromosome Conference, Brunel University, London, United Kingdom, September 5-10, 2004.

Koehler D., J. Gao, J. Mattes, R. Eils, T. Cremer and I. Solovei: "Changes in the arrangement of chromosome territories in human cell clones." Oral presentation,

“array-CGH and Molecular Cytogenetics”, Marie Curie Meeting, July 18-23, 2004, The Queen's College, Sanger Institute, Cambridge, UK.

Koehler, D., J. Gao, J. Mattes, R. Eils, T. Cremer and I. Solovei: “Changes in the arrangement of chromosome territories in human cell clones.” Poster, “array-CGH and Molecular Cytogenetics”, Marie Curie Meeting, October 19–22, 2005, Bari, Italy.

Koehler, D., I. Solovei, J. Pendse, D. Ingber and T. Cremer: “Relation between the shape of the nucleus and the spatial chromosome arrangement”. Poster, “array-CGH and Molecular Cytogenetics”, Marie Curie Meeting, September 13–16, 2006, Leuven, Belgium.

Koehler, D., A. Brero, V. Zakhartchenko, T. Cremer, E. Wolf: “Nuclear architecture during early bovine development.” Poster, Conference on Reproductive and Developmental Biology, June 21-22, 2007, Czech University of Agriculture Prague, Prag, Czech Republic.

Koehler, D., A. Brero, T. Cremer, E. Wolf, V. Zakhartchenko: “Changes in Higher Order Chromatin Arrangements During Early Bovine Development.” Oral Presentation & Poster, 34th Annual Conference of the International Embryo Transfer Society (IETS), January 5-9, 2008, Denver, Colorado, USA.

Koehler, D., A. Brero, E. Wolf, T. Cremer, V. Zakhartchenko: “Changes of spatial chromatin organization during nuclear transfer.” Poster, Society for the Study of Reproduction (SSR) 41st Annual Meeting “Reproductive Biology: Basic Discoveries That Affect Our Lives”, May 25-30, 2008, Kailua-Kona, Hawaii, USA.

11. Curriculum Vitae

Name: Daniela Nicole Köhler

Address: Schellingstr. 126 RG
80798 München

Date of Birth: 17.04.1975 in Neuburg a.d. Donau, Germany

Marital status: Unmarried

Education: 1981-1985 Elementary school, Burgheim
1985-1995 High school (Descartes Gymnasium) Neuburg

Studies: 1995-2002 Studies in biology at the Ludwig-Maximilians-University (LMU), Munich

Main subject: Human genetics

Subsidiary subjects: Biochemistry, Pharmacology and Toxicology, Zoology

Diploma thesis: 13.02.2002 – 13.11.2002 Institute of Human Genetics (Prof. Dr. T.Cremer in Munich)
Title: „Variabilität oder Konstanz der Chromosomenanordnung während des klonalen Wachstums menschlicher Zellen“

PhD thesis: since 01.02.2003 Institute of Human Genetics (Prof. Dr. T.Cremer in Munich)
Title: „Cloning in cattle: Nuclear architecture and epigenetic status of chromatin during reprogramming of donor cell nuclei“

Languages: German: mother tongue
English: fluent in written and spoken
French: basic knowledge

12. Acknowledgement

Zunächst möchte ich mich bei meinem Doktorvater Thomas Cremer herzlich bedanken, dafür dass er mir die Promotion in seiner Arbeitsgruppe ermöglicht hat. Eine Arbeitsgruppe in der man viel lernen kann und in der neben der Wissenschaft auch die Menschlichkeit immer wichtig ist. Vielen Dank für eine tolle und lehrreiche Zeit!

Manfred Schliwa möchte ich herzlichst danken für die Übernahme der Zweitkorrektur.

Eckhard Wolf und Valeri Zakhartchenko gilt mein Dank für eine äußerst kreative und produktive Zusammenarbeit auf einem für mich komplett neuen und extrem spannenden Themengebiet.

Alessandro Brero – die beste Teamhälfte die man sich wünschen kann – war mir immer zur Seite gestanden mit cleveren, beratenden, motivierenden Worten und Taten. Danke für die schöne Zeit und Arbeit! Es war nicht nur überaus interessant, sondern hat verdammt viel Spaß gemacht!

Irina Solovei möchte ich danken für alles was sie mir beigebracht hat – und das war eine ganze Menge: Zellkultur, FISH, Mikroskopie, Datenbearbeitung und nicht zuletzt schöne Bilder machen. Boris Joffe hat den statistischen Teil ergänzt. Bei Marion Cremer möchte ich mich bedanken für all den Rat, mit dem sie mir stets zur Seite stand.

Stefan Müller, Michaela Neusser (die zusammen für den Biologennachwuchs sorgen) und Christian Lanctot (kennt sich auch aus mit Embryos) gilt mein herzlichster Dank für all die hilfreichen Diskussionen, die auch nach Feierabend kein Ende fanden. Ganz besonderer Dank gilt auch all meinen Doktoranden-/Doktorandinnenkollegen für eine wunderschöne und kreative Zeit, die längst mehr ist als nur von beruflicher Natur. Danke an Claudia Weierich (jetzt Dahlem und auch mit Nachwuchs!) für all das Essen und das Zuhören, Katrin Küpper für all die durchgeführten Nächte, Claudia Hepperger für all die Abende bei Bier, Schubbis und Tennis, Kathrin Teller & Heiner Albiez für diverse Essen und viel Spaß und Action, Roman Zinner dem größten Berg-, Foto- und Reise-Spezialist, Robert Mayer (bringt immer alles genau auf den Punkt), Andreas Zunhammer (der gute Geist und Mitose-

Spezialist), Jens Nagel (der Womenizer & „formschöner“ Bäcker), Hilmar Strickfaden (Spezialist für ganz viele Dinge, u.a. Ionbeams, Lebendzellmikroskopie, backen, Mikroinjektion, Frösche züchten u.v.m.), Florian Grasser (hervorragender Koch), Sabine Langer (Diagnostikspezialistin) und Steffen Dietzel (Mikroskopspezialist), an Alex Kölbl (großer Pferdefan) & Tobias Thormeyer (extra grosses Danke für ein super eADS Programm), Doris Illner (meine Lieblingskrankenschwester) und Barbara Hübner (gibt es doch ein Biologengen?). Und nicht zu vergessen unsere „Neuen“: Jaques Rouquette & Stan Fakan (die EM-Fraktion), Charlotte Hauser (zur Verstärkung der Embryo und Stammzellfraktion). An Nina Ketterl (Vorzeigediplomandin) ein ganz besonderes Danke für ihre Hilfe mit unzähligen Embryostacks und eine tolle Diplomarbeit über die Kerntransferembryonen.

An die organisatorische Abteilung mit Carolin Bleese, Roy Hessing, Ming Zhao und Heidi Jahn-Henninger möchte ich meinen Dank aussprechen für all die Kleinigkeiten, die einem das Unileben täglich erleichtern.

Danken möchte ich auch meiner und Romans Familie für ihr stetes Vertrauen in mich und meine Arbeit. Ebenso wie meiner WG, allen Voran Matthew Philogene (Mad Matt), Georgi Kratzer (mein Lieblingskoch) und Matthias Wohlgenannt (bald berühmter Künstler) für die Unterstützung während der ganzen Zeit.

Mein allergrößter Dank gilt meinem Freund Roman für all die Diskussionen rund um die Arbeit, die Unterstützung in jeder Hinsicht, dafür dass er mich zum lachen bringt, dass er mich auf alle möglichen (wunderschöne) Berge hetzt, seine Geduld und vor allem seine Liebe, die das Leben so schön macht! You´re the best i know...

Ehrenwörtliche Versicherung

Hiermit bestätige ich, dass ich die vorliegende Dissertation selbständig und nur mit den angegebenen Materialien und Quellen durchgeführt habe.

München, den 23.10.2008

Daniela Köhler

Erklärung über frühere Promotionsversuche

Hiermit bestätige ich, dass ich vor dieser Arbeit keine anderen Promotionsversuche unternommen habe. Dies ist meine erste und einzige Dissertation.

München, den 23.10.2008

Daniela Köhler